Development of *Synechococcus* sp. PCC 11901 as a biotechnology platform

Lauren Mills

School of Biological Sciences

University of East Anglia

Submitted for the Degree of Doctor of Philosophy

December 2022

Declaration

A thesis submitted (December 2022) to the University of East Anglia for the degree of Doctor of Philosophy.

Abstract

Cyanobacteria are key organisms in the global ecosystem and potential renewable platforms for production of chemicals. Many aspects of cyanobacterial biology are unique to this subset of prokaryotes. Characterising cyanobacterial metabolism and physiology is key to understanding their environmental role and unlocking their potential for biotechnology. This thesis provides a comprehensive summary of our knowledge on cyanobacterial physiology and the pathways in the model organism, *Synechocystis* sp. PCC 6803 (PCC 6803). One of the main issues within cyanobacterial bioindustry has been the lack of sustained fast-growing strains. The newly discovered *Synechococcus* sp. PCC 11901 (PCC 11901) reportedly demonstrates the highest, most sustained growth of any known cyanobacterium. Knowledge of PCC 11901 biology, including the factors underlying the sustained fast growth, is limited, which hinders its potential for biotechnology. Genetic tools for generating unmarked mutants in PCC 11901 are not established. This thesis confirms that PCC 11901 displays faster growth than other model cyanobacteria. Comparative genomics between PCC 11901 and PCC 6803 reveal conservation of most metabolic pathways but PCC 11901 has a simplified electron transport chain and reduced light-harvesting complex. This may underlie its efficient light use, reduced photoinhibition, and higher photosynthetic and respiratory rates. Attempts to generate unmarked knockouts using two negative selectable markers were unsuccessful, suggesting that recombinase or CRISPR-based approaches may be necessary for the industry requirement of repeated genetic manipulation. To further cement PCC 11901 as a future industrial strain, biomass and optical density measurements were carried out over a range of light intensities to aid photo-mechanistic modelling of the strain. This thesis establishes PCC 11901 as one of the most promising species currently available for cyanobacterial biotechnology and provides a useful set of bioinformatic tools and strains for advancing this field, in addition to insights into the factors underlying its fast growth phenotype.

Acknowledgements

Firstly, my sincere thanks goes to my primary supervisor Dr David Lea-Smith for the opportunity to carry out this PhD and for all his help and advice over the last four years. Thanks also goes to Dr Simon Moxon and Dr Dongda Zhang for their comments and guidance. I would also like to the thank the University of East Anglia and the UKRI-BBSRC Norwich Research Park Biosciences Doctoral Training Partnership for their services and financial support which has allowed this work to happen.

I would like to thank all the members of the Lea-Smith lab, Dr Andrew Curson, Dr Emese Bartha, Dr Ayman Abufalgha and Keanu Walsham. You guys made this experience much more enjoyable. Thank you for putting up with my insistent questions and humouring me with my relentless chatting. Of course, special thanks must go to the Golden-Gate God himself, Dr José Ángel Moreno Cabezuelo, a true world leader.

Thanks to Dr Alex Jarvis, Dr Joseph Shepherd, Dr Gareth Ashworth and Dr Sam Piper. Your support and mentorship within those first few years was invaluable. Thank you showing me there is a light at the end of the tunnel. Thanks also to Dr Kabiru (KB) Usman for always keeping me entertained and smiling.

It has been an exceptionally difficult four years, without the small matter of a PhD and I am incredibly grateful to my friends for helping me through. Thank you so much to: Ocean, for being my first friend at UEA, my coffee break buddy and my emotional confidant; Jonny, for always making me laugh, even when it felt like the world was falling apart; Tom, for his wonderful music recommendations and infamous Burn's suppers; Summer, Grace and Connor for providing me with respite from the PhD by providing wine and giggles on the weekends; Sophie, for your emotional support and for providing a friendly ear when necessary. Thanks to Connor and Matthew for being my board game and pub buddies, but most importantly for your company and inspiration.

To Alan, I would not be where I am today without you. Thank you for your love and support throughout these four years. Your unwavering belief gave me the strength to keep going and to see this through.

Finally, I would like to thank my family. I can confidently say that I would not have gotten through this without you all. Thank you to my sister, Iona, for continuing to inspire me on a daily basis. To my Mum, for trying her hardest to understand why anyone would want to study 'little green bugs' for four years, but who was always at the end of the phone full of support and love. Finally, I would

never have gotten this far in science without my Dad. Thank you for teaching me determination, meticulousness and to always pursue curiosity.

Author's Declaration

The research described in this thesis was conducted at the University of East Anglia between October 2018 and December 2022 under the supervision of Dr David Lea-Smith and Dr Simon Moxon from the University of East Anglia, and Dr Dongda Zhang from the University of Manchester. No part of this thesis has previously been submitted for a degree at this or any other academic institution. All data described here are original and were obtained by the author unless except in the cases outlined below and attributed in the text.

- Alternative *desB* mutant, described in **Chapter 4**, was created and characterised by Angelo J Victoria from the McCormick Group at the University of Edinburgh.
- The computational modelling, described in **Chapter 5**, was carried out by Bovinille Anye Cho from the Zhang Group at the University of Manchester.

Sections regarding genetic engineering of model and non-model cyanobacteria in **Chapter 1** were previously published in*:*
Emerging species and genome editing tools: future prospects in cyanobacterial synthetic biology. GAR Gale, AA Schiavon Osorio, LA Mills, B Wang, DJ Lea-Smith, AJ McCormick. Microorganisms 7 (10), 409

The results described in **Chapter 2** were subject of the following publication and are presented in text as well as **Appendix 2.1 - 2.4**:
Current knowledge and recent advances in understanding metabolism of the model cyanobacterium Synechocystis sp. PCC 6803. LA Mills, AJ McCormick, DJ Lea-Smith. Bioscience reports 40 (4), BSR20193325.

The results described in **Chapter 3 and 5** were subject of the following publication and are presented in text as well as **Appendix 3.1 - 3.4**:
Development of a Biotechnology Platform for the Fast-Growing Cyanobacterium Synechococcus sp. PCC 11901. Mills, L.A.; Moreno-Cabezuelo, J.Á.; Włodarczyk, A.; Victoria, A.J.; Mejías, R.; Nenninger, A.; Moxon, S.; Bombelli, P.; Selão, T.T.; McCormick, A.J.; Lea-Smith, D.J. Biomolecules 12 (7)

The results described in **Chapter 4** were subject of the following publication and are presented in text:
Integrated experimental and photo-mechanistic modelling of biomass and optical density production of fast versus slow growing model cyanobacteria. Cho, B. A.; Moreno-Cabezuelo, J. Á.; Mills, L. A.; del Río Chanona, E. A.; Lea-Smith, D. J.; Zhang, D. Algal Research, 70, 102997.

List of Tables

List of Figures

List of Appendices

All appendices are located within the associated OneDrive file.

Appendix Table 2.1:
Comparison of *Synechocystis* sp. PCC 6803 central metabolism and transporter proteins with predicted homologs in *Escherichia coli* K12 using NCBI's Blast Algorithm.

Appendix Table 2.2:
Comparison of *Escherichia coli* K12's proteome with its predicted homologs in *Synechocystis* sp. PCC 6803, using the NCBI's Blast Algorithm.

Appendix Table 2.3:
Comparison of *Synechocystis* sp. PCC 6803 characterised proteins that are not involved in metabolism or transport with their predicted homologs in *Escherichia coli* K12 using NCBI's Blast Algorithm.

Appendix Table 2.4:
Comparison of *Synechocystis* sp. PCC 6803 uncharacterised proteins with their predicted homologs in *Escherichia coli* K12 using NCBI's Blast Algorithm.

Appendix Table 2.5:
A modified version of Supplementary Table 3 from Baers *et al.*, for one of the input files in CyanoBLAST.

Appendix Table 2.6:
A modified input file for CyanoBLAST which can be used to compare *Synechocystis* sp. PCC 6803's central metabolism and transporter proteins.

Appendix Table 2.7:
A modified input file for CyanoBLAST which can be used to compare *Synechocystis* sp. PCC 6803 characterised proteins that are not involved in metabolism or transport.

Appendix Table 2.8:
A modified input file for CyanoBLAST which can be used to compare *Synechocystis* sp. PCC 6803 uncharacterised proteins.

Appendix Table 3.1:
Comparison of *Synechocystis* sp. PCC 6803 central metabolism and transporter proteins with predicted homologs in *Synechococcus* sp. PCC 11901 using NCBI's Blast Algorithm.

Appendix Table 3.2:
Comparison of *Synechocystis* sp. PCC 6803 proteins involved in processes other than central metabolism, light harvesting and photosynthesis, and proteins of unknown function with predicted homologs in *Synechococcus* sp. PCC 11901 using NCBI's Blast Algorithm.

Appendix Table 3.3:
Synechococcus sp. PCC 11901 proteins with no homologues in *Synechocystis* sp. PCC 6803 using NCBI's Blast Algorithm.

Appendix Table 3.4:
Potential *Synechococcus* sp. PCC 11901 homologues of *Synechocystis* sp. PCC 6803 proteins involved in electron transport and light harvesting using NCBI's Blast Algorithm.

List of Abbreviations and Acronyms

5-FC	-	5-fluorocytosine
ACP	-	Acyl carrier protein
ADP	-	Adenosine diphosphate
ARTO	-	Alternative respiratory terminal oxidase
ATP	-	Adenosine triphosphate
BLAST	-	Basic Local Alignment Search Tool
Cas	-	CRISPR-associated protein
CBB	-	Calvin-Benson-Bassham
CDS	-	Coding DNA sequence
COX	-	Cytochrome-*c* oxidase complex
CRISPR	-	Clustered regularly interspaced short palindromic repeats
cyd	-	Cytochrome *bd*-quinol oxidase
cyt b_6f	-	Cytochrome b_6f complex
cyt c_6	-	Cytochrome c_6
DNA	-	Deoxyribonucleic acid
dNTPs	-	2'deoxyribonucleoside triphosphate
EDTA	-	Ethylenediaminetertraacetic acid
EMP	-	Embden-Meyerhof-Parnas
Eqs.	-	Equation
FAD	-	Flavin adenine dinucleotide
FAR	-	Acyl-ACP reductase
Fd	-	Ferredoxin
FLP	-	Flippase
Flv1/3	-	Flavodiiron 1/3 complex
Flv2/4	-	Flavodiiron 2/4 complex
FRT	-	FLP recognition targets
g	-	Gravitation, unit of gravity
gDNA	-	Genomic DNA
HPC	-	High performance computer
kb	-	Kilo base pairs
kDa	-	Kilo Dalton
LB	-	Luria-Bertani Broth
LPS	-	Lipopolysaccharide

M	-	Molar
MoClo	-	Modular cloning
NAD^+	-	Nicotinamide adenine dinucleotide
$NADP^+$	-	Oxidised β-nicotinamide adenine dinucleotide phosphate
NADPH	-	Reduced β-nicotinamide adenine dinucleotide phosphate
NDH	-	NAD(P)H dehydrogenase complex
NCBI	-	National Centre for Biotechnology Information
OD	-	Optical density
ODE	-	Ordinary differential equation
OM	-	Outer membrane
OPP	-	Oxidative Pentose phosphate
PBPs	-	Penicillin-binding proteins
PBR	-	Photobioreactor
PBS	-	Phycobilisome
PC	-	Plastocyanin
PCC 6803	-	*Synechocystis* sp. PCC 6803
PCC 7002	-	*Synechococcus* sp. PCC 7002
PCC 7942	-	*Synechococcus elongatus* PCC 7942
PCC 11901	-	*Synechococcus* sp. PCC 11901
PCR	-	Polymerase chain reaction
PDE	-	Partial differential equation
PM	-	Plasma membrane
PP	-	Pentose phosphate
PQ	-	Plastoquinone
PSI	-	Photosystem I
PSII	-	Photosystem II
RNA	-	Ribonucleic acid
ROS	-	Reactive oxygen species
rpm	-	Rotations per minute
RuBisCO	-	Ribulose 1.5-biphosphate carboxylase/oxygenase
SD	-	Standard deviation
SDH	-	Succinate dehydrogenase
SE	-	Standard error
TCA	-	Tricarboxylic acid

TM	-	Thylakoid membrane
TMH	-	Transmembrane helical domain
Tris	-	2-amino-2-hydroxy-methylpropane-1,3-diol
tRNA	-	Transfer RNA
UDP	-	Uridine diphosphate
UTEX 2973	-	*Synechococcus elongatus* UTEX 2973
v/v	-	Volume per volume
w/v	-	Weight per volume

Table of Contents

Chapter 1

General Introduction

Sections of this chapter have previously been published in

Emerging species and genome editing tools: future prospects in cyanobacterial synthetic biology
GAR Gale, AA Schiavon Osorio, LA Mills, B Wang, DJ Lea-Smith, AJ McCormick
Microorganisms 7 (10), 409

Chapter 1: General Introduction

1.1 Cyanobacteria

Cyanobacteria are a large and diverse group of photosynthetic prokaryotes found in nearly all environments on Earth. They were likely the main organisms involved in generating an oxygenic environment starting approximately 2.4 billion years ago and are currently responsible for approximately a quarter of global primary production (1–3). Cyanobacteria also play a key role in the global nitrogen cycle due to the ability of certain species to fix nitrogen (4). It has been proposed that chloroplasts almost certainly descend from an internalized cyanobacterium (5). Certain physiological and biochemical features are conserved in higher photosynthetic organisms, making cyanobacteria excellent chassis for production of plant-derived natural products, like terpenes, and as model systems for genetic studies of the processes conserved between cyanobacteria and chloroplast-containing phototrophs. Many key processes conserved throughout the photosynthetic lineages were first characterised in cyanobacteria (6,7), and there is significant interest in engineering cyanobacterial enzymes and CO_2-concentrating mechanisms into crop plants to improve productivity (8–12).

1.1.1 Ultrastructure of cyanobacteria

Cyanobacteria incorporate a cell envelope similar to other Gram-negative bacteria, containing a plasma membrane, peptidoglycan layer and an outer membrane containing lipopolysaccharides (13) (**Figure 1.1**). However, cyanobacteria are unique, in terms of Gram-negative bacteria, due to the presence of internal thylakoid membranes, the site of photosynthesis and respiration (14). Thylakoid membranes are arranged in pairs, surrounding a distinct cellular compartment called the thylakoid lumen (15). Cyanobacteria also contain large microcompartments called carboxysomes, which concentrate carbon dioxide, resulting in more efficient carbon fixation and therefore production of biomass (14). Most cyanobacteria contain multiple chromosomal copies, but this can vary greatly depending on the species. For example, in *Synechocystis* sp. PCC 6803 (PCC 6803), chromosomal number can vary between 4 - 53 copies depending on growth conditions and strain (16). Fluorescent staining of deoxyribonucleic acid (DNA) shows 92% of chromosomal material localises to the central cytoplasm, whilst 8% is found at the periphery of the cytoplasm, adjacent to the membranes (17).

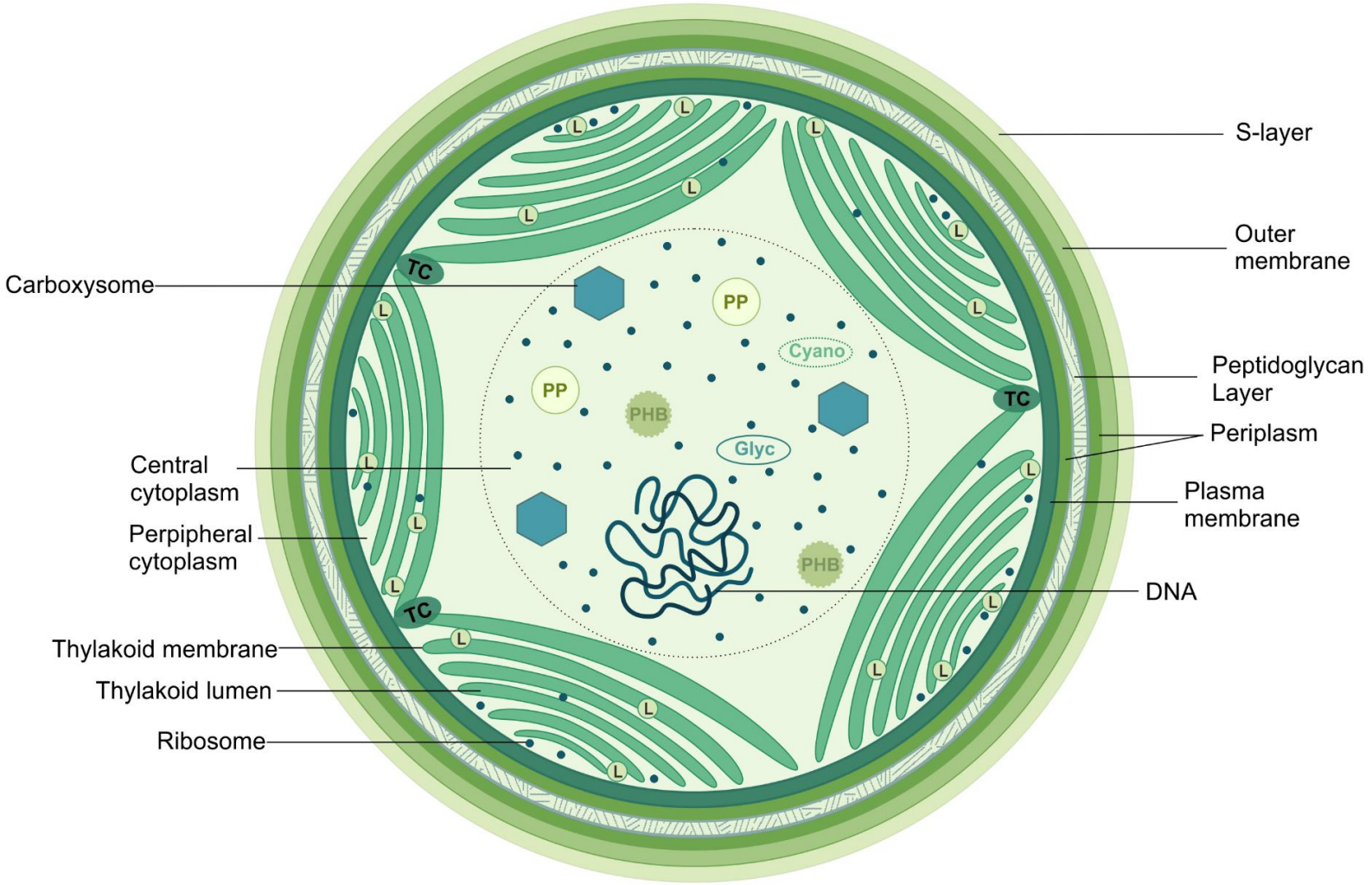

Figure 1.1 The ultrastructure of *Synechocystis* showing various subcellular components. L, Lipid body; C, Carboxysome; PHB, Polyhydroxybutyrate granule; PP, Polyphosphate body; Glyc, Glycogen granule; Cyano, Cyanophycin granule; TC, Thylakoid centre

1.1.2 Photosynthesis and respiration in cyanobacteria

In the majority of cyanobacterial species, photosynthesis occurs in the thylakoid membrane. The photosynthetic electron transport chain is largely similar between cyanobacteria, algae and plants (Figure 1.2). Photosynthesis is initiated in photosystem II (PSII), which uses light energy to split water into oxygen and protons, and the concomitant release of electrons. These electrons are then transferred to plastoquinone (PQ), reducing it to plastoquinol. The electrons are then transferred to the cytochrome b_6f complex (cyt b_6f), resulting in transport of further protons across the thylakoid membrane to the lumen, and from there, to a soluble electron carrier. The soluble electron carrier can be either plastocyanin or cytochrome c_6 (cyt c_6), depending on the species and the availability of copper (18). This reaction occurs on the luminal side of the thylakoid membrane. The electron is transferred to photosystem I (PSI), where it replaces a newly excited electron which is transferred to ferredoxin (Fd), then ferredoxin-$NADP^+$ reductase, leading to production of NADPH. The transfer of electrons during photosynthesis leads to the formation of a proton gradient which is utilised by ATP synthase for ATP production. The NADPH and ATP formed during these processes is used for CO_2 fixation and other cellular processes (18,19). CO_2 fixation occurs within the carboxysome, a compartment that increases the efficiency of carbon assimilation and limits photorespiration. The process of photorespiration results in production of 2-phosphoglycolate, which involves an energetically costly process to recycle.

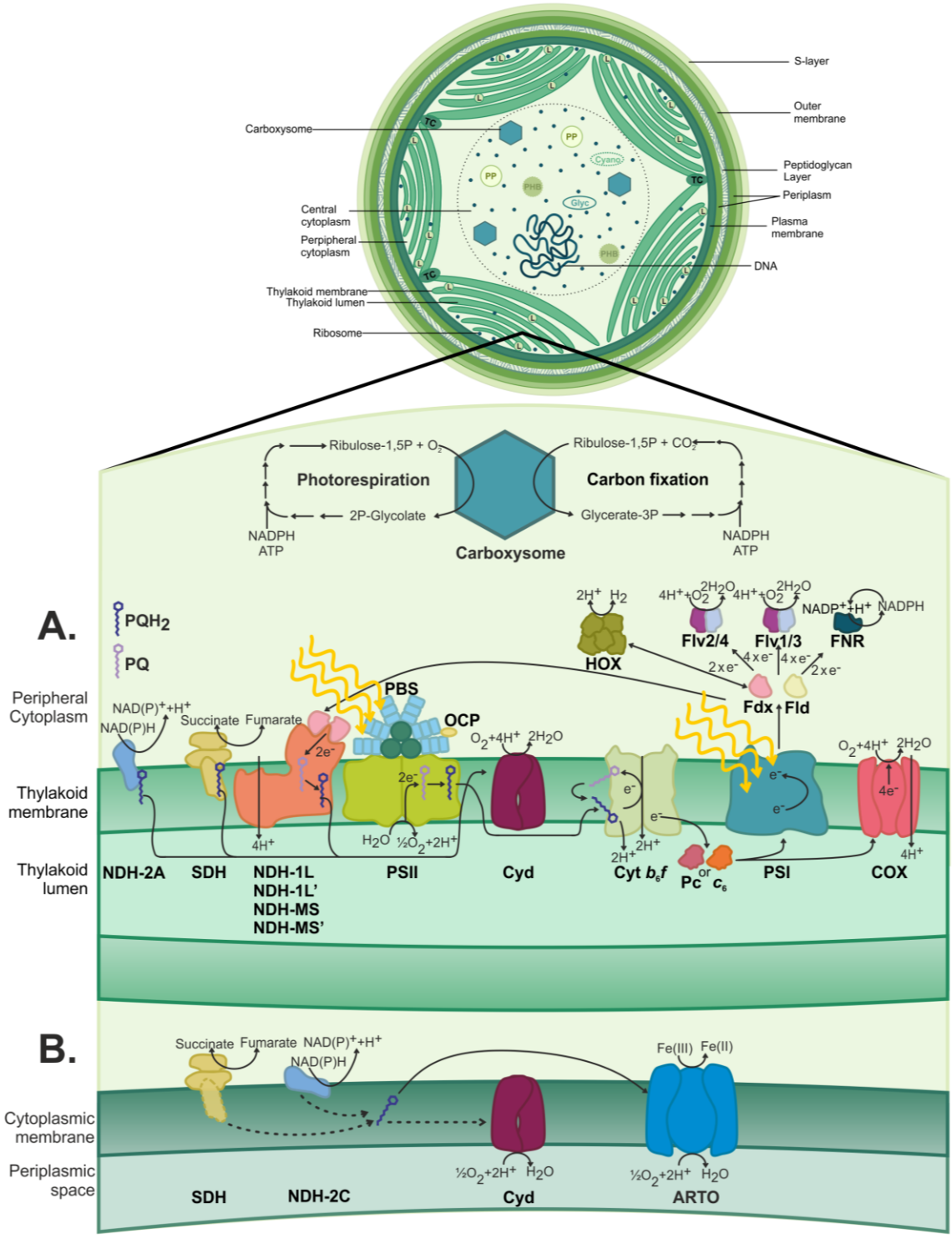

Figure 1.2 Schematic diagram of the (A) photosynthetic and (B) respiratory electron transfer chains in cyanobacteria. NDH-2A, NAD(P)H dehydrogenase; SDH, succinate dehydrogenase; NDH-1-, NAD(P)H dehydrogenase; PQ, plastoquinone; PQH_2, plastoquinol; PSII, photosystem II; PBS, phycobilisome; OCP, orange carotenoid protein; Cyd, cytochrome bd-quinol oxidase; ARTO, alternative plastoquinone oxidase; cyt b_6f, cytochrome b_6f; c_6, cytochrome c_6; Pc, plastocyanin; PSI, photosystem I; Fdx, ferredoxin; Fld, flavodoxin, COX, cytochrome oxidase; HOX, hydrogenase; Flv1/3, flavodiiron 1/3; Flv2/4, flavodiiron 2/4; FNR, ferredoxin-$NADP^+$ reductase; NDH-2C, NAD(P)H dehydrogenase.

Many cyanobacteria harvest light via large protein complexes called phycobilisomes (PBSs). PBSs consist of phycobiliproteins and can associate with PSII or PSI. Phycobiliproteins absorb light at different wavelengths from the chlorophyll and carotenoid pigments found in photosystems. PBSs are considerably larger than photosystems. This vastly increases the spectral range and amount of light harvested by cyanobacteria (20).

In the absence of light, cyanobacteria can switch to generating energy via respiration. The thylakoid membrane contains both the photosynthetic and respiratory electron transport chains. The cytoplasmic membrane contains a separate electron transport chain solely which may have multiple roles in the cell. In the thylakoid membrane there are three complexes, succinate dehydrogenase (SDH), NAD(P)H dehydrogenase-like complex I (NDH-1) and NAD(P)H dehydrogenase-like complex 2A (NDH-2A), which can donate electrons to PQ (21–23). Following the reduction of PQ, electrons are transferred to cytochrome *bd*-quinol oxidase (Cyd), or to cyt b_6f, then Pc/cyt c_6 before terminating at the cytochrome *c* oxidase (COX) (23,24). In the cytoplasmic membrane, PQ is reduced by the NAD(P)H dehydrogenase (NDH-2C. It is believed that SDH may also play a role in the cytoplasmic membrane, however this is yet to be confirmed. Additional protein complexes, flavodiiron 1/3 and 2/4, and a bi-directional hydrogenase, also act as electron acceptors from Fd (25,26).

1.1.3 Genetic engineering of model and non-model cyanobacteria

Cyanobacterial research has focused primarily on model organisms that are straightforward to culture under laboratory conditions, amenable to genetic modification and can be frozen for long-term storage (27–30). The uptake of more recalcitrant, non-model species for laboratory research can present significant challenges. Some of the basic features that are desirable for culturing and engineering cyanobacteria are: 1. Capacity to grow on agar plates and generate isolated colonies; 2. Amenability to heterologous DNA uptake, either naturally using native DNA import systems (31,32), or via conjugation (i.e., tri- or bi-parental mating), or electroporation; 3. Sensitivity to antibiotics for selection following DNA uptake (33); 4. Lack of native endonucleases that digest heterologous DNA. If present, the efficiency of DNA uptake can be improved by selecting for strains where endonucleases have been inactivated (32). Otherwise specific methylases, restriction inhibitors and liposomes could be employed during delivery (34–37); 5. Ability to take up broad-host-range self-replicating plasmids (e.g., RSF1010-based) for heterologous gene expression; 6. Capacity for genomic integration via allelic exchange (e.g., homologous recombination to facilitate the generation of gene knockouts or genomic integration of gene expression cassettes). Ideally,

species will be amenable to the generation of unmarked mutants, which is important for industrial applications. Unmarked mutants can be generated using negative selection markers (e.g., *sacB*) (20,38) or by CRISPR/Cas (39).

In this thesis, several model, known "non-model" and new organisms used in cyanobacterial research are discussed, A summary table (Table 1.1) gives an overview of genetic manipulation in a range of cyanobacterial species with wider applications to the field.

1.1.4 *Synechocystis* sp. PCC 6803

PCC 6803 is the most widely studied cyanobacterium and an ideal model organism for biotechnology. PCC 6803 is commonly used in laboratories due to its ability to naturally take up exogenous DNA, which facilitates genetic manipulation (40). It is also the most amenable species to generate unmarked mutants (40,41). Generation of unmarked mutants involves introducing chromosomal alterations into a strain via insertion of an antibiotic resistance cassette into the genomic site of interest, followed by subsequent removal of this cassette using a negative selectable marker. It is a particularly powerful technique as unmarked mutants can be genetically manipulated repeatedly, allowing as many alterations to be introduced into a strain as desirable. The PCC 6803 genome has low operon abundance and most genes are organised as single transcriptional genes. Therefore any polar effects on generating knockouts are likely to be minimal for most genes (42). PCC 6803 also has the capacity for photoautotrophic, mixotrophic, and heterotrophic growth (43). It grows rapidly under high light intensities when carbon saturated, and tolerates a wide range of temperatures (42,44), salinity and high pH (>10) conditions

Table 1.1 Summary of genetic manipulations carried out in some model and non-model cyanobacterial species.

Species	Strain	Transformation Method	Reported Selection/Counter SelectionMarkers	Agar Medium	References
Synechococcus sp.	UTEX 2973	Conjugation CRISPR/Cas *pilN* mutants are naturally transformable	Apramycin Chloramphenicol Kanamycin Spectinomycin Streptomycin	BG-11	(31,42,45,46)
	PCC 7002	Naturally transformable	Kanamycin Gentamycin	A+	(47,48)
	PCC 11801	Naturally transformable	Spectinomycin	BG-11	(49)
	PCC 11802	Naturally transformable	Spectinomycin	BG-11	(50)
	PCC 11901	Naturally transformable	Acrylic acid Spectinomycin	AD7	(51)
Nostoc punctiforme	ATCC 29133	Conjugation	Chloramphenicol Neomycin *sacB* markers Streptomycin	Allen and Arnon	(52–54)
Cyanothece sp.	PCC 7822	Electroporation	Spectinomycin	BG-11	(55)
	ATCC 51142	Conjugation	Kanamycin	BG-11 ASP2	(56)
Arthrospira platensis	C1	Electroporation	Spectinomycin	Zarrouk	(37)

Leptolyngbya sp.	BL0902	Conjugation	Chloramphenicol Erythromycin Neomycin Spectinomycin Streptomycin	BG-11	(57,58)
Fremyella diplosiphon	SF33	Conjugation	Kanamycin Neomycin *sacB* markers	BG-11/HEPES	(59–61)
Marine *Synechococcus* sp.	WH7803 WH8102 WH8103	Conjugation Electroporation	Kanamycin	SN	(62–64)
Marine *Prochlorococcus* sp.		-	Spectinomycin	Pro99	(62,65)
Thermosynechococcus elongatus	BP-1	Naturally transformable	Chloramphenicol Kanamycin	BG-11	(66)
	PKUAC-SCTE542	Naturally transformable	Spectinomycn	BG-11	(67)
Chlorogloeopsis fritschii	PCC 6912	Biolistic Conjugation	Kanamycin Neomycin	Allen and Arnon	(54,68)
Fischerella muscicola	PCC 7414	Biolistic Conjugation	Kanamycin Neomycin	Allen and Arnon	(54,68)
Chroococcidiopsis thermalis		Conjugation	Neomycin	BG-11	(69)
Gloeobacter violaceus	PCC 7421	Conjugation	Streptomycin	BG-11	(70)

1.2 Industrial applications and challenges of cyanobacterial biotechnology

1.2.1 Current industrial products derived from cyanobacteria

Cyanobacteria are important biotechnology platforms due to their ability to convert solar light and CO_2 into valuable industrial and pharmaceutical commodities (71,72) (Figure 1.3). They are also a source of nutraceuticals, while certain species can be used as a highly nutritious food source (73,74). Many species produce secondary metabolites with anticancer (74); antibacterial (75); antiviral (76); antiprotozoal (77); antioxidant (78) and anti-inflammatory properties (79).

Thus far, the most lucrative use of cyanobacteria in industry has been in the production of dyes and food colouring. Chlorophyll, phycobiliproteins and carotenoids have commercial value as natural colouring agents, nutraceuticals, dyes within the cosmetic industry and as compounds for biomedical research due to their fluorescent properties (80–82). The agricultural industry is also aiming to use cyanobacteria as potential biofertilizers or biostimulants for increased plant growth and development. Specific applications include: provision of fixed nitrogen via heterocyst-forming cyanobacteria, e.g. *Anabaena* spp.; secreting plant growth promoting hormones, e.g. inodole-3-acetic acid, gibberellins and cytokinins (83–85); secreting plant growth promoting vitamins such as cobalamin, folic acid, nicotinic acid and pantothenic acid (86,87).

1.2.2 Industrial companies utilising cyanobacteria as a biotechnology platform

Several companies have formed over the last few years with the purpose of using cyanobacteria and eukaryotic algae species for industrial purposes. Algenol Biofuels Inc. have filed several patent applications for using specific cyanobacterial strains for the bioproduction of ethanol (88–90), 1,2-propanediol (91), 1,3-propanediol (92), isoprene (93), heme-containing proteins (94) and mycosporine-like amino acids (95), as well as methods for the extraction of phycocyanin (96). The biomaterials company Living Ink Technologies LLC use a plurality of cyanobacteria, including PCC 6803, *Synechococcus* sp. PCC 7002 and *Arthrospira* spp., to create a bio-based and renewable coloured pigment, carbon black, to replace the petroleum-derived product used in printing ink (97–99). Recently the large sportwear shop, Nike, have collaborated with Living Ink to create a range of graphic T-shirts using the carbon black ink (100).

In 2008, the confectionery companies Nestlé and Mars replaced the controversial synthetic, petroleum-derived blue food colouring Brilliant Blue FCF in their products used to make blue Smarties with the natural blue colourant, phycocyanin (101). In 2019, the Japanese chemical company, DIC Corporation (DIC), marketed the *Linablue® G1* colourant from *Arthrospira plantensis*, which has received approval from the FDA as a food colourant, and, under the COSMetic Organic and Natural Standard, for use within the cosmetics industry (102). DIC successfully cultivates approximately 1,000 tons of *Arthrospira* spp. annually in large raceway ponds in China and the USA (103).

ScotBio, a UK-based business, also produces blue pigments for cosmetics, food and dyes by growing *Arthrospira* spp. in indoor bioreactors instead of raceway ponds. ScotBio successfully grows *A. plantensis* under a specific wavelength of LED light, which causes *A. plantensis* to overproduce phycocyanin (104). This has resulted in an increase in production of phycocyanin by 4-fold over the last two years (105). Additional by-products of the extraction process, such as vegan protein and carotenoids, are also valuable commodities available for resale (105).

Arthrospira spp. are also being used within the pharmaceutical sector for the development and manufacturing of therapeutics. Lumen Bioscience have exploited the ability of *Arthropsira* to produce high amounts of soluble protein and generated strains capable of producing therapeutic molecules, for example antibodies (106). The biomass is dried to form a powder of cells which is then packaged into dose-specific capsules. The cells are unable to survive the drying process, however the cell membrane protects the therapeutic drug which can then be orally delivered and released into the small intestine. This system aims to lower the cost of existing, difficult to procure drugs. At present, Lumen Biosciences have five product candidates that are under clinical trials for a range of conditions: *Clostridioides difficile* colitis; SARS-CoV-2; Crohn's disease and ulcerative colitis; Cardiometabolic Disease; Traveller's diarrhoea caused by *Campylobacter jejuni* and *Escherichia coli*. At present, projects for *C. difficile* colitis and Traveller's Diarrhoea are under Phase I and Phase II of clinical trials in the US, respectively (107–110).

Despite the large industry drive to use *Arthrospira* for the production of valuable compounds, the species is highly resistant to genetic modification due to an abundance of native restriction–modification systems that can rapidly degrade heterologous DNA (111). The most efficient transformation system reported to date has been the discovery that *Arthrospira* spp. possess the ability of natural competency for transformation when co-cultured with companion

microorganisms, specifically *Microcella* and *Sphingomonas* species (106). Transformed *Arthrospira* cells were reportedly stable for >3 years. The main issue, along with the new technology only being replicated by one group, is the lengthy process of mutant generation, with full segregation taking 8 – 10 weeks (106).

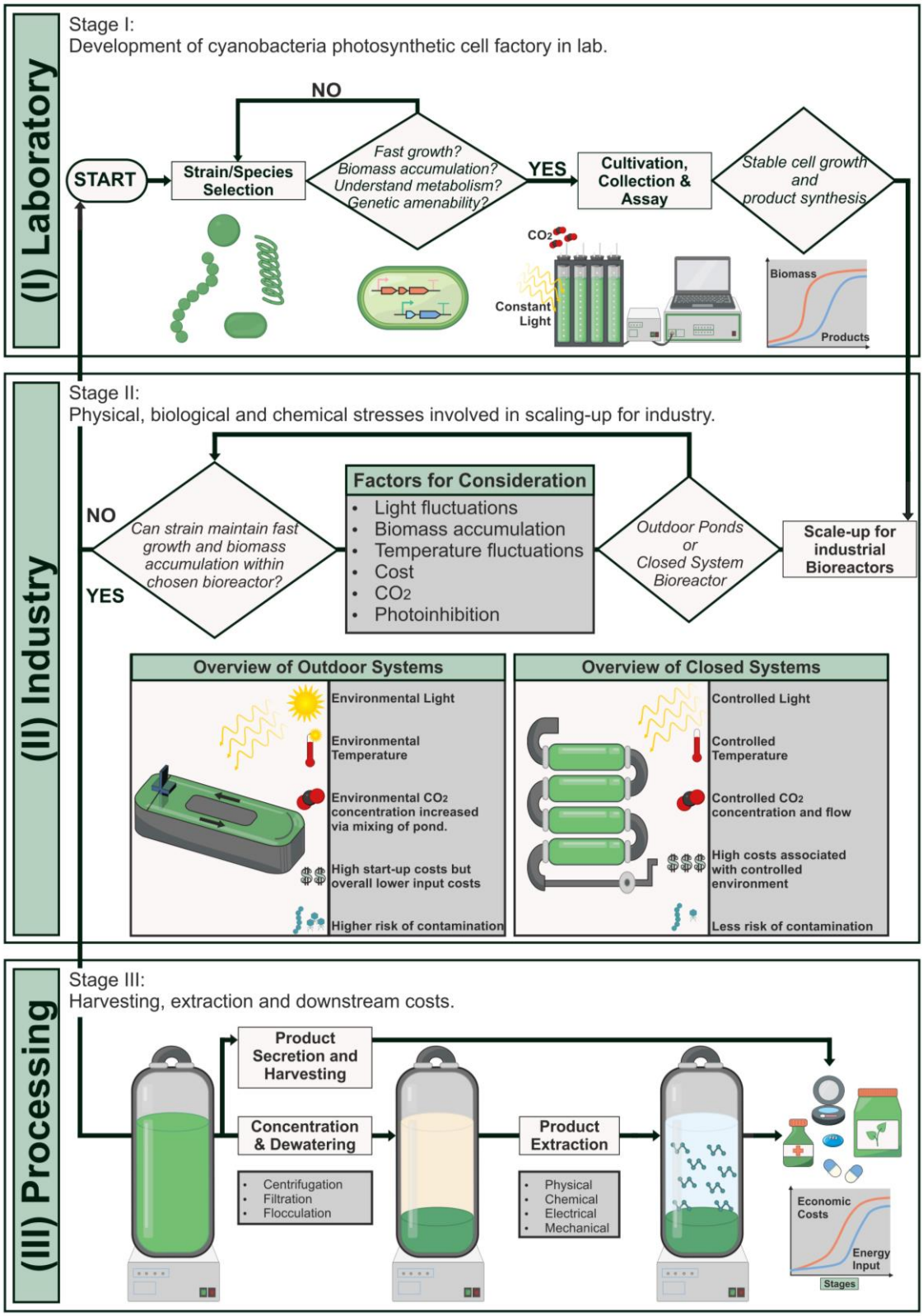

Figure 1.3 Overview of the scaling-up process required when using cyanobacteria as photosynthetic biomanufacturing chassis. (I) Laboratory: Lab-scale construction and evaluation of cyanobacterial cell factories. (II) Industry: Overview of outdoor ponds and closed system photobioreactors (PBRs) used in industry and their associated issues. (III) Processing: Overview of the downstream processing challenges associated with cyanobacterial photosynthetic biomanufacturing with the increased energy and cost required for biomass harvesting and product recoveries.

1.2.3 Advantages of using cyanobacteria in industry

1.2.3.1 Efficient solar capture

Cyanobacteria have multiple characteristics favourable for green technology. They offer distinctive advantages over both plants and most algae as a biotechnology platform due to their efficiency at solar energy capture. Cyanobacteria are able to convert as much as 9% of solar energy into biomass compared to only 0.5-3% seen in higher plants (112–114). This equates to faster growth compared to plants and therefore a higher yield per hectare (115,116).

1.2.3.2 Reduced nutrient requirements compared to other industrial microbes

Unlike many plant species, cyanobacteria can be cultivated on arid or otherwise unfarmable land in large-scale photobioreactors (PBRs) or raceway ponds. Cultures only require sunlight, mixing, a source of inorganic carbon, freshwater or seawater depending on the species, nitrogen, phosphorus and a few mineral nutrients. To further minimise nutrient feedstocks, it has been demonstrated that certain species can be grown in reactors using seawater or waste water (117–120). Another benefit to using cyanobacteria over alternative heterotrophic microorganisms, such as *Saccharomyces cerevisiae* and *E. coli*, is that cyanobacterial cultures require no carbohydrate feedstock, typically derived from an agricultural source. Growing crops as feedstocks for microbial cultures utilises land and resources which could be better used for food production or restored to natural environments. It also requires transport of the high volume feedstock from the farm to the reactor, adding to costs and energy use (121,122).

1.2.3.3 Genetic amenability

Mutant generation is a key tool in bacterial research and for altering species for biotechnology applications. Individual research laboratories currently generate mutants of interest via a variety of different experimental methods, using a range of plasmid systems in sub-strains that can vary significantly at both the phenotypic and genotypic level (e.g., in PCC 6803 (16,123,124)). There are many well-developed genetic techniques for cyanobacteria, with the most advanced being a new standardised genetic toolset, CyanoGate, based on the Plant Golden Gate Modular Cloning (MoClo) kit (42). The MoClo system makes use of plasmid vector assembly standards, along with a library consisting of parts, and allows for rapid construction of plasmids. This system enables marked/unmarked knockouts to be generated, as well as the integration of multi-gene expression and repression systems using a range of different promoters and terminators. As part of this

modular system, a new level of acceptor vectors were designed to enable integrative (i.e. chromosomal manipulation) or replicative (plasmid gene expression) transformation.

Similar to other industrially and scientifically important species, such as *Arabidopsis thaliana* (125), *Chlamydomonas reinhardtii* (126), *E. coli* (127) and *S. cerevisiae* (128), a mutant library for PCC 6803 is being created to aid and standardise cyanobacterial research. This resource, termed CyanoSource, generates plasmids and mutants using the CyanoGate system (42). The aim is to target all 3,456 genes in PCC 6803. The construction of mutant libraries is a consistent and efficient method for the study of protein regulation and function. The existence of such a library will accelerate the pace of research, avoid unnecessary replication between research groups and help improve experimental design. Targeted mutant libraries also provide knowledge on the essential gene set required for survival, further avoiding wasteful laboratory replication (129). In addition, many research groups, particularly in developing countries, lack the resources to generate cyanobacterial mutants (130).

1.2.4 Disadvantages of using cyanobacteria in industry

Despite the many advantages of using cyanobacteria as an industrial phototroph, as well as the successful businesses mentioned in Section 1.2.1, the application of cyanobacteria compared to heterotrophs in industry is not at similar scale. Although cultivation of cyanobacteria, specifically *Arthrospira* spp., can be dated as far back as the Aztecs in the 16th century, scientific research into the biotechnology applications of these organisms only started in the late 1960s and is still a relatively small area of research. Because of this, the genetic and metabolic networks of cyanobacteria are not as well understood as commonly used heterotrophs. Despite PCC 6803 being the fourth organism in history to have its genome sequenced (131), only ~30% of the genome has been characterised. Of these coding sequences, only a small proportion have been characterised in cyanobacteria, the remainder assigned function via homology with characterised genes in heterotrophic bacteria such as *E. coli.*

1.2.4.1 Limitations with current bioreactor designs

The biological advantages of cyanobacteria have contributed to their success at colonising the planet. However, these properties are not always ideal for growing dense cultures in PBRs and raceway ponds required for industry (132). Under such industrial conditions, cells at the surface-level receive saturating light causing them to absorb more photons than can be

utilised. The light intensity may also cause photoinhibition to the surface-level cells which will have a detrimental effect on the photosynthetic rate, as well as causing the production of reactive oxygen species (ROS) which can affect the whole culture, no matter the depth. There is a narrow window for optimum depth, where maximum photosynthesis is achieved, and below this at interior depths, the light energy is insufficient for optimal photosynthesis.

In closed-system bioreactors, the essential inorganic carbon source required for phototrophic growth is acquired by sparging a CO_2 enriched gas through the medium. By sparging cultures with CO_2, this significantly promotes the gas-liquid mixing of the suspension and therefore enhances light acquisition, as well as CO_2 and nutrient utilisation by individual cells (133). Although CO_2 is an additional cost to the overall system, work is being carried out to investigate the potential for bioremediation using CO_2 from emitting power stations, refineries and factories (134–138). Mixing of cultures, by CO_2 sparging or alternative methods such as mechanical agitation, can also help prevent sedimentation, facilitate heat transfer and ensures uniform exposure to nutrients, as well as light (133). It is important to note however, that not all cyanobacteria can tolerate vigorous mixing, such as the filamentous species *Aphanizomenon flos-aquae* and *A. platensis,* due to the hydrodynamic stress caused (139,140). This is an important factor when determining the potential of newly discovered species for biotechnology. It is also important to note that cyanobacteria are more resistant to shear stress compared to microalgae such as haptophytes, diatoms and dinoflagellates thanks to their rigid Gram-negative cell walls (Section 1.1.1) (140).

1.2.4.2 Cyanobacterial biomass production

A major issue facing cyanobacterial biotechnology is the limitations associated with the relatively low biomass accumulation and slow growth rates compared to well-established industrial heterotrophs. Under existing industrial practices, growth of cyanobacterial cells in large scale PBR systems results in lower productivity than predicted from *in silico* laboratory experiments (141). Certain traits are now known to inhibit biomass accumulation, such as PBR design (141,142), photoinhibition (143), shear stress (140) and biocontamination (144). To overcome some of these challenges it is important to identify species and/or strains with fast growth rates and biomass accumulation, that grow under a range of light intensities, temperatures, salinity, and that are genetically amenable.

1.2.4.3 Biocontamination of cultures

Stable and reliable production of biomass is required by industry for projects to be economically feasible. One of the most economically feasible ways of cultivating cyanobacteria is to use, or partially use, wastewater, especially nitrogen and phosphorus rich effluent, or seawater as the base for growth medium. Over 95% of commercial algae cultivation use open systems, such as raceway or open ponds, under non-sterilised conditions (145). While cheaper and easier to run, these systems can be rapidly contaminated with non-desirable organisms, especially species adapted to the local environment. Biocontaminants can lead to delayed, lower or even completely decimated biomass accumulation and therefore production of the bioproduct (146). To reduce contaminants, closed system PBRs reduce the contact time the culture has with the external environment. However, CO_2 must then be efficiently sparged through the culture, and although usually this air is filtered via a microporous membrane, maintaining an axenic culture over long periods is likely to be challenging. Regardless of whether PBRs or raceway and open ponds are used, if cultures become overwhelmed with contaminants, production may need to stop in order for PBRs to ne adequately sterilised before reinoculation of cyanobacterial cultures. This is costly and time consuming from an industrial standpoint. In conclusion, biological pollutants will inevitably infect cultures by water or gas during the mass cultivation of cyanobacteria and so alternative approaches of control must be looked at.

A potential method to reduce contamination is to grow cultures under extreme pH conditions. Zhu *et al.* demonstrated that increasing pH to approximately 11 via the addition of sodium bicarbonate led to a reduction of the common contaminant, *Pannonibacter phragemitetus,* which under lower pH conditions (pH ~8), would outcompete the cyanobacteria culture and consume the ethanol produced from the recombinant, ethanol-synthesising strain of PCC 6803. High pH conditions have been successfully used in open pond production, but are limited to a few species, such as *Synechocystis* or the halophilic algae species, *Dunaliella* (147). *Arthrospira* spp. optimal pH range is pH 9 – 10.5 (148) which also reduces the contamination potential in these cultures (149). The ability to grow at extreme pH ranges is an important factor to consider when looking at potential strains for biotechnology (146). It has also been shown that manipulating the pH of a suspension can aid flocculation of the culture (150). However, the addition of CO_2, particularly at high concentrations, can lead to an accumulation of inorganic carbon and overall reduction of the pH in the medium. This can be overcome by recycling the medium in a semi-continuous culture, as has been performed for *A. plantensis* over 18 days (151).

Monocultures have been the preferred route for a long time within the bioindustry, however, recent work within the field has shown the promising idea of co-cultivation. Co-cultivation, or co-culture, makes use of microbial communities, similar to those found in natural conditions. Controlled symbiotic co-cultures have been shown to minimise or completely eliminate contamination issues within industrial cultures (152–154). Co-cultivation systems have also shown to improve yields of biomass, lipids (155) and high-value products (156). Eukaryotic algae and cyanobacteria have been noted as good candidates for growth in co-cultures, and work has been carried out in wastewater treatment and anaerobic digestion. Research into algal co-culture has shown antibiotic compounds produced by the symbiont *Phaeobacter inhibens* has a mutualistic effect on the health of co-culture containing the coccolithophore, *Emiliana huxleyi* (157). Little work has been carried out from a large-scale, biomanufacturing perspective, however, a detailed case study has been published by Padmaperuma *et al.* (158). This method has the potential to work well in reducing contamination seen in open ponds systems, as well as aiding closed system bioreactors.

Competition from other phototrophs can be a major issue in cultures as they directly compete for light, nutrients and CO_2. Species able to sustain fast growth in dense cultures will be particularly useful for industrial applications, due to their ability to outcompete slower growing phototrophs. Cell size and morphology can also play an important role in protection against grazing contaminants. It has been documented that larger or filamentous cyanobacteria have significant advantages in resisting predation (159–161). All these factors should be considered when choosing a cyanobacterial chassis.

1.2.4.4 Harvesting cyanobacterial biomass

Cyanobacteria can range in size from 0.6 µm in diameter, for some *Prochlorococcus* species, to filaments of cells up to millimetres in length (162). Due to these small size ranges plus the water-equal densities of cyanobacterial cells, this can make it difficult to separate biomass from liquid medium, especially at large industrial-scale volumes. Centrifugation and filtration techniques rely on energy demanding equipment. This can add to the overall cost and carbon footprint..

A review by Beattie *et al.* concluded that harvesting cellular biomass for product extraction is one of the most costly processes in industrial biotechnology, utilising the second largest share of the economic burden within a biorefinery, second only to combustion of fuel. This is largely due to the high operational costs and electricity consumption, mainly heating delivered by natural gas, of the harvesting module (163). Morphology and size of cells can play an important role against predation,

but these properties also have importance in biomass recovery. Cells with larger sizes and/or that are filamentous in shape are significantly easier to harvest via filtration or sedimentation approaches. Particular species, such as *Arthrospira* sp., possess these desirable characteristics (164), but smaller, single celled species may require genetic engineering approaches to manipulate morphology. Work has been carried out to increase cell shape, size and morphology in a number of cyanobacteria. Jordan *et al.* were able to increase the size of *Synechococcus elongatus* PCC 7942 (PCC 7942) by regulating the Min system allowing for controlled cell extension (165). Hu *et al.* showed that inactivation of MreB, an actin-like protein, increased the cell size of *Anabaena* sp. PCC 7120 by ~100% (166). Similar results were seen in *Fremylla diplosiphon* when the regulation of *mreB* was disrupted and filament length increased by 5-fold (167). Although, these mutants were able to produce cell shape morphology that allows for better and easier harvesting of biomass, potential negative downstream effects must not be ruled out and further testing to check levels of the final product is required.

Cellular surface also plays a role in aiding biomass harvesting of cells. Flocculation is a widely used strategy within the field of microbial biotechnology. This strategy uses the addition of chemicals to induce aggregation of cellular cultures, henceforth easing the filtration or sedimentation methods used for harvesting biomass. Common additives include alum, lime, cellulose, salts, polyacrylamide polymers, surfactants and chitosan (147,168–170). The addition of phytic acid increased the flocculation efficiency seen in *A. plantensis* cultures by ~95% (171). Alternatives to chemical additives include manipulating the pH of the suspension (150) or co-culturing with another organism to induce aggregation, known as bioflocculation (172). Flocculation efficacy can be influenced by a variety of physical biological factors of species, including cell size, shape, surface charge and exopolymeric substances.

1.2.4.5 Extraction of products

For successful industrial application, the accrued biomass is expected to be easily harvested and lysed for product extraction. However, some products are known to be naturally secreted out of cells via native transporters or diffusion, which is more desirable for industrial applications. This includes organic acids (e.g. lactate (173), succinic acid (174)), some sugars (e.g. glycerol (175)) and alcohols (ethanol (176), propanol and butanol (177)). However, a large range of products cannot be naturally secreted or transported out of the cell for a variety of reasons including: the existence of hydrophobic cellular envelope barriers; lack of native export transporters; size limitations of the target product, with larger molecules typically accumulating within cells. With such products, cell

disruption by physical, chemical, or electrical means is required. This can add to the overall expense of the procedure, as well as increase the environmental impact if chemicals or energy inputs are required for cell disruption.

Several mechanisms have been developed to overcome these issues. Controlled autolysis via the introduction of bacteriophage genes to lyse cells under the control of a nickel-inducible promoter demonstrated by Liu and Curtis in 2009 (178). To avoid the introduction of toxic nickel into the environment, as well as the negative associated costs, it was later demonstrated that the introduction of a promoter activated under CO_2 limiting conditions could also be used to induce cell disruption and promote harvesting of fatty acids (179,180). Liu and Curtis reported that by using their described 'thermo-recovery' strategy they were able to increase yield and efficiency as well as reducing the overall costs of production by 80% on a laboratory scale. However, this system would only be feasible for closed system bioreactors where the CO_2 level can be controlled and may be challenging to implement in large scale cultures.

Another strategy is to introduce targeted and controlled expression of transporter proteins. However, this can be challenging in cyanobacteria due to our lack of knowledge on how proteins are targeted to the plasma membrane and ensuring correct orientation of the protein within the membrane to enable export of the compound (181). For a detailed review on all engineered transporters attempted in cyanobacteria see Sengupta *et al.* (182). A detailed description of the native transporters, and their cellular location, found in PCC 6803 is described in more detail in Chapter 2. For information regarding localisation of specific transporter proteins in PCC 6803, the work by Baers *et al*. (183) and Liberton *et al*. (184) should be consulted. For this to be considered an option, species would need to be amenable to genetic manipulation.

Finally, a third proposal has been suggested by Liu *et al.* involving the deletion of a peptidoglycan assembly protein, thereby weakening the cell wall and improving free fatty acid secretion (185). It has been demonstrated that weakening the cell wall could potentially have benefits against predation by amoebas (186). However, the strong peptidoglycan layer has also been suggested as protection against shear stress within a PBR environment, and further work would need to be carried out to ensure that potential negative effects would not outweigh the prospective benefits from peptidoglycan synthesis modification.

1.3 The discovery of fast-growing and stress-tolerant *Synechococcus* strains

Cyanobacterial strains that can achieve growth rates comparable with heterotrophic microbes, as well as high biomass accumulation, could be of significant value to basic research and the biotechnology industry. *Synechococcus* sp. PCC 7002 (PCC 7002) has long been reported as the fastest growing cyanobacterium. However, four new *Synechococcus* strains have recently been reported with similarly high growth rates: *Synechococcus elongatus* UTEX 2973 (UTEX 2973), *Synechococcus elongatus* PCC 11801 (PCC 11801), *Synechococcus elongatus* PCC 11802 (PCC 11802) and *Synechococcus* sp. PCC 11901 (PCC 11901).

1.3.1 *Synechococcus* sp. PCC 7002

PCC 7002 is a facultative unicellular marine organism first isolated in 1961. It requires vitamin B_{12} for growth which increases cost for large-sale cultivation. PCC 7002 can tolerate high light intensities and has been reported to have higher growth rates compared to other marine cyanobacteria (187).The fastest reported doubling time for PCC 7002 is 2.27 hours under the growth conditions, 38°C, 1% CO_2 and 500 µmol photons m^{-2} s^{-1} (51).

One of the main issues with using PCC 7002 as an industrial species has been the lack of counter-selection methods to generate unmarked mutants. The current system used to generate unmarked mutants in cyanobacteria relies on the use of SacB as a negative selection marker when cells are grown on plates containing sucrose (20). However, this method is ineffective in PCC 7002 as cells expressing SacB are able to grow successfully on sucrose-containing plates (40). Alternative negative selection markers including *acsA*, which confers acrylate sensitivity, have been attempted (188). However, this method has not been used by other groups, possibly due to the safety risks associated with the use of acrylate or the requirement to delete the native *acsA* gene via insertion of an antibiotic resistance cassette prior to further modifications (188). The latter issue is highly undesirable for commercial applications. Recently, a new method has been described which exploits the polyploidy nature of cyanobacterial chromosomes by using the Cre-lox recombinase system (47). This method integrates an antibiotic resistance cassette (flanked by lox66 and lox71 recombinase sites) into the chromosomal target site to generate a marked knockout. A second plasmid encoding the Cre recombinase is then integrated into the essential *rbcLXS* locus using a second antibiotic resistance cassette. Cre is then expressed which excises the antibiotic resistance cassette flanked by the lox sites, resulting in an unmarked mutant, although parts of the lox sites

still remain. The final step involves growing the unmarked mutant strain in the absence of the second antibiotic. This results in the gene encoding the Cre recombinase being removed from the chromosomal population. While this method does not result in production of scarless unmarked mutants, strains can be repeatedly genetically manipulated.

1.3.2 *Synechococcus elongatus* UTEX 2973

UTEX 2973 was first described in 2015 as a fast-growing, stress-tolerant strain under high light (>500 µmol photons m^{-2} s^{-1}) and temperature (38 – 42°C). It was reported that UTEX 2973 can achieve doubling times similar to that of *S. cerevisiae* (ca. 2 h). UTEX 2973 is not naturally competent, however mutant strains have been engineered to confer natural transformability by substituting *pilN* and *rpaA* alleles from PCC 7942 (189). The wild-type UTEX 2973 is naturally amenable to conjugation and genome editing by CRISPR/Cas (45,46). The shortest doubling time has been reported as 1.5 hrs in BG11 medium at 42°C under continuous light of 1,500 µmol photons m^{-2} s^{-1} and sparged with 5% CO_2/air. However, at lower temperatures and light intensities this fast growth trait has not been observed (42). Therefore, this species may not be suitable for most biotechnology applications as species cultured in outdoor PBRs will be exposed to a wide range of temperatures and light intensities.

In these initial experiments analysing UTEX 2973, growth was only measured for 12-30 hours without allowing cells to surpass an OD_{730nm}= ~1 (45,190,191). For biotechnology applications, fast growth of the strain needs to be maintained over a longer time period so sufficient biomass and a high cell density is obtained. It is also important to study growth over a similar period of time that is viable for industrial bioreactors to function (3 - 12 days (146,192)), as well as good scientific practice to determine when stationary phase, and therefore maximal growth, is obtained. Further issues with these studies is the particularly low staring OD_{730nm} of 0.025, seen in Ungerer *et al*. (191), when exposing cultures to a high light intensity of 900 µmol photons m^{-2} s^{-1}. Combining a high light intensity with a low cell concentration of cells may result in selection of mutants that can resist these conditions while inhibiting growth of less light tolerant species that may show improved growth in dense cultures and therefore be more suitable for biotechnology. This makes comparison of different species under these conditions less relevant when trying to identify the most suitable for large scale growth. Another issue from these studies was the high light intensity (500 – 900 µmol photons m^{-2} s^{-1} for liquid stocks; 125 µmol photons m^{-2} s^{-1} for agar plates) used for maintaining the strains. Again, this will select for high light tolerant strains that may not be ideal for high cell density growth. This rapid strain selection is a well-documented phenomenon within laboratory strains

(124). These concerns were reported in a response (193) to the original Ungerer *et al.* paper (191) and raises questions about the suitability of this strain for further biotechnology work.

1.3.3 *Synechococcus elongatus* PCC 11801 and PCC 11802

PCC 11801 was isolated from India and first described in 2018 (49). PCC 11801 is tolerant of high NaCl conditions (i.e. it can grow at sea salt concentrations) and is naturally transformable. The genome sequence of PCC 11801 is highly similar to PCC 7942 and UTEX 2973 (ca. 83%). Thus, existing plasmid vectors used for engineering PCC 7942 are widely compatible in PCC 11801. Similar to UTEX 2973, PCC 11801 is tolerant to high light and temperatures and exhibits fast growth rates (i.e., a doubling time of 2.3 h). However, fast growth has only been observed at lower CO_2 conditions (~1% CO_2), reducing the potential for bioremediation of CO_2 from industrial waste plants. Furthermore, growth of the species has only been measured for 10 hours and the biomass plateaus at ~1 mg DW/mL after 24 hours of growth (49).

PCC 11802 was also isolated from the same location in India as PCC 11801. First reported in 2020, this organism has a close phylogenetic relationship with PCC 11801 (~97% genome identity and ~97% average protein identity) but has distinctly different metabolic and genomic characteristics (50). Exponential growth rates are much higher compared to PCC 11801 under high light-low CO_2, low light-high CO_2 and high light-high CO_2 conditions. This strain is also naturally transformable, similar to PCC 11801. However, there are issues with this study, similar to those outlined for the UTEX 2973 work: growth conditions were never compared directly against other species; growth was only reported for ~16 hours at high light (1000 µmol photons m^{-2} s^{-1})/high CO_2 concentrations (1% CO_2); and biomass only reached ~2 mg DW/mL under optimal conditions for the species.

Metabolomic studies of the two strains suggest that PCC 11802 may be a good candidate for production of compounds primarily derived from intermediates of the Calvin-Benson-Bassham (CBB) cycle due to the increased production of CBB metabolites when CO_2 levels were raised from ambient (~0.04%) to 1% CO_2 (50). PCC 11801, on the other hand, might be a good candidate for production of compounds derived from substrates in the TCA cycle due to increased levels of associated metabolites observed (50). There has been further efforts to isolate and test a range of wild-type and well-established cyanobacterial promoters in both strains in an attempt to develop them as potential biotechnology chassis (194).

1.4 *Synechococcus* sp. PCC 11901

One of the fastest growing species reported to date is PCC 11901, which was isolated in Singapore from an estuarine environment enriched with nitrogen and phosphorus compounds (51). PCC 11901 is tolerant to high light levels, achieves fast growth rates comparable to UTEX 2973, and is tolerant to a wide range of salinities, similar to PCC 11801 and PCC 11802. PCC 11901 is naturally transformable with efficiencies similar to that of PCC 7002 (51,188). PCC 11901 demonstrates promising characteristics as a potential chassis for biotechnology. It has a doubling time of ~2 hours, which was achieved at 38°C under 660 µmol photons m^{-2} s^{-1}. High growth rates were seen at a range of high light intensities and a range of salinities. The most remarkable result is the large accumulation of cellular biomass, ~33 g DW/L. This was around 1.7 to 3 times more than other strains (UTEX 2973, PCC 7942, PCC 6803, PCC 7002) tested in this experiment (51).

Apart from this initial study, there has been no further work on PCC 11901 and our understanding of this organism is limited. Although the original paper was a thorough and in-depth analysis of this new species, there is still potential avenues to explore to determine whether this is a suitable species for industry before larger scale experiments are conducted. One such issue is the lack of a developed method for generating unmarked mutants, similar to that which is available for PCC 6803. This would be a major advantage for developing the strain for industrial applications. The growth rate of PCC 11901 has only been compared with the fast-growing UTEX 2973 at light intensities ranging from 100 - 660 µmol photons m^{-2} s^{-1}, and not in direct comparison with UTEX 2973's reported optimal growth conditions of 900 µmol photons m^{-2} s^{-1} at 38°C. It is therefore difficult to conclude which species may demonstrate the fastest growth and biomass accumulation under these conditions.

PCC 11901 is also a cobalamin auxotroph, similar to 7002, and a common trait seen in marine species due to the abundant availability of cobalamin (vitamin B_{12}) in seawater. To be grown at an industrial scale using artificial media rather than seawater, the strain would need to be cobalamin independent due to the expense of adding large amounts of vitamin B_{12}. Recently, it was reported that vitamin B_{12} independent strains were generated quickly and efficiently by driving the evolution of strains by growing cells on medium deficient in vitamin B_{12} (195). When growth rates were tested, strains independent of vitamin B_{12} requirements reached equivalent optical density of cultures as the wild-type strain after 120 hours. Interestingly, the wild-type control growing in medium without the addition of vitamin B_{12} was capable of entering log phase at ~72 hours, showing substantial growth with a similar exponential slope as the vitamin B_{12} independent strain

at this time point. It has been previously hypothesised that the loss of cobalamin-synthesis is a relatively recent evolutionary event due to the presence of the *metE* gene on one of the endogenous plasmids (51) but this species may also be able to rapidly mutate to adapt to differing environmental conditions.

1.5 Project aims

This study will focus on improving our understanding of PCC 11901, quantifying its growth and photosynthetic capacity against a range of model cyanobacteria, and the development of tools to generate unmarked knockouts. One major issue facing cyanobacterial research is the lack of knowledge regarding genetic and metabolic pathways. The first aim of this project is to further understand the biochemical pathways of the model organism *Synechocystis* sp. PCC 6803 (chapter 2). This will aid future work and computational modelling within the community, as well as being used as a reference marker for future species that are discovered.

Another main issue with cyanobacterial uptake in industry is the species that are currently used have slow growth rates and low biomass accumulation. In this chapter we have highlighted several issues with existing model and non-model strains, as well as mentioning strains with the potential as future industrial chassis. This thesis will also aim to confirm whether PCC 11901 can outcompete the growth rates seen by UTEX 2973 at the optimal conditions that have been reported for UTEX 2973, as well as suggesting potential metabolic and genetic reasons for this fast growth.

Once the suitability of PCC 11901 growth rates has been confirmed, the aim will be to demonstrate the potential for genetically manipulating PCC 11901, as well as suggesting the optimal growth conditions for biomass accumulation. The overall aim of this thesis is to comprehensively analyse and evaluate the suitability PCC 11901 as a candidate species for biotechnology.

Chapter 2

Characterisation of metabolism and transport in *Synechocystis* sp. PCC 6803 via comparative genomics with *Escherichia coli*

A published version of this chapter can be found in Biosciences Report 40 (4)

Current knowledge and recent advances in understanding metabolism of the model cyanobacterium Synechocystis sp. PCC 6803. LA Mills, AJ McCormick, DJ Lea-Smith. Bioscience reports 40 (4), BSR20193325

Chapter 2: Characterisation of metabolism and transport in *Synechocystis* sp. PCC 6803 via comparative genomics with *Escherichia coli*

2.1 Introduction

2.1.1 Current understanding of metabolism in *Synechocystis* sp. PCC 6803

Despite their importance, our understanding of many key features of cyanobacterial physiology and biochemistry is poor. For example, in *Synechocystis* sp. PCC 6803 (PCC 6803), less than 1200 coding sequences (~30%) have assigned function (469 in metabolism and 115 in transport: Highlighted in red in Appendix Table 2.1; ~558 in other cellular processes (including transposons and transposon related functions): Highlighted in red in Appendix Table 2.3), which is less than half compared with *E. coli* (196). Of these 1200 coding sequences, only a small proportion have been characterised in a cyanobacterium (197), with the majority of assigned functions based on studies of homologues in other bacteria, even though the function, catalytic activity and importance of characterised genes may differ significantly between phototrophic and heterotrophic bacteria. It is also likely that a proportion of these coding sequences have incorrectly assigned functions. Several examples of PCC 6803 genes that were experimentally validated as having functions different to the original assigned function, based on homology with genes from heterotrophic bacteria, are discussed throughout this chapter.

2.1.2 Chapter aims and objectives

The aim of this chapter was to perform a comprehensive analysis of metabolism and transport in cyanobacteria via a review of the literature and comparative genomics with *E. coli*. This chapter will focus on the model unicellular species PCC 6803 and to a lesser degree, PCC 7942.

Each results section will highlight recent findings pertaining to specific metabolic pathways, including central carbon and sugar metabolism, amino acid, nucleotide, cofactor and vitamin, lipid and membrane components, isoprenoid and pigment biosynthesis, and the transporters localized in the different membrane compartments.

In the interest of brevity, the majority of enzymatic steps will not be mentioned in the text but outlined in subsequent figures. Steps to which an enzyme from PCC 6803 has not been assigned are indicated by only an arrow with no abbreviated protein name in close proximity. The discussion will primarily focus on reactions that differ in cyanobacteria compared with model heterotrophs or have been specifically investigated in model cyanobacteria. In most cases, only the abbreviated protein name is included in the text, although full names are outlined in Appendix Table 2.1 (Column C).

This chapter will also describe a comprehensive bioinformatic analysis comparing the PCC 6803 predicted proteome to *E. coli* K12. This information has been incorporated into four tables, with the aim of helping to guide future work on identifying homologues and assigning putative protein function. Appendix Table 2.1 lists the PCC 6803 proteins for each metabolic process, in the order outlined in this chapter. Also shown are the *E. coli* K12 proteins demonstrating the highest sequence similarity to individual PCC 6803 proteins. Appendix Table 2.2 is in the opposite format and includes a list of *E. coli* K12 proteins with assigned functions, and the PCC 6803 proteins with the highest homology to each *E. coli* protein. Appendix Table 2.3 includes a list of PCC 6803 proteins potentially involved in processes other than metabolism and transport, while Appendix Table 2.4 includes all remaining PCC 6803 proteins that, at the time of analysis, have no assigned function. I will also highlight the aspects of cyanobacterial physiology and biochemistry that have yet to be elucidated.

2.2 Materials and Methods

2.2.1 CyanoBLAST: A new computational tool for cyanobacterial proteome comparison

Here, we describe an applied method of performing an all vs. all proteome comparison. The tool is used to compare the proteome of species against PCC 6803. The analysis incorporates the use of the National Centre for Biotechnology Information's (NCBI) Basic Local Alignment Search Tool (BLAST) (198). The heuristic algorithm is much faster than other approaches, such as calculating an optimal alignment using the Smith-Waterman algorithm (199). The emphasis on speed is vital to making the algorithm practical due to the huge proteome databases currently available and for enabling people to carry out analysis on personal computers rather than using expensive high-performance computing (HPC) resources. CyanoBLAST can be accessed via the GitHub repository: https://github.com/laurenmills300/CyanoBLAST

2.2.1.1 Initial modification of the input data for CyanoBLAST

2.2.1.1.1 Modifying the Baers *et al*. Table

Initially, we set out to compare the proteome of the well-documented model organism *E. coli* K12 against the well-documented cyanobacterial species, PCC 6803. The initial input data for PCC 6803's proteome was based upon the findings from Baers *et al.* (2019) (183). A modified version of Supplementary Table 3 (Appendix Table 2.5) from the Baers *et al*. paper was created and formed the starting point for all the input data required for PCC 6803's proteome information for the following algorithm. This table included the important information regarding PCC 6803's proteome, including localisation and the molecular weight of proteins.

First, Appendix Table 2.5 was edited in Microsoft Excel (Version 2110 Build 16.0.14527.20234), removing column K, titled *Marker Protein*, as this information was deemed irrelevant for the subsequent analysis. New columns inserted at the column B position contained the corresponding Uniprot ID (200). This was performed by searching the list of KEGG IDs using Uniprot's Retrieve/ID Mapping tool which can be found (www.uniprot.org/uploadlists/). To check that these had been converted correctly, a random sample of 50 KEGG IDs and the corresponding Uniprot IDs were taken and manually checked to ensure the correct conversion of IDs had taken place. For an outline of the columns and the corresponding data, see **Table 2.1**.

Table 2.1 Table showing the modified input from Appendix Table 2.5 with the column names and description of the corresponding data for each column.

Column Title	Column Name	Description
Column A	Accession	KEGG IDs taken from https://www.genome.jp/kegg/.
Column B	Uniprot Accession	Uniprot Accession taken from the Uniprot's Retrieve/ID Mapping tool (https://www.uniprot.org/uploadlists/).
Column C	Gene Product	Gene product associated with corresponding accession numbers.
Column D	Gene Name	The gene name as assigned by Baers *et al.* (2019) (183).
Column E	Gene Names in Literature	All corresponding gene names found in the literature
Column F	Functional Sub-Category	The functional sub-category of the gene as assigned by Baers *et al.* (2019) (183).
Column G	Functional Category	The functional category of the gene as assigned by Baers *et al.* (2019) (183).
Column H	Localisation	The localisation of the gene product as discovered by Baers *et al.* (2019) (183).
Column I	SVM Score	Support Vector Matrix Score which shows the percentage of confidence that the gene product is localised to the area as calculated by Baers *et al.* (2019) (183).
Column J	MW (kDa)	Molecular Weight of the gene product in kilo-Daltons
Column K	No. of TMH's	Number of transmembrane helical domains (TMHs) present

2.2.1.1.2 Modifying the second input tables

A second input file was taken from either Appendix Table 2.6, Appendix Table 2.7 or Appendix Table 2.8. These three tables are split into different classes of PCC 6803's proteome: central metabolism and transport; characterised proteins not involved in central metabolism; uncharacterised proteins. These tables were used to split the protein information from the Appendix Table 2.5 table into further sub-categories.

The second input table used for comparison depends on the desired output by the user. For example, Appendix Table 2.6 can be used to compare PCC 6803's central metabolism and transporter proteins, which are further categorised by the appropriate metabolic pathways; Appendix Table 2.7 allows for the comparison of PCC 6803's characterised proteins that are not involved in metabolism or transport; and Appendix Table 2.8 can be used for the comparison of PCC 6803's uncharacterised proteins against a proteome of any species.

For sake of brevity, further description of the methods will focus on using Appendix Table 2.6 which focuses on central metabolism for comparison against *E. coli* K12. The table was modified in Microsoft Excel to remove the information after column H in Appendix Table 2.6.

2.2.1.1.3 Manipulating the input data

Both tables modified from Section 2.2.1.1.1 and Section 2.2.1.1.2 were loaded into the PyCharm (2021.1.1 (Professional Edition)) environment using the Python programming language (v. 3.8.2) and converted to a specific dataframe type using the pandas module (201). The two dataframes were then converted to individual arrays using the NumPy module (202). The arrays were then concatenated together.

2.2.1.2 Creating a local BLAST database for *E. coli* K12

In order to run a local BLAST search from a personal computer, a BLAST database must first be created. The code outlined in this chapter uses *E. coli* K12 proteome for comparison against PCC 6803. To create the local database, the most recent proteome of *E. coli* K12 (NC_000913.3) was downloaded from the NCBI database in the format of a .faa FASTA file. The most recent NCBI BLAST+ software (v.2.11.0) was also downloaded from the NCBI website. The Python subprocess module was used to access the terminal and the `-makeblastdb` function via BLAST+. CyanoBLAST will automatically create a local database for any new organism of interest.

2.2.1.3 Using PCC 6803's proteome to BLAST against *E. coli* K12

Uniprot IDs taken from the input dataframe and the `bioservices` module was then used to search IDs against the Uniprot database to access the corresponding amino acid sequence. This amino acid sequence was then "BLASTed" against the local database, see Section 2.2.1.2, using the built-in subprocess function. Parameters for the BLAST search are given below:

```
blastp -outfmt 7 -query blasting.fa -db input files\E.coliK12.faa -evalue 1
```

The output format is automatically set to `-outfmt` 7, which displays the alignment as tabular with comments (203). The E-value is set to a maximum of 1, a liberal value to aid future downstream processing. Note that the `-evalue` option sets the significance threshold for reporting hits.

CyanoBLAST allows for this number to be changed by the user if a stricter significance threshold is required.

2.3 Results

2.3.1 Central metabolism

In this chapter, cyanobacterial central metabolism will include glycolysis/ gluconeogenesis, the tricarboxylic acid (TCA) cycle, the pentose phosphate (PP) pathway and the Calvin-Benson-Bassham (CBB) cycle, including carbon fixation, in addition to pathways for production of storage compounds, fermentation products and chorismate, a key intermediate for other pathways (**Figure 2.1**). Many enzymes involved in these pathways are conserved between PCC 6803 and *E. coli* (Appendix Table 2.1). Therefore, research related to protein function has primarily focused on the processes and enzymatic steps that differ in cyanobacteria compared to model heterotrophs.

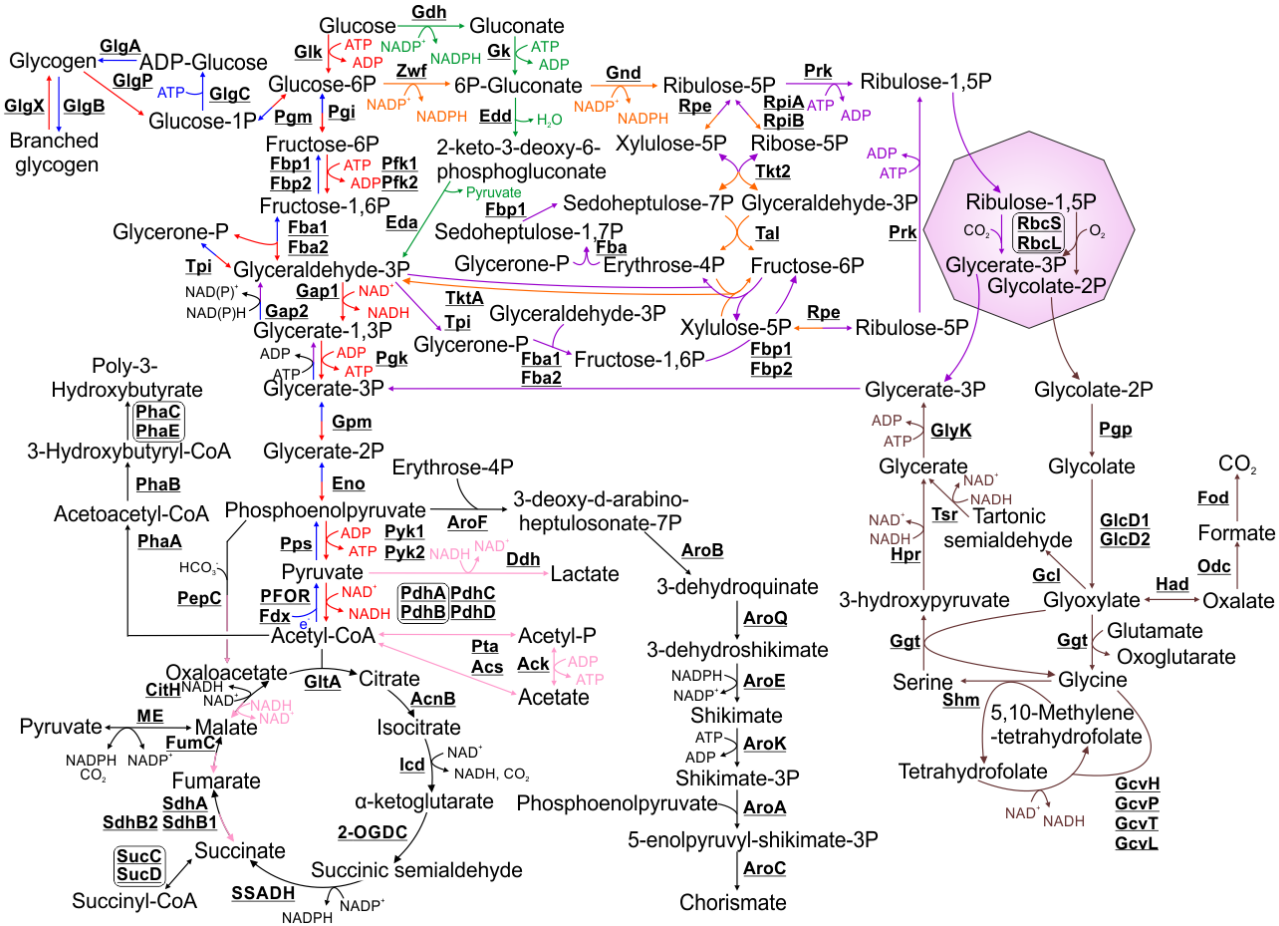

Figure 2.1 Schematic detailing the pathways involved in central metabolism. Biosynthetic steps involved in glycolysis and gluconeogenesis are highlighted in red and blue respectively. Steps in the Entner-Doudoroff pathway are highlighted in green. Steps involved in the oxidative pentose phosphate pathway and the Calvin-Benson-Bassham cycle are highlighted in orange and purple, respectively. Fermentation pathways are highlighted in pink. Photorespiration pathways are highlighted in olive. Where enzymes catalyse reactions in two pathways, the arrows are split between their respective colours. The carboxysome is represented as a purple octagon. Cofactors in each reaction are shown with the exception of protons, water, oxygen and inorganic phosphate.

2.3.1.1 Catabolism of glucose and glycogen

Carbon based inputs into central metabolism can be derived from carbon fixation, catabolism of glycogen or via the import of glucose. The ability to import glucose enables some cyanobacteria, including certain *Synechocystis* substrains, to grow heterotrophically or mixotrophically (204). Glucose is imported into the cell via the transporter, GlcP (205). There are three proposed degradation pathways, which may be active under different environmental conditions (206). Enzymes in the first two, glycolysis (the Embden-Meyerhof-Parnas (EMP) pathway) and the oxidative pentose phosphate (OPP) pathway, are generally highly conserved between PCC 6803 and *E. coli* (Appendix Table 2.1), and consequently these processes have not been extensively investigated in cyanobacteria. However, there are some differences and additional enzymes found in cyanobacteria. For example, homology between the PCC 6803 and *E. coli* PdhA and PdhB subunits of pyruvate dehydrogenase is low (E-value = 0.007 and 5.59E-04, respectively), and this complex has not been characterised in a cyanobacterium. *E. coli* encodes only a class II fructose-1,6-bisphophosphate aldolase (Fbp2) for glycolysis, while PCC 6803 also encodes a class I isoform (Fbp1). While the role of Fbp1 has not been determined in PCC 6803, expression of the native Fbp1 in the cyanobacterium *Halothece* sp. PCC 7418 expressed in PCC 7942 has been demonstrated to confer salt tolerance in this species (207). The PCC 6803 genome also encodes a protein, OpcA, which is not present in *E. coli* and has been suggested to be key for glucose-6-phosphate dehydrogenase (Zwf) activity, the first step of the oxidative PP pathway (208). However, glucose-6-phosphate dehydrogenase activity was similar to wild-type when *opcA* was deleted in PCC 6803 (209). Recently, an alternative glycolytic pathway was identified in PCC 6803 (the Entner-Doudoroff (ED) pathway) (206). This pathway allows conversion of glucose to the oxidative PP intermediate 6-P-gluconate, which is then converted to glyceraldehyde-3-P. The ED pathway is required for optimal photoautotrophic growth and glycogen catabolism, and possibly also optimal activity of the CBB cycle (210).

2.3.1.2 Carbon fixation and the Calvin-Benson-Bassham cycle

As the enzymes of the CBB cycle are not isolated in a sub-cellular organelle as in eukaryotes (i.e. the chloroplast), some reactions are shared with EMP and OPP pathways. The CBB cycle can be divided into two stages: 1) Conversion of ribulose-1,5-P and CO_2 into two molecules of glycerate-3-P via ribulose-1,5-bisphosphate carboxylase/oxygenase (RuBisCO), located in the carboxysomes; 2) Regeneration of the precursor, ribulose-1,5-P, consuming ATP and NADPH predominantly derived from photosynthesis. The requirement to regenerate ribulose-1,5-P leads to one major difference

in the EMP pathway between cyanobacteria and heterotrophs. In *E. coli*, glyceraldehyde-3-P dehydrogenase (Gap) catalyses the reversible oxidative phosphorylation of glyceraldehyde-3-P to glycerate-1,3-P, resulting in interconversion between NAD^+ to NADH. In contrast, PCC 6803 Gap1 displays only glycolytic activity and a strict affinity for NAD^+. A second isoform, Gap2, catalyses the reverse reaction required for the CBB cycle using NADH and potentially also NADPH, which is generated in large amounts via photosynthesis (211).

2.3.1.3 Photorespiration

RuBisCO can assimilate O_2 instead of CO_2, resulting in the production of one molecule each of glycerate-3-P and glycolate-2-P. The latter product is toxic to chloroplast metabolism in photosynthetic eukaryotes and likely also to PCC 6803 at high concentrations (212). Therefore, glycolate-2-P is converted to glycerate-3-P via the photorespiratory salvage pathway, a multi-step process conserved in most organisms that perform oxygenic photosynthesis (213). Glycolate-2-P is first converted to glyoxylate by GlcD1 or GlcD2. Three subsequent photorespiratory pathways for catabolism of glyoxylate have been proposed in PCC 6803 and deletion of genes in each pathway results in a mutant that requires high CO_2 conditions for survival (212). The first involves conversion of glyoxylate to glycerate-3-P via tartonic semialdehyde biosynthesis, the second, conversion of glyoxylate to glycerate-3-P via glycine and L-serine interconversion, and the third conversion of glyoxylate to oxalate, which is subsequently converted to formate. The enzymes involved in several of these pathways have been predominantly identified in *A. thaliana*, with putative homologs present in cyanobacteria (214). Of these, Shm, involved in the second pathway, and GlcD1, have been shown to display similar enzymatic activity to their *A. thaliana* homologs (214). Deletion of GlcD1 and GlcD2 in PCC 6803 results in a complete loss of photorespiratory activity (212). However, the role of the other putative cyanobacterial homologs has not been determined and many proteins currently assigned to photorespiration, as outlined in Eisenhut *et al.* (212), have been suggested to catalyse alternative reactions. Moreover, in the third pathway, only one putative enzyme, Odc, has been identified.

2.3.1.4 Synthesis of carbon storage compounds

Cyanobacteria require carbon storage compounds for periods when photosynthesis is not sufficient for cellular energy and metabolic requirements. In PCC 6803, under conditions where cells are accumulating excess sugars, a high proportion of glycerate-3-P generated via CO_2 fixation is converted to glycogen (reviewed by Zilliges (215)). In *E. coli*, ADP-glucose is used as the substrate

to generate the primary, unbranched polymer via GlgA. However, two GlgA isoforms are present in PCC 6803 with likely roles in elongating the polymer at varying length (216). Glycogen catabolism in PCC 6803 is likely catalysed by two isoforms of GlgX (GlgX1 and GlgX2) and GlgP (GlgP1 and GlgP2). The individual roles of GlgX1 and GlgX2 have not been determined. The GlgP proteins perform the same catalytic activity under different environmental conditions, cleavage of glycogen to individual glucose-1-P molecules (217). When PCC 6803 is exposed to certain stress conditions, an additional carbon storage compound, the polymer polyhydroxybutyrate, is synthesised from acetyl-CoA via PhaA, PhaB, and the PhaC/PhaE complex (218–220).

2.3.1.5 The tricarboxylic acid cycle

The tricarboxylic acid (TCA) cycle differs in cyanobacteria compared to heterotrophic bacteria, as highlighted by work in the last decade. Cyanobacteria lack the enzyme α-ketoglutarate dehydrogenase, which catalyses the fourth step of the TCA cycle in *E. coli*: conversion of α-ketoglutarate to succinyl-CoA. Instead, some cyanobacteria, including PCC 6803, have genes encoding two enzymes, α-ketoglutarate decarboxylase (2-OGDC) and succinic semialdehyde dehydrogenase (SSADH), which convert α-ketoglutarate to succinic semialdehyde, then succinic semialdehyde to succinate, respectively (221). Compared to the standard TCA cycle, where conversion of α-ketoglutarate to succinate results in production of one NADH and one GTP, the 2-OGDC/SSADH pathway results in production of one NADPH (221). Only the soluble subunits of succinate dehydrogenase, catalysing the sixth step, have been identified in cyanobacteria (73). Succinate dehydrogenase is integrated into the thylakoid membrane interlinked photosynthetic and respiratory electron chain (22). PCC 6803 also encodes a succinyl-CoA synthetase complex (SucC/SucD), which likely catalyses the reversible conversion of succinate to succinyl-CoA in cyanobacteria (222), and is potentially required for biosynthesis of methionine and lysine. Several recent papers have investigated the enzymatic properties of TCA enzymes conserved between cyanobacteria and heterotrophic bacteria (223–225). In contrast to many heterotrophic bacteria, PCC 6803 citrate synthase (GltA) was shown only to catalyse generation of citrate, not its cleavage. PCC 6803 GltA has a lower substrate affinity and turnover rate than the *E. coli* homologue, is not inhibited by ATP and NADH, but is inhibited by phosphoenolpyruvate (223).

2.3.1.6 Alternate biosynthetic pathways linking metabolites of the tricarboxylic acid cycle, photorespiration and glycolysis

A range of additional pathways link the TCA cycle with glycolysis and photorespiration. Glyoxylate, produced via photorespiration, also plays a role in the glyoxylate cycle. This cycle consists of three TCA enzymes and two additional enzymes unique to this pathway: the first, isocitrate lyase (Icl), converts the TCA cycle intermediate isocitrate to succinate and glyoxylate; the second, malate synthase (Msy), converts glyoxylate and acetyl-CoA to the TCA cycle intermediate, malate. While activity of glyoxylate cycle enzymes has been detected in some cyanobacteria (reviewed by Knoop *et al.* (226)), it is unclear whether PCC 6803 encodes active variants of Icl and Msy.

Phosphoenolpyruvate carboxylase (PepC) catalyses the conversion of phosphoenolpyruvate, a glycolysis intermediate, and HCO_3^- to oxaloacetate, a TCA intermediate (227). PepC can therefore be considered an inorganic carbon fixing enzyme (i.e. akin to RuBisCO). Metabolic flux analysis has shown that as much as 25% of all inorganic carbon fixation occurs via PepC in PCC 6803 cultured under mixotrophic or heterotrophic conditions (228). An additional protein, malic enzyme (ME), catalyses the reversible conversion of malate, a TCA intermediate, and pyruvate (229). Deletion of ME in PCC 6803 results in a mutant that displays poor growth when exposed to continuous but not diurnal light (230). It was hypothesised that ME is required for pyruvate biosynthesis under continuous light.

2.3.1.7 Fermentation pathways

Three possible fermentation pathways are present in PCC 6803 that generate D-lactate, acetate or succinate, respectively. Presumably fermentation plays a role in energy generation when cyanobacteria are exposed to long periods of darkness under anoxic conditions, but the importance of these pathways during changing environmental conditions has not been determined. D-lactate, acetate and succinate production has been observed in wild-type PCC 6803 cells but only after three days growth under dark, anaerobic conditions (174). A homolog of lactate dehydrogenase (Ddh), which converts pyruvate and NADH to lactate and NAD^+, is encoded by PCC 6803. Two possible pathways for acetate production may be present in PCC 6803: 1) Conversion of acetyl-CoA to acetyl-P, then acetate, via phosphotransacetylase (Pta) and acetate kinase (Ack), respectively; 2) Direct reversible conversion of acetyl-CoA to acetate via acetyl-CoA synthetase (Acs) (174). Production of succinate relies primarily on phosphoenolpyruvate as the initial substrate, which is subsequently converted to oxaloacetate via PepC and then fed into the reverse TCA cycle (231).

2.3.1.8 Chorismate biosynthesis

Chorismate is the precursor for biosynthesis of a range of amino acids and cofactors, and has further importance in cyanobacteria as the substrate for production of phylloquinone, plastoquinone, phenylalanine, tyrosine, folate and molybdopterin, in addition to tocopherols and carotenoids. The glycolytic and PP pathway intermediates phosphenolpyruvate and erythrose-4-P are the substrates for production of chorismate via a 7-step pathway in *E. coli*. However, the enzyme catalysing the first step, condensation of phosphoenolpyruvate and erythrose-4-P, has not been identified in PCC 6803 (232). PCC 6803 proteins demonstrating high sequence similarity to five other enzymes in the *E. coli* pathway have been identified (Appendix Table 2.1) with the exception of the third enzyme, AroQ (No BLAST match). It is unclear from the literature how function was assigned to PCC 6803 AroQ, putatively encoded by *sll1112* in the KEGG database.

2.3.2 Metabolism and degradation of nucleotide sugars and sugar osmolytes

A range of nucleotide sugars required for lipopolysaccharide (LPS) biosynthesis or as cofactors for other reactions (i.e. UDP-glucose), are synthesised by PCC 6803 (**Figure 2.2**). LPSs contain a range of sugar residues including rhamnose, galactose, glucosamine, mannose and fucose, which in PCC 6803 are incorporated as 2,3-di-methyl-fucose and 2-methyl-fucose. 2-methylxylose has also been reported in PCC 6803 (233). Only some of the biosynthetic pathways synthesising the LPS sugar precursors have been identified in cyanobacteria, although predominantly on the basis of identifying proteins with high sequence similarity to characterised enzymes from heterotrophic bacteria. TDP-β-L-rhamnose is synthesised by a four step pathway from glucose-1-P. There are two potential homologs in PCC 6803 for the last three enzymes in the pathway, RfbB, RfbC and RfbD, but the function of these isoenzymes has not been determined. UDP-N-acetylglucosamine is synthesised by a three step pathway from fructose-6-P and is the precursor not just for LPSs but also peptidoglycan. UDP-glucose is synthesised from glucose-1-P by CugP, a non-GalU UDP-glucose pyrophosphorylase, which differs from the GalU UDP-glucose pyrophosphorylase reaction conducted in most proteobacteria, including *E. coli* (234). A UDP-glucose 4-epimerase (GalE) then catalyses the conversion of UDP-glucose to UDP-galactose. GDP-mannose is synthesised from fructose-6-P by a three step reaction and GDP-fucose from GDP-mannose by a two-step pathway. None of the proteins in these pathways have been characterised in cyanobacteria although deletion of the last gene in this pathway in PCC 6803, WcaG, a GDP-fucose synthase, resulted in production of carotenoids lacking fucose, specifically myxoxanthophyll (myxol 2'fucoside) (235).

Several sugars act as osmolytes, notably sucrose and glucosylglycerol. Osmolytes play a role in PCC 6803 in salt tolerance (236,237). In PCC 6803, sucrose is synthesised from UDP-glucose (or ADP-glucose) and fructose-6-P by two enzymes, SpsA and Spp (238,239). Sucrose breakdown in PCC 6803 is catalysed by an invertase (Inv) (240), resulting in production of glucose and fructose, which are likely phosphorylated to glucose-6-P by Glk and fructose-1-P by FrkA, and cycled back into glycolysis. A putative glucose kinase and fructose kinase are encoded in the PCC 6803 genome but have not been characterised. Glucosylglycerol is synthesised from ADP-glucose and glycerol-3-P via two enzymes, GgpS and GgpP (241). Glycerol-3-P is derived from either the intermediate glycerone-P generated during glycolysis or the Calvin cycle, or it is possibly imported.

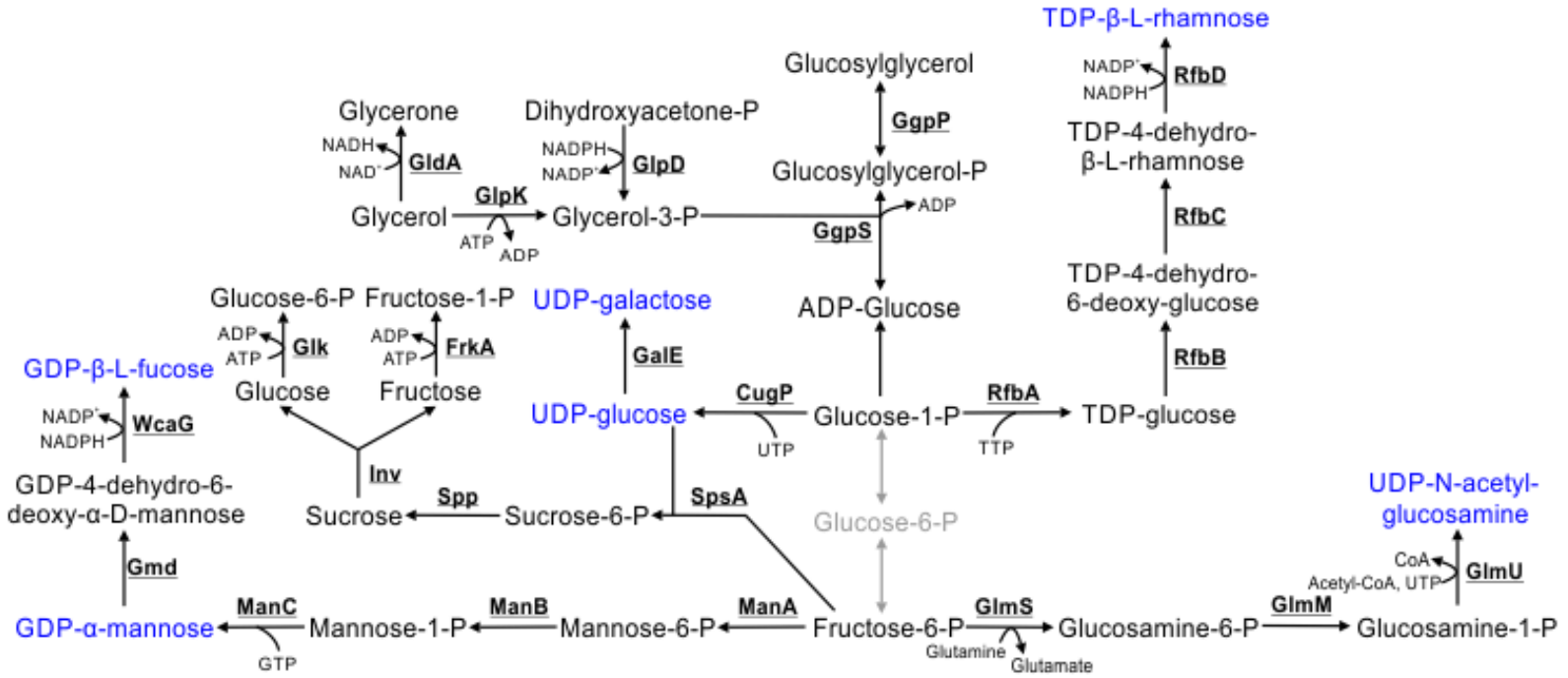

Figure 2.2 Metabolism and degradation of nucleotide sugars and sugar osmolytes. Compounds highlighted in blue are substrates for lipopolysaccharide biosynthesis. Steps highlighted in grey are compounds and reactions not involved in these pathways but detailed in **Figure 2.1**. Cofactors in each reaction are shown with the exception of protons, water, oxygen and inorganic phosphate.

2.3.3 Amino acid biosynthesis and degradation

PCC 6803 synthesises twenty L-amino acids and two D-amino acids (**Figure 2.3**). The majority of enzymes involved in amino acid biosynthesis display high sequence similarity between PCC 6803 and *E. coli* (Appendix Table 2.1). Amino acids are synthesised from a range of substrates, including pyruvate, the TCA cycle intermediates α-ketoglutarate and oxaloacetate, chorismate, the nucleotide intermediate, 5-phosphoribosyl-1-pyrophosphate (discussed further in Section 2.3.4), and glycerate-3-P or glyoxylate. Biosynthesis of amino acids is divided into sections below based on the substrates utilised.

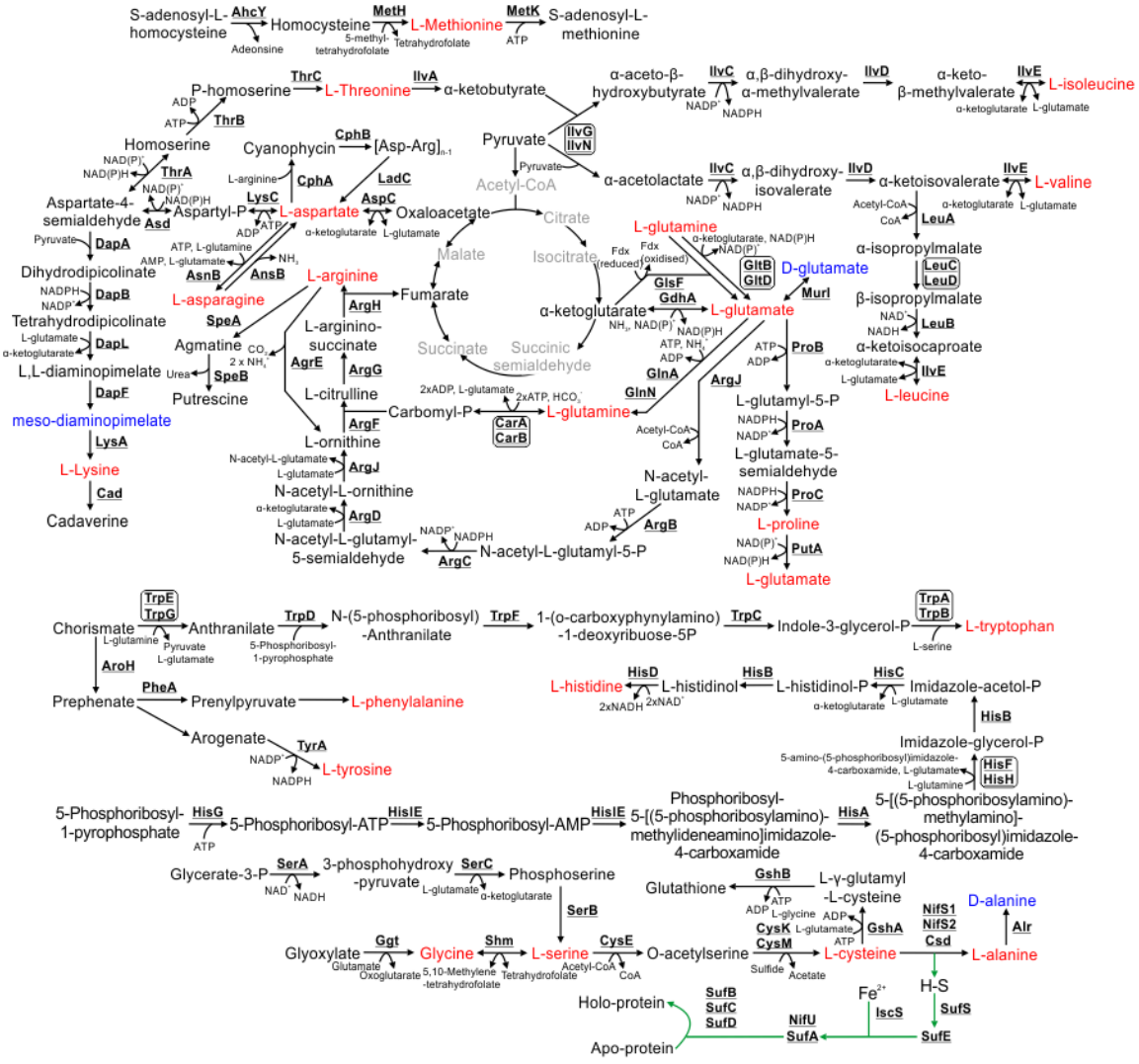

Figure 2.3 Metabolism of amino acids, cyanophycin, glutathione and iron-sulphur clusters. The twenty L-amino acids are highlighted in red while amino acids incorporated into peptidoglycan are highlighted in blue. The iron-sulphur biosynthetic pathways is highlighted in green. Steps highlighted in grey are compounds and reactions not involved in these pathways but detailed in **Figure 2.1**. Cofactors in each reaction are shown with the exception of protons, water, oxygen and inorganic phosphate.

2.3.3.1 Isoleucine, valine and leucine biosynthesis

α-ketobutyrate (synthesised from L-threonine by IlvA) and pyruvate are the substrates for biosynthesis of L-isoleucine, while pyruvate is the sole substrate for L-valine and L-leucine biosynthesis. The enzymatic steps in PCC 6803 are similar to those in *E. coli*, with the exception of the first step. In *E. coli* biosynthesis of α-acetolactate and α-aceto-β-hydroxybutyrate are typically catalysed by the IlvB/IlvN complex. However, in PCC 6803, the homologue for IlvB was identified as 2-OGDC in the TCA cycle (Section 2.3.1.5) (221). An alternate acetolactate synthase, IlvG, demonstrates high sequence similarity to *E. coli* IlvG (E-value = 0). IlvG may form a complex with IlvN and catalyse this step (242) but this requires further verification.

2.3.3.2 Glutamate, glutamine and proline biosynthesis

The TCA cycle intermediate α-ketoglutarate is the substrate for L-glutamate biosynthesis which in turn is the substrate for production of L-glutamine, D-glutamate and L-proline. D-glutamate is synthesised by MurI and is incorporated into peptidoglycan. Two different glutamine synthetases, GlnA and GlnN, convert L-glutamate to L-glutamine (243), and in the process incorporate ammonia into amino acid biosynthesis. Alternatively, several enzymes catalyse the opposite reaction where L-glutamine is converted to L-glutamate, including an NAD(P)H or possibly ferredoxin-dependent glutamate synthase (GltB/GltD) and a ferredoxin-dependent glutamate synthase (GlsF) (244). L-proline is synthesised via three enzymes (ProA, ProB, ProC). PCC 6803 also encodes a putative proline oxidase, PutA, which catabolises L-proline to L-glutamate, reducing $NADP^+$ and possibly a quinone in the process (245).

2.3.3.3 Arginine biosynthesis

L-arginine is synthesised from L-glutamate via eight enzymatic steps, the sixth requiring carbomyl-P, which is synthesised from L-glutamine via CarA/CarB. This pathway is very similar to that in *E. coli*. However, PCC 6803 does not encode ArgA or ArgE, catalysing the first and fifth steps of the pathway. Instead, it encodes ArgJ, a bifunctional enzyme which catalyses both these enzymatic reactions. Recently, an ornithine-ammonia cycle was identified in PCC 6803 (246). This cycle utilises ArgF, ArgG, ArgH, and an additional, alternative enzyme, AgrE. AgrE converts L-arginine to L-ornithine, releasing ammonia in the process (247). PCC 6803 also encodes two putative SpeA and two putative SpeB proteins, which play a role in degradation of L-arginine to putrescine, a polyamine. In *E. coli*, putrescine can be used as a nitrogen and carbon source via conversion to succinate (247). Whether putrescine has a similar role in cyanobacteria has not been determined.

2.3.3.4 Aspartate, cyanophycin and lysine biosynthesis

L-aspartate is synthesised from oxaloacetate and L-glutamate by AspC. L-aspartate and L-arginine are the substrates for cyanophycin, a nitrogen storage polymer. Cyanophycin is synthesised by CphA and then converted back to L-aspartate and L-arginine by CphB and LadC (248). L-aspartate is converted to aspartate-4-semialdehyde, which is the substrate for biosynthesis of L-threonine and L-lysine. PCC 6803 encodes all the enzymes in the five step diaminopimelate aminotransferase pathway required for L-lysine biosynthesis (249,250). The third reaction, conversion of tetrahydrodipicolinate to L,L-diaminopimelate, is catalysed by DapL. In contrast, *E. coli* requires three enzymes, DapC, DapD and DapE, for this conversion. L-lysine is the substrate for production of the siderophore cadaverine by Cad. Three enzymes, ThrA, ThrB and ThrC, convert aspartate-4-semialdehyde to L-threonine by a pathway similar to that in *E. coli*.

2.3.3.5 Methionine biosynthesis

In *E. coli*, L-methionine is also synthesised from aspartate-4-semialdehyde. However, the PCC 6803 genome does not encode homologues to MetA, MetB or MetC (Appendix Table 2.2), the first three enzymes in the pathway. However, the genome does encode a putative MetH enzyme, which catalyses the last step, conversion of homocysteine to L-methionine. The enzymatic steps prior to this have not been determined, nor has the original substrate from which L-methionine is synthesised. The PCC 6803 genome also encodes a putative MetK enzyme, which converts L-methionine to S-adenosyl-L-methionine, a cofactor utilised in many other reactions, most notably in biosynthesis of cyanocobalamin (Vitamin B_{12}; Section 2.3.8.4). A putative AhcY enzyme is also encoded, which converts S-adenosyl-L-homocysteine, the product of reactions which use S-adenosyl-L-methionine as a cofactor, back to homocysteine.

2.3.3.6 Tryptophan, phenylalanine and tyrosine biosynthesis

Chorismate is the substrate for L-tryptophan, L-phenylalanine and L-tyrosine biosynthesis. The majority of enzymes involved in L-tryptophan biosynthesis are highly conserved between *E. coli* and PCC 6803. Attempts to generate an auxotrophic mutant of TrpB, one of the subunits catalysing the final step of L-tryptophan biosynthesis, were unsuccessful (251), suggesting that it cannot be imported from the external environment. The pathway for L-phenylalanine and L-tyrosine biosynthesis differs between the two species and has not been completely determined in cyanobacteria. Both amino acids are synthesised from prephenate. However, only the second step of tyrosine biosynthesis, conversion of arogenate to L-tyrosine, has been determined, although

sll1662 (PheA) has been speculated to catalyse the first step of L-phenylalanine biosynthesis, conversion of prephenate to prenylpyruvate (252).

2.3.3.7 Histidine biosynthesis

L-histidine, synthesised from the nucleotide precursor, 5-phosphoribosyl-1-pyrophosphate, is synthesised via a nine-step pathway in *E. coli*. Proteins demonstrating high sequence similarity to all characterised histidine biosynthetic enzymes in *E. coli* have been identified in PCC 6803. However, there are two putative HisC and HisD enzymes in PCC 6803. The function of these isoenzymes has not been determined.

2.3.3.8 Serine, glycine, cysteine and alanine biosynthesis

L-serine can potentially be synthesised via two routes. The first is via a three step light-independent pathway, which has been characterised in PCC 6803 (253). However, the second enzyme in this pathway, SerC has also been suggested to catalyse the transanimation reaction in photorespiration (Section 2.3.1.3) (212). In the second pathway, L-serine (and also glycine) is synthesised from glyoxylate via the photorespiratory pathway or glyoxylate cycle in those species that encode the relevant enzymes. L-cysteine is then produced from L-serine via a two-step pathway, the second of which could potentially be catalysed by either CysK or CysM. L-cysteine is subsequently desulphonated to produce L-alanine by Csd (254), which is subsequently converted to D-alanine, a component of peptidoglycan, via Alr.

2.3.3.9 Glutathione biosynthesis

L-cysteine and L-glutamate are the substrates for the first step of glutathione biosynthesis. Glutathione is a thiol that plays a key role in metal detoxification and tolerance of oxidative stress in PCC 6803 (255). The first step of glutathione biosynthesis is catalysed by GshA, encoded by an essential gene in PCC 6803 (256). In contrast, the enzyme catalysing the second step, GshB is non-essential, suggesting that glutathione is not required for PCC 6803 viability but that the precursor, L-γ-glutamyl-L-cysteine, is required (256).

2.3.3.10 Iron-sulphur cluster biosynthesis

Conversion of L-cysteine to L-alanine by Csd releases sulphur which is incorporated into iron-sulphur clusters. Two additional cysteine desulfarases have been identified in PCC 6803 but unlike Csd, neither are essential (257–259). Iron-sulphur clusters are incorporated into many proteins involved in photosynthesis, respiration and nitrogen fixation (260). **Figure 2.3** outlines iron-sulphur biosynthesis (highlighted in green) and subsequent transfer to proteins, based on characterisation of proteins in other bacterial species (261). SufE acts as a sulphur donor, and IscA as a Fe^{2+} donor to the scaffold proteins required for cluster formation (SufA/NifU) (262). Additional subunits (SufB/SufC/SufD) aid in transfer of the iron-sulphur cluster to proteins. NifU is possibly involved in repairing iron-sulphur clusters in proteins but has not been characterised in cyanobacteria.

2.3.4 Nucleotide biosynthesis

Enzymes involved in nucleotide biosynthesis (**Figure 2.4**) are highly conserved between *E. coli* and PCC 6803 (Appendix Table 2.1), and therefore this pathway has not been investigated in great detail in cyanobacteria. Pyrimidines and purines require the same precursor, 5-phosophoribosyl-1-pyrophosphate, which is synthesised from the PP pathway intermediate, ribose-5P, after which the pathways diverge.

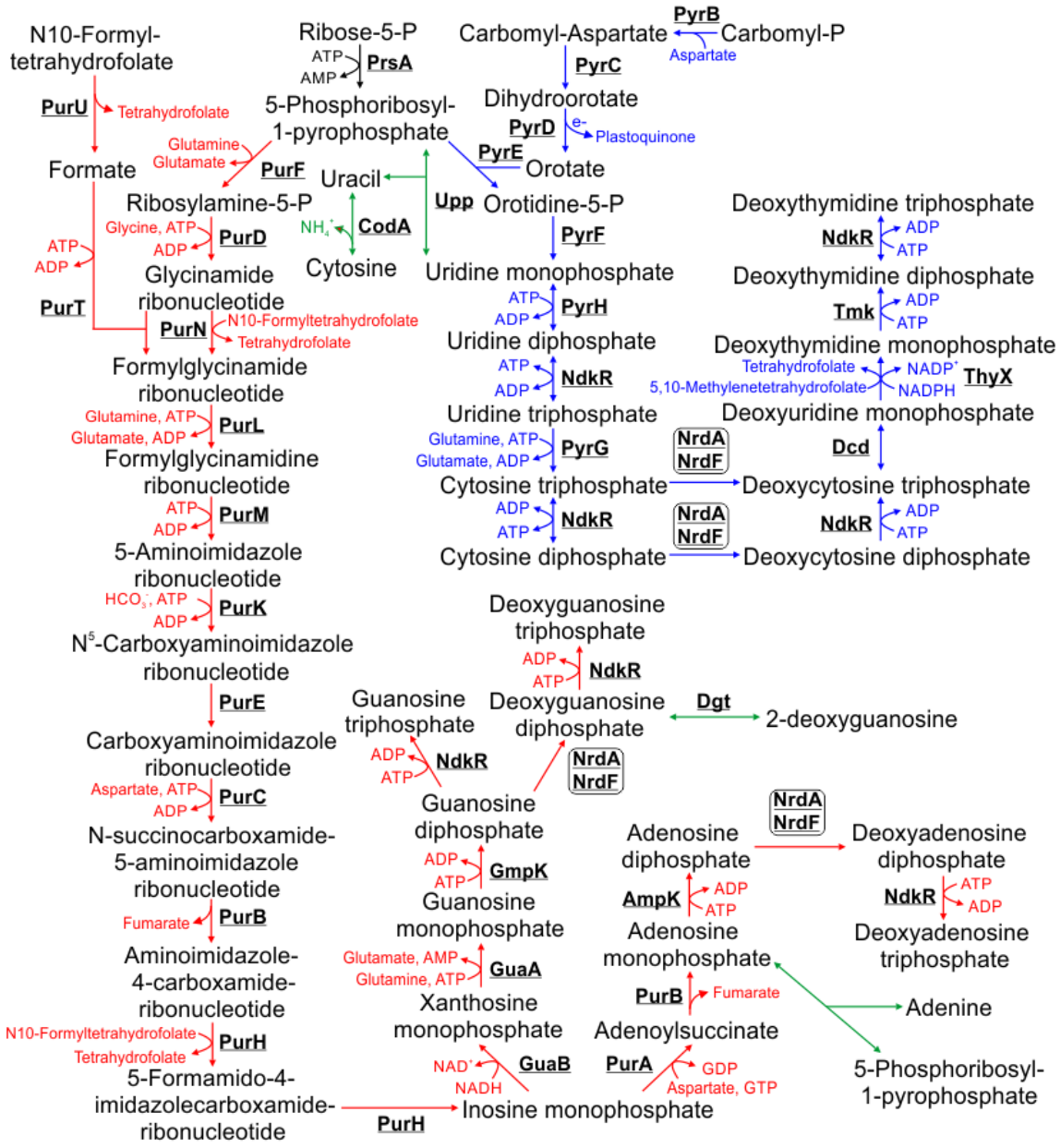

Figure 2.4 Metabolism of nucleotides. The purine and pyrimidine biosynthesis pathways are highlighted in red and blue respectively. Possible nucleotide salvage pathways are highlighted in green. Cofactors in each reaction are shown with the exception of protons, water, oxygen and inorganic phosphate.

2.3.4.1 Purine biosynthesis

In *E. coli*, purine biosynthesis requires eleven enzymatic steps for production of inosine monophosphate, the precursor of guanosine and adenosine based nucleotides (reviewed by Kappock *et al.* (263)). PCC 6803 encodes genes with high homology to all the purine biosynthetic enzymes required for inosine monophosphate in *E. coli*, including PurN and PurT, which are both capable of catalysing the third step (Appendix Table 2.1). PurB and PurH each catalyse two different steps in the pathway. In *E. coli*, inosine monophosphate is converted to guanosine diphosphate by GuaB, GuaA and GmpK, and adenosine diphosphate by PurA, PurB and AmpK (264). All nucleoside-diphosphates are converted to nucleoside-triphosphates via NdkR (265) and to deoxyribonucleotides via the NrdA/NrdF complex (266). All these enzymes are highly conserved between *E. coli* and PCC 6803 (Appendix Table 2.1).

2.3.4.2 Pyrimidine biosynthesis

In *E. coli*, pyrimidine biosynthesis requires six enzymatic steps for production of uridine diphosphate, the precursor of cytosine-, uridine- and thymidine-based nucleotides. Carbomyl-P, synthesised from glutamine and bicarbonate by CarA/CarB, is the initial substrate. Carbomyl-P is converted to orotate via a three-step pathway. Orotate phosophoribosyltransferase (PyrE) transfers a ribosyl group from 5-phosophoribosyl-1-pyrophosphate to orotate, forming oritidine-5-P, which is subsequently converted to uridine diphosphate via PyrF and PyrH. In *E. coli*, uridine diphosphate is converted to uridine triphosphate via NdkR, then cytosine triphosphate via PyrG (267). The NrdA/NrdF complex then converts cytosine triphosphate to deoxycytosine triphosphate. The pathway for biosynthesis of deoxythymidine nucleotides has not been determined. However, enzymes homologous to those identified in the *Lactococcus lactis* pathway are conserved in PCC 6803 (268). Via this pathway, deoxycytosine triphosphate is converted to deoxyuridine monophosphate via Dcd, which is subsequently converted to deoxythymidine monophosphate via ThyX, which in turn is converted to deoxythymidine diphosphate via Tmk. However, experimental evidence is required to confirm whether this pathway is utilised by PCC 6803.

2.3.4.3 Nucleotide salvage pathways

PCC 6803 also encodes a number of enzymes that display high sequence similarity to *E. coli* proteins involved in the nucleotide salvage pathway (267). However, the role of the salvage pathway in cyanobacteria and how nucleotides are catabolised has not been investigated.

2.3.5 Cofactor biosynthesis

Unlike many cyanobacterial species, PCC 6803 does not require the addition of any vitamins or cofactors for growth, suggesting that it encodes complete biosynthetic pathways for each essential compound. However, these pathways have not been extensively investigated. The majority of proteins in these pathways (**Figure 2.5**) have been assigned a function in cyanobacteria based on their homology to characterised enzymes from *E. coli*, with only a few enzymes characterised in PCC 6803 or other model cyanobacterial species. Tocopherol biosynthesis is discussed in Section 2.3.7.4, since this cofactor is synthesised from the same initial substrates as other isoprenoids. Pseudocobalamin (Vitamin B_{12}) biosynthesis is discussed in Section 2.3.8.4 , since this cofactor is synthesised from the same initial substrates as bilins and chlorophyll.

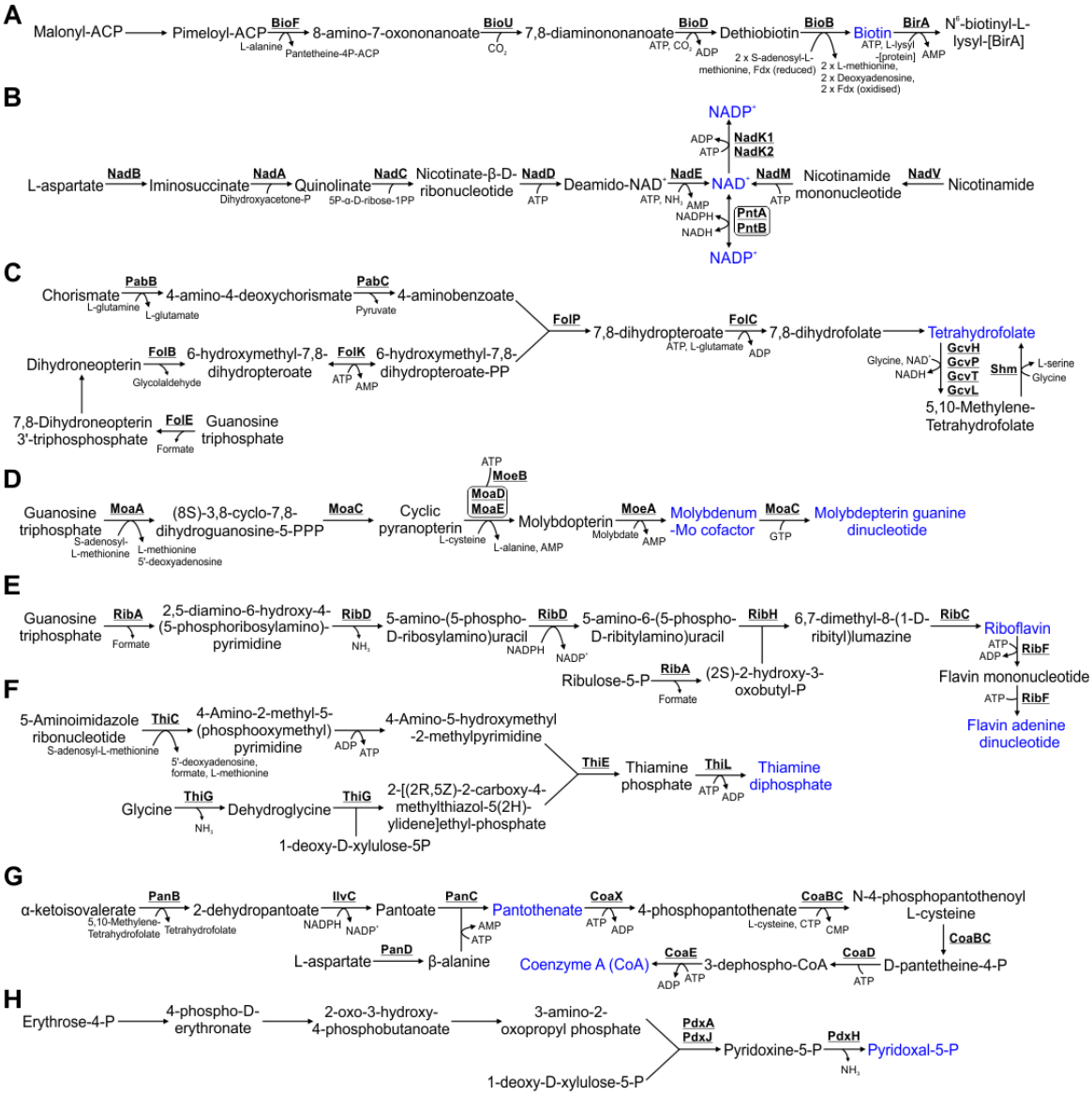

Figure 2.5 Metabolism of vitamins and cofactors. Detailed are the pathways for biosynthesis of A) Biotin, B) NAD+ and NADP+, C) folate, D) molybdenum cofactors, E) riboflavin and FAD, F) thiamine, G) pantothenate and coenzyme A, H) pyridoxal-5P. Vitamins and cofactors are highlighted in blue. Cofactors in each reaction are shown with the exception of protons, water, oxygen and inorganic phosphate.

2.3.5.1 Biotin biosynthesis

In PCC 6803, biotin (vitamin B_7) is an essential cofactor required by acetyl-CoA carboxylase (AccA/AccB/AccC/AccD; Section 2.3.6.1), which is involved in fatty acid biosynthesis (269). The biotin biosynthetic pathway has been determined in *E. coli* (270). In *E. coli*, biotin is synthesised from malonyl-ACP-methyl ester, which undergoes two cycles of fatty elongation to form pimeloyl-ACP-methyl ester. This is subsequently converted to biotin via five enzymatic steps. Synthesis of the pimeloyl-ACP precursor has not been determined in PCC 6803 (271). Putative homologues of only three enzymes in the biotin biosynthetic pathway, BioF, BioD and BioB (and not BioH, BioC and BioA) are encoded in the PCC 6803 genome (**Figure 2.5**A) (270). Recently, a novel enzyme, BioU, was demonstrated to catalyse the same reaction as BioA, conversion of 8-amino-7-oxononoate to 7,8-diaminononanoate (272). The enzymatic activity of BioU is different from BioA. BioU utilises then reforms NADPH, consumes CO_2, and acts as a suicide enzyme, meaning it catalyses only a single reaction due to loss of a lysine group. PCC 6803 also encodes a putative BirA protein, which reacts with biotin to form a biotin-BirA complex that represses biotin biosynthesis (271).

2.3.5.2 NAD^+ and $NADP^+$ biosynthesis

Nicotinamide adenine dinucleotide (NAD^+) is synthesised in cyanobacteria from L-aspartate by a five-step pathway encoded by most bacterial species (**Figure 2.5**B) (273). The last two enzymes in the pathway, NadD and NadE, have low sequence similarity to the equivalent *E. coli* proteins but the activity of the enzymes has been confirmed in PCC 6803 (274). A second two-step pathway for NAD^+ biosynthesis from nicotinamide has also been proposed (274,275), although how nicotinamide is produced has not been determined. NAD^+ is converted to $NADP^+$, required as an electron acceptor in linear photosynthetic electron transport, by NAD kinases, of which two are present in PCC 6803 (NadK1, NadK2) (276). The $NAD^+/NADP^+$ ratio is regulated by pyridine nucleotide transhydrogenase (PntA/PntB), which catalyses electron transfer between the two compounds (277).

2.3.5.3 Folate biosynthesis

Folate (vitamin B_9) based cofactors (e.g. tetrahydrofolate, 5-methyl tetrahydrofolate, 5,10-methylene tetrahydrofolate) are required in certain enzymatic reactions for biosynthesis of the amino acids L-methionine, L-serine and glycine (**Figure 2.3**), the cofactors pantothenate and coenzyme A (**Figure 2.5**G), purine nucleotides and thymidylate pyrimidines (**Figure 2.4**) and certain tRNAs (278). Folate is synthesised from the precursors, chorismate and guanosine triphosphate

(**Figure 2.5**C). A two-step pathway (PabB/PabC) results in conversion of chorismate to 4-aminobenzoate. A four-step pathway (FolE/FolB/FolK and possibly FolQ) catalyses the conversion of guanosine triphosphate to 6-hydroxymethyl-7,8-dihydropteroate-PP, which together with 4-aminobenzoate, catalyses the formation of 7,8-dihydropteroate. FolQ (designated as NudB in *E. coli*) (279) has not been characterised in PCC 6803 but slr0920 shows low sequence similarity to NudB (E-value = 4.56E-06) and may perform FolQ enzymatic activity (Appendix Table 2.2). 7,8-dihydropteroate is subsequently converted to the different folate variants, although only one enzyme catalysing these steps, FolC, has been identified. Whether 5-methyl tetrahydrofolate is synthesised by PCC 6803 is unknown, since the genome does not encode MetF, which synthesises this compound from 5,10-methylene tetrahydrofolate in *E. coli* (278).

2.3.5.4 Molybdenum cofactor biosynthesis

Molybdenum cofactors (molybdopterin guanine dinucleotide or molybdopterin-Mo) act as catalytic centres in a range of enzymes. In PCC 7942, a molybdenum cofactor is required for nitrate reductase (NarB; Section 2.3.9.1) activity (280). Whether any other enzymes in cyanobacteria also require molybdenum cofactors has not been determined. Molybdenum cofactors are synthesised from guanosine triphosphate (**Figure 2.5**D). This pathway has been characterised in *E. coli* and proteins demonstrating high sequence similarity to each enzyme have been identified in PCC 6803 (280). Moreover, several enzymes in the pathway have been characterised in PCC 7942 (280,281). MoaC is likely a bifunctional enzyme catalysing the second step, formation of pyranopterin, and the fifth step, synthesis of the cofactor molybdopterin guanine dinucleotide. The third step, conversion of cyclic pyranopterin to molybdopterin is catalysed by MPT synthase (MoaD/MoaE), which is regenerated by MoeB (282).

2.3.5.5 Riboflavin and flavin adenine dinucleotide biosynthesis

Riboflavin (vitamin B_2) and flavin adenine dinucleotide (FAD) are also synthesised from guanosine triphosphate (**Figure 2.5**E). In cyanobacteria, FAD is a cofactor involved in flavoprotein-mediated redox reactions. The pathway is similar between *E. coli* and PCC 6803 and enzymes are highly conserved between the species (Appendix Table 2.1). Three enzymes, RibA, RibD and RibF, catalyse two separate reactions in the pathway.

2.3.5.6 Thiamine biosynthesis

Thiamine diphosphate (vitamin B_1) is a cofactor for several enzymes, including pyruvate dehydrogenase (Section 2.3.1.1), transketolase in the OPP/CBB pathways (TktA, Section 2.3.1.2), and acetolactate synthase, catalysing the first step of L-valine, L-leucine and L-isoleucine biosynthesis (IlvG/IlvN; Section 2.3.3.1) (283). It is synthesised from the purine biosynthetic intermediate, 5-aminoimidazole ribonucleotide (Section 2.3.4.1; Figure 2.4), glycine and 1-deoxy-D-xylulose-5-P (**Figure 2.5**F). The pathway has been largely characterised in *E. coli* (284), but in PCC 6803, homologues have not been identified for every protein in the pathway (Appendix Table 2.1). Notably, there is no protein in PCC 6803 with high sequence similarity to ThiD (Appendix Table 2.2), which catalyses the second biosynthetic step starting at 5-aminoimidazole ribonucleotide.

2.3.5.7 Pantothenate and coenzyme A biosynthesis

The majority of enzymes involved in biosynthesis of pantothenate (vitamin B_5; **Figure 2.5**G) and coenzyme A are highly conserved between *E. coli* and PCC 6803 (Appendix Table 2.1). Coenzyme A is required for formation of acetyl-CoA and in fatty acid biosynthesis. Three enzymes convert α-ketoisovalerate, an intermediate required for L-valine and L-leucine biosynthesis (Section 2.3.3.1; **Figure 2.3**), to pantothenate. An additional enzyme, PanD, catalyses the third step, conversion of L-aspartate to β-alanine (285). The second reaction can be catalysed by PanE, not encoded in the PCC 6803 genome (Appendix Table 2.2) or IlvC, which is also involved in L-isoleucine, L-valine and L-leucine biosynthesis (**Figure 2.3**). Coenzyme A is synthesised from pantothenate via five enzymatic steps (285). Only the first step (conversion of pantophenate to 4-phosphopantophenate) is catalysed by a different enzyme from that in the *E. coli* pathway, specifically a type III pantophenate kinase (CoaX) (286).

2.3.5.8 Pyridoxal-5P biosyntheis

Pyridoxal-5-P (vitamin B_6) is a cofactor required by a range of enzymes involved in amino acid biosynthesis and catabolism, iron, cell wall component and carbon metabolism, and biosynthesis of other cofactors (For a full list refer to Richts *et al.* (287)). Biosynthesis of pyridoxal-5-P in *E. coli* utilises 1-deoxy-D-xylulose-5-P and 3-amino-2-oxopropyl phosphate as substrates, and is catalysed via PdxA/PdxJ, then PdxH (**Figure 2.5**H) (288). PdxA, PdxJ and PdxH are conserved in PCC 6803 but the enzyme pathway for 3-amino-2-oxopropyl phosphate biosynthesis has not been determined.

2.3.6 Membrane and cell wall biosynthesis

Cyanobacterial membrane composition differs from that of heterotrophic bacteria. Five classes of lipids accumulate in PCC 6803 plasma and thylakoid membranes: Phosphatidylglycerol, monogalactosyl-diacylglycerol, digalactosyl-diacylglycerol, sulfoquinovosyl-diacylglycerol and hydrocarbons (289,290). Like other Gram-negative prokaryotes, cyanobacteria are encompassed by a peptidoglycan layer and an outer membrane (OM) containing lipopolysaccharides (LPSs).

2.3.6.1 Lipid biosynthesis

Cyanobacterial lipids are synthesised from acyl-ACPs (acyl carrier proteins), which in turn are synthesised from acetyl-CoA by a pathway similar to that in *E. coli* (Appendix Table 2.1; **Figure 2.6**). Predominantly C16 and C18 acyl-ACPs are synthesised with various degrees of saturation catalysed by four possible desaturases (DesA, DesB, DesC, DesD) (291). A plasma membrane (PM) associated protein, Aas (183), mediates import of acyl-ACPs and fatty acids from the PM and periplasm (292,293).

Hydrocarbons are synthesised directly from acyl-ACPs (294,295), with the majority of cyanobacteria (including PCC 6803) producing C15 or C17 alkanes via a two-step pathway (Aar/Ado) (296), while the remainder produce C17 or C19 alkenes via a polyketide synthase (Ols) (297). The other lipids are synthesised from 1,2-diacyl-glycerol-3-P, which is produced from acyl-ACPs via three enzymes (PlsX, PlsY, PlsC) (298). A further three enzymatic steps are required for phosphatidylglycerol biosynthesis. The enzyme catalysing the second step, PgsA, is non-essential in PCC 6803, when the mutant is supplemented with phosphatidylglycerol (299). There is no PCC 6803 protein with any sequence similarity to PgpB, the enzyme in *E. coli* that catalyses the third step (Appendix Table 2.2).

1,2-diacyl-glycerol-3-P is likely converted to diacylglycerol, the common substrate for synthesis of the other membrane lipids. The enzyme catalysing this step has not been identified. The reverse reaction is likely catalysed by DgkA. MgdA catalyses conversion of diacylglycerol to monoglucosyl-diacylglycerol, which is likely converted to monogalactosyl-diacylglycerol by an unidentified epimerase (300). Monogalactosyl-diacylglycerol is then converted to digalactosyl-diacylglycerol by DgdA (301). Sulfoquinovose, synthesised from UDP-glucose and sulphate by SqdB (302,303), is reacted with diacylgycerol by SqdX to form sulfoquinovosyl-diacylglycerol (304).

The PCC 6803 genome encodes no proteins with homology to enzymes involved in β-oxidation (Appendix Table 2.2), although one report has suggested the capacity for fatty acid catabolism is

retained (305). If so, there must be an alternate, uncharacterised pathway responsible for lipid degradation.

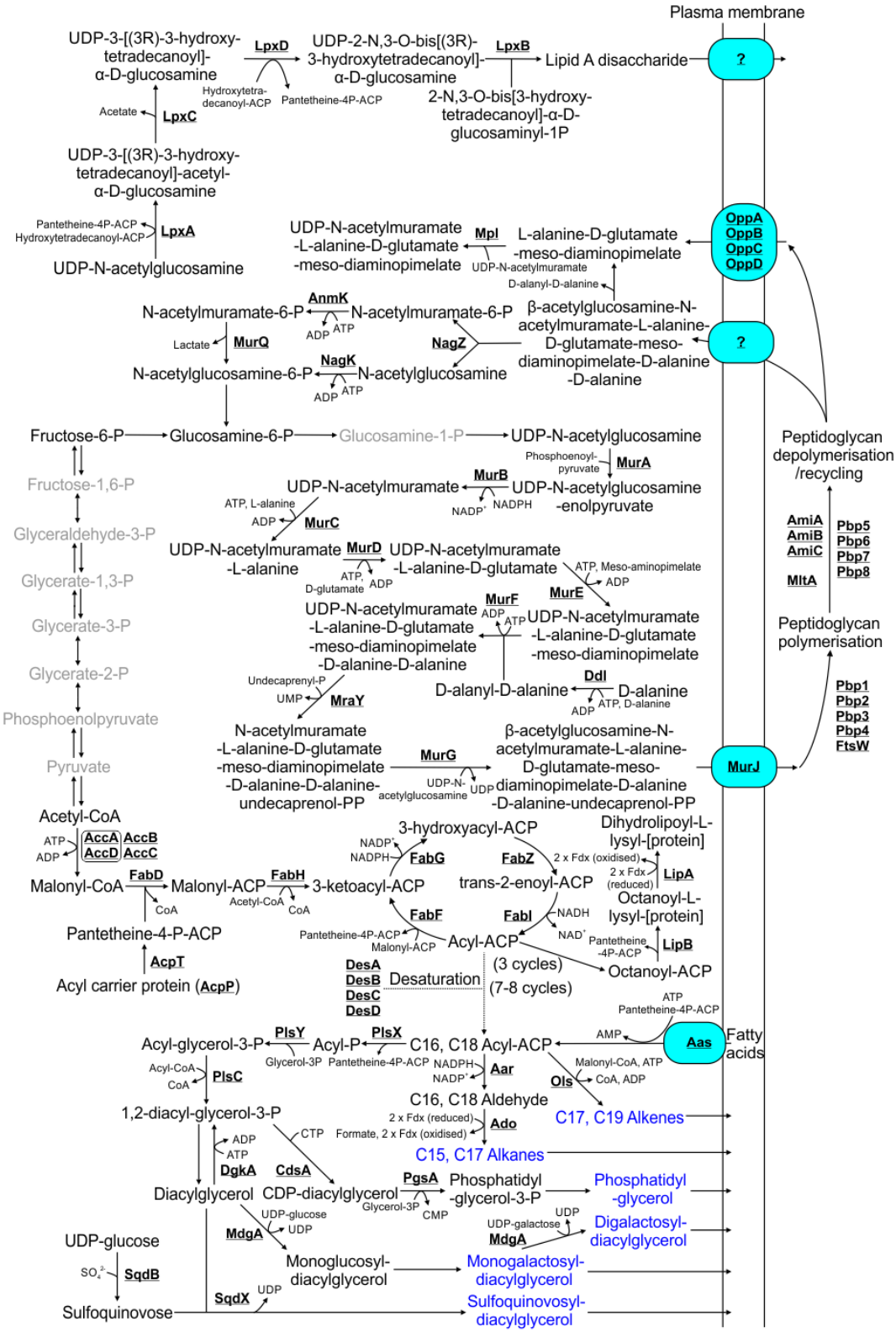

Figure 2.6 Metabolism of membrane lipids, peptidoglycan and lipopolysaccharides. Membrane lipids are highlighted in blue. Steps highlighted in grey are compounds and reactions not involved in these pathways but detailed in **Figure 2.1**. Cofactors in each reaction are shown with the exception of protons, water, oxygen and inorganic phosphate.

2.3.6.2 Lipoic acid biosynthesis

Lipoic acids are cofactors required for a range of enzymes, including pyruvate dehydrogenase and the glycine cleavage system (GcvH/GcvP/GcvT/GcvL; **Figure 2.1**) (306). The biosynthetic pathway has been elucidated in *E. coli* (307). Lipoic acids are covalently attached to enzymes via LipB and then sulfonated via LipA. In contrast to *E. coli*, there are two putative LipA proteins in PCC 6803 (Appendix Table 2.1).

2.3.6.3 Peptidoglycan biosynthesis and depolymerisation

The structure of PCC 6803 peptidoglycan has not been determined. However, peptidoglycan in the closely related species, *Synechocystis* sp. PCC 6714, incorporates L-alanine, D-alanine, D-glutamate and meso-diaminopimelate into peptide bridges, which are linked to polymers consisting of alternating acetylglucosamine and acetylmuramate monomers. The enzymes synthesising peptidoglycan monomers (acetylglucosamine-N-acetylmuramate-pentapeptides) from UDP-N-acetylglucosamine are highly conserved between *E. coli* and PCC 6803 (Appendix Table 2.1). Surprisingly, the last two enzymes in the pathway, MraY and MurG have been localised to the TM in PCC 6803 (183,308), suggesting that an additional protein or process must transport these monomers to the PM. The flippase involved in translocating the acetylglucosamine-N-acetylmuramate-pentapeptide monomers to the periplasmic side of the PM in *E. coli* (MurJ) has not been identified in cyanobacteria (309). However, the protein encoded by slr0488 in PCC 6803 demonstrates some sequence similarity to MurJ (E-value = 1.04E-28; Appendix Table 2.1) but its function needs to be confirmed experimentally.

Polymerization of peptidoglycan is catalysed by the penicillin-binding proteins (PBPs) 1-4 and FtsW (310), while depolymerisation and recycling of peptidoglycan monomers is catalysed by PBPs 5-8 and AmiA-C (311). Four proteins in *E. coli* have been implicated in importing depolymerised peptidoglycan components (NagE, MurP, AmpG, Opp) (312), but only Opp, an oligopeptide transporter consisting of four subunits, is encoded in the PCC 6803 genome (Appendix Table 2.2). A series of cytosolic enzymes conserved in PCC 6803 (Mpl, NagZ, AnmK, NagK, MurQ) likely recycle depolymerised peptidoglycan components back into peptidoglycan biosynthesis (312). Other *E. coli* enzymes involved in recycling (NagA, NagB, AmiD, AmpB) have no homologues in PCC 6803 (Appendix Table 2.2).

2.3.6.4 Lipopolysaccharide biosynthesis

LPSs are incorporated into the OM of cyanobacteria, including PCC 6803 (233). Four enzymes synthesise the Lipid A disaccharide core of the LPS and are highly conserved between *E. coli* and PCC 6803 (Appendix Table 2.1). The protein involved in translocating Lipid A disaccharide to the periplasmic side of the PM has not been identified, although four PM localised proteins with high sequence similarity to MsbA (slr2019: E-value = 8.64E-91; sll1276: E-value = 2.28E-84; sll1725: E-value = 7.22E-83; slr1149: E-value = 1.82E-73; Appendix Table 2.2), the characterised Lipid A disaccharide flippase from *E. coli* (313), are encoded in the PCC 6803 genome (183). Biosynthesis of the polysaccharide portion of the LPS has not been determined in cyanobacteria (314). Five PM-localised glycosyltransferases are encoded by the PCC 6803 genome which may play a role in saccharide polymerisation (Appendix Table 2.1). However, the PCC 6803 genome encodes no proteins with homology to those in *E. coli* involved in transporting polysaccharides across the PM (i.e. Wzm/Wzt or Wzx), ligation of the polysaccharide to the Lipid A disaccharide core (WaaL) or transport of the fully synthesised LPS to the OM (LptA, LptC, LptD, LptE), with the possible exception of LptB (Appendix Table 2.2).

2.3.7 Isoprenoid, quinol and carotenoid biosynthesis

Isoprenoids play a key role in electron transport, photoprotection, light harvesting, membrane integrity and organisation, and are incorporated into a range of compounds including LPSs, peptidoglycan and chlorophyll.

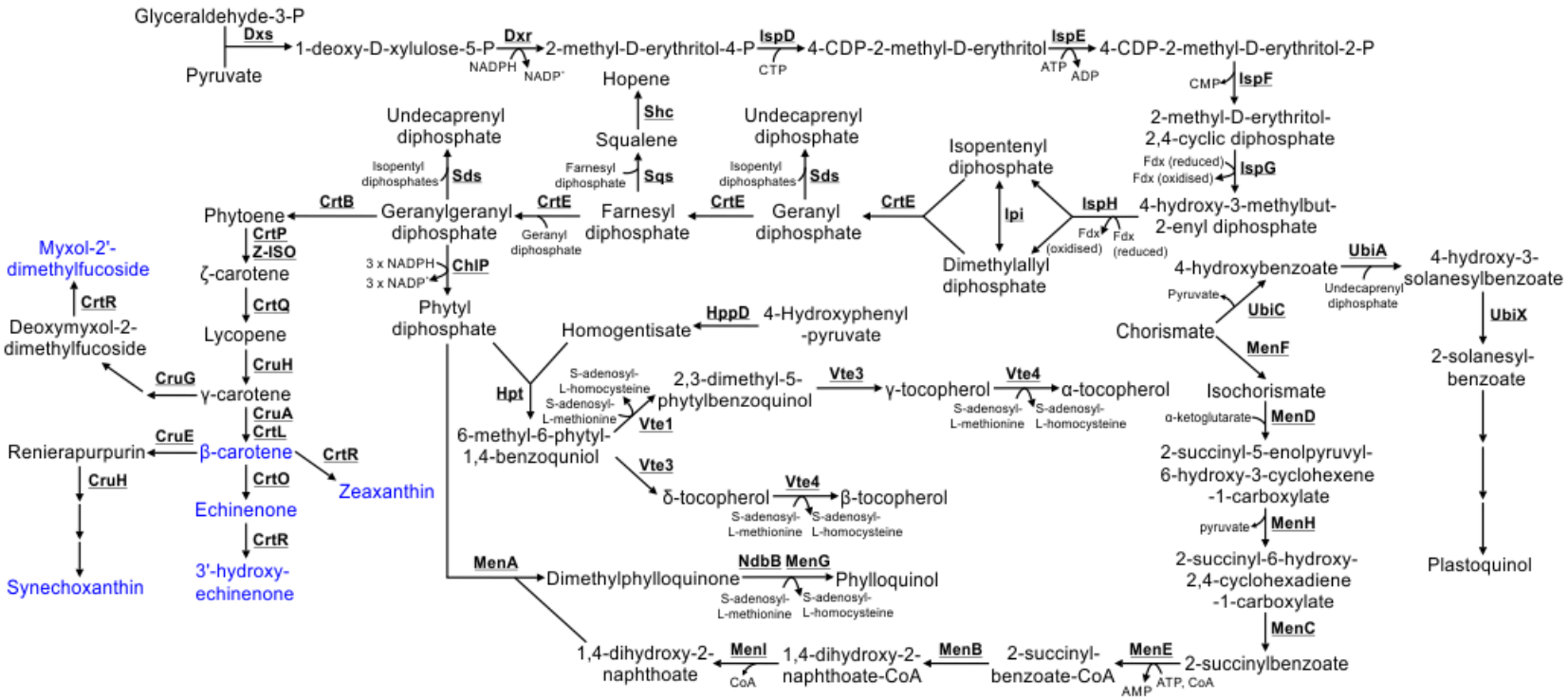

Figure 2.7 Metabolism of isoprenoids, quinols and carotenoids. Carotenoids are highlighted in blue. Cofactors in each reaction are shown with the exception of protons, water, oxygen and inorganic phosphate.

2.3.7.1 Isoprenoid biosynthesis

Isoprenoids, specifically undecaprenyl diphosphate, farnesyl diphosphate and geranylgeranyl diphosphate, are substrates required for biosynthesis of a wide range of compounds including hopenes, LPSs, peptidoglycan, carotenoids, phylloquinone, plastoquinone, chlorophyll and tocopherols. Geranylgeranyl diphosphate is synthesised from pyruvate and glyceraldehyde-3-P via eight enzymes, all of which are highly conserved between *E. coli* and PCC 6803 (Appendix Table 2.1; **Figure 2.7**) (315). An additional enzyme, Ipi, is involved in isomerisation of isopentenyl diphosphate and dimethylallyl diphosphate (316). PCC 6803 mutants lacking Ipi demonstrate deficient isoprenoid biosynthesis, smaller cell size and reduced TMs, and an altered cell wall (317).

2.3.7.2 Hopene biosynthesis

Hopenes are synthesised from farnesyl diphosphate in PCC 6803 via two enzymes, Sqs and Shc (318). While the exact role of hopenes has not been determined in cyanobacteria, they have been suggested to play a role in membrane integrity in non-sulphur purple photosynthetic bacteria (319). Hopenes have been detected in the TM, PM and OM of *Synechocystis* sp. PCC 6714 (320). Sqs and Shc are expressed under photoautotrophic conditions in PCC 6803 (183).

2.3.7.3 Carotenoid biosynthesis

Geranylgeranyl diphosphate is the substrate for carotenoid biosynthesis. Carotenoids play a key role in assembly of photosynthetic complexes (321), membrane integrity and thylakoid organisation (322), and as light-harvesting and photoprotective pigments. Seven carotenoids have been detected in PCC 6803: synechoxanthin, myxol-2'-dimethylfucoside (myxoxanthophyll), zeaxanthin, 3'-hydroxy-echinenone, *cis*-zeaxanthin, echinenone and β-carotene (323). The pathway has not been completely elucidated (324–326), but twelve enzymes have been demonstrated to play a role in carotenoid biosynthesis. A newly identified enzyme 15-*cis*-*zeta*(ζ)-carotene isomerase (Z-ISO), was found to catalyse the *cis*-to-*trans* isomerization of the central 15–15' *cis* double bond in 9,15,9'-tri-*cis*-ζ-carotene to produce 9,9'-di-*cis*-ζ-carotene during the four-step conversion of phytoene to lycopene (327).

2.3.7.4 Tocopherol biosynthesis

Tocopherols (Vitamin E) play a role in protecting cyanobacteria from lipid peroxidation (328), cold tolerance (329) and potentially optimising photosynthetic activity (330). All tocopherols are

synthesised from the precursor 6-methyl-6-phytyl-1,4-benzoquinol, which is synthesised by Hpt utilising the substrates phytyl diphosphate and homogentisate (331–333). Phytyl diphosphate is synthesised from geranylgeranyl diphosphate by ChlP (334). Homogentisate is synthesised from 4-hydroxyphenyl-pyruvate (335), which is typically synthesised from prephenate by TyrA. However, PCC 6803 TyrA demonstrates specificity only to arogenate (336), suggesting that 4-hydroxyphenyl-pyruvate may be synthesised by an alternate route. Four tocopherols (α, β, δ, γ) are produced by PCC 6803 (337), although it has not been determined if each has separate roles in the cell. α- and γ- tocopherols are synthesised from 6-methyl-6-phytyl-1,4-benzoquinol via VTE1, VTE3 and VTE4, while β and δ tocopherols are synthesised via VTE3 and VTE4 (338).

2.3.7.5 Phylloquinone and plastoquinone biosynthesis

Phylloquinone (Vitamin K_1) and plastoquinone are synthesised from chorismate. Phylloquinone acts as an electron acceptor in photosystem I (339), and while not essential under photoautotrophic conditions, loss of this compound results in a severe growth defect when cells are exposed to high light conditions (340). Phylloquinone is synthesised by ten enzymes of which several have been characterised in PCC 6803 (340,341). The majority have been identified based on homology with proteins synthesising menaquinone (Vitamin K_2) and characterised in other bacteria (342). The second last enzyme in the pathway, MenA, utilises phytyl diphosphate, while the last enzyme requires that dimethylphylloquinone be reduced via NAD(P)H dehydrogenase NdbB to dimethylphylloquinol, prior to synthesis of phylloquinone by MenG (343).

Plastoquinone is an essential electron carrier required for photosynthesis and respiration (73). Despite the importance of plastoquinone, the entire biosynthetic pathway has not been determined (344). Catalytic activity of only the first three enzymes in the pathway, UbiC, UbiA and UbiX, has been determined by expression of the PCC 6803 genes in *E. coli* (344,345). Deletion of a putative 4-hydroxy-3-solanesylbenzoate decarboxylase, encoded by *sll0936*, results in reduced plastoquinone levels (344), suggesting an uncharacterised role for this protein in its biosynthesis.

2.3.8 Chlorophyll, phycobilin and pseudocobalamin biosynthesis

Chlorophyll and phycobilins are the light harvesting pigments incorporated into photosystems and phycobilisomes, respectively. Pseudocobalamin (vitamin B_{12}) is synthesised from the same precursor substrate, uroporphyrinogen III, and is therefore included in this section.

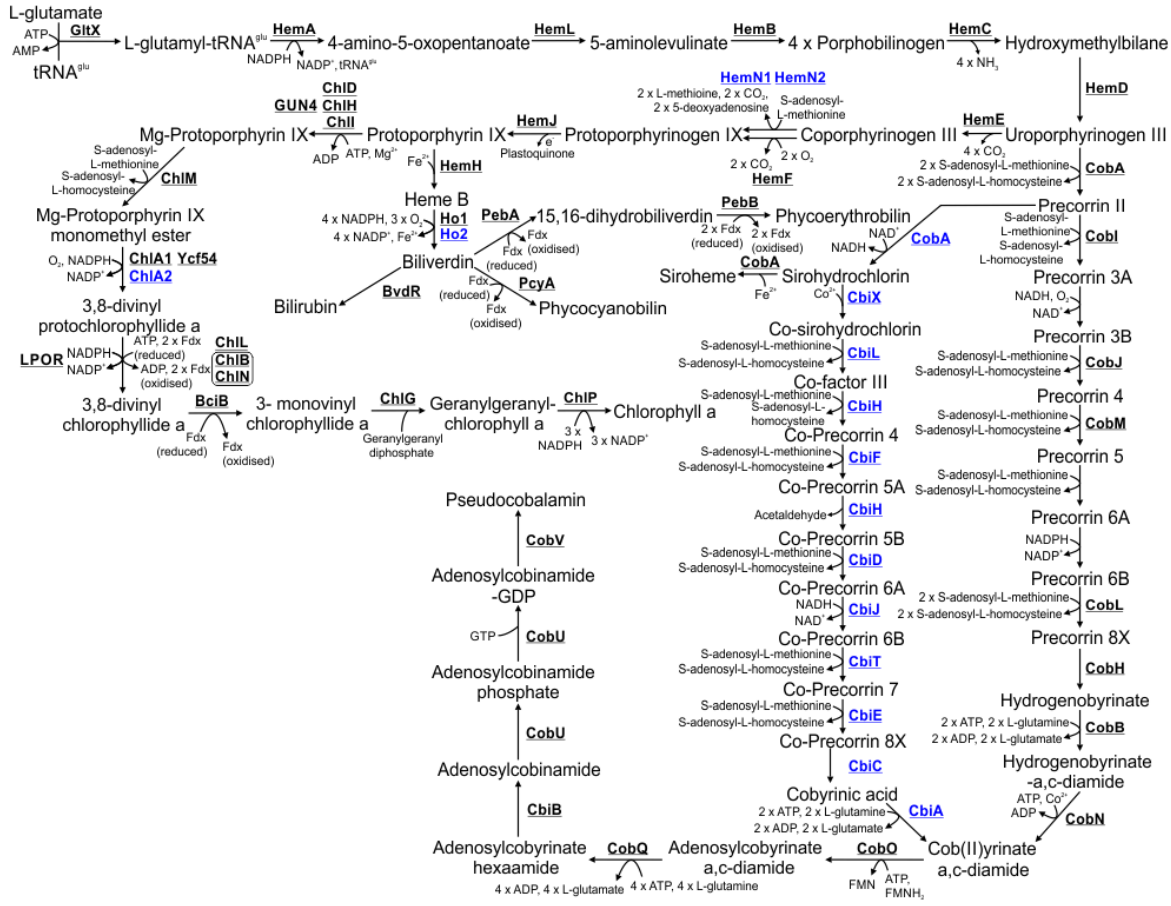

Figure 2.8 Metabolism of chlorophyll, phycobilin and pseudocobalamin. Proteins involved in anaerobic or low oxygen environment enzymatic steps are highlighted in blue. Cofactors in each reaction are shown with the exception of protons, water and inorganic phosphate.

2.3.8.1 Heme biosynthesis

Heme, the precursor of phycobilins, is synthesised from L-glutamate and $tRNA^{Glu}$ via ten enzymatic steps (**Figure 2.8**). All enzymes, apart from HemJ, are highly conserved between *E. coli* and PCC 6803 (Appendix Table 2.1) (346). In contrast to *E. coli*, HemJ, not HemG or HemY, is the protoporphyrinogen IX oxidase most commonly found in cyanobacteria (347). HemJ likely requires plastoquinone as an electron acceptor in *C. reinhardtii* (348) and localisation of PCC 6803 HemJ to the TM (183) suggests a similar enzymatic reaction (347,349). The PCC 6803 genome also encodes additional enzymes expressed under micro-oxic conditions, including HemN1 (and possibly HemN2) (350), which can catalyse the eighth enzymatic step of heme biosynthesis, in addition to Ho2 (351,352) and ChlA2 (353), which are involved in bilin and chlorophyll biosynthesis, respectively. It should be noted that these enzymes still require oxygen for catalytic activity. However, they may bind oxygen with greater affinity than the enzymes catalysing the same step which are expressed under non-microoxic conditions. Heme does not accumulate in mutants deficient in Ho1 and Ho2, which catalyse the first steps in bilin biosynthesis, suggesting that heme is rapidly degraded by an uncharacterised pathway (352) or is exported.

2.3.8.2 Bilin biosynthesis

Heme is the substrate for biosynthesis of biliverdin, which in turn is the substrate for production of the pigments phycocyanobilin and phycoerythrobilin. These pigments are subsequently incorporated into the light-harvesting phycobilisome complex (354). PCC 6803 only produces phycocyanobilin via the enzyme PcyA (354). PCC 6803 also encodes a biliverdin reductase, BvdR, resulting in production of bilirubin (355). While the exact role of bilirubin has not been determined, deletion of BvdR results in a mutant with severely attenuated phycobilisomes.

2.3.8.3 Chlorophyll biosynthesis

Chlorophyll, the main pigment in photosystems, is synthesised from protoporphyrin IX, the immediate precursor of heme, via seven enzymatic steps. The complete pathway has been characterised in PCC 6803. The first step of chlorophyll biosynthesis is catalysed by three magnesium chelatase enzymes, ChlD, ChlH and ChlI, resulting in production of Mg-protoporphyrin IX (356). GUN4 is also essential for magnesium chelatase activity (357–359). The second step is catalysed by ChlM (360), while the third is catalysed via ChlA1 (AcsF) or ChlA2 (361). Ycf54 is also required for ChlA1 activity (362). Two independent enzymes, a ferredoxin-dependent DPOR complex or a light-dependent NADPH:protochlorophyllide reductase (LPOR), can catalyse the

following step (363), while BciB catalyses the step after this (364,365). Geranylgeranyl is incorporated into chlorophyll by ChlG in the second last step. In a landmark paper, expression of ChlDHI and GUN4, ChlM, AcsF, LPOR, BciB, ChlG and ChlP in *E. coli* was sufficient for chlorophyll biosynthesis (366), demonstrating that no other enzymes are required in this pathway.

2.3.8.4 Pseudocobalamin biosynthesis

Cobalamin (Vitamin B_{12}) is required for activity of MetH, involved in methionine biosynthesis (**Figure 2.3**), and may be required by certain enzymes in the quinone and folate biosynthesis pathways (367). Cyanobacteria produce an alternate form of vitamin B_{12} termed pseudocobalamin (368). Vitamin B_{12} is synthesised from the heme biosynthetic intermediate, uroporphyrinogen III. The cob(II)yrinate a,c-diamide component of vitamin B_{12} can be synthesised by either an aerobic or anaerobic pathway, which share certain enzymes (369). These pathways have been characterised in a range of heterotrophic bacteria (369,370) but relatively few cyanobacterial enzymes have been investigated. PCC 6803 encodes all the enzymes in the anaerobic pathway but is missing five in the aerobic pathway (CobG, CobF, CobK, CobS, CobT), suggesting that this biosynthetic route is not utilised (Appendix Table 2.1). Several enzymes involved in converting cob(II)yrinate a,c-diamide to pseudocobalamin (CobO, CobQ, CbiB, CobU, CobV) are potentially encoded in the PCC 6803 genome. However, the exact biosynthetic steps have not been determined and the pathway in PCC 6803 can only be speculated based on characterised pathways from species that synthesise cobalamin (369).

PCC 6803 also has the genetic potential to produce siroheme from the pseudocobalamin biosynthetic intermediate, sirohydrochlorin. Siroheme is a cofactor required for nitrite reductase (371) and possibly for other enzymes.

2.3.9 Transport systems

The majority of proteins potentially involved in metabolite transport localise to the PM (**Figure 2.9**) (183). However, there are many putative transporters in PCC 6803 with no assigned function (Appendix Table 2.4), suggesting that our knowledge of cyanobacterial metabolite transport is still incomplete.

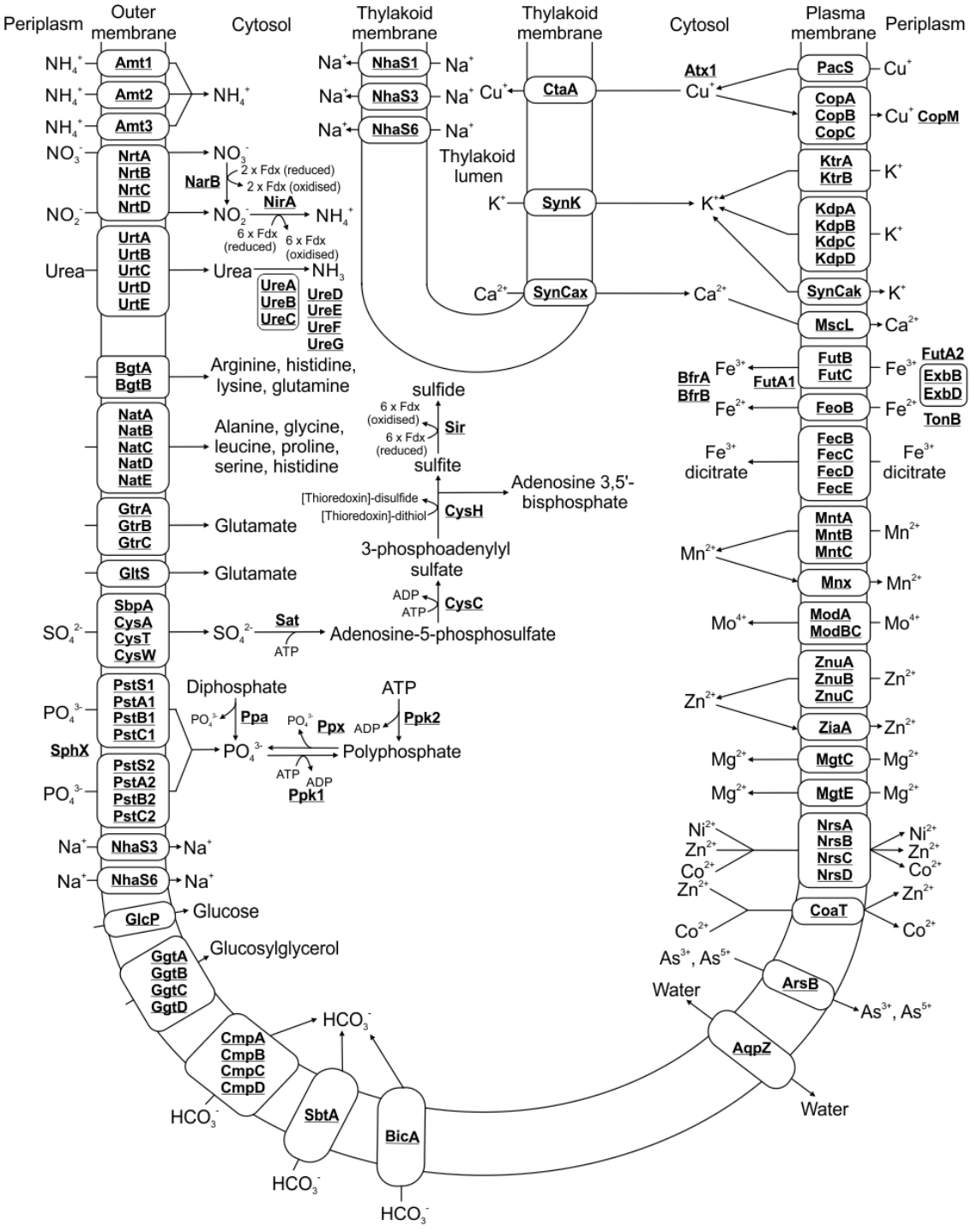

Figure 2.9 Proteins involved in metabolite transport and conversion of nitrogen, sulfur and phosphate based compounds. Localisation of transporters in either the PM or TM is detailed. Subunits in each complex may not all be membrane localised but soluble. Cofactors in each reaction are shown with the exception of protons, water, oxygen and inorganic phosphate.

2.3.9.1 Ammonia, nitrate, nitrite and urea transport

A range of transporters are responsible for import of nitrogen-based compounds. PCC 6803 encodes three ammonium transporters (Amt1, Amt2, Amt3), with Amt1 being responsible for the majority of uptake (372). Another transporter complex, comprising four subunits, NrtA-D, imports nitrate and nitrite (373–375). Nitrate is reduced to nitrite by NarB (376), while NirA converts nitrite to ammonium (377). Both enzymes require electrons supplied by ferredoxin (371). PCC 6803 can also utilise urea, which is imported into the cell via a transporter complex composed of five subunits, UrtA-E (378). Urea is converted to two molecules of ammonia via the urease complex comprising three subunits, UreA-C, which is assembled by four accessory proteins, UreD-G (379).

2.3.9.2 Amino acid transport

A range of permeases with affinity for different amino acids have been characterised in PCC 6803 in an extensive study conducted by Quintero *et al.* (380). The basic amino acid transporter encoded by BgtA and BgtB mediates transport of L-arginine, L-histidine, L-lysine and L-glutamine. Two transporters, the Gtr complex composed of GtrA-C, and the single protein GltS system, mediate L-glutamate transport. The neutral amino acid system encoded by NatA-E mediates transport of L-alanine, glycine, L-leucine, L-proline, L-serine and L-histidine. A separate study also implicated this transporter in import of L-cysteine (381). Whether these transporters can export amino acids or transport any of the other ten amino acids is unknown. It is also possible that uncharacterised permeases may play a role in transport of other amino acids.

2.3.9.3 Metal ion transport

The PCC 6803 genome encodes a range of transporters mediating import of metal ions into the cytosol, and in the case of Cu^+, into the thylakoid lumen. Additional transporters are also required for metal homeostasis and efflux.

2.3.9.3.1 Copper transport

Three copper (Cu^+) transporters, CtaA, PacS and the Cop complex, have been characterised in PCC 6803. Cyanobacteria require Cu^+ in the thylakoid lumen for the electron carrier plastocyanin. Proteome mapping of PCC 6803 localised PacS to the PM and CtaA to the TM (183), suggesting these are the main Cu^+ importers in each membrane (382). A chaperone, Atx1, likely localises to the cytosol but possibly also the thylakoid lumen, binds Cu^+ and delivers it to proteins requiring it

for enzymatic activity (383,384). The Cop complex, composed of CopA-C, is involved in Cu^+ efflux (385). An additional protein, CopM, binds Cu^+ in the periplasm and mutants lacking this protein are highly sensitive to elevated levels of Cu^+ (386).

2.3.9.3.2 Potassium transport

PCC 6803 encodes two PM localised potassium (K^+) uptake systems, Ktr (KtrA/KtrB) and Kdp (KdpA, KdpB, KdpC, KdpD) (387). The Ktr system mediates rapid K^+ uptake while the Kdp system maintains K^+ levels under limiting conditions in the environment (387,388). KtrC was initially incorrectly assigned as a subunit of the Ktr complex (389), but was later assigned to monoglucosyldiacylglycerol synthesis, not K^+ import (301). A third TM localised transporter, SynK (390), is responsible for K^+ efflux from the thylakoid lumen (391). An additional calcium activated transporter, SynCak, localised to the PM, may also be involved in potassium transport (392). Deletion of SynCak in PCC 6803 results in a mutant with altered membrane potential and greater resistance to zinc.

2.3.9.3.3 Calcium transport

Calcium (Ca^{2+}) transport is not well understood in cyanobacteria. A putative Ca^{2+}/H^+ antiporter, SynCax, has been identified (393,394), and localises to the TM (183). A PM localised Ca^{2+} importer has not been identified. MscL has been proposed to be involved in Ca^{2+} export (395).

2.3.9.3.4 Iron transport

Iron is potentially imported into PCC 6803 via multiple transporters. FeoB, which imports Fe^{2+}, is one of the main iron transporter in PCC 6803 (396). In the Fut system, a periplasmic protein, FutA2, bind Fe^{3+} (397,398) prior to uptake by the FutB/FutC membrane transporter (399). A second FutA protein, FutA1, has been postulated to bind Fe^{3+} in the cytosol (396), although proteome mapping localised it to the PM (183). Three ExbB-ExbD complexes identified in PCC 6803, possibly in association with TonB and one to three putative FhuA OM transporters, are also required for iron uptake (400,401). Once imported, iron is stored in ferritin complexes (BfrA, BfrB) in the cytosol (402). PCC 6803 also encodes subunits of a putative Fe^{3+} dicitrate transporter, although this system is reportedly less important for iron import (271).

2.3.9.3.5 Manganese, molybdate, zinc and magnesium transport

Manganese (Mn^{2+}) is imported into PCC 6803 via the MntABC complex (403), although other low-affinity transport systems may be present. Mn^{2+} plays a key role in the oxygen evolving centre of photosystem II. Mnx, is essential for tolerance of PCC 6803 to high manganese levels and may play a role in exporting Mn^{2+} from the cytosol to the thylakoid lumen (404). The PCC 6803 genome encodes proteins (ModA and ModBC) with high homology to the characterised molybdate transporter of *E. coli* (E-values = 6.25E-37 and 9.E-51, respectively) (405), but this complex has not been characterised in a cyanobacterium. The zinc (Zn^{2+}) transporter, composed of the ZnuA, ZnuB and ZnuC subunits, is highly conserved between *E. coli* and PCC 6803 (Appendix Table 2.1). Only the ZnuA protein has been characterised in PCC 6803 (406). A separate protein, ZiaA, is involved in Zn^{2+} export (407). Atx1 may also act as a Zn^{2+} chaperone, in addition to its role as a Cu^{2+} chaperone (408). The PCC 6803 genome also encode two putative magnesium transport proteins, MgtC and MgtE (409), both of which localise to the PM (183).

2.3.9.3.6 Cation efflux systems

A number of cation efflux systems are encoded by the PCC 6803 genome. The Nrs complex (NrsA, NrsB, NrsC, NrsD) was induced when cells were exposed to excess Ni^{2+}, Co^{2+} and Zn^{2+}, the CoaA transporter when cells were exposed to Co^{2+} and Zn^{2+}, and the ArsB transporter by exposure to arsenic (410).

2.3.9.3.7 Sulphate transport

Sulphate is transported into cells by the SbpA/CysA/CysW/CysT system, which is highly conserved between *E. coli* and PCC 6803 (Appendix Table 2.1). Sulphate is converted to sulphide by the assimilatory pathway divided into four enzymatic steps. The enzymes catalysing the final three steps are conserved between *E. coli* and PCC 6803. The first enzyme in the pathway, Sat, is widely conserved in bacteria capable of sulphate reduction.

2.3.9.3.8 Phosphate transport

PCC 6803 contains two systems for phosphate uptake, Pst1 and Pst2, each composed of four subunits (411,412). The PstS subunits of each system, in addition to SphX, bind phosphate in the periplasm, prior to uptake (412). Following uptake, phosphate can be stored in polyphosphate, which consists of polymers containing tens to hundreds of phosphates. Phosphate is converted to

polyphosphate by polyphosphate kinase (Ppk1), via sequential addition of single residues (413). A second Ppk enzyme, Ppk2, homologous to an enzyme characterised in *Pseudomonas aeruginosa* (414), likely synthesises polyphosphate from ATP. Ppx catalyses depolymerisation of polyphosphate, releasing inorganic phosphate (413). Another enzyme, Ppa, converts diphosphate to phosphate and is essential in PCC 6803 (413).

2.3.9.4 Sodium antiporters

PCC 6803 encodes six putative sodium (Na^+) antiporters (415), three of which localise to the TM (NhaS1, NhaS3, NhaS6) and two to the PM (NhaS2, NhaS5) (183). Only NhaS3 is essential in PCC 6803 (416). NhaS3 has been suggested to play a role in maintaining not just H^+ and Na^+, but also K^+ homeostasis (417). Deletion of the remaining Nha antiporters did not affect growth, even when cells were exposed to high salt concentrations, suggesting that these proteins can compensate for loss of each other (416).

2.3.9.5 Organic and inorganic carbon transport

PCC 6803 encodes transporters that import a range of organic carbon compounds. These include GlcP that imports glucose (205) and the Ggt complex, which imports glucosylglycerol and possibly sucrose and trehalose (418,419). A number of transporters for inorganic carbon have been characterised in PCC 6803. These play a key role in the CO_2-concentrating mechanism during photosynthesis, and include the Cmp complex (BCT1 transporter) (420,421), the SbtA transporter (422,423) and the BicA transporter (424).

2.3.9.6 Water transport

PCC 6803 encodes an aquaporin water channel, *aqpZ*, which is required for regulating osmotic stress (425), and is essential for mixotrophic growth (426).

2.4 Discussion

2.4.1 Future directions in understanding cyanobacterial metabolism

This work provides a basis for better understanding of cyanobacterial metabolism and transport processes. However, gaining a complete understanding of cyanobacterial metabolism will likely be dependent on optimising the slow process of mutant generation and characterisation, or developing bioinformatics tools which provide better insight into protein function. To bypass the laborious step of mutant generation, the novel cyanobacterial mutant library, CyanoSource, has been constructed. This mutant library aims to target every gene in PCC 6803. Construction of the library is outlined in Gale *et al*. (130). Building on transformation of PCC 6803 and Modular Cloning (MoClo) techniques (40,42) (Section 1.2.3.3), the generation of a whole genome library of gene insertion plasmids (representing 3,456 coding sequences (CDSs)), will be transformed into PCC 6803 to generate the largest available collection of known and novel cyanobacterial mutant strains.

This library will allow the field to determine the essential PCC 6803 gene set, which can be compared to the one generated in PCC 7942 via transposon mutagenesis (129). This will provide insight into the essential gene set of the phylum. CyanoSource may also provide insights into the function of many proteins involved in metabolism within a consistent strain background (427). Generation of auxotrophic mutants will provide strong evidence that the encoded protein is involved in the same pathway as putative characterised homologues from other species. However, deletion of these genes may only be possible if the metabolite the encoded protein plays a role in synthesising can be imported into the cell. Research groups with expertise in enzyme and pathway characterisation but lacking expertise in generation of cyanobacterial mutants may also be encouraged to investigate the function and enzymatic activity of cyanobacterial proteins, especially in light of recent high-impact publications on characterisation of PCC 6803 enzymes and pathways (246,272). The formation of detailed metabolic pathways and maps will also aid future bioinformaticians and computational biologists in their work, such as modelling of flux within cyanobacteria.

2.4.2 Applying this dataset to understanding metabolism and transport in other cyanobacteria

As mentioned above, Section 1.1.4, PCC 6803 is a model organism for studying cyanobacteria due to a number of traits. Since it is likely that a high proportion of the pathways discussed in this chapter are conserved throughout the phylum, understanding PCC 6803 metabolism, along with

detailed metabolic maps, will aid our characterisation of cyanobacterial species that play a key role in the environment e.g. marine *Prochlorococcus* and *Synechococcus* species or which have characteristics ideal for biotechnology, such as the fast growing cyanobacteria, *Synechococcus* sp. PCC 11901 (51). This will be critical in the optimisation of biotechnologically relevant species which have the potential as renewable platforms for production of chemicals which are currently derived from fossil fuels.

2.4.3 Concluding Remarks

Although this work will aid scientists in better understanding metabolism and transport within the model organism PCC 6803, and in cyanobacteria in general, it also highlights the large gaps in our knowledge about this phylum. Better understanding will require extensive analysis of the kinetics and localisation of enzymes which are homologous to characterised enzymes from heterotrophic bacteria but also identification of novel cyanobacterial enzymes that may perform functions specific to this phylum.

Chapter 3

Characterisation of growth, metabolism and the photosynthetic properties of *Synechococcus* sp. PCC 11901

Sections of this chapter have previously been published in Biomolecules 12 (7)

Development of a Biotechnology Platform for the Fast-Growing Cyanobacterium Synechococcus sp. PCC 11901.

Mills, L.A.; Moreno-Cabezuelo, J.Á.; Włodarczyk, A.; Victoria, A.J.; Mejías, R.; Nenninger, A.; Moxon, S.; Bombelli, P.; Selão, T.T.; McCormick, A.J.; Lea-Smith, D.J. Biomolecules 12 (7)

Chapter 3: Characterisation of growth, metabolism and the photosynthetic properties of *Synechococcus* sp. PCC 11901

3.1 Introduction

3.1.1 Fast-growing strains with the potential for large biomass accumulation

Developing innovative carbon-neutral technologies to substitute for fossil fuel-derived synthetic routes for bulk chemical and high-value material production is one of the great challenges of the 21st century. However, commercialisation of cyanobacteria as potential green platforms is dependent on genetically engineering fast-growing strains with high biomass and compound production.

Fast-growing, heterotrophic species already used in industry, such as *E. coli* and *S. cerevisiae*, have doubling times of approximately 20 and 90 minutes, respectively (428,429). In recent years, several newly discovered cyanobacterial species with faster doubling times similar to *S. cerevisiae* have been described including *Synechococcus* sp. PCC 7002 (PCC 7002) *Synechococcus elongatus* UTEX 2973 (UTEX 2973) (45) *Synechococcus elongatus* PCC 11801 (49) and *Synechococcus* sp. PCC 11901 (PCC 11901) (51). PCC 11901 reportedly maintains fast growth over extended periods and achieves higher biomass accumulation than PCC 6803, PCC 7942, UTEX 2973 and the closely related species, PCC 7002, when cultured at 30°C and 38°C (51). In comparison, two separate studies have shown that the growth of UTEX 2973 was slower than PCC 6803 and PCC 7942 when cultured at 30°C (42,51). However, PCC 11901 has not been tested under optimal growth conditions for UTEX 2973, as described in Ungerer *et al.* (191), at 38°C with 900 µmol photons m^{-2} s^{-1} and sparged with 5% CO_2.

Like other model cyanobacteria, PCC 11901 is naturally transformable but has the added advantage of maintaining a fast growth phenotype over a wide temperature range and can be grown in media with similar salinity to seawater, suggesting it may be suitable for outdoor cultivation without utilizing freshwater resources. In contrast, UTEX 2973 is a freshwater species and is sensitive to salt stress. Although attempts have been made to generate a salt-tolerant mutants by introducing the glucosylglycerol pathway and overexpression of glycerol-3-phosphate dehydrogenase. The growth rates of the mutants were still reduced compared to the wild-type UTEX 2973 strain and so therefore may not be compatible for commercial applications (430,431).

3.1.2 *Synechococcus* sp. PCC 11901: truly a better strain for biotechnology?

Although PCC 11901 demonstrates many characteristics that make it potentially useful for biotechnology, further testing and adaptation of this species is required to determine whether it is suitable for commercial applications. A further disadvantage is that our understanding of metabolism and the photosynthetic properties of PCC 11901 is limited. This knowledge is required to perform metabolic modelling, flux analysis and may also provide insight into the physiological features underlying the fast, sustained growth phenotype of PCC 11901. Moreover, a recent analysis suggests that factors other than fast growth are also critical for high phototrophic productivity, including the rate of light absorption, photosynthetic efficiency and the conversion rate of photons to biomass (432).

Although PCC 11901 has shown great potential as a biotechnology platform, only one, in-depth study has been carried out at the time of writing. Despite its ability to accumulate biomass at an unprecedented rate, PCC 11901 has not been compared directly with UTEX 2973 at the optimal growth conditions of UTEX 2973. This is required to determine whether PCC 11901 outperforms other fast growing species.

3.1.3 Chapter aims and objectives

There are two main goals for this chapter. The first is to determine if PCC 11901 grows faster and accumulates higher biomass compared to a range of model organisms, even under the optimal growth conditions for UTEX 2973. The second aim is to understand the underlying metabolic, genetic and biochemical properties which may contribute to the fast growth phenotype seen in PCC 11901. This was carried out using a compilation of bioinformatic and oxygen evolution analysis.

3.2 Materials and Methods

3.2.1 Strains and culture conditions

3.2.1.1 Synechocystis sp. PCC 6803

The *Synechocystis* sp. PCC 6803 glucose tolerant strain (204) was originally obtained from the Saul Purton laboratory, University College London.

3.2.1.1.1 Routine growth conditions

Liquid cultures of PCC 6803 cells were routinely grown at 30°C under continuous 40 µmol photons m^{-2} s^{-1} warm white LED light in liquid BG11 minimal media (433), with shaking at 120 rpm in an Algaetron Growth Chamber (Photon Systems Instruments). PCC 6803 was maintained on BG11 1.5% (w/v) agar plates supplemented with 10 mM of TES (pH 8.2) and 19 mM $Na_2S_2O_3$. Plates were also stored at 30°C under continuous 40 µmol photons m^{-2} s^{-1} warm white LED light in an Algaetron Growth Chamber (Photon Systems Instruments). For long-term storage, 50 mL of culture in exponential growth phase was pelleted by centrifugation at 3,200 x *g*, washed twice in BG11 medium, and re-suspended in 0.8 mL BG11 medium. The re-suspended cells were thoroughly mixed with 0.2 mL filter-sterilised 80% (v/v) glycerol in water, flash-frozen in liquid nitrogen, and stored at -80°C. Strains were revived by streaking a small amount onto a solid BG11 plate (40).

3.2.1.2 *Synechococcus* sp. UTEX 2973

Two UTEX 2973 strains were used for this study. One strain was obtained from The UTEX Culture Collection of Algae (434). The other was kindly gifted from the Himadri Pakrasi laboratory, University of Washington in St Louis. These are henceforth known as UTEX 2973 and UTEX 2973 Washington, respectively. Growth conditions were the same as described in Section 3.2.1.1.1.

3.2.1.3 *Synechococcus* sp. PCC 7942

The *Synechococcus* sp. PCC 7942 strain was obtained from the Pasteur Culture Collection of Cyanobacteria (PCC). Growth conditions were the same as described in Section 3.2.1.1.1.

3.2.1.4 *Synechococcus* sp. PCC 11901

The *Synechococcus* sp. PCC 11901 glucose tolerant strain was a kind gift from the Peter Nixon laboratory, Imperial College London.

3.2.1.4.1 Routine growth conditions

Liquid cultures of PCC 11901 cells were grown at 30°C under continuous 40 µmol photons m^{-2} s^{-1} warm white LED light in liquid AD7 with shaking at 120 rpm in an Algaetron Growth Chamber (Photon Systems Instruments). PCC 11901 was maintained on AD7 1.2% (w/v) agar plates supplemented with 12.6 mM $Na_2S_2O_3$ as described by Włodarczyk *et al.* (51). Plates were also stored at 30°C under continuous 40 µmol photons m^{-2} s^{-1} warm white LED light in an Algaetron Growth Chamber (Photon Systems Instruments). Long-term storage was carried out as described in Section 3.2.1.1.1, but cells were grown in AD7 media instead of BG11.

3.2.2 Growth curve conditions

3.2.2.1 Quantification of strains using optical density

To quantify the growth of cells, 1 mL of liquid culture was used to record the optical density (OD) at 750 nm using a Jenway 6305 Genova spectrophotometer. If the optical density was >1.0, then cultures were diluted with their corresponding media appropriately. This is due to the linear relationship between OD and concentration being accurate at low concentrations (OD < 1.0), according to the laws of Beer-Lambert (435).

3.2.2.2 Multicultivator MC-1000 growth conditions

To determine growth rates, starter cultures were used to inoculate 80 mL cultures in cylindrical cultivation tubes with a diameter of 30 mm to an OD_{750nm} of ~0.1. Tubes were placed into a MC-1000 multicultivator bioreactor (Photon Systems Instruments) and grown at 38°C under 125 µmol photons m^{-2} s^{-1} warm white LED light and sparging with 5% CO_2. After 24 hours of growth, the light intensity was increased to 500 µmol photons m^{-2} s^{-1}. After a further 24 hours of growth, cultures were diluted to an OD_{750nm} of ~0.1 to continue log-phase growth and the light intensity was increased to 900 µmol photons m^{-2} s^{-1}. The cultures were left for approximately 16 hours at 900 µmol photons m^{-2} s^{-1} to adapt cells to the new conditions of the bioreactor.

Samples were then diluted to an OD_{750nm} of 0.25 to start the growth experiment. Samples were collected every 12 hours for 72 hours for measurements. Parameters for the growth experiments were adapted from Ungerer *et al.* (191).

3.2.2.3 Measuring Biomass

After 72 hours of growth at 900 µmol photons m^{-2} s^{-1} and 38°C, 5 mL of culture was harvested from each strain. Cells were centrifuged at 5,000 x *g* and washed twice with sterile H_2O. Whatman 0.7 µM GF/B Glass Microfibre Filters of 70 mm diameter were measured on a microbalance three times to obtain an average filter weight. The washed cells were then added to the filter paper and left to dry for 24 hours at 70°C. Filter papers were then weighed again three times to obtain the average weight of the filter plus the biomass for each species. A student's unpaired *t* test was used to compare growth and biomass accumulation of PCC 11901 against the other cyanobacterial species, $P < 0.05$ being considered statistically significant.

3.2.3 Bioinformatic analysis

3.2.3.1 Bioinformatics analysis and generation of a metabolic and electron transport map for PCC 11901

Analysis similar to that described in Section 2.2, was carried out. However, for this analysis the proteome of PCC 11901 (CP040360.1) was used instead of *E. coli* K12. The metabolic pathway maps described in Chapter 2 were also altered to represent our findings from the analysis.

3.2.3.2 Identifying proteins in PCC 11901 that are truly unique when compared to PCC 6803 proteins

A list of all the sequences in PCC 11901's proteins which had no significant BLAST hit against any of the PCC 6803's proteins was generated. This was performed by extracting all the RefSeq IDs from the BLAST results taken from the tables generated in Section 3.2.3.1. This list was checked against the original proteome FASTA file for PCC 11901 downloaded from NCBI's proteome database. Any NCBI IDs that are present in the proteome FASTA file and not from the list generated from the BLAST output table were considered as truly unique proteins in the PCC 11901 proteome, compared to PCC 6803's proteins.

3.2.4 Oxygen electrode measurements

3.2.4.1 Determination of chlorophyll concentration in different species of cyanobacteria

Cultures were grown in an MC-1000 multicultivator bioreactor at 30°C under 125 µmol photons m^{-2} s^{-1} warm white LED light and sparging with 5% CO_2, until cultures reached an OD_{750nm} = ~1.0.

Cultures were then diluted/concentrated to an OD_{750nm} range between 0.02 – 10.0. For each sample the OD_{750nm} and OD_{680nm} was measured and recorded.

Chlorophyll in each sample was quantified by centrifuging 1 mL at 10,000 x *g* for 2 minutes. The supernatant was removed and the cells washed twice with phosphate buffered saline. Pre-cooled methanol, 1 mL, was then added and the cells were homogenized by vortexing at 2,000 rpm. Samples were covered in aluminium foil and cooled in the fridge for 20 minutes. Samples were centrifuged again, and the supernatant was measured at OD_{665nm} and OD_{720nm}. Chlorophyll *a* concentration (nmol/mL) was calculated using the equation $14.4892(OD_{665nm} - OD_{720nm})$ = Chl*a* nmol/mL from Ritchie, 2006 (436). Values were plotted to generate standard curves for each species chlorophyll content. The amount of chlorophyll in each species was determined by subtracting the 750nm OD value from the 680nm value and multiplying the total by the slope of the regression line calculated from the standard curves, as previously performed in Lea-Smith *et al*. for PCC 6803 (437).

3.2.4.2 Standard oxygen electrode conditions

Cultures were grown in an MC-1000 multicultivator bioreactor at 30°C under 125 µmol photons m^{-2} s^{-1} warm white LED light and sparging with 5% CO_2. Cells were harvested during log phase at an OD_{750nm} of ~1 and diluted to 1 nmol Chl^{-1} mL^{-1} for analysis of photoinhibition or 4 nmol Chl^{-1} mL^{-1} for photosynthesis and respiration measurements. All oxygen measurements were carried out using the appropriate media for each strain, and measurements were taken using the Oxytherm+ photosynthesis Clark-electrode (Hansatech Instruments, Kings Lynn, UK). Samples were maintained at 30°C and $NaHCO_3$ was added to each sample to a final concentration of 10 µM to act as a carbon source whilst samples were kept in the chamber.

3.2.4.3 Measuring the photosynthetic capacity of each species

For photosynthesis measurements cultures were first dark equilibrated for a 10 minutes dark period, before being subject to increasing levels of light for 10 minutes at 10, 25, 50, 150, 350, 900 and 2000 µmol photons m^{-2} s^{-1}, respectively. A 10 minutes dark period preceded each increase in light intensity. A total of 5-10 biological replicates was tested for each experiment.

3.2.4.4 Measuring the respiratory rate of each species

To determine the respiration rate, oxygen consumption was measured using the output from the oxygen electrode in the 10 minutes dark periods following the light intensities of 10, 25, 50, 150, 350, 900 and 2000 µmol photons m^{-2} s^{-1} for 10 minutes respectively. $NaHCO_3$ was added to each sample to a final concentration of 10 µM. A total of 5-10 biological replicates was tested for each experiment.

3.2.4.5 Measuring photoinhibition rates in each species

For photoinhibition experiments, samples were kept at 30°C in the oxygen electrode chamber in the dark for a 10 minutes period before being subjected to 2000 µmol photons m^{-2} s^{-1} of light. Photoinhibition experiments were conducted either in the absence or presence of lincomycin (200 µg mL^{-1}).

3.3 Results

3.3.1 PCC 11901 is the fastest growing species at 38°C with 900 µmol photons m^{-2} s^{-1} and 5% CO_2/Air

In a recently published comparison, PCC 11901 demonstrated faster growth and higher biomass accumulation than PCC 7002, UTEX 2973, PCC 7942 and PCC 6803 at 30°C under 750 µmol photons m^{-2} s^{-1} continuous light (51). PCC 11901 also outperformed PCC 7002 and UTEX 2973 at a higher temperature of 38°C and continuous light of 300 and 660 µmol photons m^{-2} s^{-1}. However, in each growth experiment 25 mL cultures were grown in 125 mL extra deep baffled flasks (Corning) in a chamber sparged with air/1% CO_2. This differs from the growth conditions in which UTEX 2973 was demonstrated to have optimal growth, specifically at 38°C under 900 µmol photons m^{-2} s^{-1} continuous light and with direct sparging of air/5% CO_2, in a MC-1000 multicultivator (191). In this study, we therefore cultured PCC 11901, UTEX 2973, PCC 7942 and PCC 6803 under these exact growth conditions to determine whether PCC 11901 would still outperform the other species. Two different UTEX 2973 strains were examined, one obtained from the UTEX collection, the other from the laboratory that performed the initial growth studies. Under these growth conditions, both UTEX 2973 strains demonstrated fast growth in the first 24 hours, similar to previous studies (45,191) and comparable to growth of PCC 11901 (**Figure 3.1**A). However, after this period, growth of both UTEX 2973 strains was considerably slower than PCC 11901 and by 48 hours had entered stationary phase at an OD_{750nm} = ~6. In contrast, after 72 hours PCC 11901 was OD_{750nm} = ~10 and growth was still in exponential phase. As demonstrated previously, growth of UTEX 2973 was faster than PCC 7942 and PCC 6803 (45). Moreover, biomass accumulation was significantly higher in PCC 11901 than the other species after 72 hours (**Figure 3.1**B). However, the OD_{750nm}/biomass (g/L) ratio was 1.7 in PCC 11901, compared to 2.88 in PCC 6803, 3.26 in PCC 7942, 2.9 in UTEX 2973 (UTEX) and 2.85 in UTEX 2973 (Washington), suggesting that spectrophotometry alone may not be a good method of determining growth of PCC 11901. This could be due to an increase in size of PCC 11901 cells, which has been reported to occur at later stages of growth (51) or to the other species entering or being in stationary phase when biomass was quantified. Overall, PCC 11901 demonstrated the fastest sustained growth of the species tested under these conditions, further emphasising its potential for biotechnology applications.

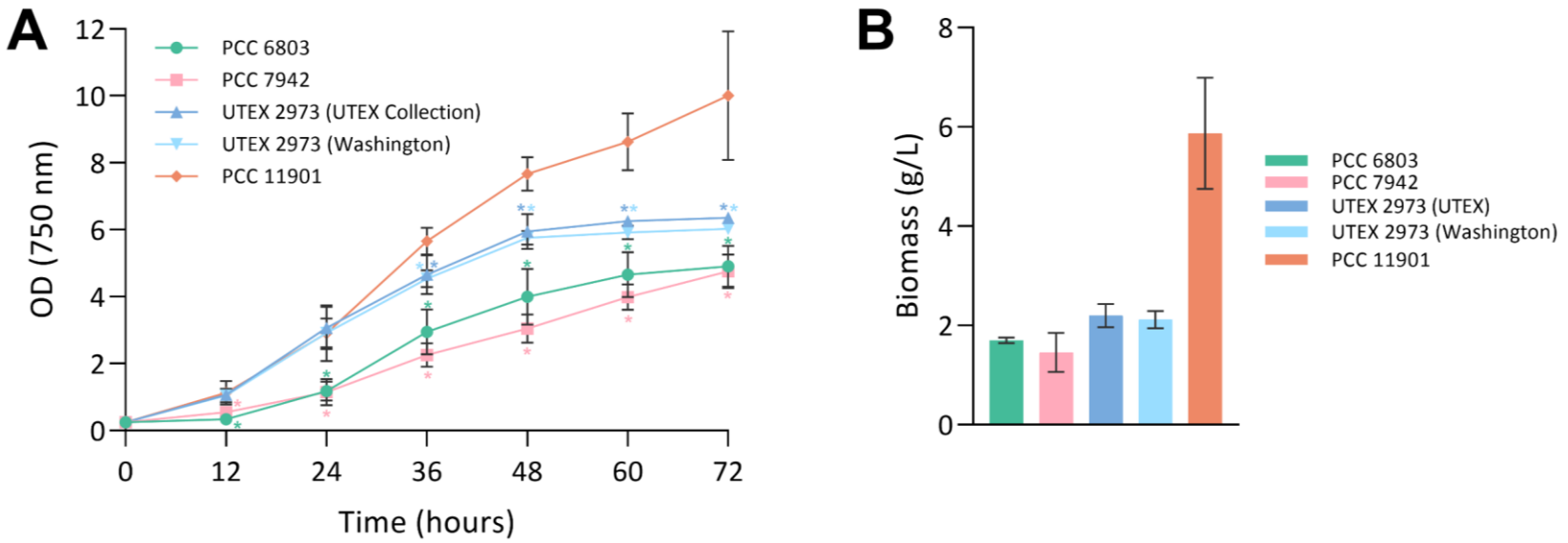

Figure 3.1 (A) Growth and (B) biomass accumulation of cyanobacterial species. Strains were cultured at 38°C under 900 µmol photons m^{-2} s^{-1} continuous light intensity and with direct sparging of air/5% CO_2. Error bars indicate standard deviation. Asterisks indicate significant differences between PCC 11901 and the other cyanobacterial species ($P < 0.05$).

3.3.2 Metabolism pathways are highly conserved between PCC 11901 and PCC 6803

The biological traits of PCC 11901 leading to faster growth have not been identified. To determine whether differences in metabolism are potentially responsible for differing growth rates and to develop a metabolic network which would aid future modelling, flux balance analysis and metabolic engineering, we performed a comparative genomics analysis of PCC 6803 versus PCC 11901 using the BLAST local databases (Appendix Table 3.1). To evaluate the metabolic and transport capacity of PCC 11901 we compared it to the pathways outlined in Chapter 2.

The PCC 11901 genome contains genes encoding most of the enzymes required for central metabolism, with a predicted 3,377 open reading frames (438)(**Figure 3.2**). However, there are a few exceptions. RpiB, a probable ribose phosphate isomerase is absent. However, a homologue encoding its isoenzyme, RpiA, is present in PCC 11901 and is likely sufficient for catalysing this reaction in the oxidative pentose phosphate (OPP) and Calvin-Benson-Bassham (CBB) pathways. Fba1 is also absent but is likely compensated by expression of Fba2. AckA, encoding acetate kinase, required for production of acetate via the Pta/AckA pathway is absent, although the homologue for Acs, required for an alternative acetate biosynthesis pathway, is present. Poor homology of PCC 11901 proteins is demonstrated to several enzymes involved in the OPP pathway (Transaldolase (Tal): E-value = 8.89e-08), branched glycogen catabolism (Isoamylase (GlgX1 and GlgX2): E-value = 2.54e-09 and 1.48e-12, respectively) and the TCA cycle (Isocitrate dehydrogenase (NADP+; Icd): E-value = 3.69e-15). However, a putative NADP+ dependent isocitrate dehydrogenase, encoded by WP_138073772.1 in the PCC 11901 genome, likely performs this last function. There are four putative phosphoglycolate phosphatase enzymes in PCC 6803, encoded by slr0458, slr0586, sll1349, and slr1762 (439), but only two of these (slr0458 and slr1762) have homologues in PCC 11901 with strong similarity (WP_138072486.1; E-value = 2.32e-62 and WP_030006614.1; 4.19e-46, respectively). The last enzyme in the photorespiration pathway, GlyK, is also absent in PCC 11901, which is also the case in PCC 7002. A comparison to PCC 7002 also demonstrated poor similarity of Tal (1e-07) and Icd (4e-15) with PCC 6803 homologues. Genes encoding proteins involved in polyhydroxybutyate biosynthesis are not present, as previously reported (51).

The majority of proteins involved in metabolism and degradation of nucleotide sugars and sugar osmolytes are present (**Figure 3.2**), except for genes encoding the proteins involved in sucrose degradation (Inv, Glk (sll0593)) and possibly FrkA (E-value = 3.4e-19). Homologues to RfbC, the third

enzyme in the TDP-rhamnose biosynthetic pathway, are not present in PCC 11901 or PCC 7002 and it is not known whether PCC 11901 synthesises rhamnose.

Pathways involved in metabolism of amino acids, cyanophycin, glutathione and iron-sulphur clusters are conserved between both species (**Figure 3.3**), with the exception of *gltD*, encoding the small subunit of the NADH-dependent glutamate synthase. Likewise, pathways involved in nucleotide metabolism are highly conserved between both species (**Figure 3.4**) with the exception of the putative thymidylate synthase ThyX. The Dgt and CodA nucleotide salvage pathways (440) are absent in PCC 11901. Metabolism of vitamins and co-factors is similar between both species (**Figure 3.6**), except for the absence of homologs encoding NadV and NadM, which convert nicotinamide to NAD^+.

Compared to PCC 6803, cell wall metabolism in PCC 11901 is similar except it lacks one of the desaturases encoded by PCC 6803 (DesD), produces hydrocarbons via the Ols pathway, instead of via FAD/FAR, which is similar to PCC 7002 (**Figure 3.7**) (294), and does not contain genes encoding penicillin binding proteins 6 and 7. Metabolism of isoprenoids, quinols, carotenoids, chlorophyll, phycobilin and pseudocobalamin is also similar, except PCC 11901 does not contain genes encoding the hopene biosynthetic pathway and as previously reported, it lacks multiple genes in both the anaerobic and aerobic pseudocobalamin (vitamin B_{12}) pathway (**Figure 3.8**, **Figure 3.9**) (51).

Genes encoding subunits of many transporters are also absent in the PCC 11901 genome (**Figure 3.10**). These include transporters importing basic amino acids (Bgt complex) and glutamate (Gtr complex, GltS), suggesting that only the Nat complex can import amino acids. Potassium transport systems are greatly reduced in PCC 11901, which lack the Kdp K^+ import complex and the thylakoid membrane localised SynK protein, required in PCC 6803 for optimal photosynthesis (391). Subunits of the magnesium (MgtC) and the sulphate import complexes (SbpA) and the Nrs complex, exporting nickel, zinc and copper (**Figure 3.8**) are also absent in PCC 11901. GlcP, involved in glucose uptake is absent in PCC 11901, possibly explaining the inability of this species to grow heterotrophically on glucose (51).

Genes not encoding proteins involved in central metabolism, electron transport and light harvesting, or with unknown function, but conserved in PCC 6803 and PCC 11901, are listed in Appendix Table 3.2. We did not investigate pathways absent in PCC 6803 that may be present in PCC 11901 (Appendix Table 3.3). There are 353 PCC 11901 genes which are distinctly different from

any homologues in PCC 6803 and it is possible that some may encode for enzymes synthesising metabolites that could play a role in enhancing growth in this organism.

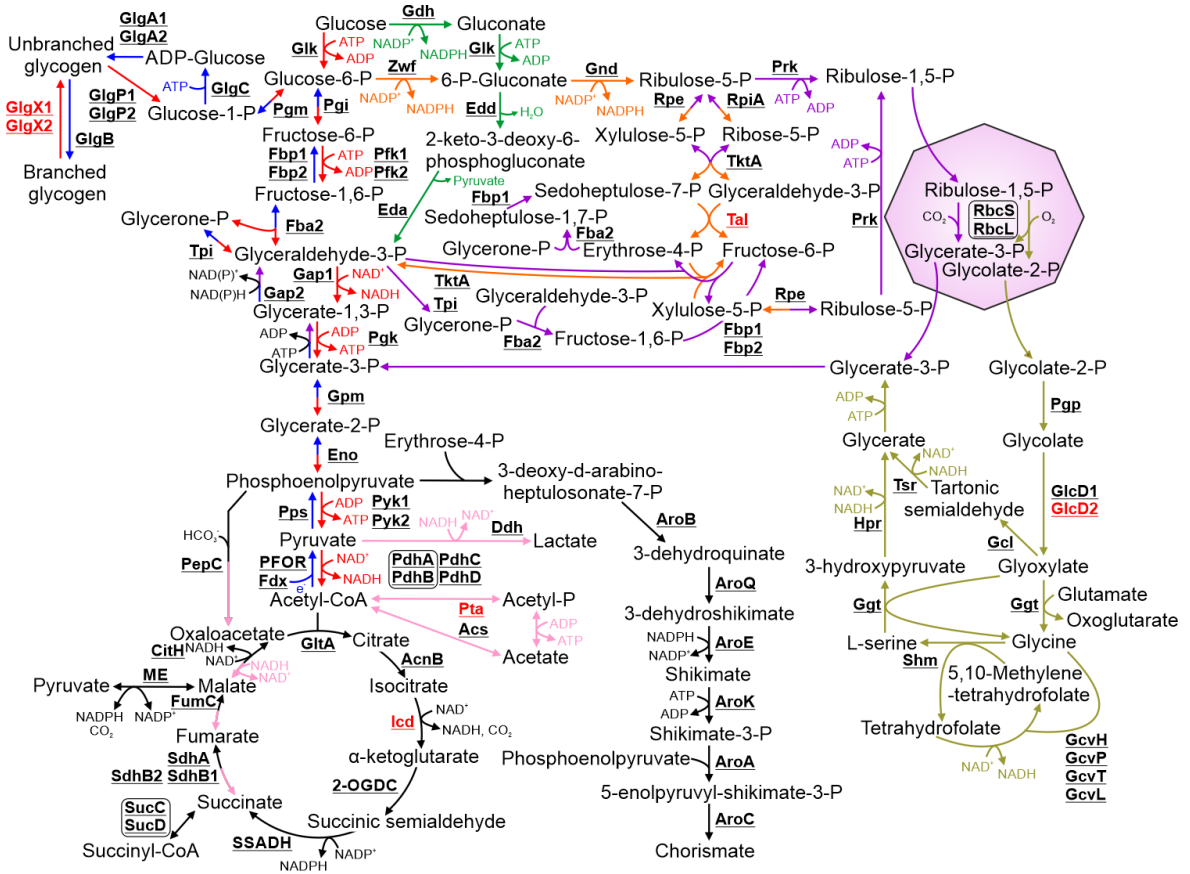

Figure 3.2 Schematic detailing the pathways involved in PCC 11901 central metabolism. Biosynthetic steps involved in glycolysis and gluconeogenesis are highlighted in red and blue respectively. Steps in the Entner-Doudoroff pathway are highlighted in green. Steps involved in the oxidative pentose phosphate pathway and the Calvin-Benson-Bassham cycle are highlighted in orange and purple, respectively. Fermentation pathways are highlighted in pink. Photorespiration pathways are highlighted in olive. Where enzymes catalyse reactions in two pathways, the arrows are split between their respective colours. The carboyxsome is represented as a purple octagon. Cofactors in each reaction are shown with the exception of protons, water, oxygen and inorganic phosphate. Proteins with low sequence similarity to PCC 6803 enzymes are highlighted in red.

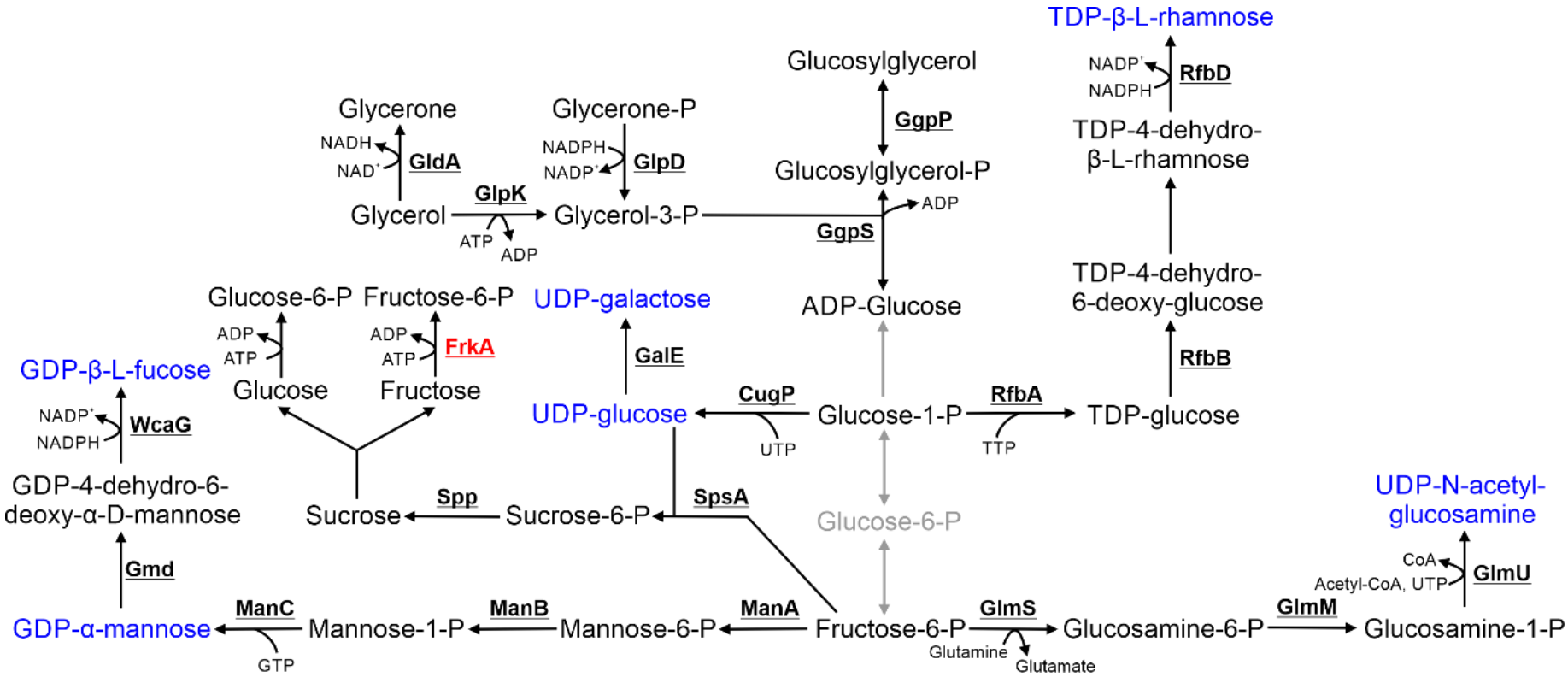

Figure 3.3 Metabolism and degradation of nucleotide sugars and sugar osmolytes in PCC 11901. Compounds highlighted in blue are substrates for lipopolysaccharide biosynthesis. Steps highlighted in grey are compounds and reactions involved in these pathways but detailed in Figure 3.2. Cofactors in each reaction are shown with the exception of protons, water, oxygen and inorganic phosphate. Proteins with low sequence similarity to PCC 6803 enzymes are highlighted in red.

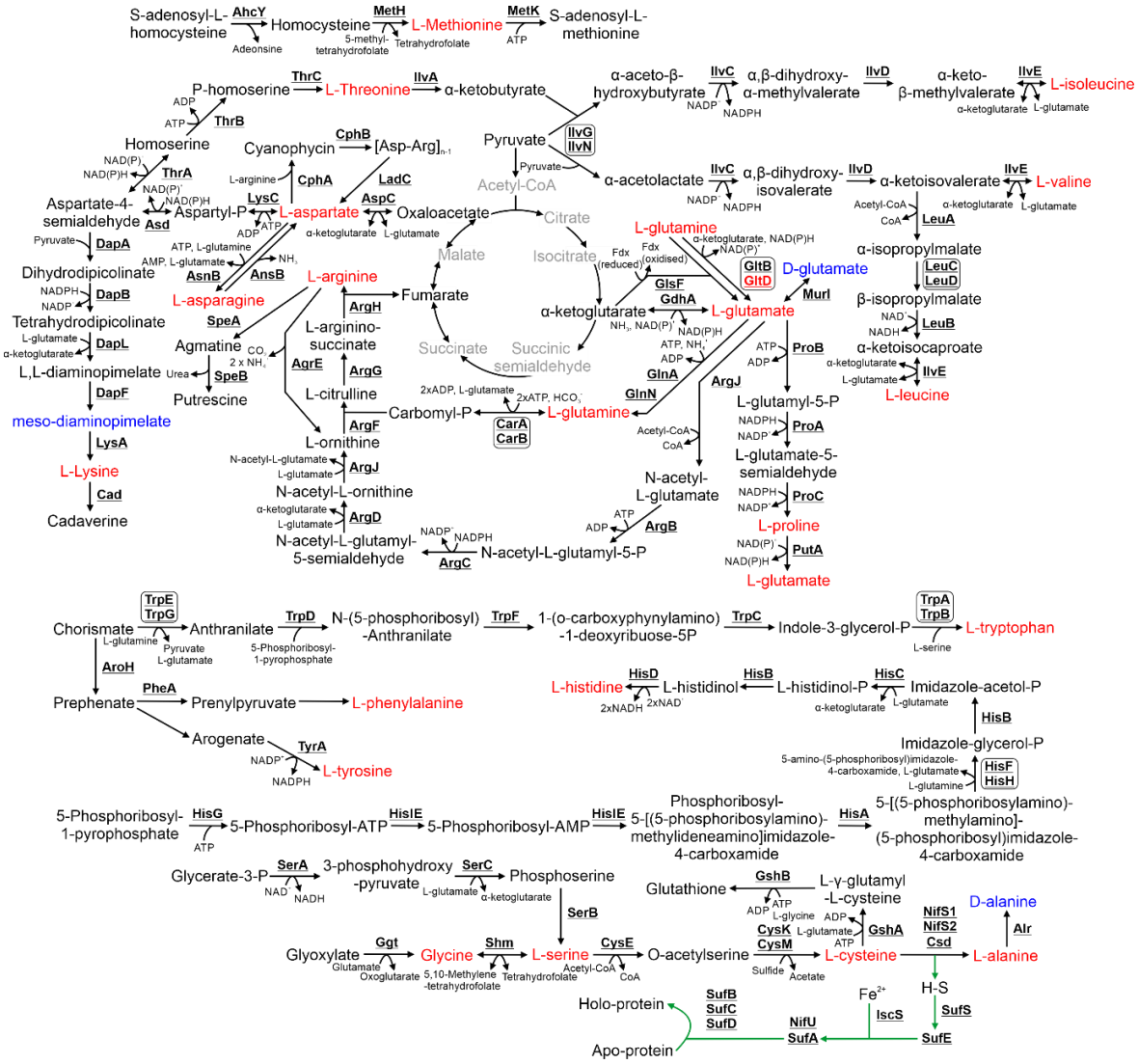

Figure 3.4 Metabolism of amino acids, cyanophycin, glutathione and iron-sulphur clusters in PCC 11901. The twenty L-amino acids are highlighted in red while amino acids incorporated into peptidoglycan are highlighted in blue. The iron-sulphur biosynthetic pathway is highlighted in green. Steps highlighted in grey are compounds and reactions involved in these pathways but detailed in Figure 3.2. Cofactors in each reaction are shown with the exception of protons, water, oxygen and inorganic phosphate. Proteins with low sequence similarity to PCC 6803 enzymes are highlighted in red.

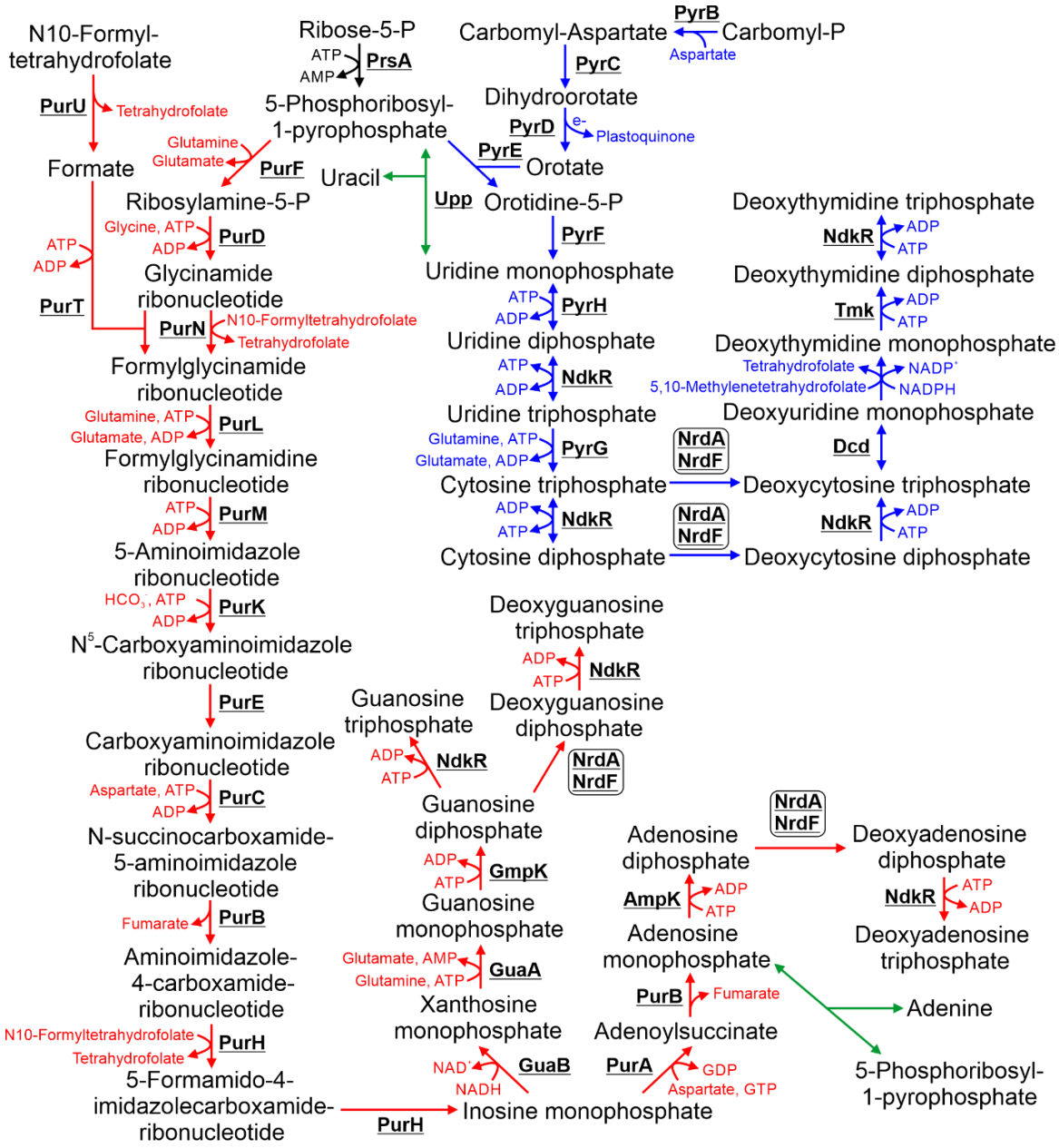

Figure 3.5 Metabolism of nucleotides in PCC 11901. The purine and pyrimidine biosynthesis pathways are highlighted in red and blue respectively. Possible nucleotide salvage pathways are highlighted in green. Cofactors in each reaction are shown with the exception of protons, water, oxygen and inorganic phosphate.

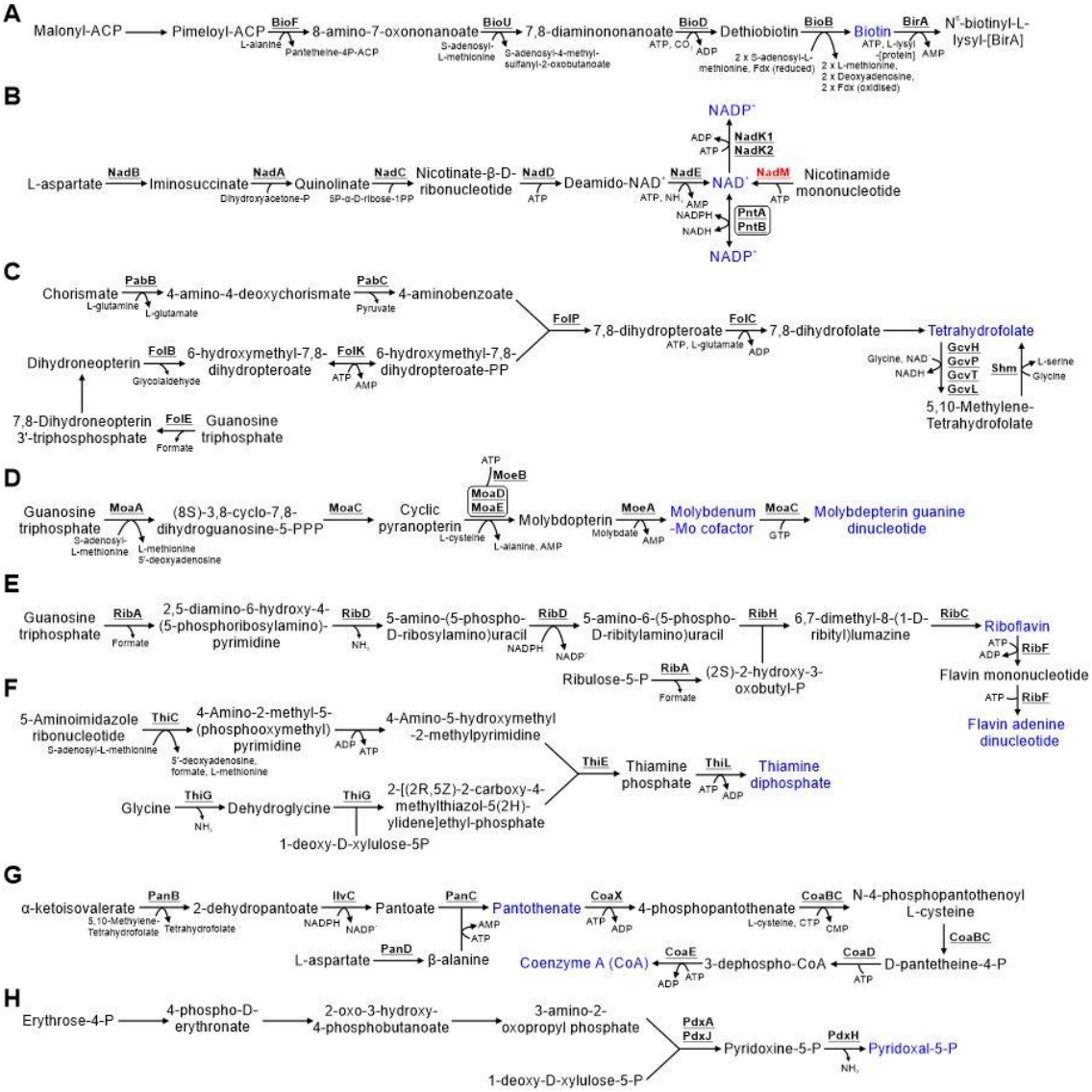

Figure 3.6 Metabolism of vitamins and cofactors in PCC 11901. Detailed are the pathways for biosynthesis of A) biotin, B) NAD^+ and $NADP^+$, C) folate, D) molybdenum cofactors, E) riboflavin and FAD, F) thiamine, G) pantothenate and coenzyme A, H) pyridoxal-5P. Vitamins and cofactors are highlighted in blue. Cofactors in each reaction are shown with the exception of protons, water, oxygen and inorganic phosphate. Proteins with low sequence similarity to PCC 6803 enzymes are highlighted in red.

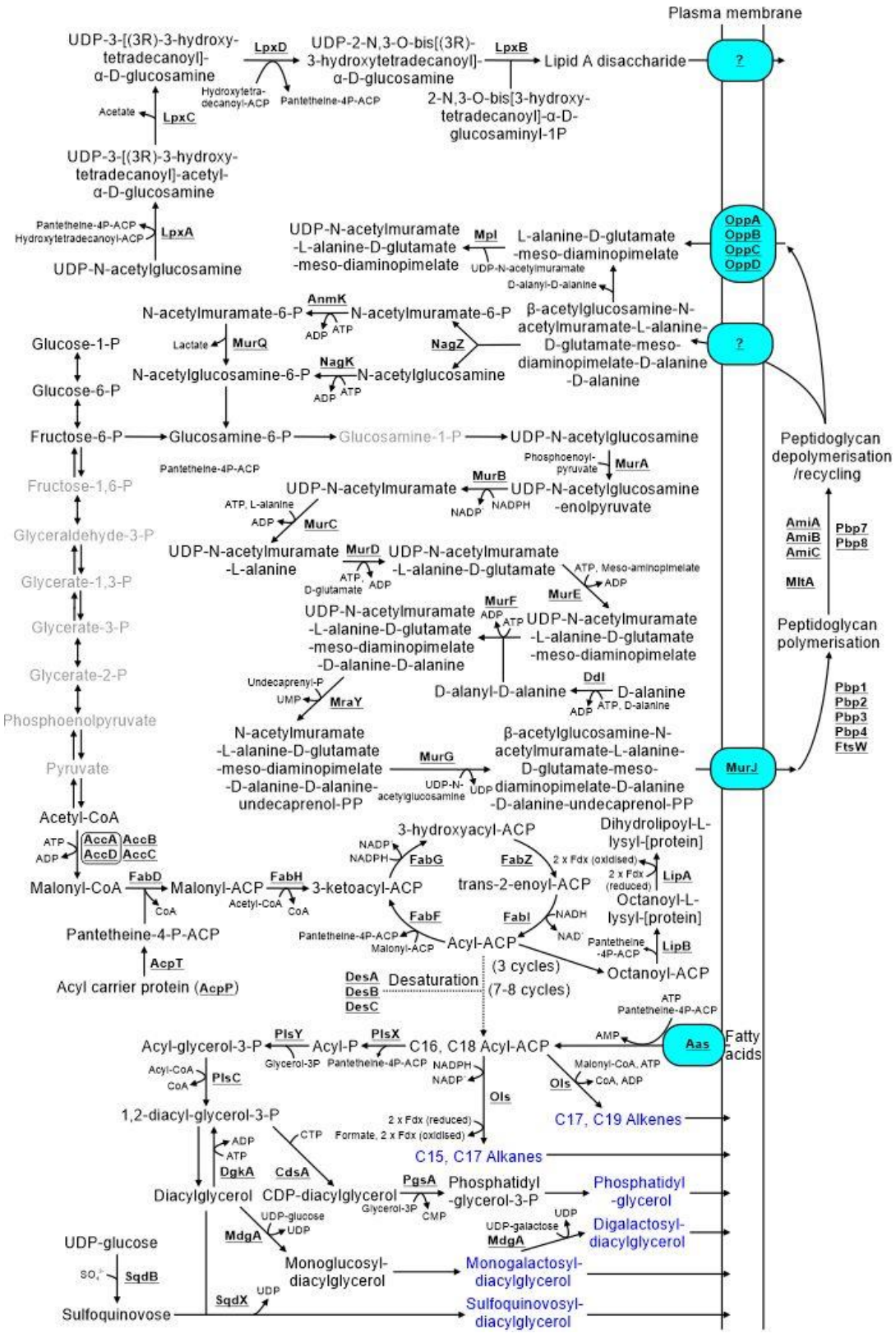

Figure 3.7 Metabolism of membrane lipids, peptidoglycan and lipopolysaccharides in PCC 11901. Membrane lipids are highlighted in blue. Steps highlighted in grey are compounds and reactions involved in these pathways but detailed in Figure 3.2. Cofactors in each reaction are shown with the exception of protons, water, oxygen and inorganic phosphate.

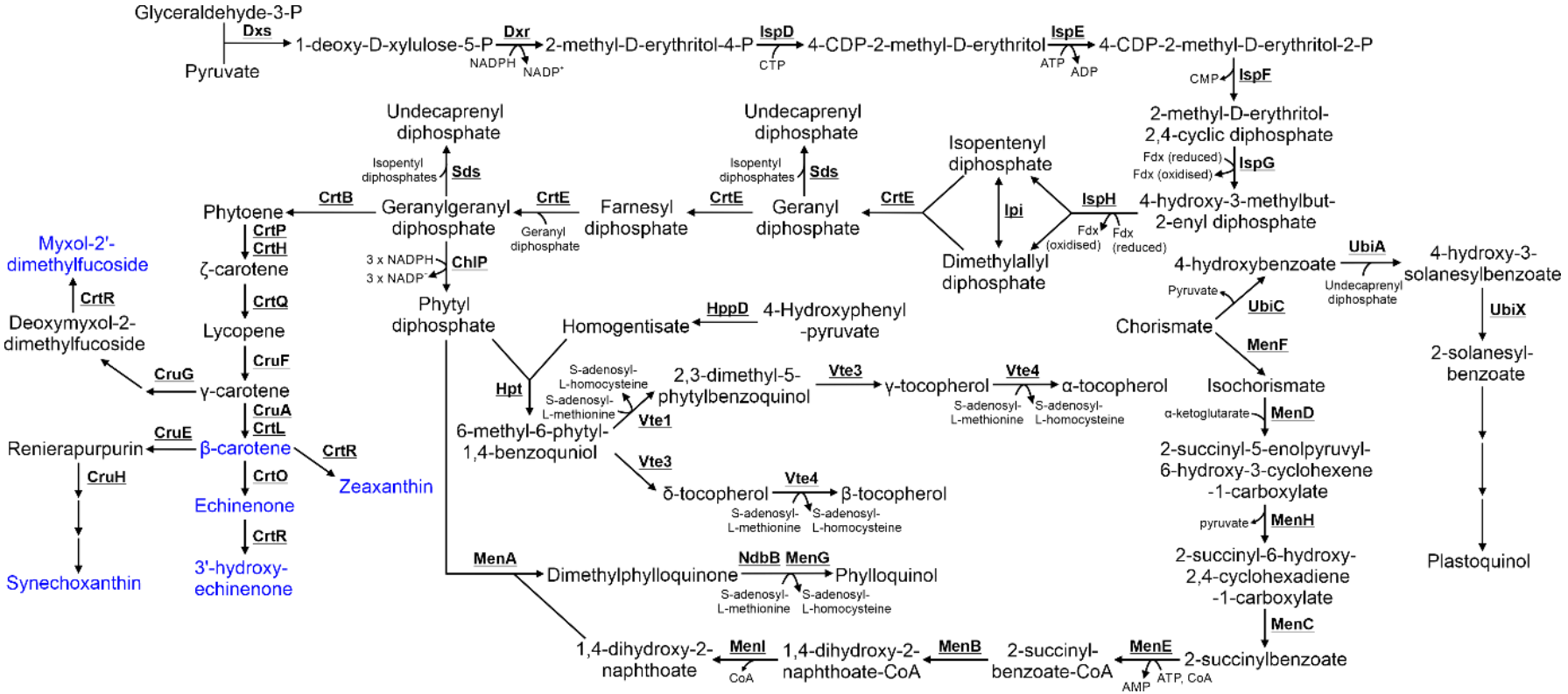

Figure 3.8 Metabolism of isoprenoids, quinols and carotenoids in PCC 11901. Carotenoids are highlighted in blue. Cofactors in each reaction are shown with the exception of protons, water, oxygen and inorganic phosphate.

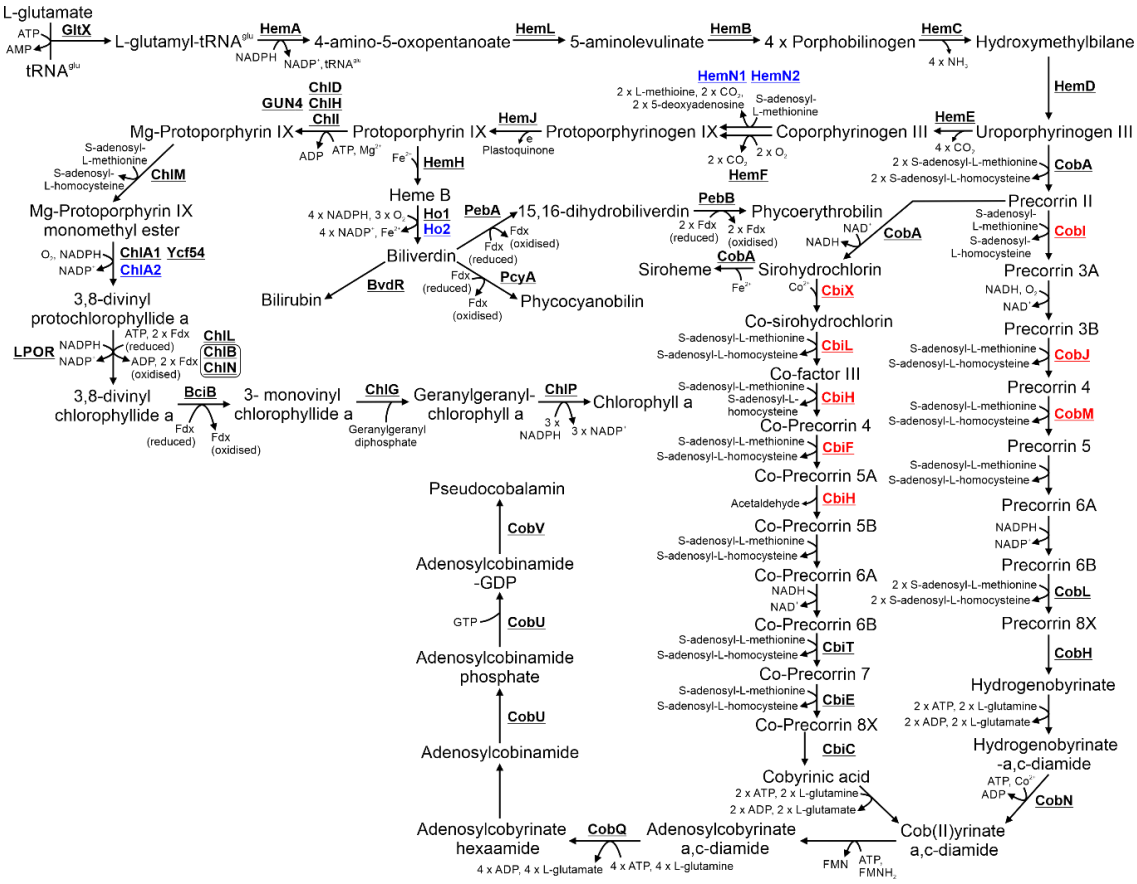

Figure 3.9 Metabolism of chlorophyll, phycobilin and pseudocobalamin in PCC 11901. Proteins involved in anaerobic or low oxygen environment enzymatic steps are highlighted in blue. Cofactors in each reaction are shown with the exception of protons, water and inorganic phosphate. Proteins with low sequence similarity to PCC 6803 enzymes are highlighted in red.

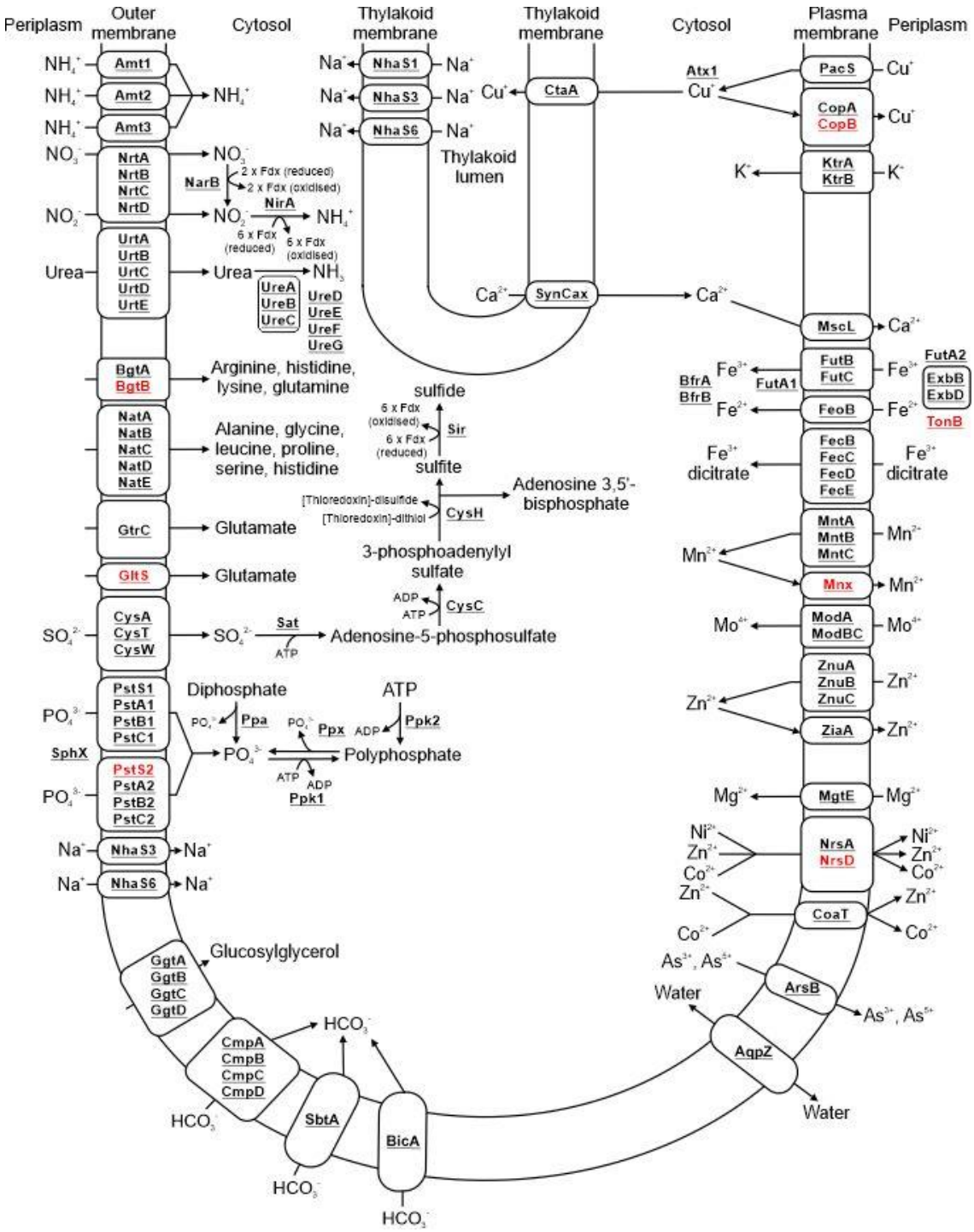

Figure 3.10 Proteins involved in metabolite transport and conversion of nitrogen, sulphur and phosphate based compounds in PCC 11901. Localisation of transporters in either the plasma or thylakoid membrane is detailed. Subunits in each complex may not all be membrane localised but soluble. Cofactors in each reaction are shown with the exception of protons, water, oxygen and inorganic phosphate. Proteins with low sequence similarity to PCC 6803 enzymes and transporter subunits are highlighted in red.

3.3.3 Electron Transport and light harvesting is streamlined in PCC 11901 compared to PCC 6803

Next we compared the differences between PCC 11901 and PCC 6803 in cellular processes, including electron transport and light harvesting (Appendix Table 3.4; **Figure 3.11**) (441). All subunits of the three main complexes, photosystem II and I, and cytochrome b_6f, are present. Similar to PCC 7002, PCC 11901 encodes cytochrome c_6 (c_{553}) but plastocyanin is not present (442). Both electron carriers, ferredoxin (Fdx) and flavodoxin (Fld), required for cyclic electron transport, in addition to ferredoxin-$NADP^+$ reductase, are present. Only two flavodiiron proteins are encoded in the PCC 11901 genome and these demonstrate the closest similarity to PCC 6803 Flv1 and Flv3, suggesting that only the Flv1/Flv3 complex is present in this species. All the subunits of the hydrogenase are also present. Other putative electron transport proteins, including the CytM and Pgr5 proteins, are present (43,443). Ten putative ferredoxins are also potentially encoded in the PCC 11901 genome, of which only Fed2, involved in iron response (444), has been characterised in PCC 6803.

Subunits specific to each of the four NAD(P)H dehydrogenase-like complexes (NDH-1L, NDH-1L', NDH-MS, NDH-MS') are present in PCC 11901 (445). Subunits of succinate dehydrogenase (SDH) are present, including the recently discovered putative third subunit encoded by Slr0201 in PCC 6803 (446). Two NAD(P)H dehydrogenase II proteins (NdbA, NdbB) are also present but there is no homologue to NdbC. Of the terminal oxidases, only genes encoding subunits of the quinone oxidising bo_3-type alternative respiratory terminal oxidase (ARTO) and the aa_3-type cytochrome-*c* oxidase complex (COX) are present in the genome. In PCC 7002, deletion of ARTO and COX increased reduction rates of photosystem I, suggesting that both complexes are thylakoid membrane localised (447). While PCC 6803 incorporates a separate electron transport chain into the plasma membrane, the lack of a third terminal oxidase suggests that this chain may not be present in PCC 11901. However, proteome mapping, as recently performed in PCC 6803 (183), would be required to confirm this.

In terms of light harvesting, the phycobilisome (PBS) has only one CpcC linker protein, suggesting that each rod consists of only two stacked disc-shaped phycocyanin hexamers radiating out of the allophycocyanin core. This PBS structure is similar to PCC 7002 but differs from PCC 6803, UTEX 2973 and PCC 7942, which encode two CpcC linker proteins and have three stacked disc-shaped phycocyanin hexamers per rod. Given that PCC 7002 and PCC 11901 demonstrate faster sustained growth at high cell densities compared to the other three species this suggests that PBSs with two

stacked disc-shaped phycocyanin hexamers may be optimal for light harvesting. The orange carotenoid protein is also present.

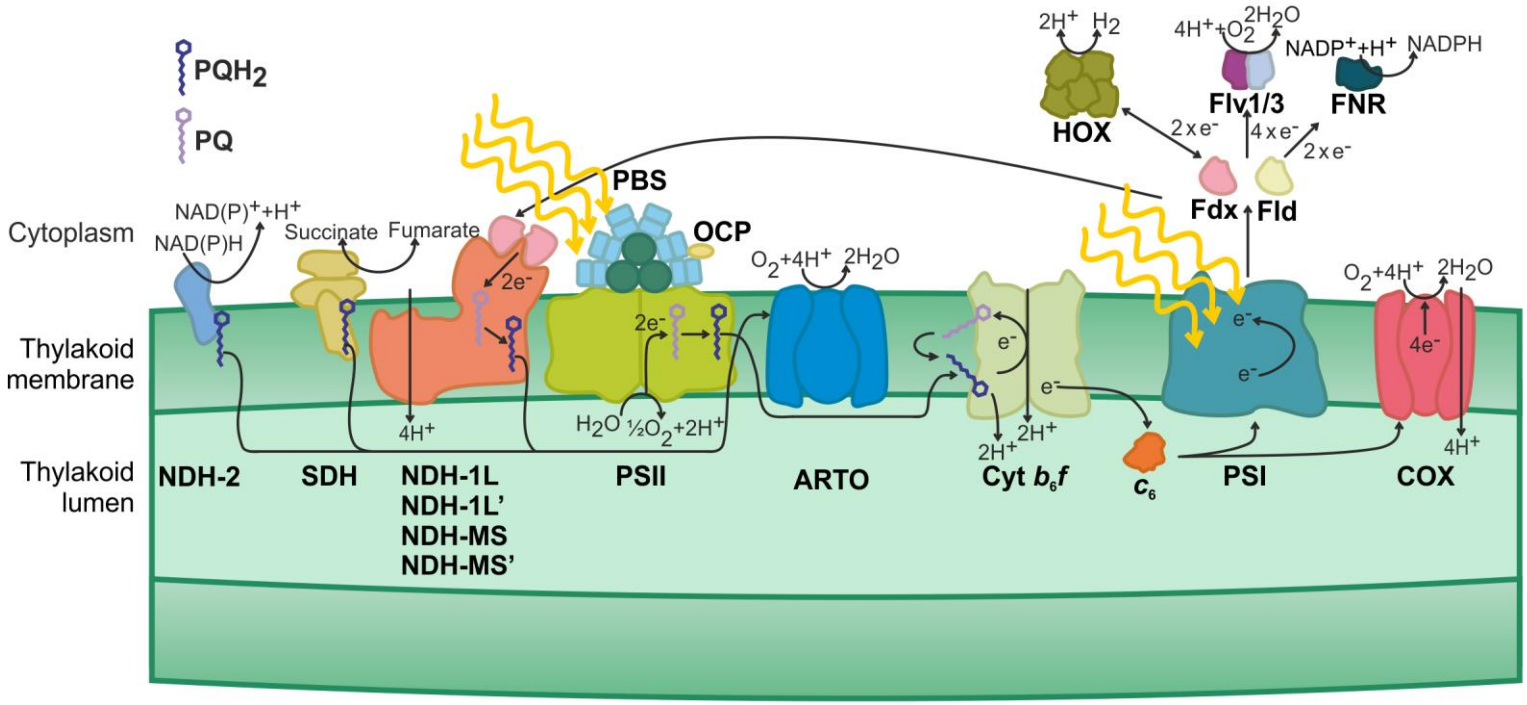

Figure 3.11 Schematic diagram of the PCC 11901 light-harvesting complex and thylakoid membrane electron transport chains. NDH-2- NAD(P)H dehydrogenase 2, SDH- Succinate dehydrogenase, NDH-1- NAD(P)H dehydrogenase 1, PQ- plastoquinone, PQH_2- plastoquinol, PSII- Photosystem II, PBS- phycobilisome, OCP- Orange carotenoid protein, ARTO- alternative cytochrome oxidase, cyt b_6f- cytochrome b_6f, Cyt c_6- cytochrome c_6,, PSI- Photosystem I, Fdx- ferredoxin, Fld- flavodoxin, COX- cytochrome-c oxidase, HOX- hydrogenase, Flv1/3- Flavodiiron 1/3, , FNR- ferredoxin-$NADP^+$ reductase.

3.3.4 PCC 11901 demonstrates higher photosynthetic and respiratory rates, lower photoinhibition and higher quantum efficiency compared to other model cyanobacteria

Chlorophyll concentration standard curves were calculated for each species tested in the oxygen electrode (**Figure 3.12**). This allowed for rapid analysis of the chlorophyll content for species and adjustment of the sample to ensure that each replicate had similar chlorophyll concentrations. This would not be possible with standard measurements of chlorophyll concentration via methanol extraction, which typically takes approximately one hour.

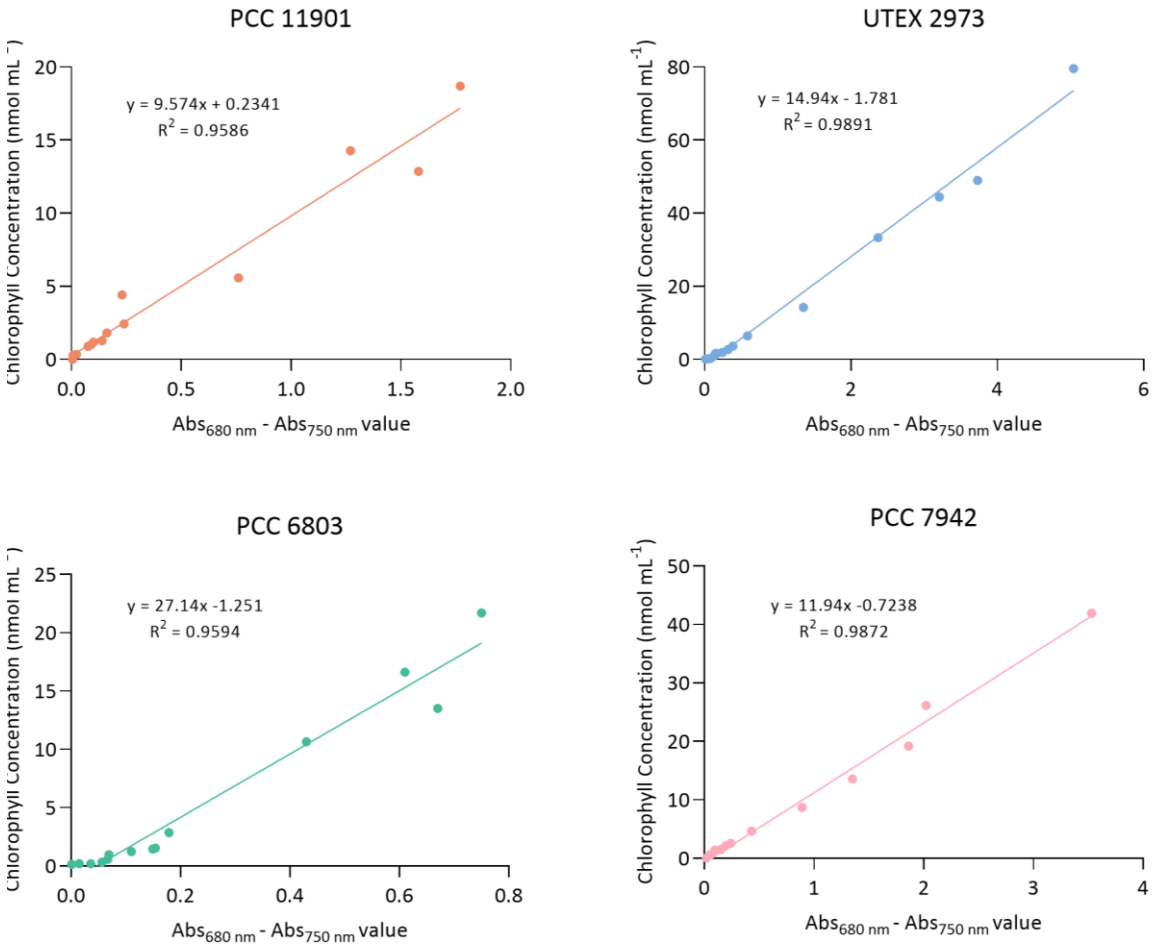

Figure 3.12 Correlation between the Abs(680nm) - Abs(750nm) value and amounts of chlorophyll measured following methanol extraction. Samples were measured at absorbance of 750nm and 680nm, followed by extraction with methanol to measure chlorophyll concentration. Amount of chlorophyll was correlated with absorbance (A_{680nm} - A_{750nm}). The regression line is shown. The slope of the regression line (R^2) was then calculated.

The next step was to determine whether the photosynthetic properties of PCC 11901 may play a role in the higher growth rates observed in this species. This was performed with cultures grown at 30°C under 125 µmol photons m^{-2} s^{-1} warm white LED light and sparging with air/5% CO_2 to test species under the high carbon saturation conditions optimal for PCC 11901. A lower light intensity was selected to avoid stress on the cells whilst the cells were cultured at 30°C to allow direct comparison to previous experiments performed on PCC 6803 (20,188) and because this is the optimal temperature for PCC 6803 and PCC 7942. UTEX 2973 also demonstrates similar growth to PCC 11901 under the first 48 hours of growth at 30°C (51), allowing a direct comparison between this species and PCC 11901 during this period. Photosynthetic rates were measured at different light intensities to generate a saturation curve, with a dark period preceding each increase in light intensity (**Figure 3.13**A). In such curves, the rate of oxygen evolution levels off as saturating light intensity is approached, with the maximum rate of oxygen evolution designated as P_{max}. The P_{max} of PCC 11901 was 32%, 52% and 566% higher than PCC 7942, UTEX 2973 and PCC 6803, respectively. The rate of oxygen depletion in the dark after each period of illumination (i.e. cellular respiration) can also be plotted as a function of the light intensity prior to the dark period, giving the respiration curve (**Figure 3.13**B). The maximum rate of oxygen depletion was measured after the highest light intensity. The maximum rate of oxygen depletion of PCC 11901 was 30%, 212% and 552% higher than PCC 7942, UTEX 2973 and PCC 6803, respectively.

To test for photoinhibition, all species were first incubated in the dark for 10 minutes, followed by exposure to constant saturating light of 2000 µmol photons m^{-2} s^{-1} for 75 minutes in the absence and presence of lincomycin (**Figure 3.13**D and **Figure 3.13**E, respectively), during which times oxygen evolution was measured. Photoinhibition, as determined by a decrease in oxygen evolution, was lowest in PCC 11901. In the absence of lincomycin the rate of oxygen evolution decreased to 85.7% ± 5.5%, 76.6% ± 9.7%, 57.8% ± 8.8% and 33.2% ± 10.5% for PCC 11901, UTEX 2973, PCC 7942 and PCC 6803, respectively. Addition of lincomycin, an inhibitor of protein synthesis and thus repair of PSII, resulted in similar levels of photoinhibition between PCC 11901 and UTEX 2973, with the rate of oxygen evolution decreasing to 75.4 ± 5.4% and 73.6% ± 18.3%, respectively. Higher rates of photoinhibition were observed in PCC 7942 and PCC 6803, with the rate of oxygen evolution decreasing to 45.4 ± 6.9% and 26.1% ± 17.4%, respectively.

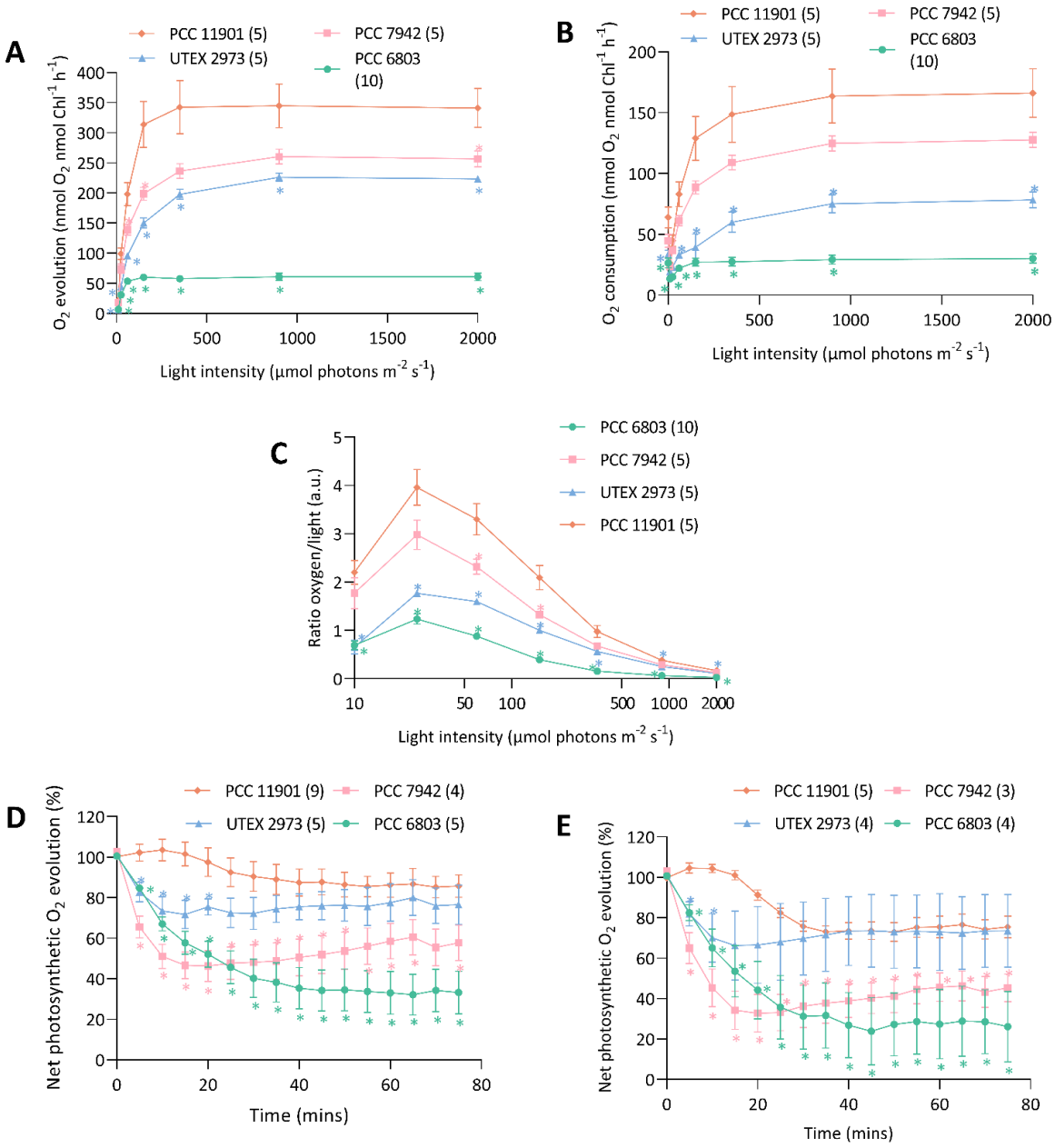

Figure 3.13 Characterization of the photosynthetic and respiratory rates, light utilization and photoinhibition of cyanobacterial species. A) Oxygen evolution was measured at different light intensities, and B) oxygen consumption was measured following each light period. C) The coefficient of light utilization was calculated by dividing the net rate of oxygen evolution by the correspondent light photon flux. Photoinhibition was quantified by determining photosynthetic oxygen evolution in the D) absence and E) presence of lincomycin. All results are from three to ten biological replicates (number indicated in brackets after species legend). Errors bars indicate SE. Colour-coded asterisks indicate significant differences between PCC 11901 and the other cyanobacterial species ($P < 0.05$).

3.4 Discussion

3.4.1 Future work testing growth rates of PCC 11901 for biotechnology applications

PCC 11901 has enormous potential as a chassis for biotechnology and as a model species to identify factors leading to high growth and biomass accumulation in photosynthetic organisms. Our data confirms that PCC 11901 outperforms all other model cyanobacterial species in terms of sustained growth, at least in small-scale laboratory experiments. However, growth of this species has not been tested at larger scales and in outdoor photobioreactors. Also, the optimal light intensity for growth has not yet been established.

3.4.2 Potential factors underlying the fast growth of PCC 11901

There are several factors identified in this chapter that could underlie the fast growth of this species. Photoinhibition was lowest in PCC 11901, although not significantly different from UTEX 2973 after 20 minutes (**Figure 3.13**D and **Figure 3.13**E). This could be one factor underlying the fast growth of both species at low cell densities, when photoinhibition has the greatest impact. Photosynthetic and respiratory rates, in addition to quantum efficiency, were significantly higher in PCC 11901 compared to the other species (**Figure 3.13**A-C). This could be due to differences in the electron transport chain or more efficient light harvesting (**Figure 3.11**). The photosynthetic rate of PCC 6803 was far lower compared to the other species. The negative effect on oxygen generation could be due to the conditions which these cells were grown under prior to oxygen measurements (i.e. 125 µmol photons m^{-2} s^{-1} with 5% CO_2 sparging), which may have resulted in higher levels of cyclic electron transport. Another possibility is that oxygen generation was impeded by the transition from a high CO_2 environment to the ambient air level in the oxygen electrode.

Comparative genomics suggest that the PBS of PCC 11901 is smaller than the other species examined in this study. This may be advantageous in dense cultures, since it may reduce light absorption of cells at the surface, reducing photoinhibition, while allowing additional light to penetrate into the interior of the photobioreactor, thereby increasing productivity. This could be a major factor leading to the faster growth of PCC 11901 observed at higher cell densities. Many studies have tried to attenuate PCC 6803 PBSs to achieve a similar outcome (20,448–450). However, PBS attenuation has not always led to an increase in growth in dense cultures, most likely due to unintended consequences, such as differences in cell size (20,451), thylakoid membrane

morphology (451,452) and altered production of other proteins, including many involved in photosynthesis (453).

Metabolic pathways were largely conserved between PCC 6803 and PCC 11901, although carbon flux may differ greatly between the two species. Given that PCC 11901 displays its fast growth phenotype under high carbon dioxide conditions it is possible that RuBisCO carboxylation rates may differ greatly between the species examined in this study. The carboxylation rate of RuBisCO from PCC 7002 is higher than that of *Synechococcus elongatus* PCC 6301 (13.4 vs 11.6, respectively [1/s]) (14), a species which is almost identical to PCC 7942 (454). Higher carboxylation rates would result in greater turnover of $NADP^+$/NADPH and ADP/ATP, thereby increasing photosynthetic rates and limiting over-reduction of the electron transport chain. In-depth carbon flux studies and enzyme kinetics of PCC 11901 RuBisCO would be required to resolve this.

3.4.3 Future Work

In this chapter, we demonstrate that PCC 11901 displays the fastest, sustained growth when compared to a range of model cyanobacterial species, even under the optimal growth conditions for UTEX 2973. This further demonstrates that PCC 11901 is the best candidate identified to date, in terms of fast growth, for cyanobacterial biotechnology when cells are cultured under high CO_2 conditions. Moreover, we show that the fast growth phenotype of PCC 11901 is linked to lower photoinhibition, higher photosynthetic rates and a higher quantum efficiency compared to other model cyanobacteria. Via comprehensive analysis of PCC 11901 central metabolism, we demonstrate that most pathways are conserved between this species and PCC 6803. Further development of this species for biotechnology applications can be aided by the bioinformatics analysis provided in this study.

Overall, this chapter lays the foundation for the use of PCC 11901 as a robust chassis for renewable biotechnological applications, paving the way for efficient photosynthetic recovery of industrial CO_2 waste streams and towards carbon-efficient biomanufacturing.

Chapter 4

Experimental and photo-mechanistic modelling of growth and biomass production for the cyanobacterium *Synechococcus* sp. PCC 11901

A published version of this chapter can be found in Algal Research 70: 102997

Integrated experimental and photo-mechanistic modelling of biomass and optical density production of fast versus slow growing model cyanobacteria.
Cho, B. A.; Moreno-Cabezuelo, J. Á.; Mills, L. A.; del Río Chanona, E. A.; Lea-Smith, D. J.; Zhang, D.
Algal Research, 70, 102997

Chapter 4: Experimental and photo-mechanistic modelling of growth and biomass production for the cyanobacterium Synechococcus sp. PCC 11901

4.1 Introduction

4.1.1 Identifying the optimal light intensity for growth of cyanobacteria

The faster growth and higher biomass accumulation of PCC 11901 could be attributed to lower photoinhibition, higher photosynthetic rates and higher light utilisation efficiency compared to other model cyanobacterial strains. In addition, a comprehensive analysis into the central metabolism of both the PCC 11901 and PCC 6803 concluded that most of the metabolic pathways were conserved between the two species. Despite these observed similarities, an in-depth analysis across a range of light intensity parameters could provide additional information on the factors underlying the fast growth and high biomass accumulation phenotype of PCC 11901, as well as to aid the construction of mathematical models which could predict the optimal parameters for growth in larger scale photobioreactors.

Growth of dense, healthy cultures (i.e. not photolimited) is a prerequisite for bioindustry. Generally speaking, increasing light intensity results in improved growth till the point at which cells become photoinhibited (455). Accounting for light attenuation and photomechanisms (i.e., photolimitation, photosaturation and photoinhibition) in computational models is of utmost importance when analysing fast growing strains (20,456). Growth of PCC 11901 has only been reported at four continuous light intensities: 300, 660, 750 and 900 µmol photons m^{-2} s^{-1}, with only growth at 750 µmol photons m^{-2} s^{-1} being tested for longer than 96 hours (51,195) Therefore, the optimal light intensity for growth and biomass has not been identified.

4.1.2 Chapter aims and objectives

The aim of this chapter was to determine the optimal light intensity for sustained growth and biomass accumulation of PCC 11901 and how this compares to PCC 6803. This may allow us to

determine the optimal conditions to cultivate PCC 11901 cultures to a high density for industrial applications. These experiments will also aid systems modelling for optimal light intensities for the culturing of cyanobacteria at industrial scales as well as improving PBR design for mass cultivation, conducted by our collaborators at the University of Manchester.

4.2 Materials and Methods

4.2.1 Strain and culture conditions

PCC 6803 was maintained on BG11 agar plates (40) and PCC 11901 was maintained on AD7 plates (51) as described in Section 3.2.1.1.1 and Section 3.2.1.4.1, respectively. Liquid cultures used as starter cultures for growth experiments were grown in their corresponding liquid medium in 50 mL volumes in 100 mL conical flasks at 30°C under 40 µmol photons m^{-2} s^{-1} warm white LED light in an Algaetron growth chamber (Photon Systems Instruments) and shaken at 120 rpm.

4.2.2 Quantification of strains using optical density

To quantify growth of cells, 1 mL of liquid culture was used to record the optical density at 750 nm using a Jenway 6305 Genova spectrophotometer. If the optical density was >1.0, cultures were diluted with their corresponding media appropriately.

4.2.3 Multicultivator MC-1000 growth conditions

To determine growth rates, starter cultures were used to inoculate 80 mL cultures in cylindrical cultivation tubes with a diameter of 30 mm to an OD_{750nm} = ~0.1. Tubes were placed into a MC-1000 multicultivator bioreactor (Photon Systems Instruments) and grown at 38°C under 150 µmol photons m^{-2} s^{-1} warm white LED light and sparging with 5% CO_2. After 24 hours of growth, the light intensity was increased gradually depending on the final light intensity (**Table 4.1Error! Reference source not found.**). After a further 24 hours of growth, cultures were diluted to an OD_{750nm} of ~0.1 to continue log-phase growth and the light intensity was increased to the final light intensity (**Table 4.1Error! Reference source not found.**). The cultures were left overnight at this intensity to adapt samples to the new conditions of the bioreactor. Samples were then diluted to an OD_{750nm} = 0.25 to start the growth experiment. Samples were collected every 12 hours for 120 hours. Parameters for the growth experiments were adapted from Chapter 3.

Table 4.1 Light intensity increased steps in the PBR dependent to achieve the final desired light intensity. The light increasing steps were implemented every 24 hours before the experiment was started. n/a applies to stages where the light intensity was not increased.

Initial light intensity (µmol photons m^{-2} s^{-1})	Second step in light intensity (µmol photons m^{-2} s^{-1})	Final Light intensity (µmol photons m^{-2} s^{-1})
150	n/a	300
150	300	450
150	300	600
150	450	750
150	500	900

4.2.4 Measuring dry cell weight

After 120 hours of growth at the corresponding light intensities and 38°C, 50 mL of culture was harvested from each replicate. Cells were centrifuged at 5,000 x *g* and washed twice with sterile H_2O. Samples were then diluted with sterile H_2O to 10%, 20%, 40%, 60%, 80% and 100% of the original culture. The OD_{750nm} value was measured again for each diluted sample. Whatman GF/B Glass Microfibre Filters of 70 mm diameter were dried for 48 hours at 70°C and then measured on a microbalance three times to obtain an average filter weight. Post wash and dilution, 5 mL of each diluted sample was added to the filter paper, and dried for 24 hours at 70°C. The filter papers were then weighed again three times to obtain the average weight of the filter plus the dry cell weight (*X*) for each species. The biomass concentrations were determined from the standard curves between *X* and OD_{750nm} and reported in Eq. (1) and (2) for PCC 11901 and PCC 6803 respectively.

$$X_{\mathrm{PCC\_11901}}(\mathrm{g\,L^{-1}}) = 0.222 \cdot OD_{750nm\_\mathrm{PCC\_11901}}\,, \quad \mathrm{R^2} = 0.998 \qquad (1)$$

$$X_{\mathrm{PCC\_6803}}(\mathrm{g\,L^{-1}}) = 0.2406 \cdot OD_{750nm\_\mathrm{PCC\_6803}}\,, \quad \mathrm{R^2} = 0.996 \qquad (2)$$

4.2.5 Mathematical model construction

The mathematical modelling for predicting the optimal light intensity for the two species used the biomass concentrations and optical densities from this study. The computational modelling

(Section **Error! Reference source not found.**) was carried out by our collaborator, Bovinille Anye Cho from the Zhang Laboratory at The University of Manchester.

The constructed dynamic models were used to simulate variables under the influences of (i) incident light intensity, (ii) light attenuation, and (iii) photomechanisms. However, the differing levels of light related influences among the two investigated species required their experimental data sets to be subjected to statistical student *t*-tests to incorporate either all (i.e., (i), (ii) and (iii)) or a selective combination (e.g., (i) and (iii) only) of these influences.

4.2.5.1 Modelling of biomass concentrations

The two cyanobacterial species were expected to exhibit four distinct growth phases, namely the (i) lag phase, (ii) primary growth phase (iii) secondary growth phase and (iv) stationary phase, as reported in other studies (20,457,458). The lag phase was not noticeable due to the starter cultures being adapted to the operational light intensity of the PBR by using the light stepping up strategy as reported in **Table 4.1Error! Reference source not found.**. The dynamic model structure in Eq. (3) was constructed to capture the three remaining phases. This model permits the incorporation of strain dependent biological knowledge which may influence the trajectories of the state variables.

$$\frac{dX}{dt} = u\,(I) \cdot X - \mu_d \cdot X^2 \qquad (3)$$

Where X is the biomass concentration (g L^{-1}), $u\,(I)$ represents the effects of the PBR's light intensities on the biomass growth (h^{-1}) and $\mu_d(I)$ denotes the specific cell decay rate (L g^{-1} h^{-1}).

4.2.5.2 Modelling of optical densities

Although often disputed as to whether there exist a linear or a non-linear correlation between the biomass concentration and optical density, the optical density profiles of -PCC 11901 and PCC 6803 strains has been shown (20,51,195) to have sigmoidal shapes typical of bioprocesses. Thus, the model structure of the optical density and biomass concentration (i.e., Eq. (3)) were assumed to be similar. Hence, Eq. (4) was constructed to simulate the optical density profiles of the two cyanobacterial species.

$$\frac{d\ \mathrm{OD}_{750}}{dt} = u\ (I) \cdot\ \mathrm{OD}_{750} - \mu_d \cdot\ {\mathrm{OD}_{750}}^2 \quad (4)$$

Where OD_{750nm} is the optical density at a wavelength of 750 nm (dimensionless), $u\ (I)$ represents the effects of the PBR's light intensities on the optical density build up (h^{-1}) and μ_d denotes the specific rate of vanishing optical density (h^{-1}).

4.2.5.3 Modelling of optical densities

The effect of light on growth rates are often characterised mechanistically by three distinguishable photomechanisms: (i) photolimitation, (ii) photosaturation and (iii) photoinhibition (204,457,459,460), via the Aiba model structure (Eq. (5)). These three photomechanisms occur under low, optimal and high light intensities, respectively. In order to capture all three stages cultures were grown at different light intensities between 300 and 900 µmol photons m^{-2} s^{-1} which was required to implement a model. Student *t*-tests were first performed on the experimental data sets for statistical significance to confirm the validity of the light influences on the two cyanobacterial strains.

$$u\ (I) = u_m \cdot \frac{I(z)}{I(z) + k_s + \frac{I(z)^2}{k_i}} \quad (5)$$

Where u_m is the maximum specific growth rate (h^{-1}), $I(z)$ denotes the light attenuation model (see Eqs. (6) and (7) below), k_s and k_i represent the light saturation (µmol photons m^{-2} s^{-1}) and light inhibition (µmol photons m^{-2} s^{-1}) coefficients.

4.2.5.4 Modelling PCC 11901 growth associated terms

From the student's *t*-test performed over the wide operational light intensity range (300 to 900 µmol photons m^{-2} s^{-1}), statistical significance ($P<0.05$) of light intensity influences were observed in the data sets of PCC 11901. Eq. (5) was employed to encompass all the above mentioned photomechanisms on the associated growth terms. Eq. (5)'s light attenuation model, based on the unidirectional illumination of the PBR, was defined by Eq. (6) for the biomass production model and Eq. (7) for the optical density model. To overcome light scattering phenomena seen in dense cell cultures (461,462), the embedded light attenuation model within the biomass model (Eq. (3)) included both the light absorption and light scattering terms. Only pigment dominated light

absorption influences were therefore accounted for within the optical density model. These assumptions were concluded to be rational for a PBR of this size with a short light path length and low aeration rate (no visible gas bubbles during cultivation experiments). We therefore assumed light scattering induced by insignificant gas bubbles to be negligible in the models, especially for the optical density model.

$$I(z) = I_0 \cdot \exp[-(\tau \cdot X + \beta) \cdot z] \quad (6)$$

$$I(z) = I_0 \cdot \exp[-(\tau \cdot \mathrm{OD}_{750}) \cdot z] \quad (7)$$

Where I_0 is the operational incident light intensity (µmol photons m^{-2} s^{-1}), z is the light path length (mm) and β is the light scattering coefficient (mm^{-1}). τ is the light attenuation coefficient with units of (mm^2 g^{-1}) and (mm^{-1}) for Eq. (6) and Eq. (7) respectively.

Simplified light attenuation model structures (as seen with Eq. (6) and Eq. (7)) have been reported by Anye Cho *et al.*, (462) to be numerically stable for dynamic parameter estimation solvers without compromising the high solution accuracy. However, incorporation of the PBR's cylindrical curvature effects in Eq. (6) and Eq. (7) will further increase the model's complexity and computational burden for the dynamic parameter estimation solver. Therefore, further simplifications by approximating the observed circular cross-section with a rectangular cross-sectional area as reported in (462,463), and altering the light path length to 23.9 mm, was implemented.

When embedding Eq. (5), Eq. (6), Eq. (7) into Eq. (3) and Eq. (4), the overall predictive model is now a partial differential equation (PDE) due to the presence of both temporal and spatial dimensions, thus challenging to resolve both dimensions for the non-linear optimisation solver. To utilise a less complex ordinary differential equation (ODE) solver, a 20-step trapezoidal rule, as shown in Eq. (8), was employed to eliminate the spatial dimensions (456,464) in the model. The predictive models of PCC 11901 required more integration steps to better approximate its spatial dimension related parameters (i.e., u_m, k_s and k_i) during the parameter estimation process. Hence, Eqs. (6), (7), and (8) were then substituted into Eqs. (3) and (4) for the remainder of this study.

$$(I) = \frac{u_m}{40} \cdot \sum_{n=1}^{19} \left(\frac{I_0}{I_0 + k_s + \frac{I_0^2}{k_i}} + \frac{2 \cdot I_{\frac{n \cdot L}{20}}}{I_{\frac{n \cdot L}{20}} + k_s + \frac{I_{\frac{n \cdot L}{20}}^2}{k_i}} + \frac{I_L}{I_L + k_s + \frac{I_L^2}{k_i}} \right) \quad (8)$$

4.2.5.5 Modelling PCC 6803 growth associated terms

Contrary to the statistical significance observed in PCC 11901 (P<0.05), the final biomass and optical density data sets of PCC 6083 showed statistical insignificance (P>0.05) over the light intensity range (300 - 900 µmol photons m^{-2} s^{-1}) and was therefore not experiencing the above mentioned photomechanisms. However, upon performing dynamic student's *t*-test(s) over each state trajectory, two to three discrete time points on each growth trajectory did show some level of statistical significance as seen in **Error! Reference source not found.**D, thereby implying a partial presence of these photomechanisms. Since these points were observed mostly around the exponential growth phase (i.e., between 20 and 60 hours), light saturation to a smaller extent was assumed present. Meanwhile, photoinhibition was completely ruled out (i.e., $\left[\frac{I(z)^2}{k_i}\right] \sim 0$ in Eq. (5)) as the growth of PCC 6083 was not observed to decline over time and operational light intensities. However, the very small extent of light saturation implied that the influence of light attenuation on growth of PCC 6083 was also negligible (i.e., $\tau = \beta = 0$ in Eqs. (6) and (7)), thereby leading to Eq. (9). This resulting Monod-like model structure theoretically implies that the growth of PCC 6083 will increase linearly at lower operational light intensity until a saturation threshold is attained whereby the growth becomes maximal and independent of the operational light intensity. Herein, the former linear increase was assumed to only occur below 300 µmol photons m^{-2} s^{-1}, and the proposed model was therefore valid to simulate the saturating threshold (300 - 900 µmol photons m^{-2} s^{-1}) when embedding Eq. (9) into Eq. (3) and (4).

$$u\,(I) = u_m \cdot \frac{I_0}{I_0 + K_s} \tag{9}$$

Where K_s represent the light saturation (µmol photons m^{-2} s^{-1}).

4.2.5.6 Model parameter estimation methodology

To estimate the model parameters, a weighted non-linear least-square regression problem (Eqs. (10a) to (10e)) was formulated. Due to the stiffness and high non-linearity of the proposed biomass and optical density models, orthogonal collocation over finite elements in time was utilised to numerically discretise the differential equations, thus transforming them into a series of non-linear algebraic equations. Thereafter, the resulting non-linear optimisation problem was solved with an interior point-based solver (i.e., IPOPT (465) version 3.11.1) through an open-source interface Pyomo (466,467).

$$\min_{P} \Phi(\boldsymbol{p}) = \sum_{k=1}^{Nspp} \sum_{j=1}^{NV} \sum_{i=1}^{NP} \left(\frac{\hat{y}_{i,j,k} - y_{j,k}(t_i, \boldsymbol{p})}{\hat{y}_{i,j,k}} \right)^2 \cdot w_{i,j,k} \tag{10a}$$

Subject to:

$$\frac{d\boldsymbol{y}}{dt} = f(\boldsymbol{y}(t), p)\,, \qquad t \in [t_0, t_f] \tag{10b}$$

$$\boldsymbol{y_{lb}} \leq \boldsymbol{y} \leq \boldsymbol{y_{ub}} \tag{10c}$$

$$\boldsymbol{p_{lb}} \leq \boldsymbol{p} \leq \boldsymbol{p_{ub}} \tag{10d}$$

$$\boldsymbol{y}(t_0) = \boldsymbol{y_0} \tag{10e}$$

whereby $\boldsymbol{p}$ denotes a vector of parameters, $Nspp$, NV and NP are the number of species (i.e., PCC 11901 and PCC 6803), number of state variables (i.e. biomass concentration and optical density) and number of experimental data points, respectively, $\boldsymbol{y}$ denotes dynamic model output, $\hat{y}_{i,j,k}$ represents the experimental data point of species k with state variable j at time instant t_i, w_i is a weighting factor of species k for the data point of state variable j at time instant t_i, $\boldsymbol{y_{lb}}$, $\boldsymbol{y_{lb}}$, $\boldsymbol{p_{lb}}$ and $\boldsymbol{p_{ub}}$ denotes the lower and upper bounds of the state variables and parameters, respectively, t_0 and t_f represents the initial and final cultivation times, $\boldsymbol{y_0}$ denotes the initial concentration of the state variables.

To simultaneously identify all model parameters, as well as their confidence intervals, a bootstrapping technique was applied. This has increasingly been used in the machine learning community (468–470) for quantification of uncertainties. By implementing the bootstrapping methodology, the entire experimental dataset (i.e., 300 - 900 µmol photons m^{-2} s^{-1}) were repartitioned into several partitions (i.e., PE1, PE2 and PE3), as illustrated in **Table 4.2Error! Reference source not found.**. Eqs. (10a) to (10e) were solved on every partition for the dynamic model parameter's estimation. The obtained parameter estimates were statistically aggregated by averaging for the mean and standard deviation. As a caveat, the upper and lower bounds of the experimental data sets (i.e., 300 and 900 µmol photons m^{-2} s^{-1}) were included in all three data partitions (**Table 4.2Error! Reference source not found.**). This was to guarantee the models high-fidelity extrapolations within the investigated range. This was later confirmed with a separate cross validation data set which was not utilised during parameter estimation (**Table 4.2Error! Reference source not found.**).

Table 4.2 Bootstrapping design of experiments for model parameter estimation.

Label	Training data sets (µmol photons m^{-2} s^{-1})	Cross validation data sets (µmol photons m^{-2} s^{-1})
Parameter estimation 1 (PE 1)	300, 900, 600, 750	450
Parameter estimation 2 (PE 2)	300, 900, 450, 750	600
Parameter estimation 3 (PE 3)	300, 900, 450, 600	750

To evaluate the impact of the parameter confidence intervals on the various model prediction uncertainties, a Latin Hypercube Sampling methodology was used to draw 100 probabilistic samples from the confidence intervals. For each probabilistic sample, a dynamic model simulation was performed thereby amounting to a total of 100 Monte Carlo simulations whereby the mean prediction was computed and compared against the unseen experimental data sets. This implementation was carried out in Python version 3.9 using the *SMT* 1.0.0 and *Numpy* libraries.

4.3 Results

4.3.1 PCC 11901 demonstrates maximal growth at 750 µmol photons m^{-2} s^{-1}

In recently published work, PCC 11901 demonstrated faster growth over other model cyanobacteria at 38°C under 300 and 660 µmol photons m^{-2} s^{-1} of continuous light, and at 30°C under continuous light at 750 µmol photons m^{-2} s^{-1}, when cultured in 25 mL flasks and sparged with air/1% CO_2 (51). Work documented in this thesis has also demonstrated that PCC 11901 displays the fastest growth at 900 µmol photons m^{-2} s^{-1} of continuous light at 38°C with direct sparging of air/5% CO_2 in an MC-1000 cultivator, compared to other model cyanobacterial species (Chapter 3). To determine the optimal light intensity for fast growth we cultured PCC 11901 and PCC 6803 for 120 hours under the exact same growth conditions as seen in Chapter 3 but using a range of light intensities at intervals of 150 µmol photons m^{-2} s^{-1} between 300 – 900 µmol photons m^{-2} s^{-1}. Under all light intensities, PCC 11901 demonstrated much faster growth rates than PCC 6803 after just 12 hours. PCC 6803 enters stationary phase at an OD_{750nm} = 2-4 after ~48 hours in all tested light intensities (**Figure 4.1**). In contrast, PCC 11901 demonstrated slower growth at ~108 hours at an OD_{750nm} ≥15 at 300 - 600 and 900 µmol photons m^{-2} s^{-1} but was still displaying linear growth under 750 µmol photons m^{-2} s^{-1} after 120 hours of growth. The maximal growth was observed under 750 µmol photons m^{-2} s^{-1}, achieving an OD_{750nm} = 24 ± 1.35 after 120 hours. This nonlinear trend indicates photolimitation at lower light intensities, photosaturation around the optimal light intensity, and photoinhibition beyond the optimal light intensity range. The same effect was not observed with biomass accumulation, suggesting that optical density does not correlate directly to biomass.

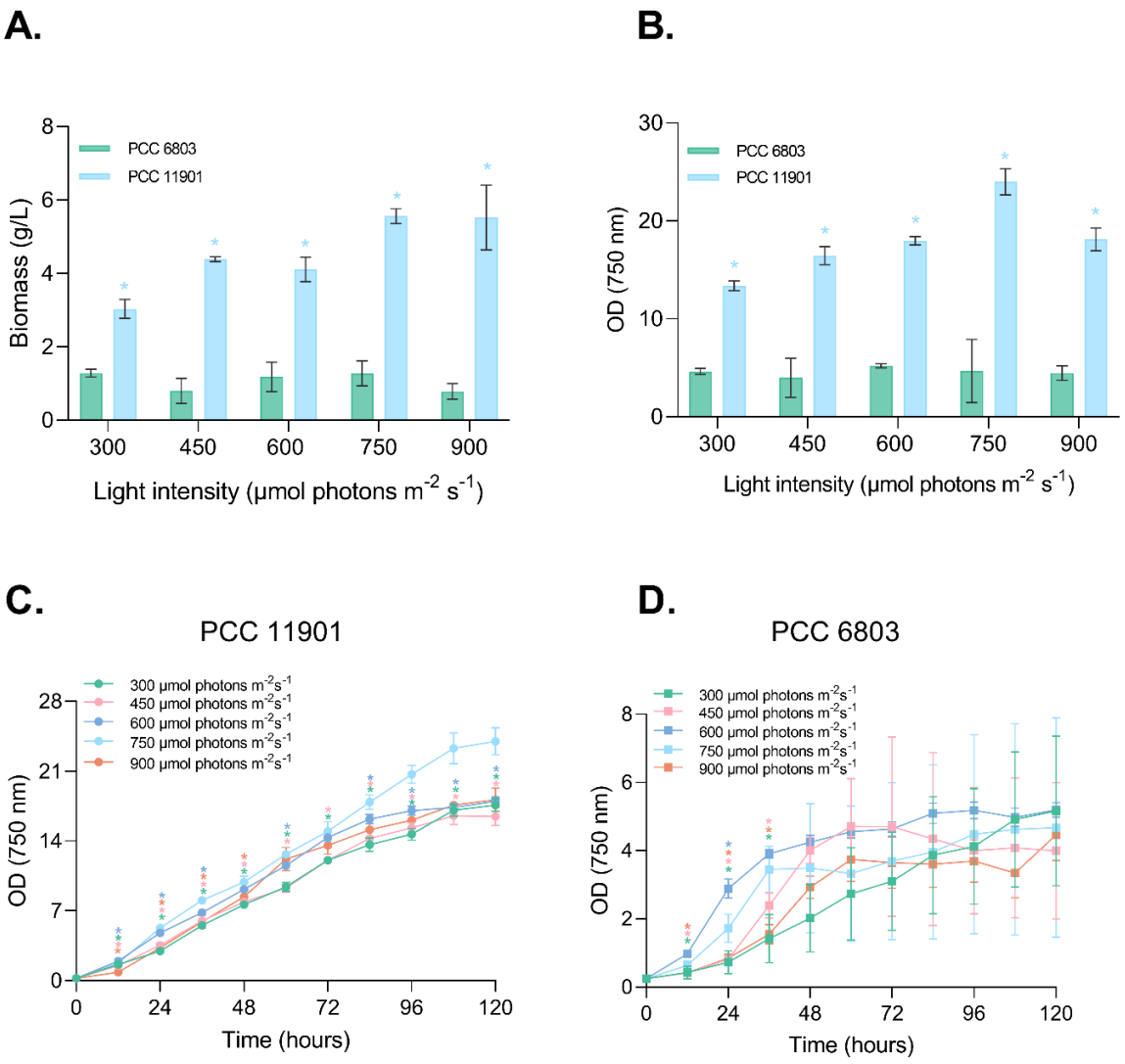

Figure 4.1 Light intensity influences on biomass production and optical density accumulation in the two cyanobacteria strains. A) Final biomass concentration and B) Final optical density (OD_{750nm}). Growth of C) PCC 11901 and D) PCC 6803 across a range of light intensities. Strains were cultured at 38°C under continuous light with direct sparging of air/5% CO_2. Asterisks indicate significant differences ($P<0.05$) at the various light intensities and time instances compared to 750 µmol photons m^{-2} s^{-1} : (i) between PCC 11901 and PCC 6803 as presented in A) and B), and (ii) individual growth profiles of PCC 11901 and PCC 6803 as presented in C) and D) respectively. Error bars indicate SD, n = 4

4.3.2 PCC 11901 and PCC 6803 accumulate maximal biomass at 750 µmol photons m^{-2} s^{-1}

Similar to the trends observed with OD_{750nm} measurements, the final biomass (g/L) obtained for each culture after 120 hours of photoautotrophic growth was more than double in PCC 11901 compared to PCC 6803 under each of the trialled light intensities (**Figure 4.1**). This further demonstrates the faster growth and higher biomass accumulation of PCC 11901 shown in previous findings in this thesis and published work (51,195). The highest biomass accumulated was 5.56 gDW/L ± 0.2 obtained under 750 µmol photons m^{-2} s^{-1} of continuous light, followed closely by 5.52 gDW/L ± 0.8 under 900 µmol photons m^{-2} s^{-1}, correlating with the trends observed with the OD_{750nm} data. Sustained biomass accumulation at high light intensities suggest PCC 11901 is an excellent candidate for growth in outdoor bioreactors exposed to environmental light conditions.

4.4 Mathematical and mode-based analysis

Analysis from the mathematical models was performed by Bovi Anye Cho from Manchester University. I interpretated the computational analysis in relation to biological aspects.

4.4.1.1 Parameter estimation of the model is statistically reliable

To ensure the constructed dynamic model was able to yield reliable predictions, the bootstrapping method, commonly used to calculate the uncertainty quantification in machine learning models, was adapted for this analysis (468,469,471). **Figure 4.2** and **Figure 4.4** show the predicted biomass model fit against the experimental data points from which the optimal parameter results in **Table 4.3Error! Reference source not found.** were obtained via the bootstrapping technique (468,469,471). The OD_{750nm} model fittings were presented in **Figure 4.3** for PCC 11901 and **Figure 4.5** for PCC 6803. Analysis of the model results were carried out by computing the overall average percentage relative errors (%RE), which showed that the experimental data of PCC 11901 was 13.8% and PCC 6803 18.0%, with equally obtained percentages for cross validation runs were 9.3% and 18.8%, respectively. Whilst this was expected due to the larger standard deviation between the experimental data sets observed in PCC 6803 (**Figure 4.4** and **Figure 4.5**), this percentage of error was deemed acceptable for computational modelling when considering that typical light driven bioprocesses are often associated with larger uncertainties (462,472). All the model's trajectories were seen to represent the experimental data points and thereby captured the underlying complex behaviours with a small subset of biokinetic parameters. This confirms that the postulated mechanistic hypothesis during the model construction and implemented model structural simplifications for the dynamic parameter estimation solver were all valid.

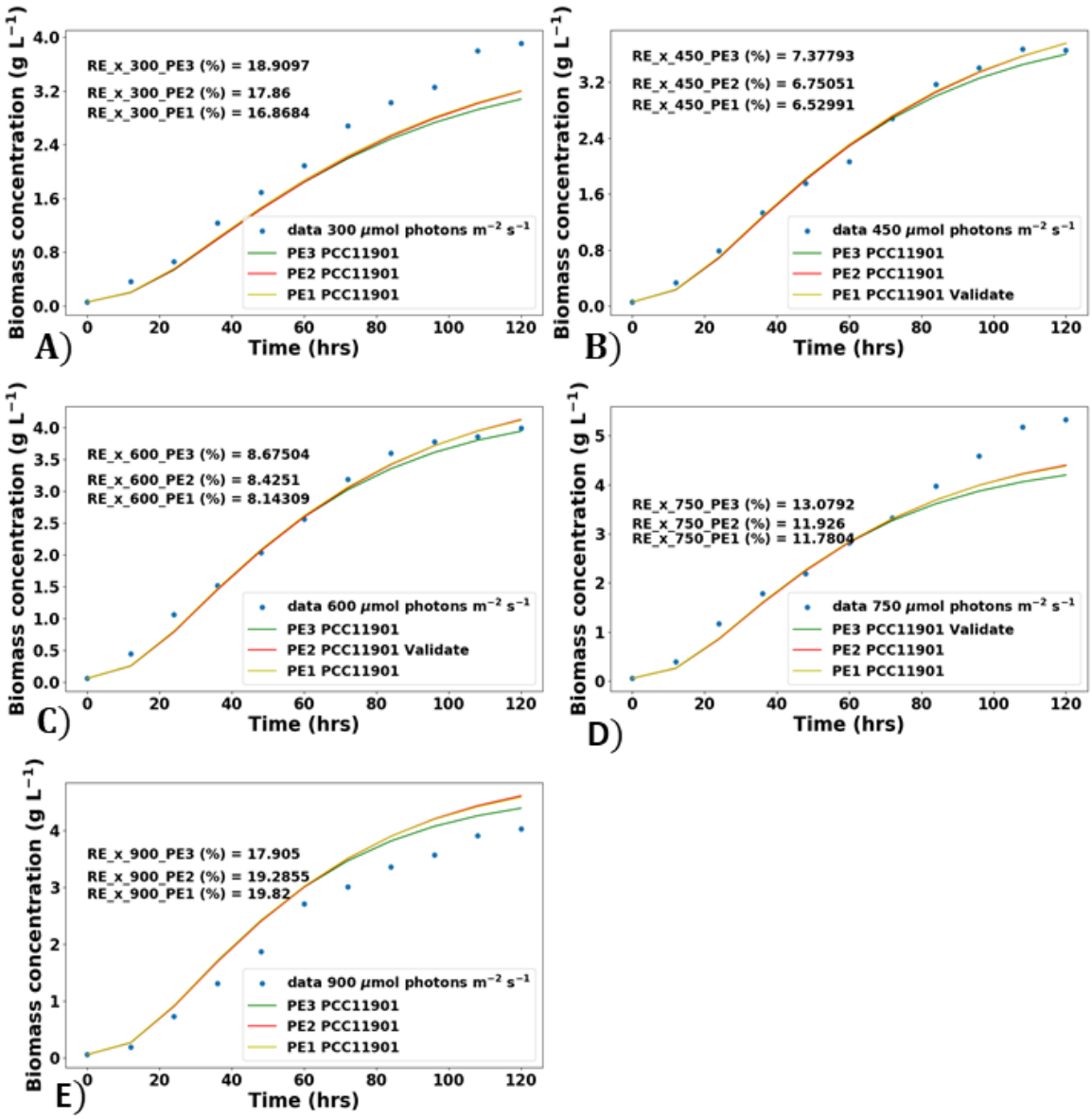

Figure 4.2 Bootstrapping biomass model fitting results for PCC 11901 at: (A) 300 µmol photons m^{-2} s^{-1}, (B) 450 µmol photons m^{-2} s^{-1}, (C) 600 µmol photons m^{-2} s^{-1}, (D) 750 µmol photons m^{-2} s^{-1}, (E) 900 µmol photons m^{-2} s^{-1}. The percentage relative error (%RE) of each fitting is as indicated.

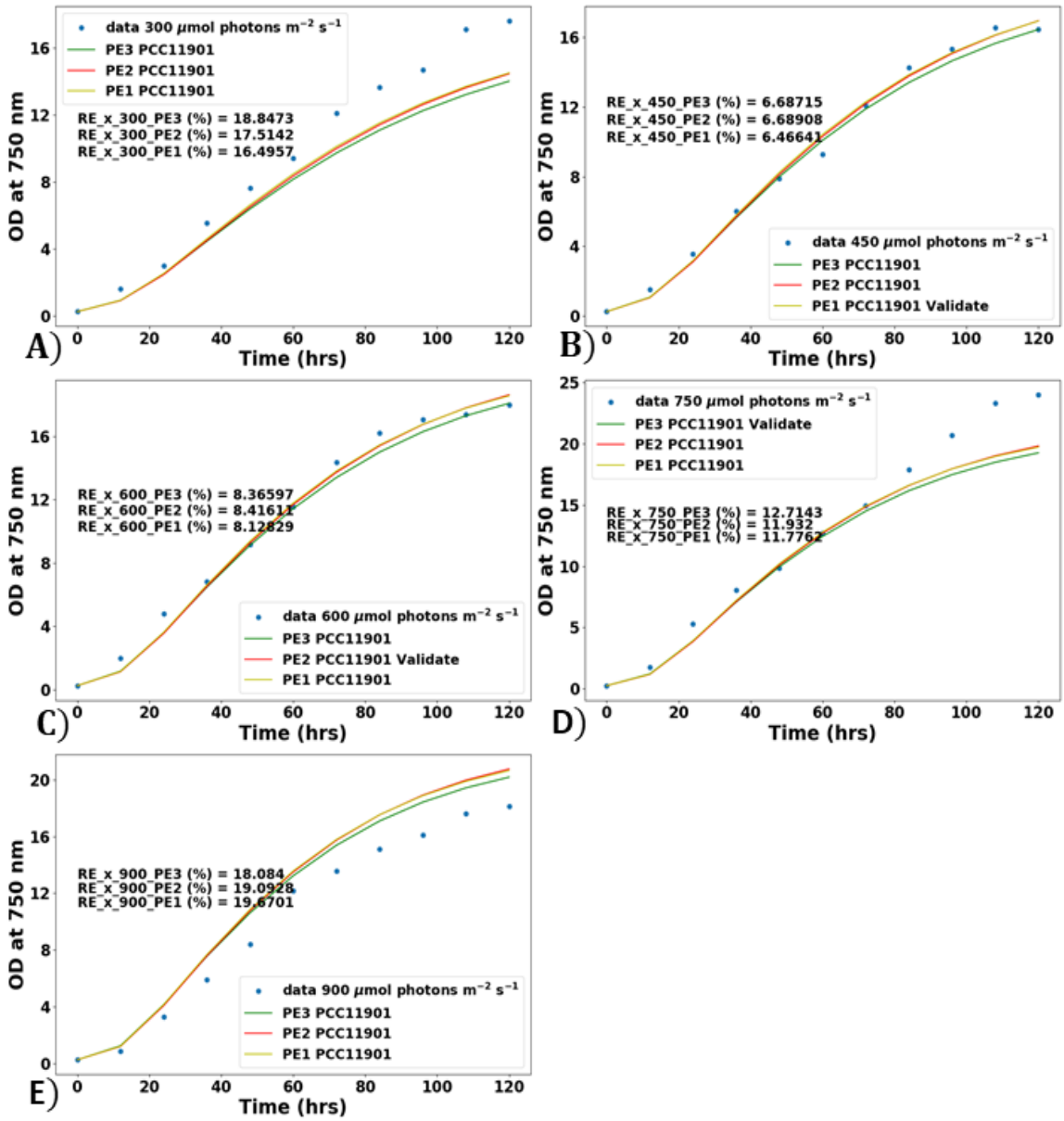

Figure 4.3 Bootstrapping optical density (OD_{750nm}) model fitting results for PCC 11901 at: (A) 300 µmol photons m^{-2} s^{-1}, (B) 450 µmol photons m^{-2} s^{-1}, (C) 600 µmol photons m^{-2} s^{-1}, (D) 750 µmol photons m^{-2} s^{-1}, (E) 900 µmol photons m^{-2} s^{-1}. The percentage relative error (%RE) of each fitting is as indicated.

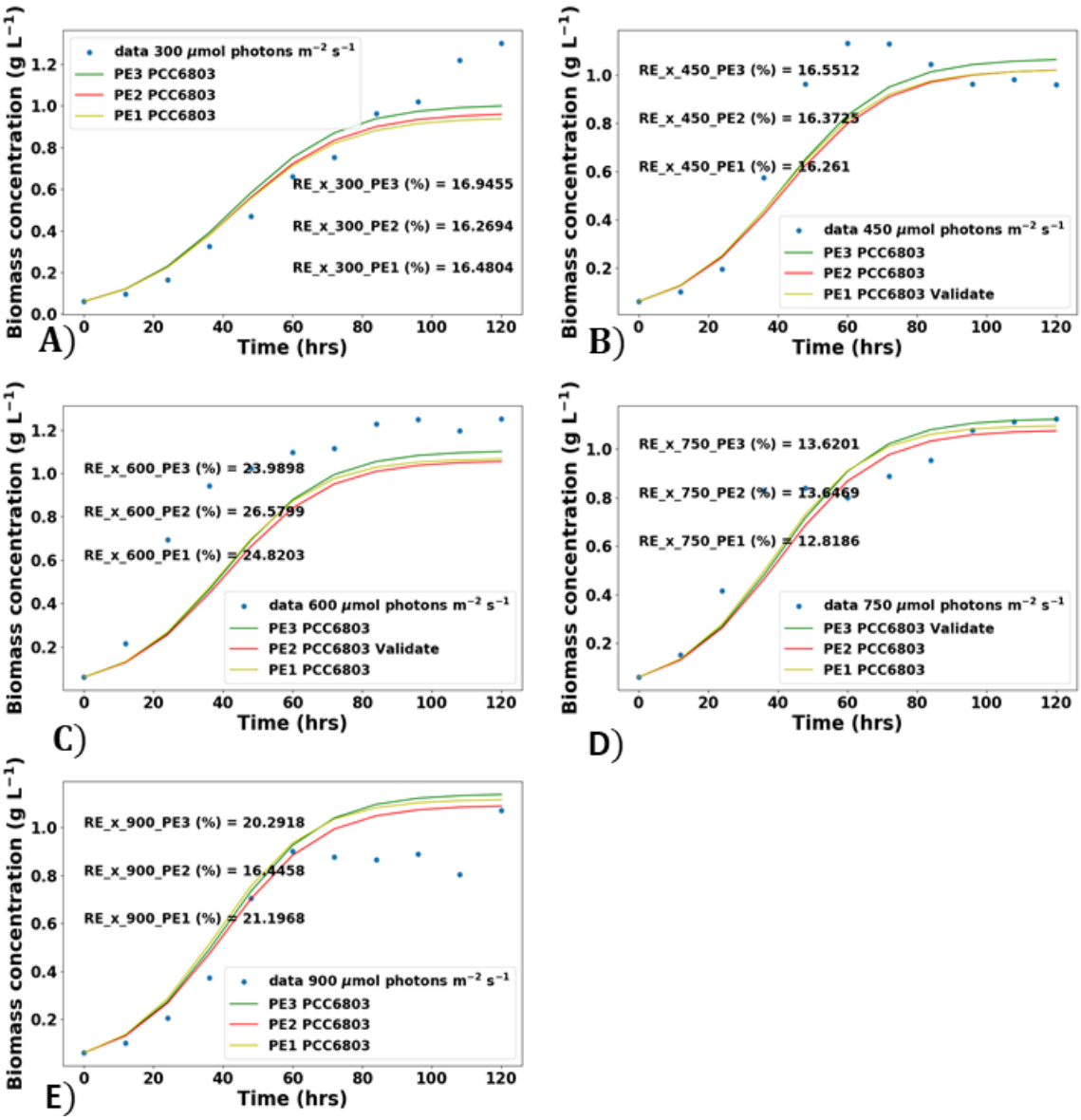

Figure 4.4 Bootstrapping biomass model fitting results for PCC 6803 at: (A) 300 µmol photons m^{-2} s^{-1}, (B) 450 µmol photons m^{-2} s^{-1}, (C) 600 µmol photons m^{-2} s^{-1}, (D) 750 µmol photons m^{-2} s^{-1}, (E) 900 µmol photons m^{-2} s^{-1}. The percentage relative error (%RE) of each fitting is as indicated.

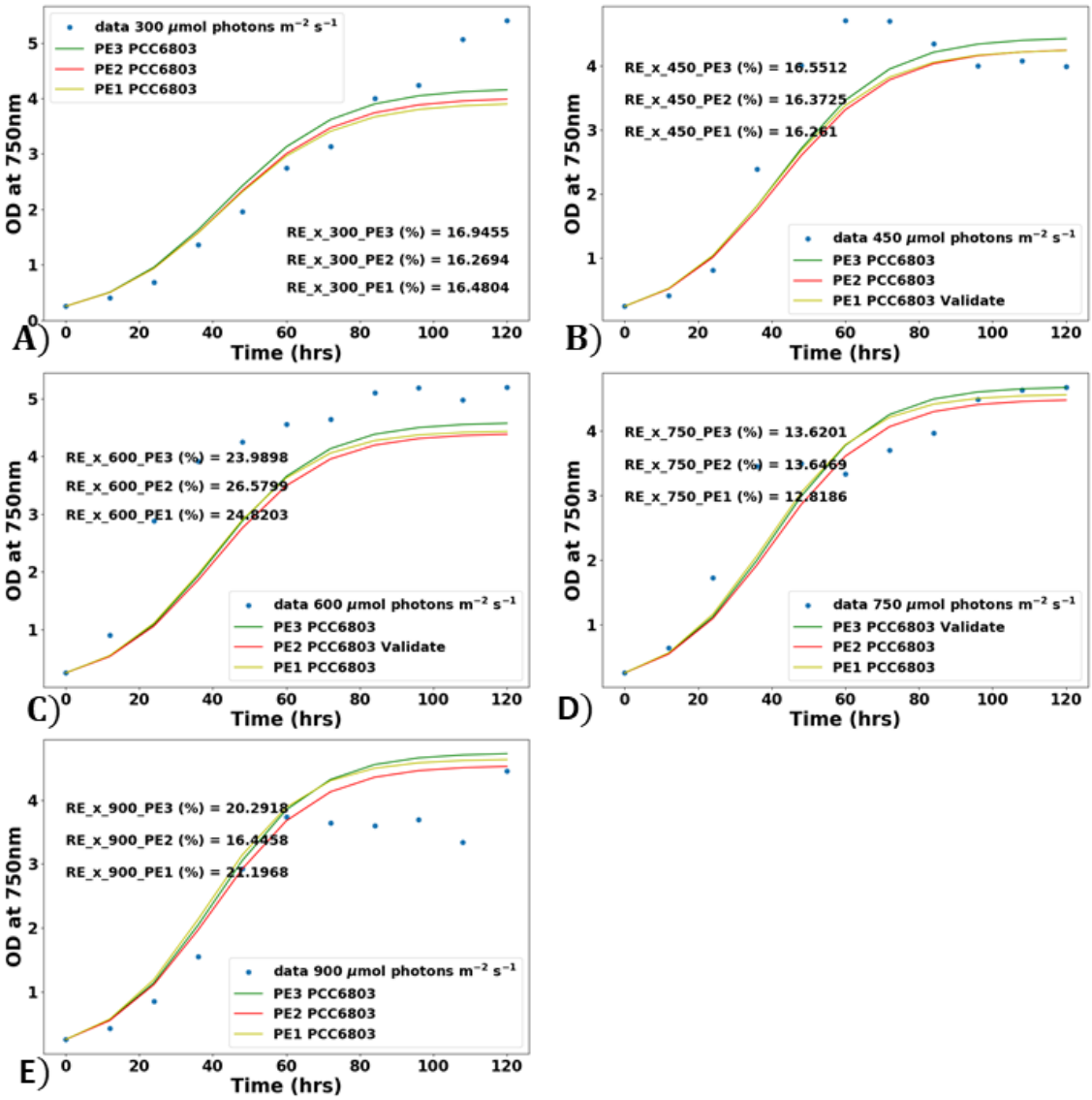

Figure 4.5 Bootstrapping optical density (OD_{750nm}) model fitting results for PCC 6803 at: (A) 300 µmol photons m^{-2} s^{-1}, (B) 450 µmol photons m^{-2} s^{-1}, (C) 600 µmol photons m^{-2} s^{-1}, (D) 750 µmol photons m^{-2} s^{-1}, (E) 900 µmol photons m^{-2} s^{-1}. The percentage relative error (%RE) of each fitting is as indicated.

Table 4.3 Bootstrapping dynamic parameter estimation results for the optical density (OD_{750nm}) and biomass models of the two cyanobacterial strains. Parameter estimates represent the mean of n=3 bootstrapping partitions ± standard deviations as the confidence intervals.

Model parameter	OD_{750} model	Biomass model	Literature range	References
		PCC 11901		
u_m (h^{-1})	$1.99\times 10^{-1} \pm 2.86\times10^{-3}$	$1.99\times 10^{-1} \pm 5.39\times10^{-4}$	(0.004, 0.28)	(51,458,473)
μ_d (h^{-1})	$6.15\times 10^{-4} \pm 8.94\times10^{-6}$	$2.96\times 10^{-3} \pm 2.64\times10^{-4}$	$(8.559\times10^{-3}, 0.005)$	(457,473,474)
k_s (µmol photons m^{-2} s^{-1})	150.0 ± 4.08	156.67 ± 6.24	(70.0, 347.0)	(458,473,475)
k_i (µmol photons m^{-2} s^{-1})	3523.33 $\pm$ 24.94	3522.33 $\pm$ 23.61	(457.0, 53370)	(474,475)
τ (mm^2 g^{-1})	48.57 ± 1.03	208.14 ± 6.62	(67, 225)	(473,475)
β (mm^{-1})	n/a	$3.16\times 10^{-7} \pm 3.07\times10^{-8}$	0.0	(476)
		PCC 6803		
u_m (h^{-1})	$7.9\times 10^{-2} \pm 2.65\times10^{-3}$	$7.9\times 10^{-2} \pm 2.65\times10^{-3}$	(0.004, 0.28)	(51,458,473)
μ_d (h^{-1})	$1.57\times 10^{-2} \pm 3.52\times10^{-4}$	$6.54\times 10^{-2} \pm 1.46\times10^{-3}$	$(8.559\times10^{-3}, 0.005)$	(457,473,474)
K_s (µmol photons m^{-2} s^{-1})	72.84 ± 12.74	72.84 ± 12.74	(70.0, 347.0)	(458,473,475)

n/a: not included in model structure

4.4.1.2 Probabilistic models predictive validations are statistically reliable

The model is also required to estimate optimal growth conditions, as well as simulating, optimising and controlling long-term bioprocessing within an industrial setting. To ensure the models function for these required processes, it was necessary to evaluate the models performance for predicting unseen experimental data sets. Monte Carlo simulations were performed by sampling the model parameter confidence intervals in **Table 4.3Error! Reference source not found.** and propagating their influences on the dynamic models output. **Figure 4.6** shows the biomass model predictions and **Figure 4.7** shows the OD_{750nm} model predictions under uncertainty for the two cyanobacterial strains. Whilst the uncertainty bands reflect the degree of variability imposed by the parameter confidence intervals, those for the biomass and optical density models were similar. The mean prediction from the uncertainty bands (in grey) were computed to compare against the experimental data points. These uncertainty bands are observed to increase in bandwidth size with time, indicating the model to be responsive to changes of these parameters. To evaluate the model's prediction under uncertainty versus the pure model outputs, the overall %RE in **Figure 4.6** were computed and compared to that of the bootstrapping cross validation runs. From this analysis, a 4.5% prediction improvement in PCC 11901 and 3.1% prediction deterioration in PCC 6803, respectively, were observed under uncertainty. The improvement seen with the predictions for PCC 11901 was expected due to the responsive model parameters which tend to improve accuracy (462). However, the prediction deterioration in PCC 6803 was unexpected but could potentially be attributed to the noisy experimental data sets. It is expected that the small prediction deterioration of 3.1% would be reversed if presented with a less noisy experimental data sets.

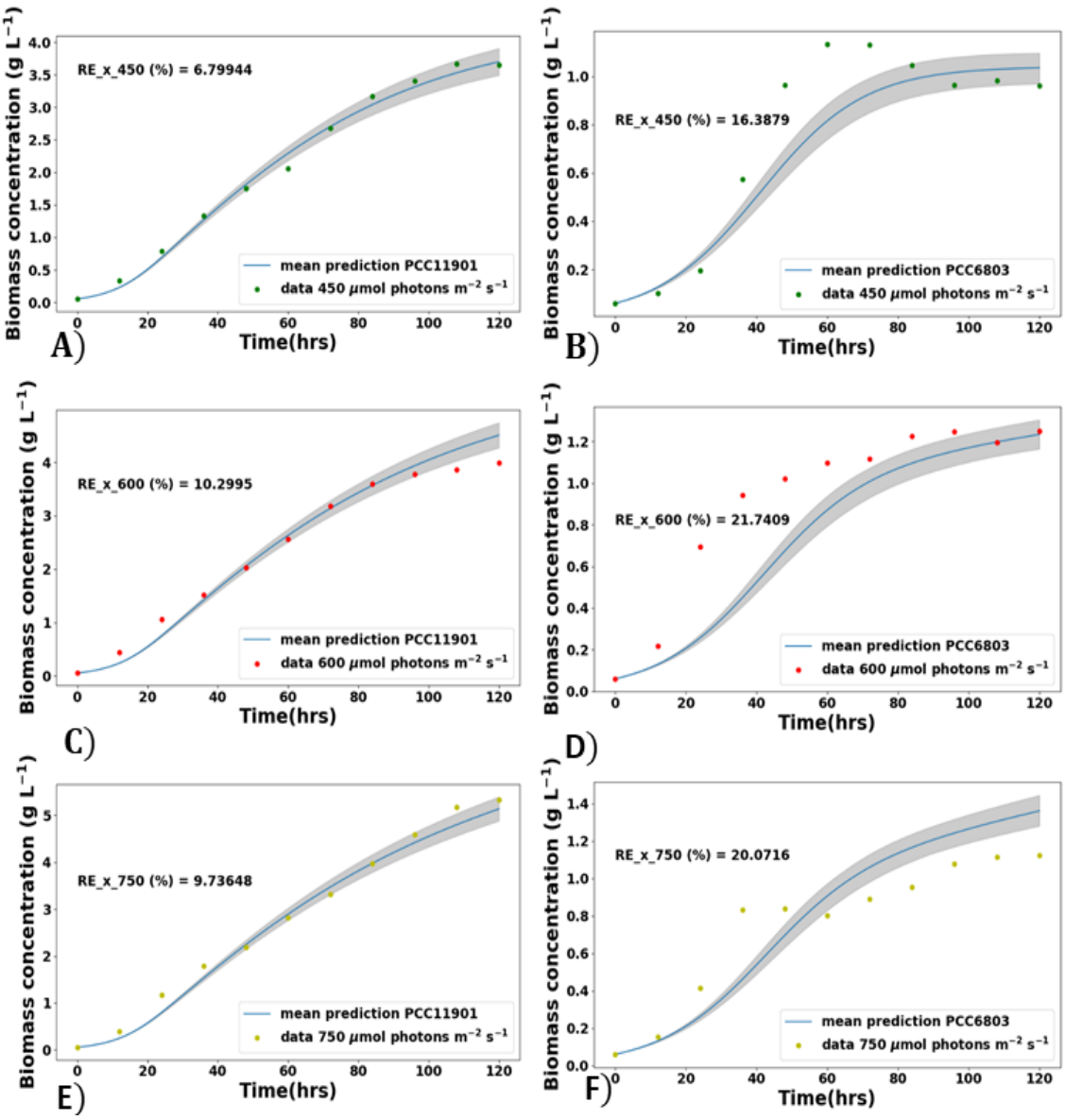

Figure 4.6 Prediction of biomass models under uncertainty. (A), (C) and (E) for PCC 11901, and (B), (D) and (F) for PCC 6803, at 450, 600 and 750 µmol photons m^{-2} s^{-1}, which were unseen experimental data sets during the bootstrapping parameter estimation. The percentage relative error (%RE) of each fitting is as indicated in grey.

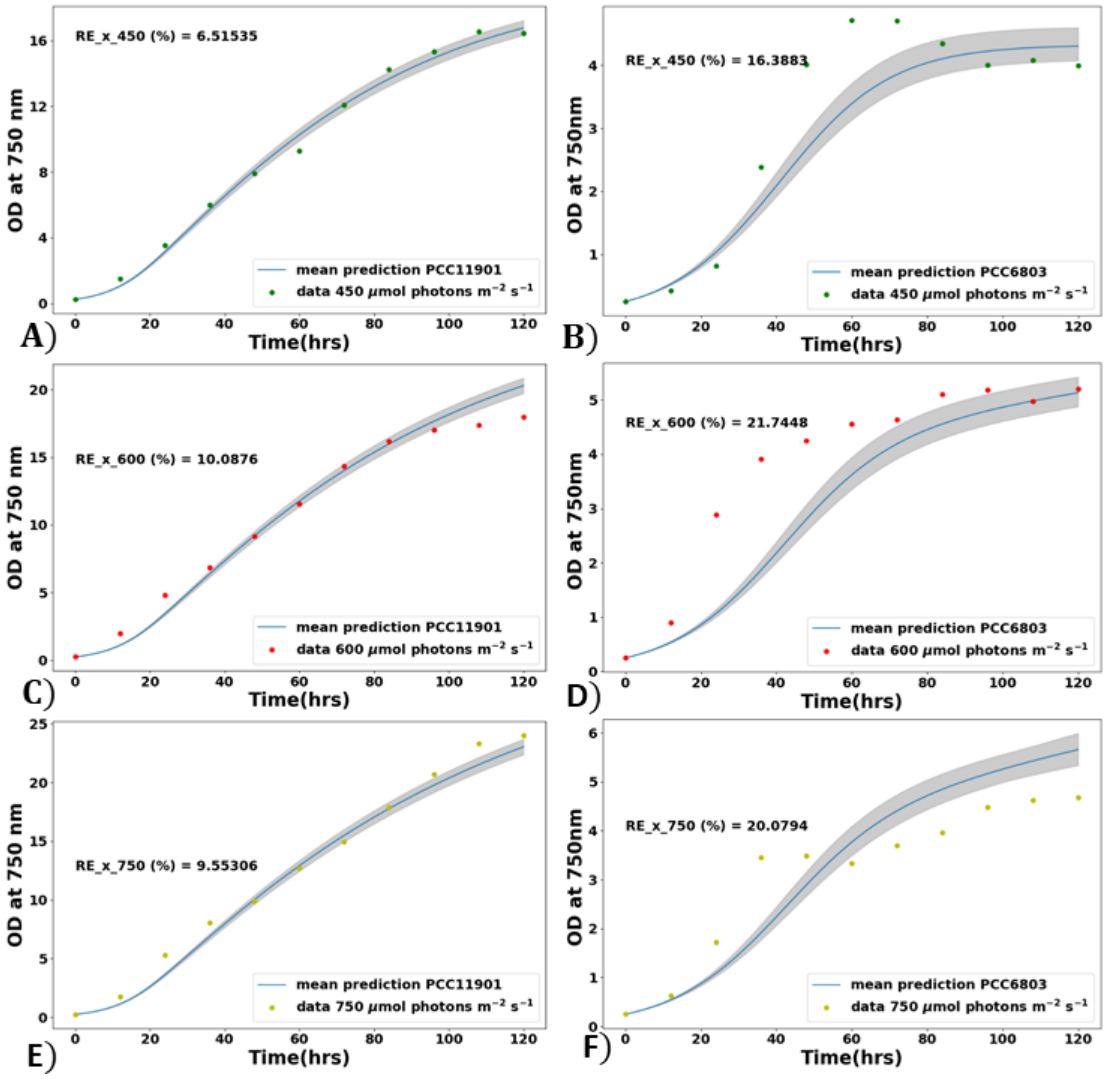

Figure 4.7 Prediction of optical density (OD_{750nm}) models under uncertainty: (A), (C) and (E) for PCC 11901, and (B), (D) and (F) for PCC 6803, at 450, 600 and 750 µmol photons m^{-2} s^{-1}, which were unseen experimental data sets during the bootstrapping parameter estimation. The percentage relative error (%RE) of each fitting is as indicated in grey.

4.4.1.3 Predicted optimal light intensity from computational modelling

From the growth characteristics of the two strains outlined in **Table 4.3Error! Reference source not found.**, it was observed that the maximum specific growth rate of PCC 11901 was over two-fold higher than that of PCC 6803. Whilst this increase was consistent with the experimental data sets, the order of magnitude was however about four-fold higher when comparing the final biomass concentration and optical densities as illustrated in **Error! Reference source not found.**.

Table 4.4 Analysis of the experimental data sets to determine the magnitude of difference in biomass and optical density accumulation among the two cyanobacterial strains at various light intensities. The scale of ratio corresponds to PCC 11901: PCC 6803.

Species	**Highest observed value at different light intensities (µmol photons m^{-2} s^{-1})**		
	300	750	900
Biomass concentration			
PCC 11901	3.91	5.33	4.02
PCC 6803	1.24	1.37	1.07
Scale of ratio	**3.15**	**3.89**	**3.76**
OD_{750}			
PCC 11901	17.61	24	18.13
PCC 6803	5.40	5.20	4.46
Scale of ratio	**3.26**	**4.62**	**4.07**

These disparities indicate that the results outlined in **Table 4.4Error! Reference source not found.** are insufficient for characterising the strain specific growth properties as the dynamic model and estimated parameters is capable of predicting these results, but the reverse is not possible. The light saturation coefficient of PCC 6803 was about two-fold lower than that of PCC 11901, indicating superior light affinity and utilisation efficiency. This implies that PCC 6803 should be the faster growing strain which contradicts previous studies (51,195). Explaining this inconsistency is far beyond the capabilities of the linearised curve fitting literature methods for estimating and

comparing maximum specific growth rate. This was addressed with the dynamic mechanistic modelling approach by analysing the maximum specific growth and decay rates in **Table 4.4Error! Reference source not found.**. Those of PCC 6803 were seen to be of similar order of magnitudes while the decay rate of PCC 11901 was about 67-fold lower than its maximum specific growth rate. This implies that for the portion of absorbed and utilised light intensities within the 300 to 900 µmol photons m^{-2} s^{-1} range, PCC 11901 was experiencing unbalanced growth dominating Eqs. (3) and (4), whereas that of PCC 6803 was balanced. Hence, the higher light affinity and utilisation efficiency of PCC 6803 compared to PCC 11901 was not directed towards growth promoting activities and was herein interpreted to be either for (i) cell maintenance, and/or (ii) fluorescence heat generation. Cell maintenance encompasses non-growth related metabolic activities performed by the cells to stay alive which usually consume energy in the form ATP. Since ATP and NADPH are products of light dependent reactions (477), it was reasonable to assume that ATP and NADPH generation in PCC 6803 was mostly directed towards cell maintenance and not for carbon fixation via the Calvin-Benson-Basshan cycle. This hypothesis was validated as the final biomass concentration ultimately derived from carbon fixation did not change within the investigated 300 to 900 µmol photons m^{-2} s^{-1} range. This also suggests that extra absorbed light above 300 µmol photons m^{-2} s^{-1} was mostly wasted as heat and not utilised for growth of PCC 6803 due to the balanced equations of Eqs. (3) and (4).

The remaining two questions were only valid for PCC 11901 since the 300 to 900 µmol photons m^{-2} s^{-1} range were observed to be above the light intensity saturation threshold for PCC 6803, suggesting growth is light independent at these intensities. As per the optimal light intensity of PCC 11901, the model derivative with respect to the light intensity was equated to zero, thereby resulting in optimal light intensities of 727.0 µmol photons m^{-2} s^{-1} and 742.9 µmol photons m^{-2} s^{-1} for the biomass and optical density models, respectively, and averaging 735.0 µmol photons m^{-2} s^{-1} to encompass both aspects. The similar optimal light intensity between the two models (i.e., biomass and OD_{750nm}) suggest that they can be used interchangeably for (i) optimal design of experiments, and (ii) online bioprocess control since OD_{750nm} measurements with a UV/VIS spectrophotometer is easier and quicker to measure than quantifying biomass. The predicted optimal light intensities are within the range seen in several other cyanobacterial species (51,195,478), supporting the validity of the models predicted output. Although the predicted light intensity was slightly lower than the reported experimental optimal intensity of 750.0 µmol photons m^{-2} s^{-1}, the 15 µmol photons m^{-2} s^{-1} difference was negligibly small (circa 2%) and indicates the accurate dynamic estimation from the model regarding the PBR light path length.

1

4.5 Discussion

4.5.1 PCC 11901 can sustain fast growth and biomass accumulation over a range of light intensities

From the results reported in Chapter 3, we confirmed that PCC 11901 was the fastest growing species amongst a range of model cyanobacterial species over 3 days at 38°C with air/5% CO_2. However, growth should be monitored over a range of light intensities to establish the optimal light intensity and tolerance. Our data demonstrates that PCC 11901 is capable of fast growth and high biomass accumulation under a wide range of light intensities when grown with 5% CO_2/air at 38°C. Furthermore, maximal biomass accumulation could be maintained in indoor photobioreactors cultured under the lowest tested light intensity (~300 µmol photons m^{-2} s^{-1}), potentially reducing costs for indoor bioreactors by lowering the need for energy intensive lighting.

4.5.2 Optimal light intensity can be predicted for PCC 11901 and PCC 6803 under different PBR growth parameters

Computational modelling was used to determine optimal light intensity for each species when grown under the conditions described in this chapter. The model can predict two objectives, biomass accumulation or high growth. Models for OD_{750nm} for PCC 11901 and PCC 6803 were previously unavailable. The similarities of their growth profile to biomass models justified the existence of similar model structures and was herein implemented for the first time. The model for PCC 11901 embedded the complicated influences of incident light intensity, light attenuation and photomechanisms, whereas the PCC 6803 model was only limited by the incident light intensity and photosaturation mechanisms. To simultaneously estimate the model parameter values and their associated confidence intervals, bootstrapping techniques with three-fold cross validations was implemented. Thereafter, the models predictions under uncertainties were thoroughly validated against unseen experimental data sets with small simulation errors averaging less than 19%. Of the two species, PCC 11901 showed superior prediction fidelities and faster growth. Whilst fluorometry measurements are recommended in future for confirming the light-stressed photosynthetic activities of PCC 6803 within the 300 to 900 µmol photons m^{-2} s^{-1} range, further model-based analysis was carried out on the PCC 11901 model parameters. As a result, 735.0 µmol photons m^{-2} s^{-1} was identified as the optimal cultivation light intensity. These findings will benefit future biotechnological upscaling, online bioprocess control and exploitation of these strains.

The model was also used to predict if upscaling the PBR used to grow PCC 11901 will be severely impacted by light intensity. The light absorption coefficient (τ) was identified as the main parameter to be compared against values from photobioreactors of different scales and configurations. This was motivated by the intrinsic nature of the light absorption coefficient to cyanobacteria and the light attenuation challenges being the primary limitation for upscaling photobiological processes, as was investigated by Anye Cho *et al*., (456). A high light absorption coefficient would indicate rapid diminishing local light transmissions within the PBR as its diameter was increased for upscaling, and vice-versa. The PCC 11901 light absorption coefficient compared well to that observed in previous studies (473,475) ($67 \leq \tau \leq 225$ $mm^2\ g^{-1}$) outlined in **Table 4.3Error! Reference source not found.**. This suggests that upscaling of PCC 11901 cultivation will not be severely impacted by light intensity since previous studies used PBRs ranging from 0.5 L cylindrical PBRs (479,480), 1.0 L flat-plate (460,475) and tubular (481) PBRs, to as large as 120.0 L flat-plate PBRs (482,483).

Chapter 5

Attempts to develop of a novel method for the production of markerless mutants in *Synechococcus* sp. PCC 11901.

Sections of this chapter have previously been published in Biomolecules 12 (7)

Development of a Biotechnology Platform for the Fast-Growing Cyanobacterium Synechococcus sp. PCC 11901.
Mills, L.A.; Moreno-Cabezuelo, J.Á.; Włodarczyk, A.; Victoria, A.J.; Mejías, R.; Nenninger, A.; Moxon, S.; Bombelli, P.; Selão, T.T.; McCormick, A.J.; Lea-Smith, D.J. Biomolecules 12 (7)

Chapter 5: Attempts to develop a novel method for the production of markerless mutants in *Synechococcus* sp. PCC 11901.

5.1 Introduction

The ability to generate mutants is key to understanding cyanobacterial photosynthesis, biochemistry and physiology, and is essential for development of strains for industrial purposes. To unlock the full potential of cyanobacteria as a biotechnology chassis it is important to be able to genetically manipulate and control gene expression. PCC 11901 demonstrates a multitude of attractive traits for genetic amenability: it is naturally transformable; there are synthetic tools which already exist for the closely related species PCC 7002 which are compatible with PCC 11901; it demonstrates sensitivity against a range of antibiotics (51). Marked genetic manipulation of PCC 11901 has been demonstrated using selectable markers (kanamycin, spectinomycin, acrylic acid) and was used to knock out the *fadD* gene, thereby increasing the production of industrially relevant free fatty acids (51). However, a system for generating unmarked mutants at different chromosomal locations in this species has not yet been demonstrated.

5.1.1 Markerless mutants and the requirement for their application within biotechnology

The standard method for generating genetically modified strains is via insertion of an antibiotic resistance cassette into the site of interest (i.e. a marked mutant). Traditional insertion of antibiotic resistance cassettes limits the number of mutations that can be introduced into a strain as only a few antibiotic resistance cassettes are available for cyanobacteria (130). The absence of genes encoding antibiotic resistance cassettes is desirable in strains that may be potentially cultured outdoors, avoiding the possibility that they may be transferred to environmental species. The generation of markerless mutants (or unmarked mutants) overcomes these limitations. Unmarked mutants are generated via insertion of an antibiotic resistance cassette into the target site, followed by subsequent removal of this cassette using a negative selectable marker. Unmarked mutants contain no foreign DNA, unless intentionally included, and can be repeatedly genetically manipulated, which is a major advantage for the development of industrial strains (42). In addition,

polar effects on genes downstream of the modification site can be minimized, allowing more precise modification of the organism (20).

5.1.2 Production of markerless mutants using *sacB*

The *sacB* gene, endogenous to *Bacillus subtilis*, encodes for the enzyme, levansucrase, which confers sensitivity to sucrose. Expression of *sacB* is regulated by the *cis*-activating regulatory locus *sacR* and is induced by the presence of sucrose (484). Levansucrase transfers fructosyl residues from sucrose via hydrolysis to different acceptors, such as levans, water and other sugars (484). Levans are branched polymers made up of fructosyl residues which cannot be metabolized by most Gram-negative bacteria (484–486). The mechanism of toxicity is still not fully understood. Two methods have been proposed, the first being that the fructosyl residues may be transferred to metabolically important acceptors and thereby disrupt cell metabolism. The second hypothesis is that the levans play a role in cell death by accumulating in the periplasm (38) and are then unable to be cleaved or exported out of the cell (486,487).

In order to generate markerless knock-out mutants in PCC 6803 using *sacB*, marked mutants are first produced (**Figure 5.1**). The suicide plasmid contains two DNA fragments identical to regions in the cyanobacterial chromosome flanking the region to be deleted (termed the 5' and 3' flanking regions). Two genes, an antibiotic resistance gene and *sacB*, are inserted between these flanking regions. The plasmid is then added to a liquid culture of cyanobacteria where the DNA is naturally taken up by the cells. Transformants are selected on agar plates containing the appropriate antibiotic and verified via colony PCR. The marked mutant is then mixed with the second plasmid containing only the 5’ and 3’ flanking regions. Selection for transformants is then carried out via growth on agar plates containing sucrose. Sucrose is lethal to cells expressing *sacB*, thereby facilitating recombination of the antibiotic resistance gene and *sacB* out of the chromosome and onto the plasmid, which is subsequently lost following cell division (40).

The *sacB*-sucrose method was established in *Anabaena* sp. PCC 7120 (488) and has been shown to successfully generate mutants in glucose tolerant PCC 6803 (40,489). This method, however, has been unsuccessful in generating markerless mutants in PCC 7002, an organism with high genetic similarity to PCC 11901 (40), as wild-type PCC 7002 is unable to grow on media containing sucrose which is required for the counter-selection stage (**Figure 5.1**).

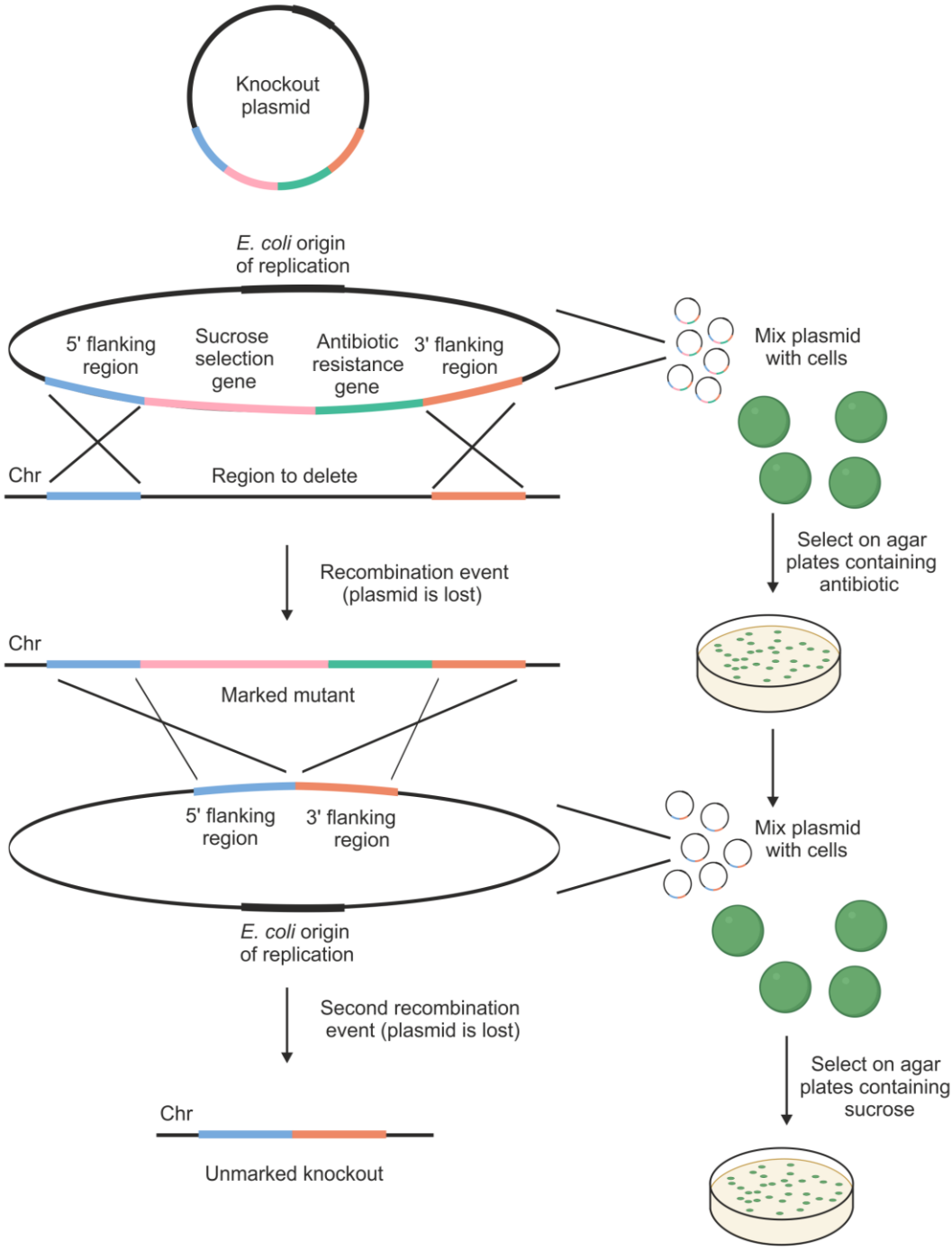

Figure 5.1 Generation of marked and unmarked mutants in cyanobacteria. Schematic detailing recombination and the experimental steps involved in mutant generation. Plasmid A is first mixed with cells. Following incubation on agar plates containing kanamycin, colonies in which a recombination event occurs between the 5' and 3' flanking regions (indicated in blue and orange, respectively) and the homologous sequence in the chromosome, are isolated. In addition, the *sacB* cassette between the 5' and 3' flanking regions is inserted into the chromosome. Following segregation, a marked mutant is generated. Marked mutant cells are then mixed with plasmid B which contains just the 5' and 3' flanking regions. A second homologous recombination event occurs between the 5' and 3' flanking regions and the homologous regions in the chromosome, resulting in removal of the antibiotic resistance/*sacB* cassette and production of an unmarked knockout. Insertion of foreign DNA between the 5' and 3' flanking regions in plasmid B will result in insertion of this region into the chromosome. Figure adapted from Lea-Smith et al. (2016) (10).

5.1.3 Alternative methods used in production of markerless mutants in cyanobacteria

Several methods have been used to produce markerless mutants in cyanobacteria, **Table 5.1**. These can be sub-classed into counter-selection methods and site-specific recombinase systems.

Table 5.1 Overview of the various methods used to produce markerless transformants in cyanobacteria. Adapted from Branco dos Santos et al., 2014 (490)

	Methods	Strains Tested	Reference
Counter-Selection	*sacB*-sucrose	*Synechocystis* sp. PCC 6803 *Anabaena* sp. PCC 7120	(40,489) (488)
	mazF-nickel	*Synechocystis* sp. PCC 6803	(491)
	acsA-acrylate	*Synechococcus* sp. PCC 7002	(188)
	upp-5-Fluorouracil	*Synechocystis* sp. PCC 6803 *Synechococcus* sp. PCC 7002 *Synechococcus elongatus* PCC 7942	(492) (492) (493)
Site-specific recombinase systems	FLP/FRT	*Synechococcus elongatus* PCC 7942 *Synechocystis* sp. PCC 6803	(494) (494)
	Cre/LoxP	*Anabaena* sp. PCC 7120 *Synechococcus* sp. PCC 7002	(495) (47)

The *mazF*-nickel method is based upon the *sacB*-sucrose technique (Section 5.1.2.) and was designed to be used in cyanobacteria that can integrate DNA by homologues recombination but are unable to take-up sucrose. Although originally designed for strains which were unable to use the *sacB*-sucrose counter selection method, this system has so far only been successfully demonstrated in PCC 6803 (491). Acrylate has been shown as a suitable counter selection compound for generating mutants in PCC 7002. Under normal conditions, acrylate inhibits PCC 7002. However, with the loss of the *acsA* gene which encodes for acetyl-CoA ligase this inhibition can be overcome (188). It is therefore possible to create markerless mutants by selecting for the loss of the *acsA* gene in the presence of acrylate, following a similar protocol to the *sacB*-sucrose method. Although successful mutants were produced, it does require the original *acsA* gene to be knocked out of the species, and to date this method has only been performed in PCC 7002. Similar difficulties are also observed using the *upp*-5-fluorouracil method, which has been performed in PCC 6803, PCC 7942 and PCC 7002, but requires the deletion of the *upp* gene (492,493). The *upp* gene encodes for the enzyme uracil phosphoribosyltransferase, which converts uracil to UMP but can also convert 5-fluorouracil to 5-fluoro-UMP, which inhibits protein synthesis and leads to cell

death. This method has only been eluded to in patents and is yet to be published in a scientific paper.

5.1.4 The potential of *codA* expression as a viable counter-selection marker

The native *E. coli codA* gene encodes the cytosine deaminase enzyme which converts cytosine and water into uracil and ammonia in prokaryotes, fungi and some eukaryotic microorganisms (**Figure 5.2**) (496). In some cases, cytosine deaminase can also convert 5-flurocytosine (5-FC), an anti-fungal drug, to 5-fluorouracil, which leads to inhibition of DNA and protein synthesis which ultimately leads to cell death (497). Attempts to use *codA*-5-FC negative selection in PCC 6803 had mixed success, with around 75% of potential markerless mutants still containing the *codA* or reverting back to a wild type genotype (19). However, *codA* has been successfully used as a negative selectable marker in a number of organisms (498–502). Due to its success in other systems, this could be a suitable method for generating markerless mutants in PCC 11901.

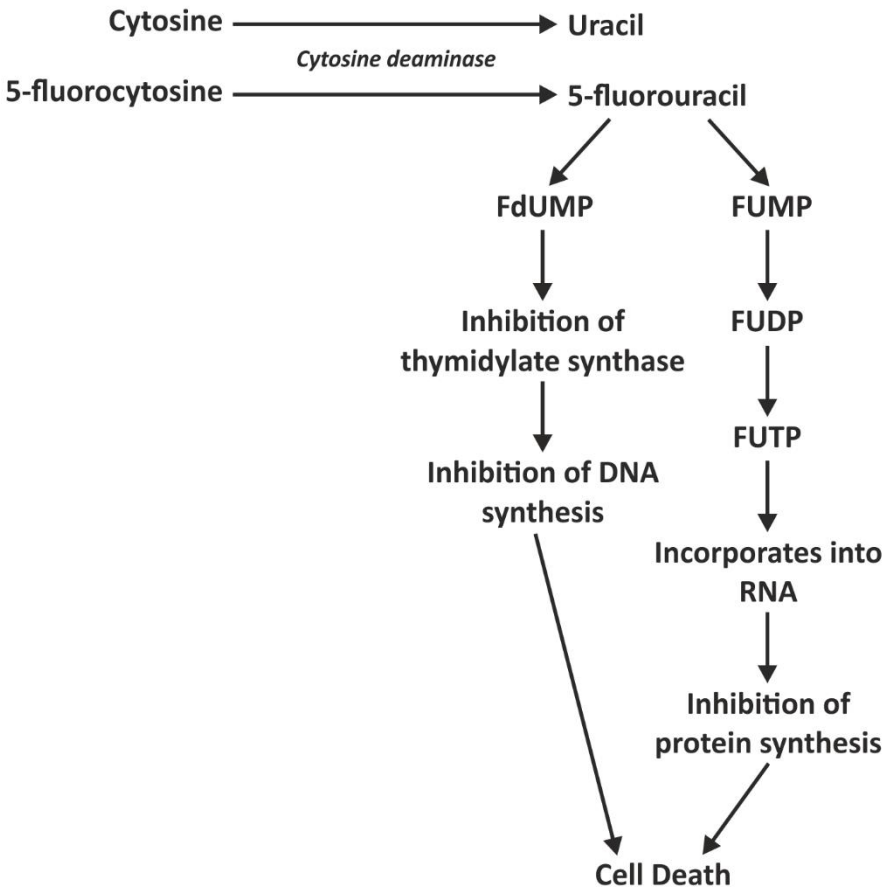

Figure 5.2 Pathway and mode of action of 5-fluorocytosine. Figure adapted from Lui (2017) (23). FUMP, 5-fluorouridine monophosphate; FUDP, 5-fluorouridine monophosphate; FUTP, 5-fluorouridine triphosphate; FdUMP, 5-fluorodeoxyuridine monophosphate

5.1.5 Site-specific recombinase unmarking systems

Another potential strategy for generating unmarked mutants in cyanobacteria is the use of site-specific recombinases such as the flippase (FLP) from *S. cerevisiae* and the Cre recombinase from *E. coli* bacteriophage P1. The FLP system recognises short target DNA sequences known as FLP Recognition Targets (FRT) and has been successfully used to generate markerless mutants in PCC 6803 and PCC 7942 (494).

The Cre recombinase enzyme works via a similar mechanism but recognises short target sequences known as lox sites. The method was originally demonstrated in *Anabaena* sp. PCC 7120 (495) and has recently been developed for generating unmarked mutants in PCC 7002 and PCC 6803 (47). This system relies on integrating an antibiotic resistance cassette flanked by lox66 and lox71 recombinase sites into the chromosomal target site to generate a marked knockout (**Figure 5.3**). A second plasmid encoding the Cre recombinase is then integrated into a non-essential region of the *rbcLXS* site (encoding for RuBisCO and the associated chaperone) using a second antibiotic resistance marker. Expression of Cre leads to excision of the original antibiotic resistance cassette, resulting in the generation of an unmarked mutant at the site of interest, although parts of the lox66 and lox71 sites are retained. Finally, culturing this strain in the absence of the second antibiotic results in the gene encoding Cre, plus the second antibiotic selection, being removed from the population. While this method does not result in production of scarless unmarked mutants or precise genetic engineering, strains can be repeatedly genetically manipulated and due to the genetic similarity between PCC 7002 and PCC 11901 it could be a viable method of generating unmarked mutants.

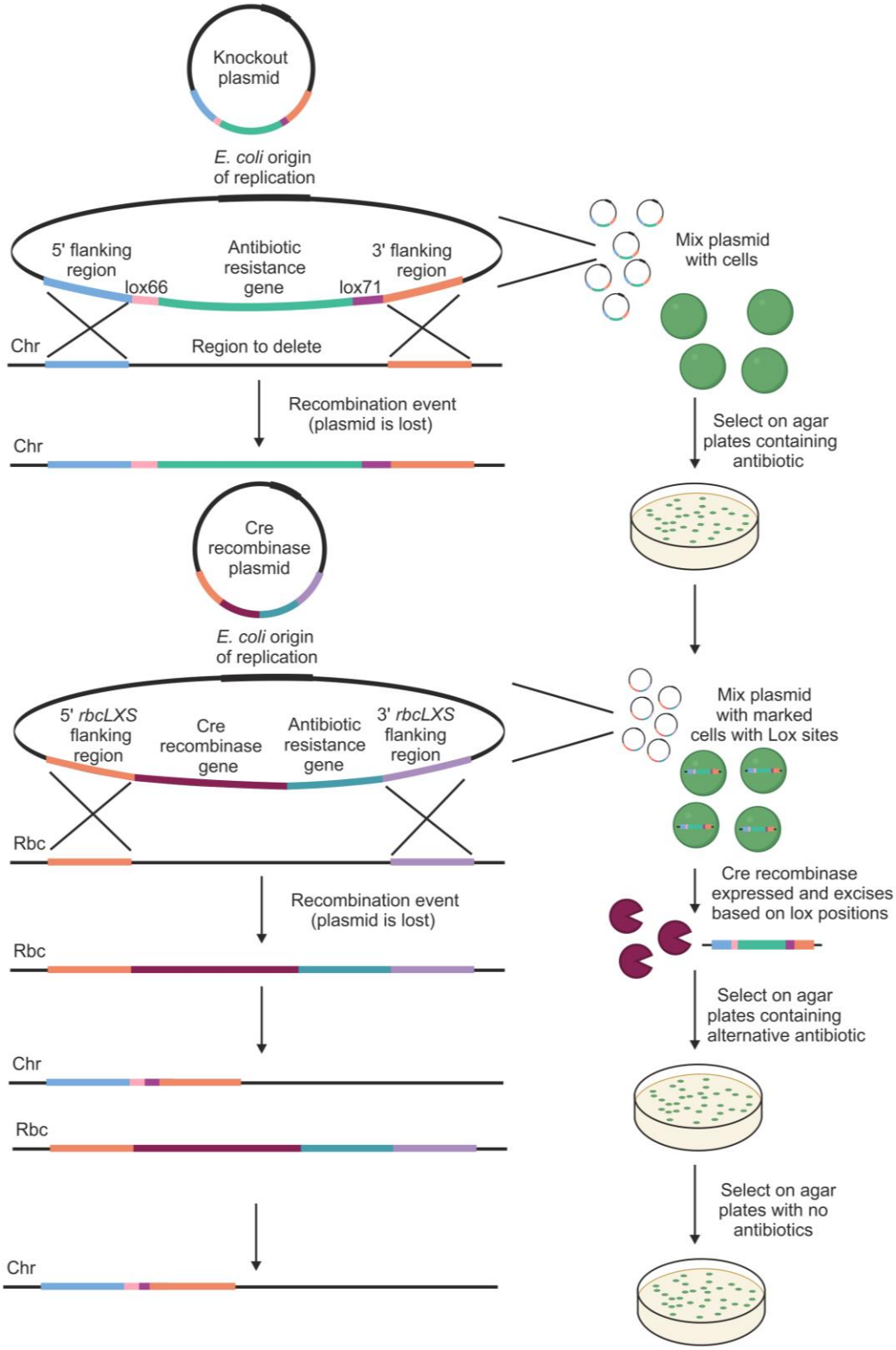

Figure 5.3 Generation of marked and unmarked mutants in cyanobacteria using the Cre-Lox recombinase method.

Schematic detailing Cre-lox recombination and the experimental steps involved in mutant generation as described for PCC 7002 and PCC 6803 in Jones et al. (47). Plasmid A is first mixed with cells. Following incubation on agar plates containing kanamycin, colonies in which a recombination event occurs between the 5' and 3' flanking regions (indicated in blue and orange, respectively) and the homologous sequence in the chromosome, are isolated. Following segregation by repeated streaking a marked mutant is generated. Marked mutant cells are then mixed with plasmid B which

contains the 5' and 3' flanking *rbcLXS* regions. A second homologous recombination event occurs between the 5' and 3' flanking *rbcLXS* regions and the homologous regions in the chromosome. Cells are incubated on agar plates containing spectinomycin with the surviving mutants expressing Cre recombinase (indicated in coral) which excises the DNA region between the lox66 (indicated in pink) and lox71 sites (indicated in dark purple). The unmarked mutants are then grown on solid agar with no antibiotic resistance and the Cre recombinase and spectinomycin resistance genes are recombined out of the *rbcLXS* site.

5.1.6 Chapter aims and objectives

The initial objective of this chapter was to demonstrate the production of markerless mutants in PCC 11901 via expression of the non-native *codA* gene and in the presence of 5-FC. Although generation of multiple marked mutants were successfully developed, attempts to create unmarked mutants were unsuccessful. This led to the second objective of attempting to generate unmarked mutants using the Cre-loxP recombinase system designed for PCC 7002. The work presented in this chapter describes the attempts carried out to generate unmarked mutants using the *codA*-5-FC method and the Cre-loxP site-specific recombinase systems in PCC 11901 which would further cement its potential as a biotechnology chassis.

5.2 Materials and Methods

5.2.1 Molecular Genetic Methods

5.2.1.1 Extraction of template DNA

A small volume of cyanobacterial cells was scraped from a plate and suspended in 50 µL of ultrapure water in a PCR tube. Tubes were then placed in a thermocycler (BioRad) at 100°C and left to incubate for 5 minutes. 5 µL was then used as template DNA in PCR reactions.

5.2.1.2 Amplification of genomic DNA

Phusion High-Fidelity DNA Polymerase (Phusion HF) (New England BioLabs (NEB)) was used to amplify DNA fragments required for plasmid construction, using the corresponding primers listed in **Table 5.2**. All primers used were synthesised by Eurofins Genomics, Germany. A typical 20 µl reaction mixture contained: 4 µl 5x Phusion HF Buffer, 0.2 µl Phusion DNA Polymerase, 0.6 µL DMSO, 0.4 µl 2'deoxyribonucleoside triphosphate (dNTP) mixture, 1 µl 10 µM forward primer, 1 µl 10 µM reverse primer, and ~10-100 ng template DNA (or 5 µl cyanobacterial DNA template; see 4.2.1.1.), made up to 20 µl with ultrapure water.

The standard Phusion HF PCR protocol consisted of an initial denaturation step at 98°C for 30 seconds, and 35 subsequent cycles of 98°C for 10 seconds (denaturation), 62°C for 30 seconds (primer annealing), 72°C for 30 seconds (primer extension), with a final extension at 72°C for 5 minutes. The annealing temperature varied depending on the primers used.

Table 5.2 Oligonucleotide primers used in this work. All primers were purchased from Eurofins Genomics.

Primer	Sequence (5' – 3')	Purpose
ARTO_LF	ATCGAGGTCTCAGGAGCGGAAACCAACCAGAGAAATTC	Generation of left flank for *codA*-5-FC method
ARTO_LR	AGCTCGGTCTCTTCATGTAATCGCTCACAAACCATGACC	Generation of left flank for *codA*-5-FC method
ARTO_RF	TGCACGGTCTCAATAACATTGGTCACTAAAGCCTCTTG	Generation of right flank for *codA*-5-FC method
ARTO_RR	GCTCAGGTCTCTAGCGTGTATGTCCACGGCACTTTG	Generation of right flank for *codA*-5-FC method
COX_LF	ATCGAGGTCTCAGGAGCCTTTAGTGGTTGACGTGAA	Generation of left flank for *codA*-5-FC method
COX_LR	AGCTCGGTCTCTTCATTCGCAAGTTCTGTGCGGACA	Generation of left flank for *codA*-5-FC method
COX_RF	TGCACGGTCTCAATAAGATGAACCGCCGCATTGCCC	Generation of right flank for *codA*-5-FC method
COX_RR	GCTCAGGTCTCTAGCGATCAGTGCCGTAATCCCGAA	Generation of right flank for *codA*-5-FC method
COXfor	AGGCAATGTTCCCCTAGAGA	Confirmation of gene segregation
COXrev	ACCCCGTCAGCACATAGAAA	Confirmation of gene segregation
ARTOfor	CGAAGAGTAACATCACCGCC	Confirmation of gene segregation
ARTOrev	ATACGATGATTTGGCACGGC	Confirmation of gene segregation
COX_LF_LOX	GTACGAAGACTCCATTCCTTTAGTGGTTGACGTGAA	Generation of left flank with lox66 sites for Cre-lox method
COX_LR_LOX	GTACGAAGACCTGGAGTCGCAAGTTCTGTGCGG	Generation of left flank with lox66 sites for Cre-lox method
COX_RF_LOX	GTACGAAGACCTAGCGGATGAACCGCCGCATT	Generation of right flank with lox71 sites for Cre-lox method
COX_RR_LOX	GTACGAAGACCTGCTTATCAGTGCCGTAATCCCGAA	Generation of right flank with lox71 sites for Cre-lox method
ARTO_LF_LOX	GTACGAAGACTCCATTCGGAAACCAACCAGAGAAATTC	Generation of left flank with lox66 sites for Cre-lox method
ARTO_LR_LOX	GTACGAAGACCTGGAGGTAATCGCTCACAAACCATG	Generation of left flank with lox66 sites for Cre-lox method

ARTO_RF_LOX	GTACGAAGACCTAGCGCATTGGTCACTAAAGCCTCTT	Generation of right flank with lox71 sites for Cre-lox method
ARTO_RR_LOX	GTACGAAGACCTGCTTTGTATGTCCACGGCACTTTG	Generation of right flank with lox71 sites for Cre-lox method
acs_LF_LOX	GTACGAAGACTCCATTGTATCGCCCACAATTTCCTG	Generation of left flank with lox66 sites for Cre-lox method
acs_LR_LOX	GTACGAAGACCTGGAGGGGTTAAGACATCCCCAATA	Generation of left flank with lox66 sites for Cre-lox method
acs_RF_LOX	GTACGAAGACCTAGCGCCTCTTCGAGGCGACTG	Generation of right flank with lox71 sites for Cre-lox method
acs_RR_LOX	GTACGAAGACCTGCTTTTATGTCCGAACAAAACATT	Generation of right flank with lox71 sites for Cre-lox method
ldhA_LF_LOX	GTACGAAGACTCCATTTTTCTAGGGACATAACTGAT	Generation of left flank with lox66 sites for Cre-lox method
ldhA_LR_LOX	GTACGAAGACCTGGAGATTTACCAGATTTGCTCACC	Generation of left flank with lox66 sites for Cre-lox method
ldhA_RF_LOX	GTACGAAGACCTAGCGTGCATAATTTTGGCAAAGCA	Generation of right flank with lox71 sites for Cre-lox method
ldhA_RR_LOX	GTACGAAGACCTGCTTTTTCACCACGAACTGTTCTT	Generation of right flank with lox71 sites for Cre-lox method
sdhA_LF_LOX	GTACGAAGACTCCATTGCGCTCTTTGGGTTCAAAAC	Generation of left flank with lox66 sites for Cre-lox method
sdhA_LR_LOX	GTACGAAGACCTGGAGATGCCATTAATGAACCGATG	Generation of left flank with lox66 sites for Cre-lox method
sdhA_RF_LOX	GTACGAAGACCTAGCGACTGCCTCCGAGATTAAAAC	Generation of right flank with lox71 sites for Cre-lox method
sdhA_RR_LOX	GTACGAAGACCTGCTTATGTTGCAACACGACGTCAT	Generation of right flank with lox71 sites for Cre-lox method
COX_LOX_for	ATCGCAAATGGACGGACTAC	Confirmation of gene segregation
COX_LOX_rev	GGATGATCGTATTCACCGTG	Confirmation of gene segregation
ARTO_LOX_for	GCATTGTAAACGGTGCGAT	Confirmation of gene segregation
ARTO_LOX_rev	ACTGGTGGATCGGCTCTTTA	Confirmation of gene segregation
acs_LOX_for	CACCGGGTAAAGGCGTAATC	Confirmation of gene segregation
acs_LOX_rev	ATGGTTTGAGAAATGGGACAA	Confirmation of gene segregation

ldhA_LOX_for	TCAATTAAGCCACCTCGACT	Confirmation of gene segregation
ldhA_LOX_rev	CTCTATCGCGCCTACAACC	Confirmation of gene segregation
sdhA_LOX_for	CTTTCTTTGCGGTGGTAAGC	Confirmation of gene segregation
sdhA_LOX_rev	TGTATCACATCGAAACTGGACAT	Confirmation of gene segregation

5.2.1.3 Confirmation and visualisation via agarose gel electrophoresis

DNA fragments were separated according to their size by agarose gel electrophoresis using 1% (w/v) agarose dissolved in Tris-acetate-EDTA (TAE; 40 mM Tris-HCl pH 7.6, 20 mM acetic acid, 1 mM ethylenediaminetertraacetic acid (EDTA)) with 3.6 µL GelRed® per 100 mL of agarose for visualisation of DNA under UV illumination using a G:BOX gel imager (Syngene). DNA samples were mixed with 6 x DNA Purple Gel Loading Dye (NEB) to monitor DNA migration. Either 5 µL of DirectLoad 1 kb DNA ladder (Sigma) or 2.5 µL of GeneRuler 1 kb plus DNA ladder (Thermo Scientific) was used to determine fragment size.

5.2.1.4 Gel Extraction of genomic DNA

DNA fragments from agarose gels were purified using the GENECLEAN® III Kit (MP Biomedicals) according to the manufacturer's instructions. DNA was eluted with 15 µL ultrapure water, and stored at -20°C.

5.2.1.5 Plasmid Generation

PCC 11901 knockouts were constructed according to a protocol similar to that utilised in PCC 6803 and outlined in Lea-Smith *et al.* (40), except plasmids were constructed using the CyanoGate system (42). All primers used for cloning and mutant verification are listed in **Table 5.3** and plasmids are listed in **Table 5.3**.

Table 5.3 Plasmids used and generated in this chapter. Those highlighted in blue were kindly generated by members of the McCormick Lab Group at the University of Edinburgh. Those highlighted in green were generated by other members of the Lea-Smith Lab Group.

Plasmid	Plasmid design	Purpose
pUC19:desB CodA-Sp	pUC19 + 5´ flanking region of *desB* (1000 bp) + *codA*/SpR cassette (3488 bp) + 3´ region of *desB* (1000 bp)	Marking plasmid: introducing *codA*-SpR into the DesB neutral site
pUC19: Unmark Linker	pUC19 + 59bp sequence	Serves as a blank/linker sequence to be inserted between the 5' flanking region and 3' flanking region of the DesB for unmarking
pUC19:desB Unmark Linker	pUC19 + 5´ flanking region of *desB* (1000 bp) + Unmark Linker (59 bp) + 3´region of *desB* (1000 bp)	Unmarking plasmid: introducing a short 60bp linker into the marked DesB::codA-SpR
pICH47742: lox66-KanR-lox71	pICH47742 + lox66 sites (34 bp) + KanR cassette (816 bp) + lox71 sites (34 bp)	Plasmid used to introduce loxP sites into the knockout plasmids for the Cre-lox recombinase method.
pICH47742: lox66-GmR-lox71	pICH47742 + lox66 sites (34 bp) + GmR cassette (534 bp) + lox71 sites (34 bp)	Plasmid used to introduce lloxP sites into the knockout plasmids for the Cre-lox recombinase method.
pUC19:ARTO CodA-KanR	pUC19 + 5´ flanking region of *ctaCII* (531 bp) + *codA*/KanR cassette (2949 bp; amplified from vector pICH47732) + 3´region of ARTO gene (526 bp)	Generating marked mutant of CtaCII in PCC 11901
pUC19:COX CodA-KanR	pUC19 + 5´ flanking region of *ctaDI* (745 bp) + *codA*/KanR cassette (2949 bp; amplified from vector pICH47732) + 3´region of *ctaDI* (658 bp)	Generating marked mutant of CtaDI in PCC 11901
pUC19:ARTO Unmark Linker	pUC19 + 5´ flanking region of *ctaCII* (531bp) + Unmark Linker (59 bp) + 3´region of *ctaCII* (526 bp)	Generating unmarked mutant of CtaCII in PCC 11901
pUC19:COX Unmark Linker	pUC19 + 5´ flanking region of *ctaDI* (745 bp) + Unmark Linker (59 bp) + 3´region of *ctaDI* (658 bp)	Generating unmarked mutant of CtaDI in PCC 11901
pUC19: COX-loxP-GmR	pUC19 + 5' flanking region of *ctaDI* (745 bp) + lox66/GmR/lox71 cassette (933 bp; amplified from vector pICH47732) + 3' region of *ctaDI* (658 bp)	Generating marked mutants of CtaDI and introducing loxP sites in PCC 11901
pUC19: COX-loxP-KanR	pUC19 + 5' flanking region of *ctaDI* (745 bp) + lox66/KanR/lox71 cassette (1292 bp; amplified from vector pICH47732) + 3' region of *ctaDI* (658 bp)	Generating marked mutants of CtaDI and introducing loxP sites in PCC 11901
pUC19:ARTO-loxP-GmR	pUC19 + 5' flanking region of *ctaCII* (531 bp) + lox66/GmR/lox71 cassette (933 bp; amplified from vector pICH47732) + 3' region of *ctaCII* (526 bp)	Generating marked mutants of CtaCII and introducing loxP sites in PCC 11901
pUC19:acs-loxP-GmR	pUC19 + 5' flanking region of acs gene (818 bp) + lox66/GmR/lox71 cassette (933 bp; amplified from vector pICH47732) + 3' region of acs gene (568 bp)	Generating marked mutants of Acs and introducing loxP sites in PCC 11901

pUC19:acs-loxP-KanR	pUC19 + 5' flanking region of acs gene (818 bp) + lox66/KanR/lox71 cassette (1292 bp; amplified from vector pICH47732) + 3' region of acs gene (568 bp)	Generating marked mutants of Acs and introducing loxP sites in PCC 11901
pUC19: ldhA-loxP-GmR	pUC19 + 5' flanking region of ldhA gene (428 bp) + lox66/GmR/lox71 cassette (933 bp; amplified from vector pICH47732) + 3' region of ldhA gene (425 bp)	Generating marked mutants of LdhA and introducing loxP sites in PCC 11901
pUC19:sdhA-loxP-GmR	pUC19 + 5' flanking region of sdhA gene (716 bp) + lox66/GmR/lox71 cassette (933 bp; amplified from vector pICH47732) + 3' region of sdhA gene (743 bp)	Generating marked mutants of SdhA and introducing loxP sites in PCC 11901
pICH47751:Cre-enzyme-rbcLXS	pICH47751 + 5' flanking region of the *rbcLXS* gene (464 bp) + Cre enzyme encoding gene (1032 bp) + SpecR cassette (792 bp; amplified from pICH41264) + 3' region of *rbcLXS* gene (336 bp)	Introduces the Cre enzyme into the essential *rbcLXS* site in PCC 11901

5.2.1.5.1 Marked plasmid assembly for *codA*-5-FC mutant generation

Assembly of the plasmid for generating marked mutants was performed using a standard Golden Gate one-pot digestion/ligation reaction (503). The *codA* gene in each cassette was placed under control of the strong promoter J23101 from the CyanoGate library of parts(42). The flanking regions were amplified using the corresponding primers and PCC 11901 genomic DNA (Section 5.2.1.1).

A 20 µL reaction was prepared by adding 2 µL of Ligase Buffer (10X); 2 µL of bovine serum albumin (BSA; 1 mg/mL); 1.5 µL of *BsaI* (NEB); 0.5 µL of T4 ligase (NEB); 40 ng of the pUC19 backbone vector; 40 ng of the *codA*/KanR (conferring kanamycin resistance) cassette, *codA*/SpecR (conferring spectinomycin resistance) or *sacB*/SpecR cassette; 10 ng of the PCR product of the left-flanking region; 10 ng of the PCR product of the right-flanking region. The reaction was then cycled in a programmed thermocycler for 35 cycles, first at 37°C for 5 minutes, then 16°C for 5 minutes, with a final hold at 60°C for 5 minutes to inactivate the enzymes.

5.2.1.5.2 Unmarked plasmid assembly for *codA*-5-FC mutant generation

Assembly of the plasmid for generating unmarked mutants was performed using a similar method as described above, Section 5.2.1.5.1, however the restriction enzyme used in the Golden Gate assembly was BpiI (Thermo Fisher). A 20 µL reaction was generated by adding 2 µL of Ligase Buffer (10X); 2 µL of BSA (1 mg/mL); 1.5 µL of *BpiI*; 0.5 µL of T4 ligase (NEB); 40 ng of the marked plasmid; 40 ng of the pUC19KL CyanoGate linker. To confirm correct assembly, either a double digest involving the restriction enzymes *SacI*-HF (NEB) and *ScaI*-HF (NEB), or a single digest with *SacI*-HF was used.

5.2.1.5.3 Linearising plasmid DNA for transformation

The plasmids were linearized by digesting 1 µg of the plasmid with 1 µL of *ScaI*-HF restriction enzyme at 65°C for 2 hours and 85°C for 20 minutes to inactivate the enzyme. The linearized plasmid size was checked on a 1% agarose gel and then used for transformation.

5.2.1.5.4 Plasmid generation for the Cre-loxP site specific recombinase system

Assembly of the plasmids for generating the marked mutants containing the loxP sites were generated using the standard Golden Gate one-pot digestion/ligation reaction, (Section 5.2.1.5.1) (503). The sequences for the lox71 (5'-ATAACTTCGTATAATGTATGCTATACGAACGGTA-3') and lox66

(5'-TACCGTTCGTATAATGTATGCTATACGAAGTTAT-3') sites were derived from Lambert *et al*. (504) The antibiotic resistance cassette within the plasmids encoded for either kanamycin or gentamycin resistance. CyanoGate Level 0 plasmids were generated for both the lox71 (pICH41276) and the lox66 site (pICH41295) for future use of these sites, as well as a Level 1 plasmid which contained both loxP sites flanking either a kanamycin or gentamycin resistance cassette. These Level 0 and Level 1 plasmids were generated by our collaborators at the University of Edinburgh. The Level T marking plasmids were generated via the standard Golden Gate digestion/ligation protocol (Section 5.2.1.5.1), containing the corresponding flanking regions which were produced via PCR amplification (Section 5.2.1.2).

The plasmid encoding the genes for the Cre recombinase was generated using the Golden Gate method (Section 5.2.1.5.1). The flanking regions targeting the *rbcLXS* site in PCC 11901 were homologous to the sites defined in the PCC 7002 method described in Jones *et al.* (47). The 5' flank (464 bp) and the 3' flank (336 bp) were inserted either side of the Cre-recombinase gene (1032 bp) and a spectinomycin resistance cassette (792 bp) (**Figure 5.4**). Flanks were generated via PCR amplification (Section 5.2.1.2).

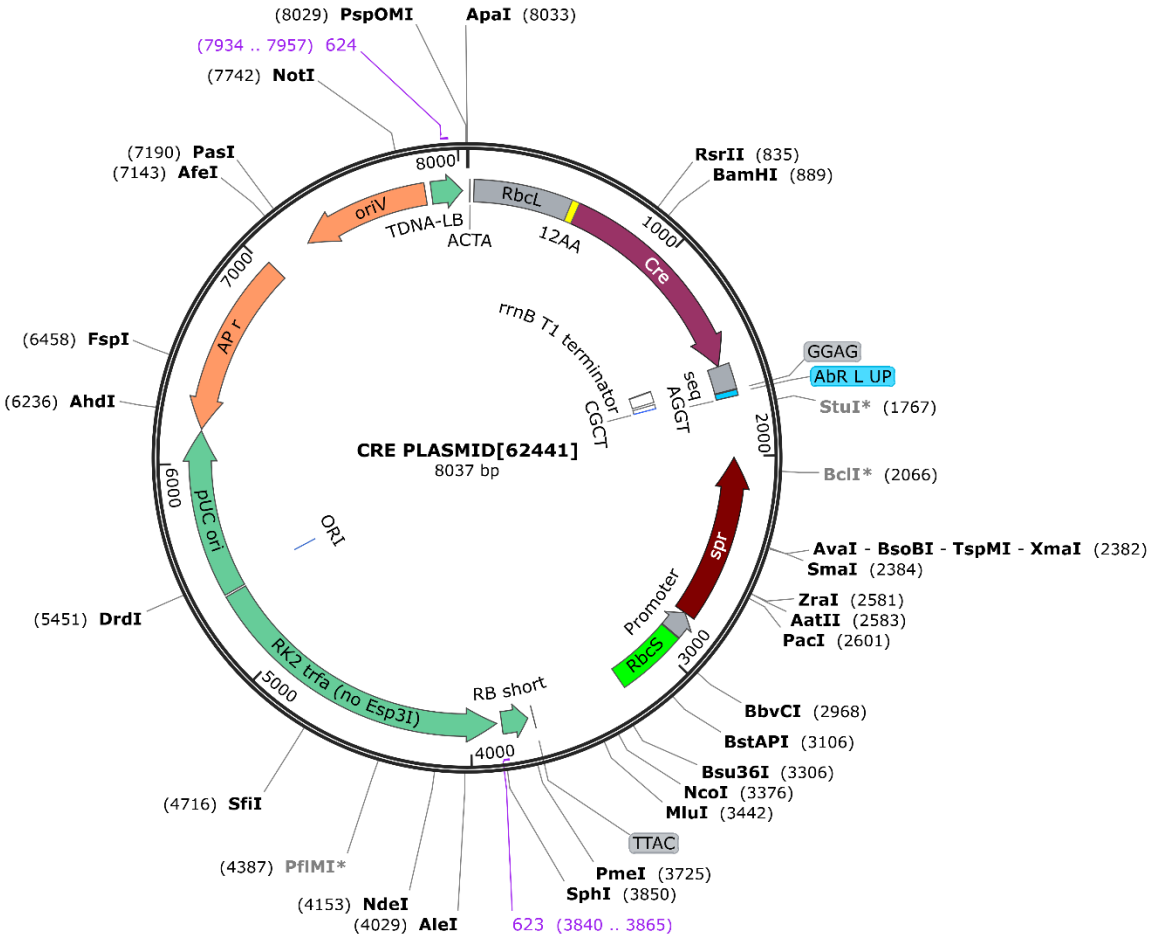

Figure 5.4 Plasmid map of the Cre recombinase expression vector. The plasmid contains the pICH47751 backbone which contains both the 5' *rbcL* and 3' *rbcS*, part of the *rbcLXS* chromosomal site, flanking the Cre recombinase gene and the spectinomycin resistance cassette.

5.2.1.6 Verification of mutants via colony PCR

Once mutants were generated, colony PCR was used to determine whether full segregation had occurred. GoTaq® DNA Polymerase (Promega) was used for colony PCR using the primers listed in **Table 5.3**. A typical 50 µL reaction mixture contained: 10 µL of GoTaq® Reaction Buffer, 0.25 µL GoTaq® DNA polymerase, 1 µL dNTP mixture (10 mM of dATP, dCTP, dGTP and dTTP), 1 µL 10 µM forward primer, 1 µL 10 µM reverse primer, 5 µL DNA template and made up to 50 µL with ultrapure water.

The standard GoTaq® PCR protocol consisted of an initial denaturation step at 95°C for 2 minutes, and 35 subsequent cycles of 95°C for 1 minute (denaturation), 60°C for 1 minute (primer annealing), 72°C for 3 minutes (primer extension), with a final extension at 72°C for 5 minutes. The PCR program was varied when the standard procedure did not yield optimal results.

5.2.2 DNA transformation of cells

5.2.2.1 Preparation of Competent DH5α *E. coli*

A single *E. coli* colony was picked from a fresh, re-streaked Luria-Bertani Broth (LB) plate and inoculated into 5 mL of LB medium before being incubated overnight at 37°C and shaken at 200 rpm. The overnight culture was used to inoculate 50 mL of LB by the addition of 0.5 mL of the overnight culture to the liquid medium. This was then left to grow at 37°C and shaken at 200 rpm until an OD_{600} of ~0.6 was reached and then the culture was placed on ice for 15 minutes. Cells were harvested by centrifugation at 8,200 x *g* for 8 minutes at 4°C and then resuspended in 20 mL of ice-cold 0.1 M $MgCl_2$. The culture was then incubated on ice for 30 minutes before the cells were harvested by centrifugation at 8,200 x *g* for 8 minutes at 4°C. Pellets were resuspended in ice-cold Solution A (250 µL of 1M $CaCl_2$, 1 mL glycerol (50% w/v) and 1.25 mL ultrapure water). 50 µL aliquots of cells were then flash-frozen in liquid nitrogen and stored at -80°C.

5.2.2.2 Transformation of DH5α *E. coli*

Competent DH5α *E. coli* cells were thawed on ice for 10 minutes and mixed with ~1 µg plasmid DNA and incubated on ice for 30 minutes. The cells were subjected to heat shock at 42°C for 45 seconds and incubated for 5 minutes on ice. Cells were recovered by the addition of 950 µL of LB medium and incubated at 37°C for 1 hour. 50-200 µL of the mix was spread onto LB 1.5% (w/v) agar plates supplemented with appropriate antibiotics and incubated at 37°C overnight.

5.2.2.3 Transformation of NEB™ Stable Competent *E. coli* (High Efficiency)

When plasmids carrying *codA* with the corresponding promoter were required for transformation, NEB® Stable Competent *E. coli* (High Efficiency) (C3040H, New England BioLabs) cells were used due to their ability to survive under this strong promoter. Competent *E. coli* cells were thawed on ice for 10 minutes and mixed with ~1 µg plasmid DNA and incubated on ice for 30 minutes. The cells were subjected to heat shock at 42°C for 30 seconds and incubated for 5 minutes on ice. Cells were recovered by the addition of 950 µL of room temperature SOC medium and incubated at 37°C for 1 hour at 250 rpm. 50-100 µL of the mix was spread onto pre-warmed LB 1.5% (w/v) agar plates supplemented with appropriate antibiotics and incubated at 37°C overnight.

5.2.2.4 Plasmid extraction and purification from *E. coli* cells

E. coli cells were harvested from a 10 mL overnight liquid LB culture by centrifugation of 3 mL at 17,000 x *g* for 1 minute. Plasmids were extracted and purified from the cell pellet using the GenElute™ Plasmid Miniprep Kit (Sigma Aldrich) according to the manufacturers instructions. Plasmids were eluted using ultrapure water and either used immediately or stored at -20°C.

5.2.2.5 Electroporation

Starter cultures prepared as standard (Section 3.2.1.4.1) were washed three times with 50 mL of ice-cold, sterile 10% (w/v) glycerol. After washes, cells were resuspended in 1 mL of ice-cold 10% glycerol. 100 µL of concentrated cells was added to a pre-chilled 1 mm electroporation cuvette (VWR® International). Plasmid DNA (1 µg) was added to the cells in the cuvette and incubated for 5 minutes on ice. Electrotransformation was performed using an Electro cell manipulator at 1000 volts, 200 Ωs and 25 µFarads. Cells were then transferred to 15 mL round bottom tube (Costar®) and 2 mL of AD7 media was added and left to incubate at 30°C with 50 µmol photons m^{-2} s^{-1} of light and shaking at 200 rpm. After 4 days, 6 days or 8 days of incubation 50 µL of culture was plated onto AD7 + 5-FC (0.25 mg/mL).

5.2.3 Mutant Generation

5.2.3.1 Transformation of PCC 11901 for marked mutant generation

Initially, to generate marked mutants, cultures were grown under standard growth conditions (as described in Section 3.2.1.4.1) to OD_{750nm} = 0.5 – 1.0. Cells were spun down at 3,200 x *g* for 20 minutes, washed once in fresh AD7 and resuspended in 1mL of AD7 in a 1.5 mL Eppendorf.

Approximately 1 µg of marked knockout plasmid was mixed with PCC 11901 cells for a minimum of 4 hours in liquid AD7 media and shaken at 180 rpm at 30°C under 50 µmol photons m^{-2} s^{-1} illumination. Cells were pelleted again at 1,500 x *g* for 5 minutes, decanting 800 µL of supernatant and resuspending the pellet in the remaining 200 µL. The resuspended culture was then spread onto AD7 agar plates containing the appropriate antibiotic concentration.

To ensure segregation of the marked knockout, the kanamycin concentration was increased from 50 to 100 µg/mL. This was in accordance with the original paper that stated PCC 11901 showed partial resistance at low kanamycin concentrations (below 50 µg/mL) (51). To ensure full segregation we conducted 'reverse' patching. Using the blunt end of a toothpick, colonies were first patched onto the AD7 5-FC (0.1 mg/mL) plates and then onto the AD7 kanamycin (100 µg/mL) plates. Those colonies that grew on the kanamycin plates, but not on the 5-FC plates, and then verified for the absence of the wild-type band via PCR, were considered fully segregated and were used for subsequent unmarked transformation attempts.

5.2.3.2 Toxicity tests for *CodA* and 5-Fluorocytosine negative selection

Once marked mutants were acquired, it was possible to test the effectiveness of 5-FC as a potential negative selection marker. Wild-type, and CtaCII and CtaDI marked mutants were grown under standard conditions, as outlined in Section 3.2.1.4.1. Starting cultures with an OD_{750nm} = 0.3 - 0.4 were used and a series dilution was carried out with 20 µL of dilutions 10^{0}, 10^{-1}, 10^{-2}, 10^{-3} and 10^{-4} spotted onto plates with differing concentrations of 5-FC (0; 0.05; 0.1; 0.25; 0.5; and 1 mg/mL).

5.2.3.3 Generation of unmarked mutants in *Synechococcus* sp. PCC 11901

As a method for generating markerless mutant in PCC 11901 had not been reported, we used the well-established protocol for generating unmarked mutants in PCC 6803 (40). Cultures of 11901 were grown in 40-60 mL of AD7 under standard culture conditions, Section 3.2.1.4.1, to an OD_{750nm} = 0.4-0.6. Cells were pelleted by centrifuging at 2,300 *x g* for 10 minutes and the supernatant was discarded. The pellets were washed with AD7 media twice and then resuspended in 200 µL of AD7. The cells were then transferred to a 14 mL round-bottomed tube and either 1 or 5 µg of the unmarked plasmid was added. Samples were incubated for 5 hours by laying tubes horizontally in the photobioreactor at 30°C under 50 µmol photons m^{-2} s^{-1} light and shaking at 200 rpm. After the incubation period, 1.8 mL of AD7 was added and samples were left to incubate for 4 days. 10 µL, 50 µL and 100 µL were then plated onto either 0.1 mg/mL 5-FC MAD or 0.1 mg/mL 5-FC AD7 plates.

Stock solution of 5-FC (10 mg/mL) was prepared and stored at room temperature; -18°C; or made fresh and added directly to the liquid agar solution post-autoclaving. BG-11 (0.1 mg/mL 5-FC) plates were also trialled.

5.2.4 Site-specific Cre-loxP recombinase mutant generation method

Marked mutants were generated using the plasmids described in Section 5.2.1.5.1. and transformation method described in Section 5.2.3.1. After marked mutants were confirmed as fully segregated, cultures were inoculated with the Cre-containing plasmid (Section 5.2.1.5.1; pICH47751: Cre-enzyme-*rbcLXS*, **Table 5.3**), again using the transformation methods described in Section 5.2.3.1. and plated onto AD7 solid agar plates containing the antibiotic corresponding to the resistance cassette within the Cre-containing plasmids, in this case spectinomycin (20 µg/mL).

5.3 Results

5.3.1 Generation of *sacB* knockout plasmids

Initially, the negative selectable marker *sacB* was tested to determine whether it was ineffective in PCC 11901, similar to what has been demonstrated in PCC 7002. This work was carried out by collaborators in the McCormick Lab at the University of Edinburgh.

The omega 3 desaturase gene, *desB*, a known neutral site in PCC 7002 (505), was targeted, using a plasmid in which cassettes containing *sacB* and a gene conferring spectinomycin resistance, were inserted between regions in the chromosome flanking the deletion site. Prior to these experiments, *desB* was confirmed as non-essential in PCC 11901 via deletion using a marked plasmid. This counter-selection plasmid (pUC19:desB-CodA-Sp, **Table 5.3**) was transformed into PCC 11901 using spectinomycin to select for potential marked knockouts. However, despite three separate transformation attempts, no colonies were observed, suggesting that expression of *sacB* is lethal to PCC 11901 even in the absence of sucrose on agar plates. This is dissimilar to PCC 7002, where marked mutants were obtained but *sacB* expression was ineffective in selecting for unmarked mutants (40). Since PCC 11901 also encodes a putative sucrose biosynthesis pathway (**Figure 3.3**), which is typically expressed in cyanobacteria under high-salt conditions (506), we also attempted to generate marked mutants on low-salt BG11 medium plates. Despite trying two different transformation methods in which the incubation time in liquid BG11 medium was altered (4 and 24 hours), and the cells plated on either BG11 or AD7 solid medium, no colonies were obtained. Therefore, it seems unlikely that this negative selectable marker can be used to generate unmarked mutants.

5.3.2 Generation of marked mutants in PCC 11901 expressing *codA*

Transformation with plasmids in which *codA* replaced *sacB* as the negative selectable marker resulted in approximately 5-40 colonies per microgram of plasmid. Marked mutants of *ctaD1* and *ctaCII*, encoding subunits of cytochrome-*c* oxidase (COX) and the alternative respiratory terminal oxidase (ARTO) respectively, were also generated (**Figure 5.4**C-D; **Figure 5.5**E-F) using kanamycin for selection. These are the only terminal oxidases in PCC 11901 and were selected because these genes are non-essential in PCC 6803 and PCC 7002 (447). Segregation of mutants was not obtained after multiple streaking on plates containing 50 µg/mL kanamycin. Segregation was only observed when the concentration was increased to 100 µg/mL. It was observed that leaving cells to incubate with the plasmid overnight (~16 hours) yielded a higher number of transformants.

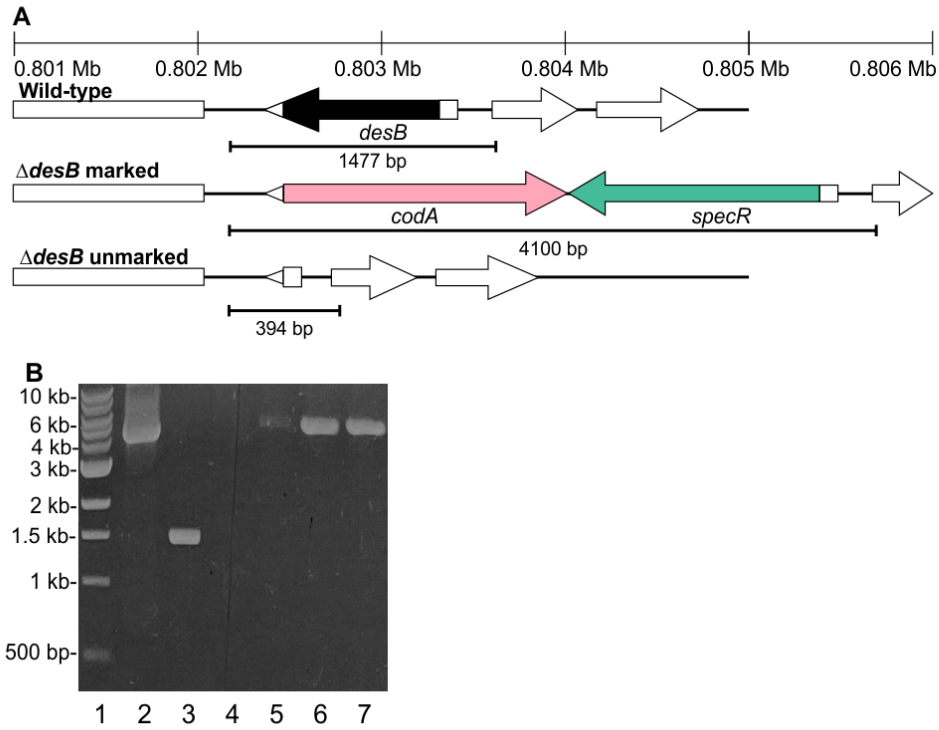

Figure 5.5A-B Generation of marked knockouts in PCC 11901. DNA ladders are shown in lane 1 in each panel. A) Schematic representations of locus location in the PCC 11901 genome (top) and profiles expected in wild-type and the *ΔdesB* marked and unmarked knockouts. B) Amplification of genomic DNA in wildtype (Lane 3; Expected band size: 1477 bp) and *ΔdesB* marked mutants (Lanes 4-7) using DesBfor and DesBrev primers. Positive control is shown in lane 2

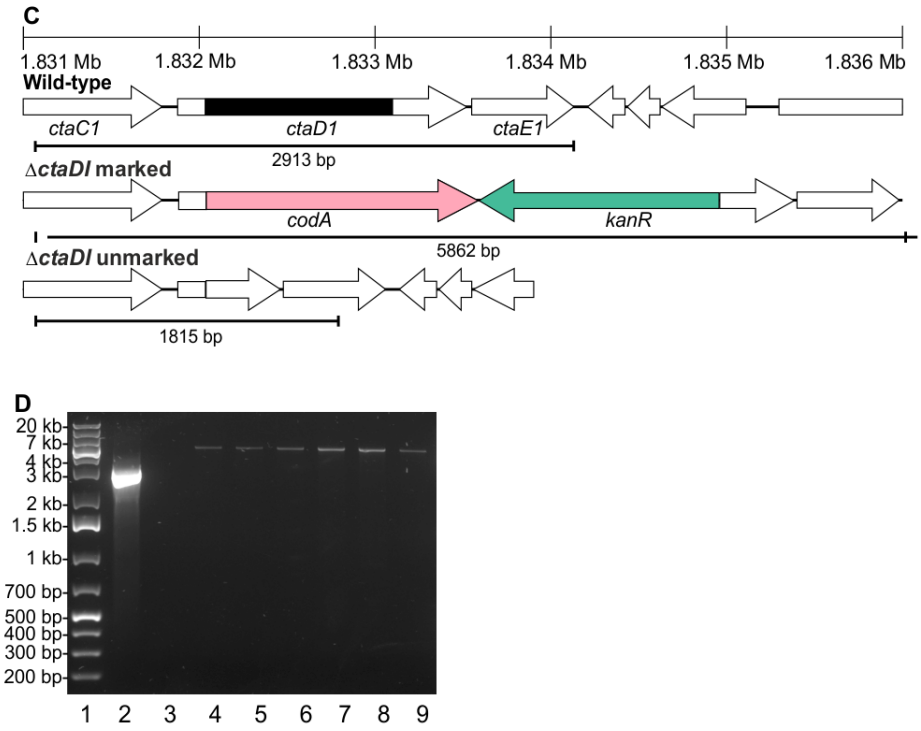

Figure 5.6C-D Generation of marked knockouts in PCC 11901. DNA ladders are shown in lane 1 in each panel. C) Schematic representations of locus location in the PCC 11901 genome (top) and profiles expected in wild-type and the *ΔctaD1* marked and unmarked knockouts. D) Amplification of genomic DNA in wild-type (Lane 2) and *ΔctaD1* marked mutants (Lanes 4-9) using COXfor and COXrev primers. Negative control (no gDNA) is shown in lane 3

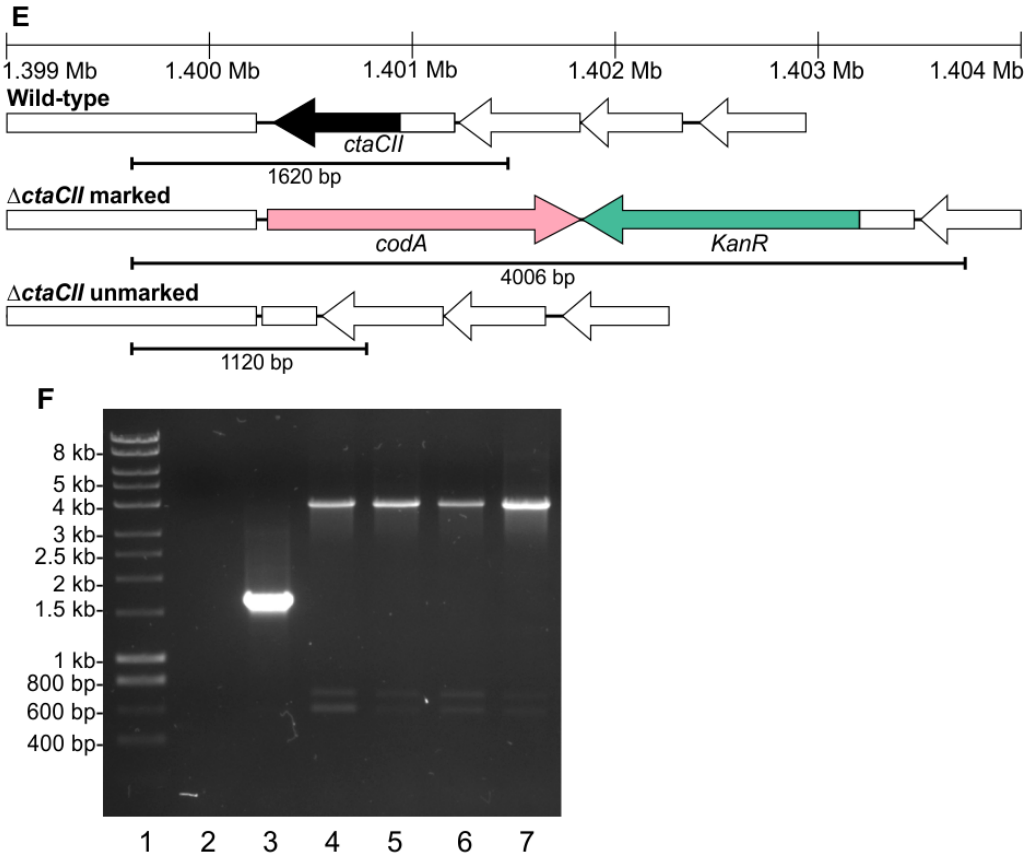

Figure 5.7E-F Generation of marked knockouts in PCC 11901. DNA ladders are shown in lane 1 in each panel. E) Schematic representations of locus location in the PCC 11901 genome (top) and profiles expected in wild-type and the *ΔctaCII* marked and unmarked knockouts. F) Amplification of genomic DNA in wild-type (Lane 3) and *ΔctaCII* marked mutants (Lanes 4-7) using ARTOfor and ARTOrev primers. Negative control (no gDNA) is shown in lane 2.

5.3.3 Testing the feasibility of a *codA*–5-FC method for producing marker-less transformants.

Prior to generating unmarked mutants, wild-type and the Δ*ctaD1* and Δ*ctaCII* marked mutants were cultured on plates with increasing concentrations of 5-FC (**Figure 5.6**). Wild-type cells grew well up to concentrations of 0.5 mg/mL but growth was poor at 1 mg/mL. Marked mutants did not grow, even on the lowest concentration of 0.05 mg/mL. This suggests that 5-FC is lethal to PCC 11901 cells expressing native *E. coli* CodA and has the potential to work as a negative selectable marker in PCC 11901.

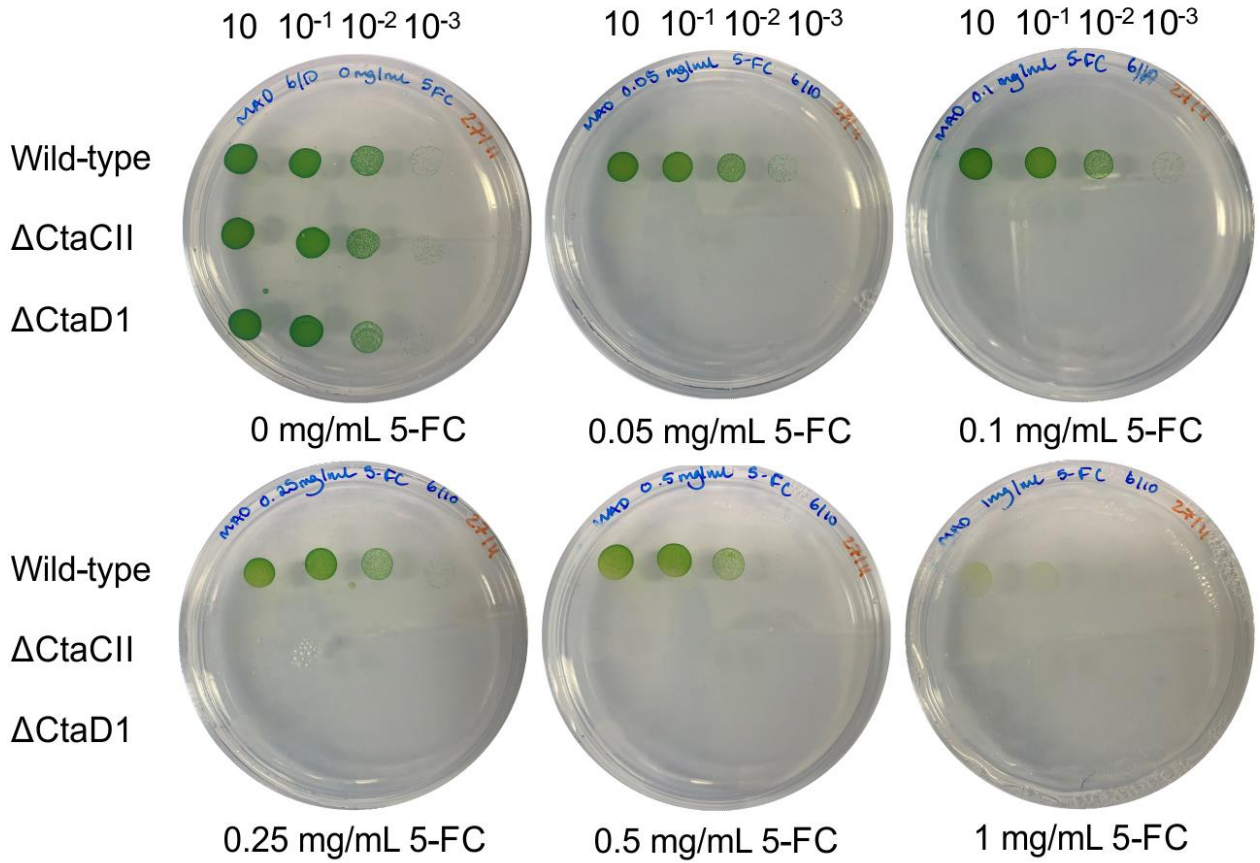

Figure 5.8 Growth of wild-type 11901 and the *ctaD1* and *ctaCII* marked mutants on plates with increasing concentrations of 5-FC. Dilutions are shown above the top row plates.

5.3.4 Markerless transformants in PCC 11901 could not be generated using the *codA*-5-FC method

As described in Section 5.2.4, multiple methods of unmarking were trialled in two different laboratories with different alterations applied in each case. Following transformation of at least six different marked mutants targeting each of the two loci with the unmarking plasmids (**Table 5.3**) and incubation for four days in a shaking incubator, transformants were selected on plates with 0.25 mg/mL 5-FC added directly to the plate or to an agar layer added 24 hours after the initial plating. No fully segregated unmarked colonies were obtained under any of these conditions at this stage. Colonies were then re-streaked on plates with increasing concentrations of 5-FC, up to 1 mg/mL. However, again no mutants were obtained with the expected unmarked profile (**Figure 5.7**A-C). Increasing the incubation time after transformation from four to six or eight days did not result in segregated unmarked colonies. Sequencing of one of these clones confirmed that there were no mutations in *codA*, or the regions upstream and downstream of this gene. All mutants contained the marked mutation or in some cases also the wild-type profile. This suggests that CodA is a poor negative selectable marker and unsuitable for generating unmarked PCC 11901 mutants.

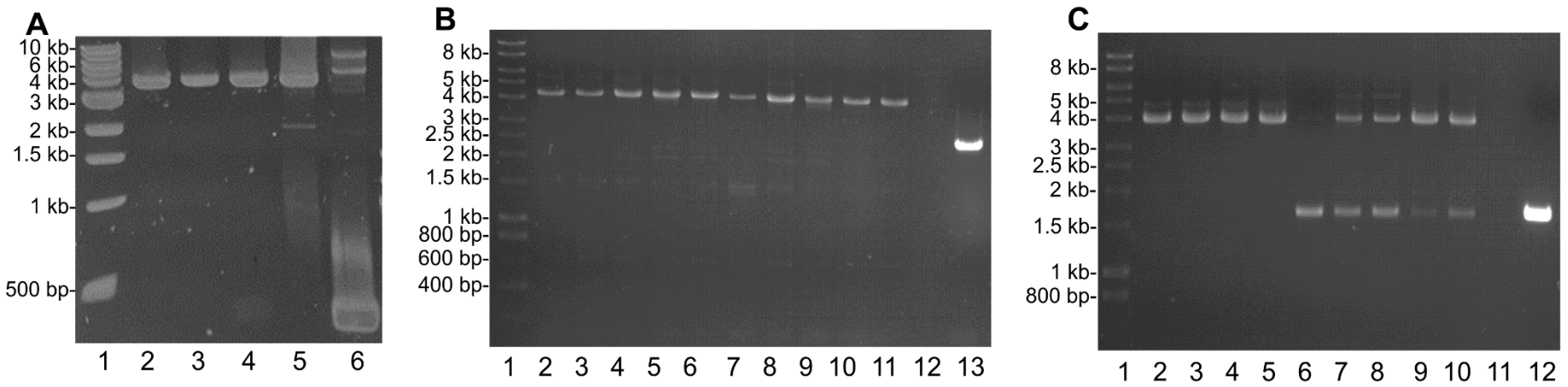

Figure 5.9 Attempted generation of unmarked knockouts in PCC 11901. A) Amplification of genomic DNA in the *ΔdesB* marked mutant (Lanes 5) and putative DesB unmarked mutants (Lanes 2-4, 6) using DesBfor and DesBrev primers. B) Amplification of genomic DNA in putative *ΔctaD1* unmarked mutants (Lanes 2-11) using COXfor and COXrev primers. Negative control (no gDNA) is shown in lane 12. Amplification of wild-type is shown in lane 13. C) Amplification of genomic DNA in putative *ΔctaCII* unmarked mutants (Lanes 2-10) using ARTOfor and ARTOrev primers. Negative control (no gDNA) is shown in lane 11. Amplification of wild-type is shown in lane 12.

5.3.5 Unsuccessful attempts at producing markerless transformants in PCC 11901 using the Cre-loxP site-specific recombinase method

The plasmids containing the loxP sites were effectively used to generate marked mutants, using either kanamycin or gentamycin for the selection pressure. Marked mutants were successfully generated within the *ctaD1* sites, as described above in Section 5.3.2. Alternative marked mutants were generated for knockouts of the succinate dehydrogenase/fumarate reductase flavoprotein (*sdhA*) gene, the acetate-CoA ligase (*acs*) gene, both located within the main chromosomal genome, and the 2-hydroxyacid dehydrogenase (*ldhA*) gene, located on plasmid NZ_CP040361.1. This method similarly resulted in approximately 3-50 colonies per microgram of plasmid and were fully-segregated after two further streaks on either 25 µg/mL gentamycin or 100 µg/mL kanamycin plates (**Figure 5.8**). *ΔctaD1* marked mutant with kanamycin resistance were successfully generated. Potential marked *ΔctaD1* mutants with gentamycin resistance were also generated, however the primers that were used amplified a product with a similar profile to the wild-type, so these were unconfirmed as marked mutants (**Figure 5.8**B). The *ΔctaD1* marked mutant with kanamycin resistance was used for further transformation (**Table 5.3**). The *ΔctaCII* mutant was never fully segregated (**Figure 5.8**D).

Once fully segregated mutants were confirmed, these were transformed with the Cre-containing plasmid (pICH47751: Cre-enzyme-*rbcLXS*, **Table 5.3**). Colonies were never successfully grown on AD7 solid agar with spectinomycin (25 µg/mL) plates, despite increasing the plasmid concentration to 5 µg, and reducing the spectinomycin concentration to 20 µg/mL. This suggests that all chromosomal *rbcLXS* sites are essential in PCC 11901, unlike in PCC 7002. This could possibly be due to a smaller number of chromosomes in this species, although this requires verification. Wild-type PCC 11901 was also inoculated with the Cre-containing plasmid to determine whether the *rbcLXS* site was suitable for genetic manipulation in PCC 11901. Again, no colonies were gained, suggesting that this site is unsuitable for genetic manipulation within this species.

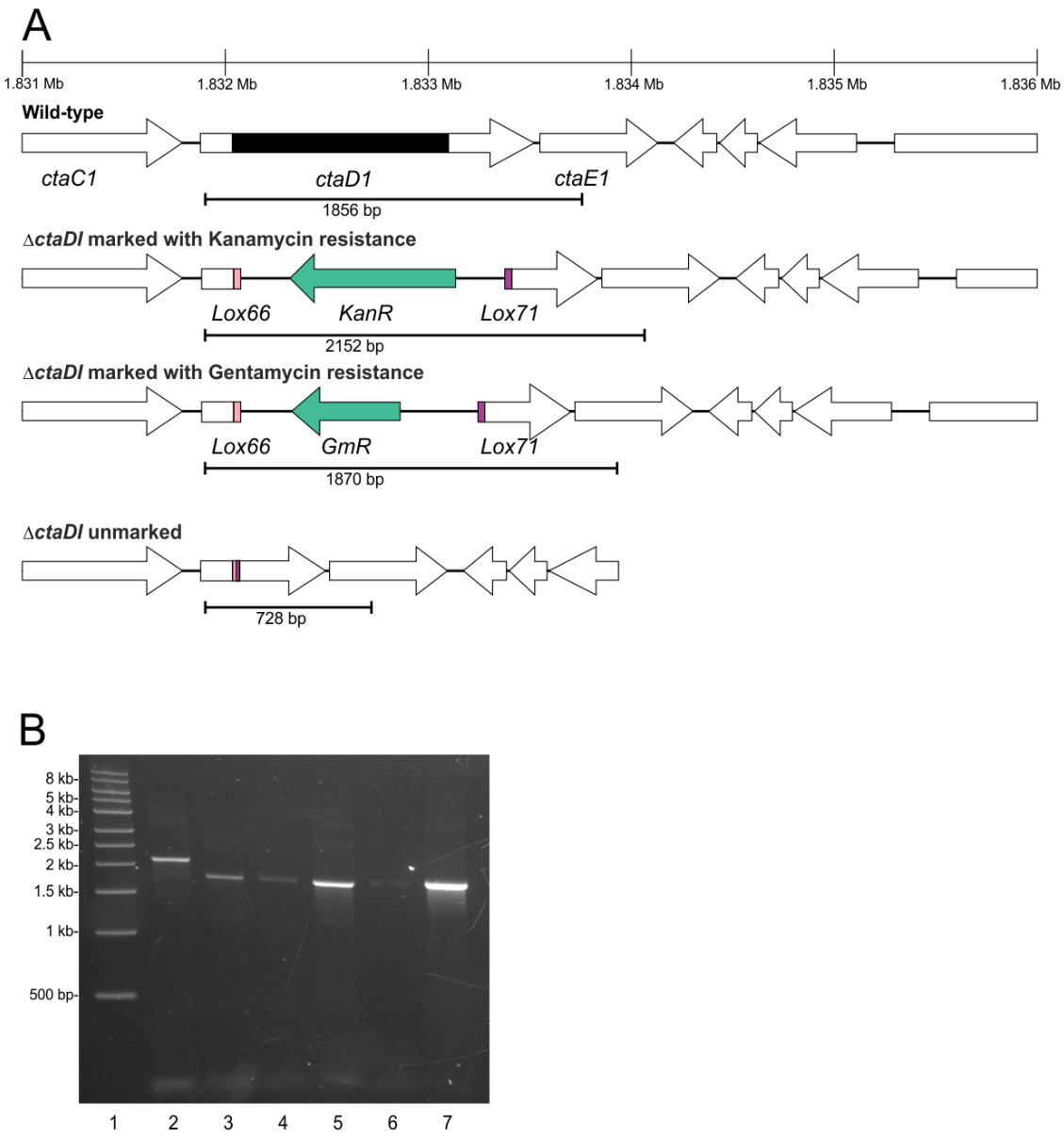

Figure 5.10A-B Generation of marked knockouts in PCC 11901 using lox plasmids. DNA ladders are shown in lane 1 in each panel. A) Schematic representations of locus location in the PCC 11901 genome (top) and profiles expected in wild-type and the *ΔctaD1* marked and unmarked knockouts using the Cre-loxP recombinase plasmids. B) Amplification of genomic DNA in wild-type (Lane 7) and *ΔctaD1* marked mutant with kanamycin resistance (Lane 2) and *ΔctaD1* potential marked mutants with gentamycin resistance (Lanes 3-7) using COX_LOX_for and COX_LOX_rev primers.

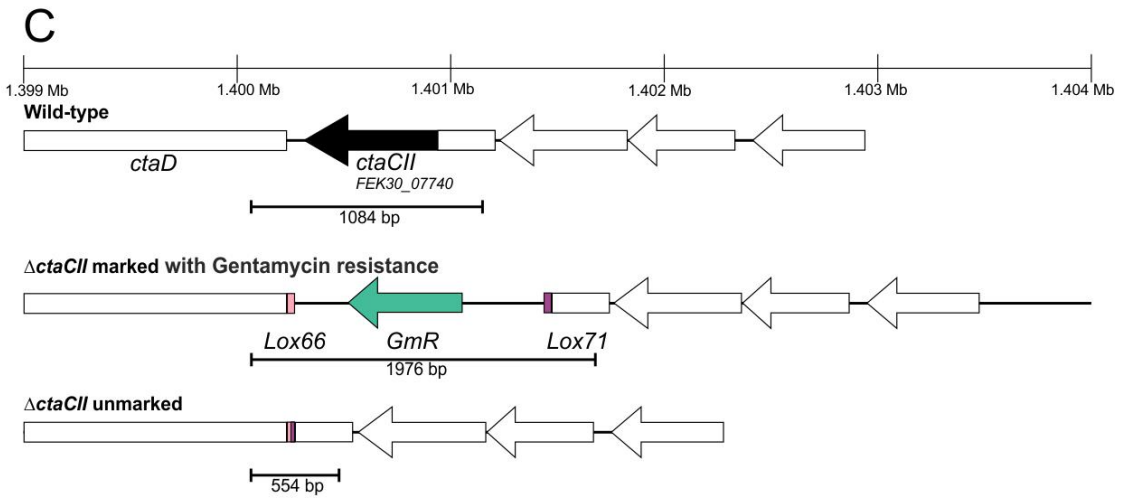

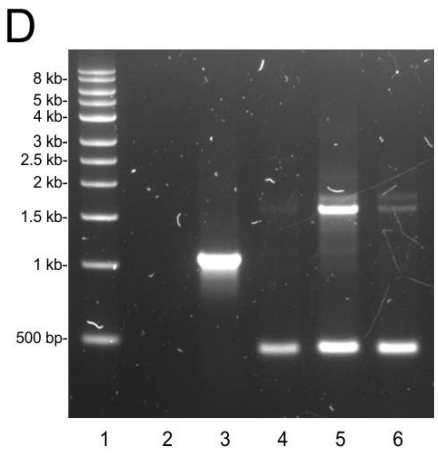

Figure 5.11C-D Generation of marked knockouts in PCC 11901 using lox plasmids. DNA ladders are shown in lane 1 in each panel. E C) Schematic representations of locus location in the PCC 11901 genome (top) and profiles expected in wild-type and the *ΔctaCII* marked and unmarked knockouts using the Cre-loxP recombinase plasmids. D) Amplification of genomic DNA in wild-type (Lane 3) and attempted *ΔctaCII* marked mutants with gentamycin resistance (Lanes 4-6) using ARTO_LOX_for and ARTO_LOX_rev primers. Negative control (no gDNA) is shown in lane 2.

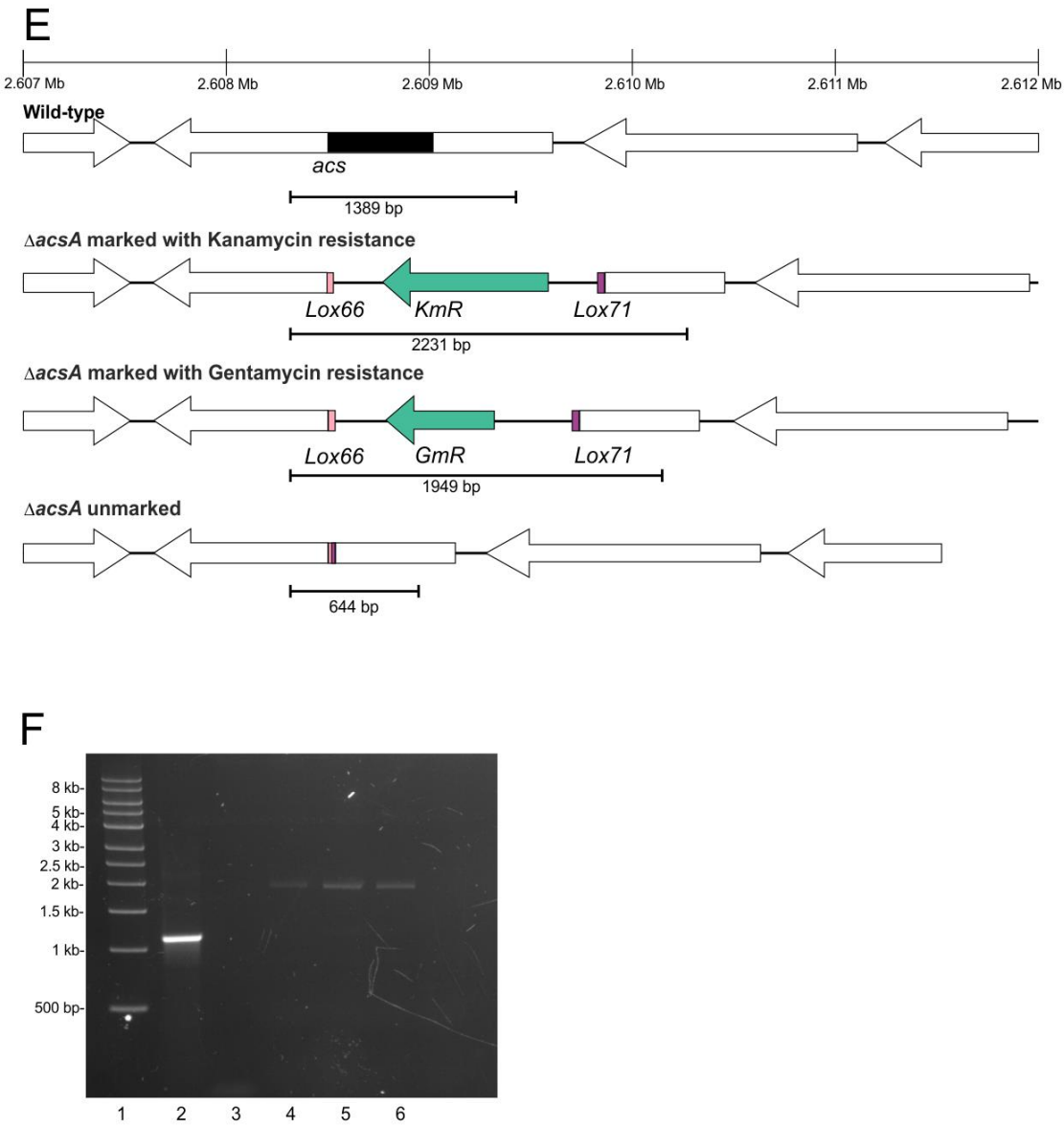

Figure 5.12E-F Generation of marked knockouts in PCC 11901 using lox plasmids. DNA ladders are shown in lane 1 in each panel. E) Schematic representations of locus location in the PCC 11901 genome (top) and profiles expected in wild-type and the *Δacs* marked and unmarked knockouts using the Cre-loxP recombinase plasmids. F) Amplification of genomic DNA in wild-type (Lane 2) and *Δacs* marked mutants with gentamycin resistance (Lanes 4-6) using acs_LOX_for and acs_LOX_for primers. Negative control (no gDNA) is shown in lane 3.

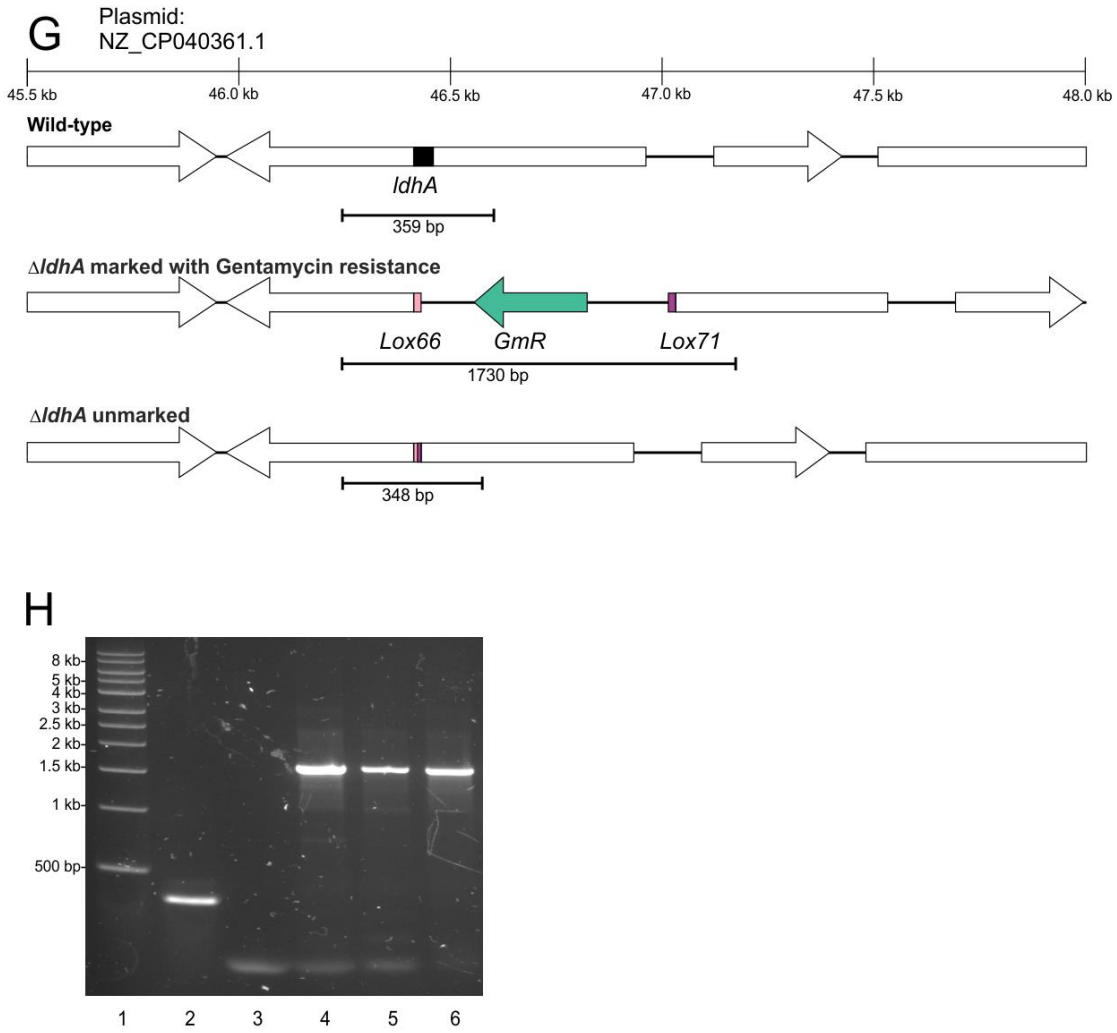

Figure 5.13G-H Generation of marked knockouts in PCC 11901 using lox plasmids. DNA ladders are shown in lane 1 in each panel. G) Schematic representations of plasmid NZ_CP040361.1 location in the PCC 11901 genome (top) and profiles expected in wild-type and the *ΔldhA* marked and unmarked knockouts using the Cre-loxP recombinase plasmids. H) Amplification of genomic DNA in wild-type (Lane 2) and *ΔldhA* marked mutants with gentamycin resistance (Lanes 4-6) using ldhA_LOX_for and ldhA_LOX_for primers. Negative control (no gDNA) is shown in lane 3.

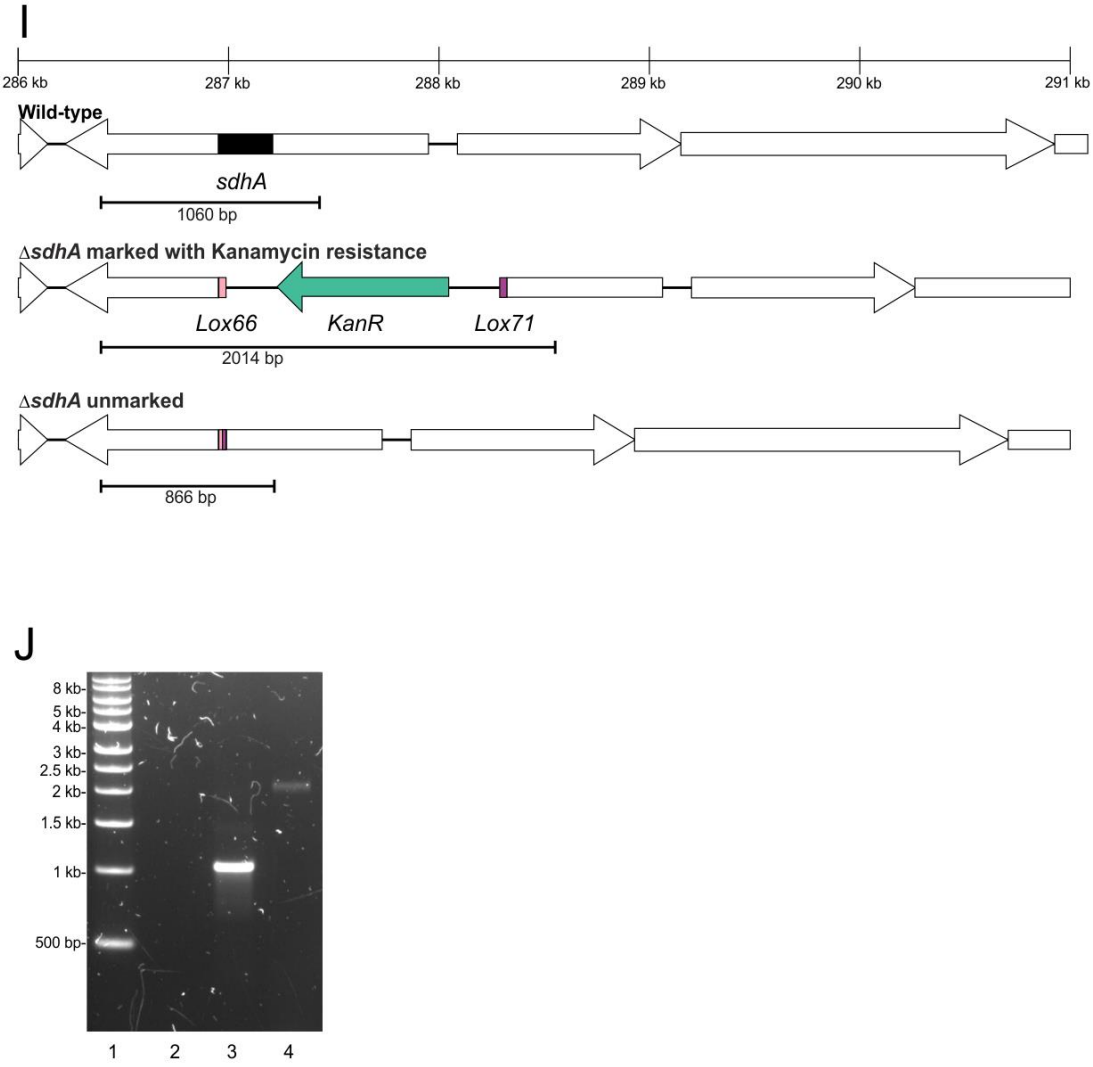

Figure 5.14 Generation of marked knockouts in PCC 11901 using Lox plasmids. DNA ladders are shown in lane 1 in each panel. I) Schematic representations of locus location in the PCC 11901 genome (top) and profiles expected in wild-type and the *ΔsdhA* marked and unmarked knockouts using the Cre-loxP recombinase plasmids. J) Amplification of genomic DNA in wild-type (Lane 3) and *ΔsdhA* marked mutant with kanamycin resistance (Lanes 4) using sdhA_LOX_for and sdhA_LOX_for primers. Negative control (no gDNA) is shown in lane 2.

5.4 Discussion

While genetic manipulation via natural transformation of PCC 11901 has been demonstrated (51), including marked gene deletions and chromosomal insertion of gene cassettes, a system for repeated chromosomal unmarked modification has not been developed. This is essential for biotechnology applications since multiple chromosomal modifications will likely be necessary to generate strains of commercial value. Generation of marked mutations in multiple chromosomal locations is limited by the number of available cassettes conferring antibiotic resistance. Currently, there are five to seven antibiotic resistance cassettes which have been successfully used in model cyanobacterial species (130). This limits the number of chromosomal modifications possible, which may be inadequate for most biotechnology applications. An additional issue is the potential release of organisms containing genes encoding resistance to antibiotics into the environment.

5.4.1 Factors underlying failure of SacB as a negative selectable marker in PCC 11901

Our inability to generate marked mutants using *sacB* containing plasmids may be due to a number of factors. Native expression of sucrose in cells may be high enough to make expression of *sacB* lethal, even in a suicide plasmid. Reducing the salt concentration in solid BG11 agar did not overcome this issue. One possibility might be to delete *spp* in a marked mutant, encoding the protein converting sucrose-6-P to sucrose (**Figure 3.3**). This gene could then be subsequently deleted via a two-step unmarked mutation process and if successful, this strain could then be utilised for further unmarked mutations. However, one issue with this approach is the potential to render the strain less fit under high salt concentrations and any reduction in growth may outweigh the advantages of developing a strain suitable for two-step *sacB* unmarked mutation.

5.4.2 Factors underlying failure of CodA as a negative selectable marker in PCC 11901

Our inability to generate fully segregated unmarked mutants using *codA* containing plasmids seems surprising given that 5-FC is lethal to PCC 11901 cells expressing CodA. However, despite multiple attempts to generate unmarked mutants, trialled across two laboratories and at different genetic sites of interest, we were unable to generate an unmarked mutant using *codA*. Future work should involve testing novel negative selectable markers in PCC 11901 as and when they are discovered.

Potential issues with the *codA* system could be down to the potentially higher polyploidy in this species compared to PCC 6803 or PCC 7002, although our inability to integrate a cassette into *rbcLXS* may suggest that there are less chromosomes in PCC 11901. For example, generation of segregated marked knockouts of *ctaD1* and *ctaCII* in PCC 6803 in our laboratory was achieved after two streaks on agar plates containing kanamycin at a concentration of 30 µg/mL (502). However, in PCC 11901, more streaks on plates containing a higher concentration of kanamycin, up to 100 µg/mL, was required. Polyploidy needs to be determined in this species under a range of growth and nutrient conditions, as has previously been performed for PCC 6803 (427). It is possible that growing PCC 11901 on low phosphate media may reduce polyploidy and make it easier and quicker to generate marked mutants, as has been shown in PCC 6803 (427).

5.4.3 The site specific Cre-loxP recombinase method

Our inability to incorporate the Cre recombinase coding gene into *rbcLXS* in the marked mutants or wild-type may be due to a number of factors. The *rbcLXS* locus, homologous to the site used in PCC 7002 (47), may be unsuitable since the cell may have a strong bias against removing any chromosomal copies. Surprisingly, culturing cells with the addition of glycerol did not overcome this. An alternative technique would be to focus on a different site, such as *psbEFLJ*, encoding for components of photosystem II, as suggested in Jones *et al*., (47).

5.4.4 Future Work

The ability to generate unmarked knockouts using available negative selectable markers is crucial for the development of PCC 11901 for biotechnology (Section 5.1.1). If new negative selectable genes are discovered which can be utilised in bacteria, then these should be tested in PCC 11901 in future studies. CRISPR based genome editing, which have been utilised to generate segregated mutants in PCC 6803 (290,507,508), PCC 7942 (191,507,509), UTEX 2973 (46,191,507) and *Anabaena* sp. PCC 7120 (507,510), could be a potential alternative strategy for genetic modification. This method is currently being investigated by our collaborators in the McCormick laboratory at the University of Edinburgh. Alternative recombinase-based approaches using alternative essential chromosome locations for insertion of the Cre enzyme or the FLP/FRP method also have the potential to successfully generate unmarked mutants. To further improve this organism as a biotechnology chassis, mutant generation should be compatible with parts from the CyanoGate library (42).

Chapter 6

General Discussion

Chapter 6: General Discussion

6.1 Overview

This thesis aimed to provide an in-depth analysis of the newly discovered species PCC 11901, assess its relevance for cyanobacterial biotechnology and develop genetic tools for generating strains suitable for applied applications. Numerous aims were achieved, including: A) Improved understanding of central metabolism and transport in PCC 6803 and PCC 11901; B) Validation of PCC 11901 as a fast growing species of potential use in biotechnology; C) Improved understanding of the factors potentially responsible for the improved growth of PCC 11901; D) Testing of a wide-range of methods for genetic manipulation of the species.

6.2 Improving our current understanding of cyanobacterial metabolism and transport

The genome of PCC 6803 contains 3,456 genes, of which only ~1,200 are functionally known, less than half-compared to *E. coli* (196). An analysis of the published literature, combined with a comparative genome analysis between *E. coli* and PCC 6803, was used to perform the most comprehensive analysis to date of PCC 6803 metabolism and transport. It is likely that many of the biochemical pathways are conserved throughout the phylum, and this analysis will aid our understanding of other cyanobacteria, including environmentally important species or those with potential for biotechnology.

By improving our overall understanding of PCC 6803, we also highlighted steps in cyanobacterial metabolism for which no enzyme has been assigned, i.e. methionine and tyrosine metabolism, and which may vary between cyanobacteria and other bacteria. Identification of these novel cyanobacterial enzymes should be the focus of future research and may require the use of comparative genomics to identify candidate genes. Analysis of mutants, possibly derived from CyanoSource (130), combined with enzyme assays, would be required to characterise such novel cyanobacterial enzymes. These could then be introduced into metabolic maps, thereby aiding metabolic engineering and future bioinformatic and computational studies, such as flux balance analysis.

Mapping of central metabolism and transport was also successfully conducted for PCC 11901. Comparative analysis with PCC 6803 did not reveal any major differences that may contribute to the fast growth phenotype of PCC 11901 as most metabolic pathways were largely conserved between the two species. However, it is possible that differences in carbon flux may play a role in the fast growth traits. This would have to be determined via *in vivo* radioactive carbon labelling experiments with $^{13}CO_2$, combined with metabolomic analysis (511). Preferably, this should be performed across a range of growth conditions (e.g. low vs high CO_2) in order to identify metabolic differences leading to high growth and biomass accumulation. For example, PCC 6803 directs 20 times more carbon towards synthesis of carbohydrates than for industrially relevant terpenoids (512). The knowledge gained from flux experiments would provide insights into how fixed carbon could be redirected towards more industrially relevant metabolic pathways. It may also allow us to identify differences in expression of certain genes responsible for the fast growth phenotype of PCC 11901 that could be introduced into other phototrophs.

6.3 Confirming the validity of PCC 11901 as an optimal species for biotechnology

PCC 11901 shows great promise as a bioindustry chassis (51). We aimed to test this species further with a particular focus on its potential application in a biotechnology environment. One of the issues with previously discovered 'fast growing' species has been insufficient testing of growth under a range of conditions, which is a prerequisite before more expensive and larger scale biotechnology experiments are conducted. The prime example of this has been UTEX 2973, which we were able to show is not able to sustain its fast growth or accumulate large quantities of biomass after 24 hours of growth when compared to PCC 11901 under the reported optimal conditions for UTEX 2973.

Our in-depth analysis of PCC 11901 demonstrated that it was able to outcompete a number of model cyanobacterial species in both biomass accumulation and growth rates and that fast growth was maintained over a broad range of light intensities (**Figure 4.1**). Combined with modelling, we were able to determine the optimum light intensity of 735 µmol photons m^{-2} s^{-1} for growth and biomass accumulation of PCC 11901 in a PBR under 5% CO_2/air. This was accomplished by testing the strain against other cyanobacteria in a small, lab-scale PBR, possibly with similar attributes to industrial PBRs. Ultimately, this must be validated by growing this species in larger scale outdoor PBRs exposed to environmental conditions.

6.4 Improved understanding of the fast-growing phenotype of PCC 11901

We were also able to identify several factors which could account for the fast growth rate and biomass accumulation of PCC 11901. Photoinhibition was lower in PCC 11901 compared to the other species tested, although not significantly different from UTEX 2973 after 20 mins. This further suggests that UTEX 2973 is a high-light tolerant strain, rather than a fast growing one. Photosynthetic and respiratory rates and quantum efficiency were significantly higher in PCC 11901 compared to the other species. This could be due to differences in the electron transport chain (**Figure 3.11**) or higher light harvesting efficiency in PCC 11901. The faster growth rate under elevated CO_2 concentrations could also be due to higher carboxylation rates of the native PCC 11901 RuBisCO. In turn this may result in higher turnover of $NADP^+$/NADPH and ADP/ATP, limiting over-reduction of the electron transport chain. Future work should investigate the carboxylation rate and CO_2/O_2 affinity of RuBisCO in PCC 11901 and slower growing cyanobacteria to confirm this. As mentioned previously, higher biomass accumulation could also be due to differences in carbon flux. Recent work carried out in PCC 6803 demonstrated that overexpression of native RuBisCO, sedoheptulose 1,7-biphosphatase, fructose-bisphosphate aldolase and transketolase (enzymes within the Calvin-Bassham-Benson cycle) resulted in a 42% increase in biomass (315,513–516).

Comparative genomics suggests that the PBS is smaller in PCC 11901 compared to PCC 6803. This may be advantageous for growing PCC 11901 in dense cultures, such as large scale industrial PBRs. In theory, an attenuated PBS will result in lower light absorption of cells at the surface, thereby reducing photoinhibition, as well as allowing additional light to penetrate into the PBR interior, thereby increasing productivity of the overall culture. Reducing the size of PBS has been attempted in PCC 6803 via deletion of various components but has had mixed results in terms of increasing biomass production (20,448–453).

6.5 Development of methods for generation of unmarked mutants

We were able to generate marked gene knockouts in numerous chromosomal sites in PCC 11901 using a range of different antibiotics for selection. Unfortunately, attempts to generate an unmarked mutant were unsuccessful and we have shown that *sacB*-sucrose and *codA*-5-FC methods are unsuitable for use in PCC 11901. We also attempted to replicate the Cre-lox site specific recombinase method which has been successful in PCC 7002, as described in Jones *et al.*

(47). Attempts at generating marked knockouts with the antibiotic cassettes flanked by the lox66 and lox71 sites were successful, but we were unable to integrate the Cre expressing gene into the essential *rbcLXS* chromosome site within PCC 11901. It is likely that this method should work in PCC 11901 due to the success demonstrated in PCC 7002. Alternative essential sites within the genome, such as *psbEFLJ*, or increasing the length of the flanking regions within the knockout plasmid should be tested. The flanking regions in our Cre plasmid were 464 bp and 336 bp in length. However, it has been shown that increasing flanking regions to >800 bp increased the number of successful transformants in PCC 7002 (505). Alternatively the FLP/FRT site specific recombinase method may be more efficient at mutant generation in PCC 11901 and should also be tested in the future (494). This work could be combined with development of CyanoGate parts for PCC 11901, including different combinations of promoters and terminators to achieve optimal production of the desired compound or protein.

Other methods for generating unmarked mutants could utilise techniques such as CRISPR/Cas genome editing tools. CRISPR has been successfully used in numerous cyanobacterial species, including PCC 6803 (290,507,508), PCC 7942 (191,507,509), UTEX 2973 (46,191,507) and *Anabaena* sp. PCC 7120 (507,510). A potential drawback to this method is the toxicity of the Cas enzyme in cyanobacteria. The native Cas9 of *Streptococcus pyogenes* (SpCas9) is the only enzyme from the Cas9 family to be successfully expressed in cyanobacterial strains (PCC 6803, PCC 7942 and UTEX 2973 (46,508,509)). However, expression of SpCas9 has been linked to toxicity and failure to recover colonies in all three species, even at low expression levels. The mechanism of toxicity of SpCas9 in cyanobacteria is unknown and perhaps other Cas9 enzymes may be more compatible. Expression of Cas12a, native to *Francisella novicida* (FnCas12a), is not toxic to UTEX 2973, PCC 6803, PCC 7942 and *Anabaena* PCC 7120 (191,507,510). New Cas enzymes, such as CasX, continue to be identified and these should be tested in PCC 11901 (and other cyanobacteria) (517). CRISPR interference (CRISPRi) should also be investigated for repressing native genes to reduce flux through competing metabolic pathways and directing energy sources towards a targeted chemical. CRISPRi has been successfully used to repress glutamine synthetase, encoded by *glnA*, in PCC 7002, which increased lactate production by two-fold (518). CRISPRi is not only a useful tool for synthetic biology but it can also aid studies into natural physiology and metabolism of a species. Since this method worked in PCC 7002, it could potentially be used in PCC 11901 in the future. However, the long-term stability of repression is unknown.

6.6 The future of PCC 11901 for cyanobacterial biotechnology

The work from this thesis strongly indicates that PCC 11901 should be considered for biotechnology applications in the future. However, to avoid repeating past mistakes with cyanobacteria and "green" technology, further experiments are required.

One of the main issues with cyanobacterial research has been the cost of scaling from laboratory settings to industrial sized PBRs which can house hundreds to thousands of litres of culture. Further experiments should focus on growing PCC 11901 in outdoor PBRs under natural sunlight with high CO_2 containing gas, preferably flue gas from industrial sources, to determine whether fast growth and biomass accumulation can be replicated at larger scale. PCC 11901 is yet to be tested under diurnal light conditions for long periods which may be vital if the strain is to be grown outdoors. Testing the upper and lower limits of temperature is also important to predict the best geographical location for outdoor bioreactors. From these experiments we could possibly identify optimal days and time for harvesting biomass, the length of the stationary phase, as well as the potential to test continuous culturing techniques. As mentioned in Chapter 1, co-culturing with other beneficial bacteria may reduce contamination of cultures. This would be useful to investigate, especially if outdoor bioreactors prove to be successful for cultivation of PCC 11901. Conversely, since cultures grown at larger scale are unlikely to remain axenic, it is important to determine how resistant PCC 11901 cultures are to contamination and mass death from invasive predators. One of the typical issues with culturing marine cyanobacterial and algal species is the requirement of vitamin B_{12}, an expensive addition to large-scale cultures which can make synthesis of lower value chemicals unfeasible. However, a spontaneous vitamin B_{12} independent mutant of PCC 11901 has been successfully isolated and shown to grow without vitamin B_{12} at a similar rate to wild-type PCC 11901 grown with vitamin B_{12} (195).

Ultimately, PBR design will be one of the main factors that will limit scaling up to an industrial level (163,519–521). The modelling carried out as part of this thesis aimed to predict the optimal conditions for fast growth and biomass accumulation for PCC 11901 under the specific parameters of the MC-1000 multicultivator used in the study. The advantage of modelling is that particular constraints can be altered with a few lines of code, thereby saving time and money, thus ensuring the limits of particular bioreactors are taken into consideration when growing photoautotrophic organisms. As computational models continue to improve with the increasing data from PBR design and cyanobacteria research, future PBR design may be less of a limiting factor in scaling up

cyanobacteria for biotechnology. However, modelling must be supported by experimental data, further emphasising the need for large scale, outdoor PBR growth experiments.

6.7 Concluding remarks

Cyanobacteria have huge potential to be an industrially valuable and renewable biomass source and chassis for production of valuable chemicals and proteins. There remain certain challenges in scaling up, PBR design and ensuring metabolic pathways can be introduced and controlled in a predictable manner. However, the future for cyanobacteria is promising as metabolic engineering and synthetic biology approaches continue to increase metabolite production in cyanobacteria, novel strains with industrially desirable traits are discovered and technology advances allowing more comprehensive computer modelling and better PBR design. With these advancements, cyanobacterial biotechnology may expand to a scale which could reduce our reliance on non-renewable and high polluting sources for a range of products which a growing world population requires.

References

1. Brocks JJ, Logan GA, Buick R, Summons RE. Archean Molecular Fossils and the Early Rise of Eukaryotes. Science. 1999 Aug 13;285(5430):1033–6.

2. Rasmussen B, Fletcher IR, Brocks JJ, Kilburn MR. Reassessing the first appearance of eukaryotes and cyanobacteria. Nature. 2008 Oct;455(7216):1101–4.

3. Schopf JW. Microfossils of the Early Archean Apex Chert: New Evidence of the Antiquity of Life. Science. 1993 Apr 30;260(5108):640–6.

4. Capone DG. Marine nitrogen fixation: what's the fuss? Current Opinion in Microbiology. 2001 Jun 1;4(3):341–8.

5. Howe CJ, Barbrook AC, Nisbet RER, Lockhart PJ, Larkum AWD. The origin of plastids. Philos Trans R Soc Lond B Biol Sci. 2008;363(1504):2675–85.

6. Silva P, Thompson E, Bailey S, Kruse O, Mullineaux CW, Robinson C, et al. FtsH is involved in the early stages of repair of photosystem II in Synechocystis sp PCC 6803. Plant Cell. 2003;15(9):2152–64.

7. Kurisu G, Zhang H, Smith JL, Cramer WA. Structure of the cytochrome b6f complex of oxygenic photosynthesis: tuning the cavity. Science. 2003;302(5647):1009–14.

8. Lin MT, Occhialini A, Andralojc PJ, Parry MAJ, Hanson MR. A faster Rubisco with potential to increase photosynthesis in crops. Nature. 2014 Sep 25;513(7519):547-+.

9. Zarzycki J, Axen SD, Kinney JN, Kerfeld CA. Cyanobacterial-based approaches to improving photosynthesis in plants. J Exp Bot. 2013 Jan;64(3):787–98.

10. Miyagawa Y, Tamoi M, Shigeoka S. Overexpression of a cyanobacterial fructose-1,6-/sedoheptulose-1,7-bisphosphatase in tobacco enhances photosynthesis and growth. Nat Biotechnol. 2001;19(10):965–9.

11. Long BM, Hee WY, Sharwood RE, Rae BD, Kaines S, Lim YL, et al. Carboxysome encapsulation of the CO2-fixing enzyme Rubisco in tobacco chloroplasts. Nat Commun. 2018 Sep 3;9(1):3570.

12. Orr DJ, Worrall D, Lin MT, Carmo-Silva E, Hanson MR, Parry MAJ. Hybrid Cyanobacterial-Tobacco Rubisco Supports Autotrophic Growth and Procarboxysomal Aggregation1 [CC-BY]. Plant Physiology. 2020 Feb 1;182(2):807–18.

13. Hoiczyk E, Hansel A. Cyanobacterial cell walls: news from an unusual prokaryotic envelope. J Bacteriol. 2000;182(5):1191–9.

14. Savir Y, Noor E, Milo R, Tlusty T. Cross-species analysis traces adaptation of Rubisco toward optimality in a low-dimensional landscape. Proceedings of the National Academy of Sciences of the United States of America. 2010;107(8):3475–80.

15. Stanier G. Fine structure of cyanobacteria. In 1988. p. 157–72.

16. Zerulla K, Ludt K, Soppa J. The ploidy level of Synechocystis sp PCC 6803 is highly variable and is influenced by growth phase and by chemical and physical external parameters. Microbiology-Sgm. 2016;162(5):730–9.

17. Schneider D, Fuhrmann E, Scholz I, Hess WR, Graumann PL. Fluorescence staining of live cyanobacterial cells suggest non-stringent chromosome segregation and absence of a connection between cytoplasmic and thylakoid membranes. BMC Cell Biol. 2007;8(1):39–39.

18. Vermaas WF. Photosynthesis and respiration in Cyanobacteria. Encyclopedia of Life Sciences. 2001;

19. Lui YT. Developing cyanobacteria as a microbial factory for the production of novel compounds [Internet] [Doctoral]. Doctoral thesis, UCL (University College London). UCL (University College London); 2017 [cited 2022 Jun 8].

20. Lea-Smith DJ, Bombelli P, Dennis JS, Scott SA, Smith AG, Howe CJ. Phycobilisome-deficient strains of Synechocystis sp. PCC 6803 have reduced size and require carbon-limiting conditions to exhibit enhanced productivity. Plant Physiology. 2014;165(2):705–14.

21. Cooley JW, Howitt CA, Vermaas WFJ. Succinate : quinol oxidoreductases in the cyanobacterium Synechocystis sp strain PCC 6803: Presence and function in metabolism and electron transport. Journal of Bacteriology. 2000;182(3):714–22.

22. Cooley JW, Vermaas WFJ. Succinate Dehydrogenase and Other Respiratory Pathways in Thylakoid Membranes of Synechocystis sp. Strain PCC 6803: Capacity Comparisons and Physiological Function. Journal of Bacteriology. 2001 Jul 15;183(14):4251–8.

23. Lea-Smith DJ, Hanke GT. Electron Transport in Cyanobacteria and Its Potential in Bioproduction. In: Cyanobacteria Biotechnology [Internet]. John Wiley & Sons, Ltd; 2021 [cited 2022 Sep 12]. p. 33–63.

24. Howitt CA, Vermaas WF. Quinol and cytochrome oxidases in the cyanobacterium Synechocystis sp. PCC 6803. Biochemistry. 1998;37(51):17944–51.

25. Zhang P, Eisenhut M, Brandt AMM, Carmel D, Silén HM, Vass I, et al. Operon flv4-flv2 provides cyanobacterial photosystem II with flexibility of electron transfer. Plant Cell. 2012;24(5):1952–71.

26. Allahverdiyeva Y, Ermakova M, Eisenhut M, Zhang PP, Richaud P, Hagemann M, et al. Interplay between Flavodiiron proteins and photorespiration in Synechocystis sp. PCC 6803. Journal of Biological Chemistry. 2011;286(27):24007–14.

27. Lin PC, Pakrasi HB. Engineering cyanobacteria for production of terpenoids. Planta. 2019 Jan 1;249(1):145–54.

28. Shestakov SV, Khyen NT. Evidence for Genetic Transformation in Blue-Green Alga Anacystis-Nidulans. Mol Gen Genet. 1970;107(4):372-+.

29. Stevens SE, Porter RD. Transformation in Agmenellum-Quadruplicatum. P Natl Acad Sci-Biol. 1980;77(10):6052–6.

30. Elhai J. Strong and Regulated Promoters in the Cyanobacterium Anabaena Pcc-7120. Fems Microbiol Lett. 1993 Dec 1;114(2):179–84.

31. Li S, Sun T, Xu C, Chen L, Zhang W. Development and optimization of genetic toolboxes for a fast-growing cyanobacterium Synechococcus elongatus UTEX 2973. Metabolic Engineering. 2018 Jul 1;48:163–74.

32. Wendt KE, Pakrasi HB. Genomics Approaches to Deciphering Natural Transformation in Cyanobacteria. Front Microbiol [Internet]. 2019 Jun 7;10. Available from: ://WOS:000470976200002

33. Taton A, Unglaub F, Wright NE, Zeng WY, Paz-Yepes J, Brahamsha B, et al. Broad-host-range vector system for synthetic biology and biotechnology in cyanobacteria. Nucleic Acids Research. 2014;42(17).

34. Elhai J, Wolk CP. Conjugal transfer of DNA to cyanobacteria. In: Methods in Enzymology [Internet]. Academic Press; 1988 [cited 2022 Jun 9]. p. 747–54. (Cyanobacteria; vol. 167).

35. Masukawa H, Inoue K, Sakurai H, Wolk CP, Hausinger RP. Site-Directed Mutagenesis of the Anabaena sp. Strain PCC 7120 Nitrogenase Active Site To Increase Photobiological Hydrogen Production. Applied and Environmental Microbiology. 2010 Oct 15;76(20):6741–50.

36. Mandakovic D, Trigo C, Andrade D, Riquelme B, Gómez-Lillo G, Soto-Liebe K, et al. CyDiv, a Conserved and Novel Filamentous Cyanobacterial Cell Division Protein Involved in Septum Localization. Frontiers in Microbiology [Internet]. 2016 [cited 2022 Jun 9];7.

37. Jeamton W, Dulsawat S, Tanticharoen M, Vonshak A, Cheevadhanarak S. Overcoming Intrinsic Restriction Enzyme Barriers Enhances Transformation Efficiency in Arthrospira platensis C1. Plant Cell Physiol. 2017 Apr 1;58(4):822–30.

38. Ried JL, Collmer A. An nptI-sacB-sacR cartridge for constructing directed, unmarked mutations in gram-negative bacteria by marker exchange-eviction mutagenesis. Gene. 1987;57(2–3):239–46.

39. Behler J, Vijay D, Hess WR, Akhtar MK. CRISPR-Based Technologies for Metabolic Engineering in Cyanobacteria. Trends in Biotechnology. 2018 Oct 1;36(10):996–1010.

40. Lea-Smith DJ, Vasudevan R, Howe CJ. Generation of marked and markerless mutants in model cyanobacterial species. Journal of visualized experiments : JoVE. 2016;(March):1–11.

41. Ermakova M, Huokko T, Richaud P, Bersanini L, Howe CJ, Lea-Smith D, et al. Distinguishing the roles of thylakoid respiratory terminal oxidases in the cyanobacterium Synechocystis sp. PCC 6803. Plant Physiology. 2016;171(2):1307–19.

42. Vasudevan R, Gale GAR, Schiavon AA, Puzorjov A, Malin J, Gillespie MD, et al. CyanoGate: A Modular Cloning Suite for Engineering Cyanobacteria Based on the Plant MoClo Syntax. Plant Physiol. 2019 May;180(1):39–55.

43. Solymosi D, Nikkanen L, Muth-Pawlak D, Fitzpatrick D, Vasudevan R, Howe CJ, et al. Cytochrome c M Decreases Photosynthesis under Photomixotrophy in Synechocystis sp. PCC 6803. Plant Physiol. 2020 Jun;183(2):700–16.

44. Zavřel T, Sinetova MA, Búzová D, Literáková P, Červený J. Characterization of a model cyanobacterium Synechocystis sp. PCC 6803 autotrophic growth in a flat-panel photobioreactor. Engineering in Life Sciences. 2015;15(1):122–32.

45. Yu JJ, Liberton M, Cliften PF, Head RD, Jacobs JM, Smith RD, et al. Synechococcus elongatus UTEX 2973, a fast growing cyanobacterial chassis for biosynthesis using light and CO2. Sci Rep-Uk [Internet]. 2015 Jan 30;5. Available from: ://WOS:000348576400001

46. Wendt KE, Ungerer J, Cobb RE, Zhao H, Pakrasi HB. CRISPR/Cas9 mediated targeted mutagenesis of the fast growing cyanobacterium Synechococcus elongatus UTEX 2973. Microb Cell Fact. 2016 Jun 23;15(1):115.

47. Jones CM, Parrish S, Nielsen DR. Exploiting Polyploidy for Markerless and Plasmid-Free Genome Engineering in Cyanobacteria. ACS Synth Biol. 2021 Sep 17;10(9):2371–82.

48. Kachel B, Mack M. Engineering of Synechococcus sp. strain PCC 7002 for the photoautotrophic production of light-sensitive riboflavin (vitamin B2). Metabolic Engineering. 2020 Nov 1;62:275–86.

49. Jaiswal D, Sengupta A, Sohoni S, Sengupta S, Phadnavis AG, Pakrasi HB, et al. Genome Features and Biochemical Characteristics of a Robust, Fast Growing and Naturally Transformable Cyanobacterium Synechococcus elongatus PCC 11801 Isolated from India. Sci Rep-Uk [Internet]. 2018 Nov 9;8.

50. Jaiswal D, Sengupta A, Sengupta S, Madhu S, Pakrasi HB, Wangikar PP. A Novel Cyanobacterium Synechococcus elongatus PCC 11802 has Distinct Genomic and Metabolomic Characteristics Compared to its Neighbor PCC 11801. Sci Rep. 2020 Jan 13;10(1):191.

51. Włodarczyk A, Selão TT, Norling B, Nixon PJ. Newly discovered Synechococcus sp. PCC 11901 is a robust cyanobacterial strain for high biomass production. Communications Biology. 2020 May 7;3(1):1–14.

52. Cohen MF, Wallis JG, Campbell EL, Meeks JC. Transposon mutagenesis of Nostoc sp. strain ATCC 29133, a filamentous cyanobacterium with multiple cellular differentiation alternatives. Microbiology. 1994 Dec;140 (Pt 12):3233–40.

53. Soule T, Stout V, Swingley WD, Meeks JC, Garcia-Pichel F. Molecular genetics and genomic analysis of scytonemin biosynthesis in Nostoc punctiforme ATCC 29133. J Bacteriol. 2007 Jun;189(12):4465–72.

54. Allen MB, Arnon DI. Studies on Nitrogen-Fixing Blue-Green Algae. I. Growth and Nitrogen Fixation by Anabaena Cylindrica Lemm1. Plant Physiol. 1955 Jul;30(4):366–72.

55. Min HT, Sherman LA. Genetic Transformation and Mutagenesis via Single-Stranded DNA in the Unicellular, Diazotrophic Cyanobacteria of the Genus Cyanothece. Appl Environ Microb. 2010 Nov;76(22):7641–5.

56. Liberton M, Bandyopadhyay A, Pakrasi HB. Enhanced Nitrogen Fixation in a glgX-Deficient Strain of Cyanothece sp. Strain ATCC 51142, a Unicellular Nitrogen-Fixing Cyanobacterium. Appl Environ Microb [Internet]. 2019 Apr;85(7).

57. Taton A, Lis E, Adin DM, Dong G, Cookson S, Kay SA, et al. Gene Transfer in Leptolyngbya sp Strain BL0902, a Cyanobacterium Suitable for Production of Biomass and Bioproducts. Plos One [Internet]. 2012 Jan 24;7(1).

58. Taton A, Ma AT, Ota M, Golden SS, Golden JW. NOT Gate Genetic Circuits to Control Gene Expression in Cyanobacteria. ACS Synth Biol. 2017 Dec 15;6(12):2175–82.

59. Busch AWU, Montgomery BL. The Tryptophan-Rich Sensory Protein (TSPO) is Involved in Stress-Related and Light-Dependent Processes in the Cyanobacterium Fremyella diplosiphon. Front Microbiol [Internet]. 2015 Dec 14;6.

60. Pattanaik B, Montgomery BL. FdTonB is involved in the photoregulation of cellular morphology during complementary chromatic adaptation in Fremyella diplosiphon. Microbiology-Sgm. 2010;156:731–41.

61. Bordowitz JR, Montgomery BL. Photoregulation of Cellular Morphology during Complementary Chromatic Adaptation Requires Sensor-Kinase-Class Protein RcaE in Fremyella diplosiphon. Journal of Bacteriology. 2008 Jun;190(11):4069–74.

62. Morris JJ, Kirkegaard R, Szul MJ, Johnson ZI, Zinser ER. Facilitation of robust growth of Prochlorococcus colonies and dilute liquid cultures by "Helper" heterotrophic bacteria. Appl Environ Microb. 2008 Jul;74(14):4530–4.

63. Brahamsha B. A genetic manipulation system for oceanic cyanobacteria of the genus Synechococcus. Appl Environ Microb. 1996 May;62(5):1747–51.

64. Waterbury JB, Willey JM. [6] Isolation and growth of marine planktonic cyanobacteria. In: Methods in Enzymology [Internet]. Academic Press; 1988 [cited 2022 Nov 19]. p. 100–5. (Cyanobacteria; vol. 167).

65. Moore LR, Coe A, Zinser ER, Saito MA, Sullivan MB, Lindell D, et al. Culturing the marine cyanobacterium Prochlorococcus. Limnology and Oceanography-Methods. 2007;5:353–62.

66. Onai K, Morishita M, Kaneko T, Tabata S, Ishiura M. Natural transformation of the thermophilic cyanobacterium Thermosynechococcus elongatus BP-1: a simple and efficient method for gene transfer. Mol Genet Genomics. 2004 Feb 1;271(1):50–9.

67. Liang Y, Tang J, Luo Y, Kaczmarek MB, Li X, Daroch M. Thermosynechococcus as a thermophilic photosynthetic microbial cell factory for CO2 utilisation. Bioresource Technology. 2019 Apr 1;278:255–65.

68. Stucken K, Ilhan J, Roettger M, Dagan T, Martin WF. Transformation and Conjugal Transfer of Foreign Genes into the Filamentous Multicellular Cyanobacteria (Subsection V) Fischerella and Chlorogloeopsis. Curr Microbiol. 2012 Nov 1;65(5):552–60.

69. Billi D, Friedmann EI, Helm RF, Potts M. Gene Transfer to the Desiccation-Tolerant Cyanobacterium Chroococcidiopsis. Journal of Bacteriology. 2001 Apr;183(7):2298–305.

70. Araki M, Shimada Y, Mimuro M, Tsuchiya T. Establishment of the reporter system for a thylakoid-lacking cyanobacterium, Gloeobacter violaceus PCC 7421. FEBS Open Bio. 2013 Jan 1;3:11–5.

71. Ducat DC, Way JC, Silver PA. Engineering cyanobacteria to generate high-value products. Trends Biotechnol. 2011;29(2):95–103.

72. McCormick AJ, Bombelli P, Lea-Smith DJDJ, Bradley RWRW, Scott AMAM, Fisher ACAC, et al. Hydrogen production through oxygenic photosynthesis using the cyanobacterium Synechocystis sp. PCC 6803 in a bio-photoelectrolysis cell (BPE) system. Energy & Environmental Science. 2013;6(9):2682–2682.

73. Lea-Smith DJ, Bombelli P, Vasudevan R, Howe CJ. Photosynthetic, respiratory and extracellular electron transport pathways in cyanobacteria. Biochimica et Biophysica Acta (BBA) - Bioenergetics. 2016 Mar 1;1857(3):247–55.

74. Tan LT. Bioactive natural products from marine cyanobacteria for drug discovery. Phytochemistry. 2007;68(7):954–79.

75. Biondi N, Tredici M r., Taton A, Wilmotte A, Hodgson D a., Losi D, et al. Cyanobacteria from benthic mats of Antarctic lakes as a source of new bioactivities. Journal of Applied Microbiology. 2008;105(1):105–15.

76. Kanekiyo K, Lee JB, Hayashi K, Takenaka H, Hayakawa Y, Endo S, et al. Isolation of an antiviral polysaccharide, nostoflan, from a terrestrial cyanobacterium, Nostoc flagelliforme. J Nat Prod. 2005 Jul;68(7):1037–41.

77. Clark BR, Engene N, Teasdale ME, Rowley DC, Matainaho T, Valeriote FA, et al. Natural Products Chemistry and Taxonomy of the Marine Cyanobacterium Blennothrix cantharidosmum. J Nat Prod. 2008 Sep;71(9):1530–7.

78. Sarnaik A, Nambissan V, Pandit R, Lali A. Recombinant Synechococcus elongatus PCC 7942 for improved zeaxanthin production under natural light conditions. Algal Research. 2018 Dec 1;36:139–51.

79. Villa FA, Lieske K, Gerwick L. Selective MyD88-dependent pathway inhibition by the cyanobacterial natural product malyngamide F acetate. Eur J Pharmacol. 2010 Mar 10;629(1–3):140–6.

80. Pandey VD, Pandey A, Sharma V. Biotechnological applications of cyanobacterial phycobiliproteins. Int J Curr Microbiol App Sci. 2013;2(9):89–97.

81. Uzair B, Tabassum S, Rasheed M, Rehman SF. Exploring marine cyanobacteria for lead compounds of pharmaceutical importance. The Scientific World Journal. 2012;2012.

82. Pagels F, Guedes AC, Amaro HM, Kijjoa A, Vasconcelos V. Phycobiliproteins from cyanobacteria: Chemistry and biotechnological applications. Biotechnology Advances. 2019 May 1;37(3):422–43.

83. Singh JS, Kumar A, Rai AN, Singh DP. Cyanobacteria: a precious bio-resource in agriculture, ecosystem, and environmental sustainability. Frontiers in microbiology. 2016;7:529.

84. Kour D, Rana KL, Yadav AN, Yadav N, Kumar M, Kumar V, et al. Microbial biofertilizers: Bioresources and eco-friendly technologies for agricultural and environmental sustainability. Biocatalysis and Agricultural Biotechnology. 2020;23:101487.

85. Rodríguez AA, Stella AM, Storni MM, Zulpa G, Zaccaro MC. Effects of cyanobacterial extracellular products and gibberellic acid on salinity tolerance in Oryza sativaL. Saline systems. 2006;2(1):1–4.

86. Misra S, Kaushik BD. Growth promoting substances of cyanobacteria. I: vitamins and their influence on rice plant. Proceedings of the Indian National Science Academy Part B Biological sciences. 1989;55(4):295–300.

87. Kaushik BD. Developments in cyanobacterial biofertilizer. In: Proc Indian Nat Sci Acad. 2014. p. 379–88.

88. Friedrich A, Piven I, Uliczka F, Enke H. Chlorogloeopsis sp. host cell for producing ethanol and method for producing ethanol using the same [Internet]. 2015 [cited 2022 Jun 13]. Available from: https://patentscope.wipo.int/search/en/detail.jsf?docId=WO2015090422&_cid=P22-L4CSYI-16642-1

89. Duehring U, Enke H, Ziegler K, Schwecke T. Metabolically Enhanced Cyanobacterial Cell for the Production of Ethanol [Internet]. 2014 [cited 2022 Jun 13]. Available from: https://patentscope.wipo.int/search/en/detail.jsf?docId=WO2014198964&_cid=P22-L4CSYI-16642-1

90. Baier K, Dühring U, Oesterhelt C, Ziegler K, Enke H. Metabolically Enhanced Photoautotrophic Ethanol Producing Host Cells, Method for Producing the Host Cells, Constructs for the Transformation of the Host Cells, and Method of Producing Ethanol Using the Host Cells [Internet]. 2011 [cited 2022 Jun 13]. Available from: https://patentscope.wipo.int/search/en/detail.jsf?docId=WO2011018116&_cid=P22-L4CSYI-16642-1

91. Ziegler K, Weissert C, Duehring U, Chin J, Anderson M, Cui J, et al. Production of 1,2-Propanediol in Cyanobacteria [Internet]. 2014 [cited 2022 Jun 13]. Available from: https://patentscope.wipo.int/search/en/detail.jsf?docId=WO2014062993&_cid=P22-L4CSYI-16642-1

92. Chin J, Anderson M, Cui J, Spieker M. Production of 1, 3-Propanediol in Cyanobacteria [Internet]. 2014 [cited 2022 Jun 13]. Available from: https://patentscope.wipo.int/search/en/detail.jsf?docId=WO2014062997&_cid=P22-L4CSYI-16642-1

93. Duehring U. Genetically Enhanced Cyanobacteria for the Production of Isoprene [Internet]. 2014 [cited 2022 Jun 13]. Available from: https://patentscope.wipo.int/search/en/detail.jsf?docId=WO2014037050&_cid=P22-L4CSYI-16642-1

94. McConnell M, Uliczka-Opitz F, Dühring U. Production of Heme-Containing Proteins in Cyanobacteria [Internet]. 2019 [cited 2022 Jun 13]. Available from: https://patentscope.wipo.int/search/en/detail.jsf?docId=WO2019079135&_cid=P22-L4CSYI-16642-1

95. Dühring U, Uliczka-Opitz F. Production of Mycosporine-Like Amino Acids Employing Enhanced Production Strains and Novel Enzymes [Internet]. 2020 [cited 2022 Jun 13]. Available from: https://patentscope.wipo.int/search/en/detail.jsf?docId=WO2020231426&_cid=P22-L4CSYI-16642-1

96. Budinoff C, Hehman L, Sweeney K, McConnell MD, Stegman MR. Methods for Extracting Phycocyanin [Internet]. US20180305413 [cited 2022 Jun 13]. Available from: https://patentscope.wipo.int/search/en/detail.jsf?docId=US232146819&_cid=P22-L4CSYI-16642-1

97. Albers S, Fulbright S. Biological Inks and Coatings and Associated Methods [Internet]. 2020 [cited 2022 Jun 17]. Available from:

https://patentscope.wipo.int/search/en/detail.jsf?docId=WO2020097402&_cid=P22-L4IBJH-00154-1

98. Nagarajan A, Davies F, Fulbright S, Albers S, Kim K. Biologically-Derived Carbon Black Alternative and Method of Making the Same [Internet]. 2021 [cited 2022 Jun 17]. Available from: https://patentscope.wipo.int/search/en/detail.jsf?docId=WO2021226552&_cid=P22-L4IBJH-00154-1

99. Albers S, Fulbright S, Zdunek J. US20180291215 Compositions, Systems, Methods and Devices for Utilizing Microorganisms in Print [Internet]. [cited 2022 Jun 17]. Available from: https://patentscope.wipo.int/search/en/detail.jsf?docId=US231564856&_cid=P22-L4IBJH-00154-1

100. Nike Prints Sustainable Graphic Tees Collection with Algae Ink [Internet]. Living Ink. [cited 2022 Jul 5]. Available from: https://livingink.co/news/nike-graphical-tee-algae-ink

101. Seaweed allows Smarties comeback. 2008 Feb 11 [cited 2022 Jul 15]; Available from: http://news.bbc.co.uk/1/hi/uk/7238247.stm

102. DIC's Linablue G1 Natural Blue Colorant Receives Approval under the COSMOS-standard Global Standard for Organic and Natural Cosmetics | News [Internet]. DIC Corporation. [cited 2022 Jul 15]. Available from: https://www.dic-global.com/en/news/2019/products/20191217133339.html

103. Corporation DIC. DIC produces algae?! Spirulina's in the news a lot, but what exactly is it? [Internet]. DIC Corporation. [cited 2022 Jul 15]. Available from: https://www.dic-global.com/en/contents/scene/spirulina/

104. Brain CM. Bioprocessing in microalgae [Internet] [Thesis]. Newcastle University; 2017 [cited 2022 Jul 15]. Available from: http://theses.ncl.ac.uk/jspui/handle/10443/3695

105. Doe J. ScotBio [Internet]. Maritime Forum - European Commission. 2020 [cited 2022 Jul 15]. Available from: https://webgate.ec.europa.eu/maritimeforum/en/node/4540

106. Jester BW, Zhao H, Gewe M, Adame T, Perruzza L, Bolick DT, et al. Development of spirulina for the manufacture and oral delivery of protein therapeutics. Nat Biotechnol. 2022 Jun;40(6):956–64.

107. Lumen Bioscience, Inc. A Phase 2, Randomized, Double-blind, Placebo-controlled Study of LMN-201 for Prevention of C. Difficile Infection Recurrence [Internet]. clinicaltrials.gov; 2022 Apr [cited 2022 Jun 15]. Report No.: NCT05330182. Available from: https://clinicaltrials.gov/ct2/show/NCT05330182

108. Lumen Bioscience, Inc. A Phase 2 Randomized, Double-Blind, Placebo-Controlled, Single Dose Regimen Study of LMN-101 in Healthy Volunteers Challenged With Campylobacter Jejuni [Internet]. clinicaltrials.gov; 2022 Mar [cited 2022 Jun 15]. Report No.: NCT04182490. Available from: https://clinicaltrials.gov/ct2/show/NCT04182490

109. Lumen Bioscience, Inc. Exploratory Study to Assess Delivery of LMN-201 Components Via Enteric Capsules in the Gut of Individuals With Ostomies [Internet]. clinicaltrials.gov; 2022 Mar [cited 2022 Jun 15]. Report No.: NCT04893239. Available from: https://clinicaltrials.gov/ct2/show/NCT04893239

110. Lumen Bioscience, Inc. A Phase 1 Randomized, Double-Blind, Placebo-Controlled, Dose-Escalation, Safety and Pharmacokinetic Study of LMN-101 in Healthy Volunteers [Internet]. clinicaltrials.gov; 2020 Jul [cited 2022 Jun 15]. Report No.: NCT04098263. Available from: https://clinicaltrials.gov/ct2/show/NCT04098263

111. Fujisawa T, Narikawa R, Okamoto S, Ehira S, Yoshimura H, Suzuki I, et al. Genomic Structure of an Economically Important Cyanobacterium, Arthrospira (Spirulina) platensis NIES-39. DNA Research. 2010;17(2):85–103.

112. Dismukes GC, Carrieri D, Bennette N, Ananyev GM, Posewitz MC. Aquatic phototrophs: efficient alternatives to land-based crops for biofuels. Curr Opin Biotechnol. 2008;19(3):235–40.

113. Ruffing AM. Engineered cyanobacteria: Teaching an old bug new tricks. Bioengineered Bugs. 2011 May 1;2(3):136–49.

114. Machado IMP, Atsumi S. Cyanobacterial biofuel production. Journal of Biotechnology. 2012 Nov 30;162(1):50–6.

115. Nozzi NE, Oliver JWK, Atsumi S. Cyanobacteria as a Platform for Biofuel Production. Front Bioeng Biotechnol. 2013 Sep 26;1:7.

116. Quintana N, Van der Kooy F, Van de Rhee MD, Voshol GP, Verpoorte R. Renewable energy from Cyanobacteria: energy production optimization by metabolic pathway engineering. Applied Microbiology and Biotechnology. 2011;91(3):471–90.

117. Christenson L, Sims R. Production and harvesting of microalgae for wastewater treatment, biofuels, and bioproducts. Biotechnology Advances. 2011;29(6):686–702.

118. Craggs RJ, Heubeck S, Lundquist TJ, Benemann JR. Algal biofuels from wastewater treatment high rate algal ponds. Water Science and Technology. 2011 Feb 1;63(4):660–5.

119. Su HY, Chou HH, Chow TJ, Lee TM, Chang JS, Huang WL, et al. Improvement of outdoor culture efficiency of cyanobacteria by over-expression of stress tolerance genes and its implication as bio-refinery feedstock. Bioresource Technology. 2017 Nov 1;244:1294–303.

120. Iijima H, Nakaya Y, Kuwahara A, Hirai MY, Osanai T. Seawater cultivation of freshwater cyanobacterium Synechocystis sp. PCC 6803 drastically alters amino acid composition and glycogen metabolism. Frontiers in Microbiology [Internet]. 2015 [cited 2022 Jun 22];6. Available from: https://www.frontiersin.org/article/10.3389/fmicb.2015.00326

121. Lai MC, Lan EI. Advances in Metabolic Engineering of Cyanobacteria for Photosynthetic Biochemical Production. Metabolites. 2015 Oct 27;5(4):636–58.

122. Yu Y, You L, Liu DY, Hollinshead W, Tang YJJ, Zhang FZ. Development of Synechocystis sp PCC 6803 as a Phototrophic Cell Factory. Mar Drugs. 2013 Aug;11(8):2894–916.

123. Zavrel T, Ocenasova P, Cerveny J. Phenotypic characterization of Synechocystis sp PCC 6803 substrains reveals differences in sensitivity to abiotic stress. Plos One [Internet]. 2017 Dec 7;12(12).

124. Morris JN, Eaton-Rye JJ, Summerfield TC. Phenotypic variation in wild-type substrains of the model cyanobacterium Synechocystis sp PCC 6803. New Zeal J Bot. 2017 Mar;55(1):25–35.

125. Alonso JM, Stepanova AN, Leisse TJ, Kim CJ, Chen H, Shinn P, et al. Genome-Wide Insertional Mutagenesis of Arabidopsis thaliana. Science. 2003 Aug;301(5633):653–7.

126. Li X, Patena W, Fauser F, Jinkerson RE, Saroussi S, Meyer MT, et al. A genome-wide algal mutant library and functional screen identifies genes required for eukaryotic photosynthesis. Nat Genet. 2019 Apr;51(4):627–35.

127. Baba T, Ara T, Hasegawa M, Takai Y, Okumura Y, Baba M, et al. Construction of Escherichia coli K-12 in-frame, single-gene knockout mutants: the Keio collection. Mol Syst Biol [Internet]. 2006;2.

128. Giaever G, Chu AM, Ni L, Connelly C, Riles L, Veronneau S, et al. Functional profiling of the Saccharomyces cerevisiae genome. Nature. 2002 Jul 25;418(6896):387–91.

129. Rubin BE, Wetmore KM, Price MN, Diamond S, Shultzaberger RK, Lowe LC, et al. The essential gene set of a photosynthetic organism. P Natl Acad Sci USA. 2015 Dec 1;112(48):E6634–43.

130. Gale GAR, Schiavon Osorio AA, Mills LA, Wang B, Lea-Smith DJ, McCormick AJ. Emerging Species and Genome Editing Tools: Future Prospects in Cyanobacterial Synthetic Biology. Microorganisms [Internet]. 2019 Sep 29;7(10).

131. Kaneko T, Sato S, Kotani H, Tanaka A, Asamizu E, Nakamura Y, et al. Sequence analysis of the genome of the unicellular cyanobacterium Synechocystis sp. strain PCC6803. II. Sequence determination of the entire genome and assignment of potential protein-coding regions. DNA Res. 1996 Jun 30;3(3):109–36.

132. Ritchie RJ, Larkum AWD. Modelling photosynthesis in shallow algal production ponds. Photosynthetica. 2012;50(4):481–500.

133. Wang B, Lan CQ, Horsman M. Closed photobioreactors for production of microalgal biomasses. Biotechnology Advances. 2012 Jul 1;30(4):904–12.

134. Chen HW, Yang TS, Chen MJ, Chang YC, Lin CY, Wang EIC, et al. Application of power plant flue gas in a photobioreactor to grow Spirulina algae, and a bioactivity analysis of the algal water-soluble polysaccharides. Bioresource Technology. 2012 Sep 1;120:256–63.

135. Francisco ÉC, Neves DB, Jacob-Lopes E, Franco TT. Microalgae as feedstock for biodiesel production: Carbon dioxide sequestration, lipid production and biofuel quality. Journal of Chemical Technology & Biotechnology. 2010;85(3):395–403.

136. Douskova I, Doucha J, Livansky K, Machat J, Novak P, Umysova D, et al. Simultaneous flue gas bioremediation and reduction of microalgal biomass production costs. Appl Microbiol Biotechnol. 2009 Feb 1;82(1):179–85.

137. Chiu SY, Kao CY, Huang TT, Lin CJ, Ong SC, Chen CD, et al. Microalgal biomass production and on-site bioremediation of carbon dioxide, nitrogen oxide and sulfur dioxide from flue gas using Chlorella sp. cultures. Bioresource technology. 2011;102(19):9135–42.

138. Li FF, Yang ZH, Zeng R, Yang G, Chang X, Yan JB, et al. Microalgae Capture of CO2 from Actual Flue Gas Discharged from a Combustion Chamber. Ind Eng Chem Res. 2011 May 18;50(10):6496–502.

139. Acién FG, Molina E, Reis A, Torzillo G, Zittelli GC, Sepúlveda C, et al. 1 - Photobioreactors for the production of microalgae. In: Gonzalez-Fernandez C, Muñoz R, editors. Microalgae-Based Biofuels and Bioproducts [Internet]. Woodhead Publishing; 2017 [cited 2022 Jun 21]. p. 1–44. (Woodhead Publishing Series in Energy).

140. Wang C, Lan CQ. Effects of shear stress on microalgae – A review. Biotechnology Advances. 2018 Jul 1;36(4):986–1002.

141. Chisti Y. Constraints to commercialization of algal fuels. Journal of Biotechnology. 2013 Sep 10;167(3):201–14.

142. Pulz O. Photobioreactors: production systems for phototrophic microorganisms. Appl Microbiol Biotechnol. 2001 Oct 1;57(3):287–93.

143. Grobbelaar JU. Microalgae mass culture: the constraints of scaling-up. J Appl Phycol. 2012 Jun 1;24(3):315–8.

144. Wang H, Zhang W, Chen L, Wang J, Liu T. The contamination and control of biological pollutants in mass cultivation of microalgae. Bioresource Technology. 2013 Jan 1;128:745–50.

145. Luan G, Lu X. Tailoring cyanobacterial cell factory for improved industrial properties. Biotechnology Advances. 2018;36(2):430–42.

146. Zhu Z, Luan G, Tan X, Zhang H, Lu X. Rescuing ethanol photosynthetic production of cyanobacteria in non-sterilized outdoor cultivations with a bicarbonate-based pH-rising strategy. Biotechnol Biofuels. 2017 Apr 14;10(1):93.

147. Parmar A, Singh NK, Pandey A, Gnansounou E, Madamwar D. Cyanobacteria and microalgae: A positive prospect for biofuels. Bioresource Technology. 2011 Nov 1;102(22):10163–72.

148. Kishi M, Yamada Y, Katayama T, Matsuyama T, Toda T. Carbon Mass Balance in Arthrospira platensis Culture with Medium Recycle and High CO2 Supply. Applied Sciences. 2020 Jan;10(1):228.

149. Zarrouk C. Contribution a l'etude d'une Cyanophycee. Influence de Divers Facteurs Physiques et Chimiques sur la croissance et la photosynthese de Spirulina mixima. Thesis University of Paris, France. 1966;

150. Sukenik A, Schröder W, Lauer J, Shelef G, Soeder CJ. Coprecipitation of microalgal biomass with calcium and phosphate ions. Water Research. 1985 Jan 1;19(1):127–9.

151. Kishi M, Toda T. Carbon fixation properties of three alkalihalophilic microalgal strains under high alkalinity. J Appl Phycol. 2018 Feb 1;30(1):401–10.

152. Brenner K, You L, Arnold FH. Engineering microbial consortia: a new frontier in synthetic biology. Trends in Biotechnology. 2008 Sep 1;26(9):483–9.

153. Williams P 2007. Quorum sensing, communication and cross-kingdom signalling in the bacterial world. Microbiology. 153(12):3923–38.

154. Sue T, Obolonkin V, Griffiths H, Villas-Bôas SG. An Exometabolomics Approach to Monitoring Microbial Contamination in Microalgal Fermentation Processes by Using Metabolic Footprint Analysis. Applied and Environmental Microbiology. 2011 Nov;77(21):7605–10.

155. Yen HW, Chen PW, Chen LJ. The synergistic effects for the co-cultivation of oleaginous yeast-Rhodotorula glutinis and microalgae-Scenedesmus obliquus on the biomass and total lipids accumulation. Bioresource Technology. 2015 May 1;184:148–52.

156. Dong QL, Zhao XM. In situ carbon dioxide fixation in the process of natural astaxanthin production by a mixed culture of Haematococcus pluvialis and Phaffia rhodozyma. Catalysis Today. 2004 Dec 14;98(4):537–44.

157. Wang R, Gallant É, Seyedsayamdost MR. Investigation of the Genetics and Biochemistry of Roseobacticide Production in the Roseobacter Clade Bacterium Phaeobacter inhibens. mBio. 2016 Mar 22;7(2):e02118-15.

158. Padmaperuma G, Kapoore RV, Gilmour DJ, Vaidyanathan S. Microbial consortia: a critical look at microalgae co-cultures for enhanced biomanufacturing. Critical Reviews in Biotechnology. 2018 Jul 4;38(5):690–703.

159. Young KD. The selective value of bacterial shape. Microbiology and molecular biology reviews. 2006;70(3):660–703.

160. Hahn MW, Höfle MG. Grazing of protozoa and its effect on populations of aquatic bacteria. FEMS Microbiology Ecology. 2001 Apr 1;35(2):113–21.

161. Jezberová J, Komárková J. Morphological transformation in a freshwater Cyanobium sp. induced by grazers. Environmental Microbiology. 2007;9(7):1858–62.

162. Nienaber M, Kannan M. A Guide to Cyanobacteria: Identification and Impact. 2018.

163. Beattie A, Vermaas W, Darzins A, Holland SC, Li S, McGowen J, et al. A probabilistic economic and environmental impact assessment of a cyanobacteria-based biorefinery. Algal Research. 2021 Nov 1;59:102454.

164. Caetano NS, Martins AA, Gorgich M, Gutiérrez DM, Ribeiro TJ, Mata TM. Flocculation of Arthrospira maxima for improved harvesting. Energy Reports. 2020 Feb 1;6:423–8.

165. Jordan A, Chandler J, MacCready JS, Huang J, Osteryoung KW, Ducat DC. Engineering cyanobacterial cell morphology for enhanced recovery and processing of biomass. Applied and environmental microbiology. 2017;83(9):e00053-17.

166. Hu B, Yang GH, Zhao WX, Zhang YJ, Zhao JD. MreB is important for cell shape but not for chromosome segregation of the filamentous cyanobacterium Anabaena sp PCC 7120. Molecular Microbiology. 2007;63(6):1640–52.

167. Singh SP, Montgomery BL. Regulation of BolA abundance mediates morphogenesis in Fremyella diplosiphon. Frontiers in microbiology. 2015;6:1215.

168. Vandamme D, Foubert I, Muylaert K. Flocculation as a low-cost method for harvesting microalgae for bulk biomass production. Trends in Biotechnology. 2013 Apr 1;31(4):233–9.

169. Zheng H, Gao Z, Yin J, Tang X, Ji X, Huang H. Harvesting of microalgae by flocculation with poly (γ-glutamic acid). Bioresource technology. 2012;112:212–20.

170. Yu SI, Min SK, Shin HS. Nanocellulose size regulates microalgal flocculation and lipid metabolism. Sci Rep. 2016 Oct 31;6(1):35684.

171. Zhu J, Wakisaka M. Harvesting of Arthrospira platensis by flocculation with phytic acid from rice bran. Bioscience, Biotechnology, and Biochemistry. 2020 Aug 2;84(8):1736–44.

172. Golueke CG, Oswald WJ. Harvesting and processing sewage-grown planktonic algae. Journal (Water Pollution Control Federation). 1965;471–98.

173. Angermayr SA, van der Woude AD, Correddu D, Vreugdenhil A, Verrone V, Hellingwerf KJ. Exploring metabolic engineering design principles for the photosynthetic production of lactic acid by Synechocystis sp PCC6803. Biotechnology for Biofuels. 2014;7.

174. Osanai T, Shirai T, Iijima H, Nakaya Y, Okamoto M, Kondo A, et al. Genetic manipulation of a metabolic enzyme and a transcriptional regulator increasing succinate excretion from unicellular cyanobacterium. Frontiers in Microbiology. 2015;6:1064.

175. Savakis P, Tan X, Du W, Branco dos Santos F, Lu X, Hellingwerf KJ. Photosynthetic production of glycerol by a recombinant cyanobacterium. Journal of Biotechnology. 2015 Feb 10;195:46–51.

176. Gao Z, Zhao H, Li Z, Tan X, Lu X. Photosynthetic production of ethanol from carbon dioxide in genetically engineered cyanobacteria. Energy & Environmental Science. 2012;5(12):9857–65.

177. Shen CR, Liao JC. Metabolic engineering of Escherichia coli for 1-butanol and 1-propanol production via the keto-acid pathways. Metabolic Engineering. 2008 Nov 1;10(6):312–20.

178. Liu X, Curtiss R. Nickel-inducible lysis system in Synechocystis sp. PCC 6803. Proceedings of the National Academy of Sciences. 2009 Dec 22;106(51):21550–4.

179. Liu X, Fallon S, Sheng J, Curtiss R. CO2-limitation-inducible Green Recovery of fatty acids from cyanobacterial biomass. Proceedings of the National Academy of Sciences. 2011 Apr 26;108(17):6905–8.

180. Liu X, Curtiss R. Thermorecovery of cyanobacterial fatty acids at elevated temperatures. Journal of Biotechnology. 2012 Nov 15;161(4):445–9.

181. Mahbub M, Hemm L, Yang Y, Kaur R, Carmen H, Engl C, et al. mRNA localization, reaction centre biogenesis and thylakoid membrane targeting in cyanobacteria. Nat Plants. 2020 Sep;6(9):1179–91.

182. Sengupta S, Sahasrabuddhe D, Wangikar PP. Transporter engineering for the development of cyanobacteria as cell factories: A text analytics guided survey. Biotechnology Advances. 2022 Jan 1;54:107816.

183. Baers LL, Breckels LM, Mills LA, Gatto L, Deery MJ, Stevens TJ, et al. Proteome Mapping of a Cyanobacterium Reveals Distinct Compartment Organization and Cell-Dispersed Metabolism. Plant Physiology. 2019 Dec 1;181(4):1721–38.

184. Liberton M, Howard Berg R, Heuser J, Roth R, Pakrasi HB. Ultrastructure of the membrane systems in the unicellular cyanobacterium Synechocystis sp. strain PCC 6803. Protoplasma. 2006 May 30;227(2):129.

185. Liu X, Sheng J, Curtiss 3rd R, Curtiss R. Fatty acid production in genetically modified cyanobacteria. Proc Natl Acad Sci U S A. 2011;108(17):6899–904.

186. Simkovsky R, Effner EE, Iglesias-Sánchez MJ, Golden SS. Mutations in Novel Lipopolysaccharide Biogenesis Genes Confer Resistance to Amoebal Grazing in Synechococcus elongatus. Applied and Environmental Microbiology. 2016 May;82(9):2738–50.

187. Bernstein HC, Konopka A, Melnicki MR, Hill EA, Kucek LA, Zhang S, et al. Effect of mono- and dichromatic light quality on growth rates and photosynthetic performance of Synechococcus sp. PCC 7002. Frontiers in Microbiology [Internet]. 2014 [cited 2022 Jul 19];5.

188. Begemann MB, Zess EK, Walters EM, Schmitt EF, Markley AL, Pfleger BF. An Organic Acid Based Counter Selection System for Cyanobacteria. Plos One [Internet]. 2013 Oct 1;8(10).

189. Wendt KE, Walker P, Sengupta A, Ungerer J, Pakrasi HB. Engineering Natural Competence into the Fast-Growing Cyanobacterium Synechococcus elongatus Strain UTEX 2973. Applied and Environmental Microbiology. 2022 Jan 11;88(1):e01882-21.

190. Ungerer J, Lin PC, Chen HY, Pakrasi HB. Adjustments to Photosystem Stoichiometry and Electron Transfer Proteins Are Key to the Remarkably Fast Growth of the Cyanobacterium Synechococcus elongatus UTEX 2973. mBio. 2018 Mar 7;9(1):e02327-17.

191. Ungerer J, Wendt KE, Hendry JI, Maranas CD, Pakrasi HB. Comparative genomics reveals the molecular determinants of rapid growth of the cyanobacterium Synechococcus elongatus UTEX 2973. P Natl Acad Sci USA. 2018 Dec 11;115(50):E11761–70.

192. Kanno M, Carroll AL, Atsumi S. Global metabolic rewiring for improved CO2 fixation and chemical production in cyanobacteria. Nat Commun. 2017 Mar 13;8(1):14724.

193. Zhou J, Li Y. SNPs deciding the rapid growth of cyanobacteria are alterable. Proceedings of the National Academy of Sciences. 2019 Mar 5;116(10):3945–3945.

194. Sengupta A, Madhu S, Wangikar PP. A Library of Tunable, Portable, and Inducer-Free Promoters Derived from Cyanobacteria. ACS Synth Biol. 2020 Jul 17;9(7):1790–801.

195. Mills LA, Moreno-Cabezuelo JÁ, Włodarczyk A, Victoria AJ, Mejías R, Nenninger A, et al. Development of a Biotechnology Platform for the Fast-Growing Cyanobacterium Synechococcus sp. PCC 11901. Biomolecules. 2022 Jul;12(7):872.

196. Ghatak S, King ZA, Sastry A, Palsson BO. The y-ome defines the 35% of Escherichia coli genes that lack experimental evidence of function. Nucleic Acids Research. 2019 Mar 18;47(5):2446–54.

197. Fujisawa T, Narikawa R, Maeda S ichi, Watanabe S, Kanesaki Y, Kobayashi K, et al. CyanoBase: a large-scale update on its 20th anniversary. Nucleic Acids Research. 2017 Jan 4;45(D1):D551–4.

198. Altschul SF, Gish W, Miller W, Myers EW, Lipman DJ. Basic local alignment search tool. J Mol Biol. 1990;215(3):403–10.

199. Smith TF, Waterman MS. Identification of common molecular subsequences. Journal of Molecular Biology. 1981 Mar 25;147(1):195–7.

200. The UniProt Consortium. UniProt: the universal protein knowledgebase in 2021. Nucleic Acids Research. 2021 Jan 8;49(D1):D480–9.

201. Wes McKinney. Data structures for statistical computing in python. In: Proceedings of the 9th Python in Science Conference. Austin, TX: Zenodo; 2010. p. 51--56.

202. Harris CR, Millman KJ, van der Walt SJ, Gommers R, Virtanen P, Cournapeau D, et al. Array programming with NumPy. Nature. 2020 Sep;585(7825):357–62.

203. BLAST® Command Line Applications User Manual. National Center for Biotechnology Information (US); 2008.

204. Williams JGK. Construction of specific mutations in photosystem-II photosynthetic reaction center by genetic-engineering methods in Synechocystis-6803. Methods in Enzymology. 1988;167:766–78.

205. Schmetterer GR. Sequence Conservation among the Glucose Transporter from the Cyanobacterium-Synechocystis Sp Pcc-6803 and Mammalian Glucose Transporters. Plant Mol Biol. 1990 May;14(5):697–706.

206. Chen X, Schreiber K, Appel J, Makowka A, Fahnrich B, Roettger M, et al. The Entner-Doudoroff pathway is an overlooked glycolytic route in cyanobacteria and plants. P Natl Acad Sci USA. 2016 May 10;113(19):5441–6.

207. Patipong T, Ngoennet S, Honda M, Hibino T, Waditee-Sirisattha R, Kageyama H. A class I fructose-1,6-bisphosphate aldolase is associated with salt stress tolerance in a halotolerant cyanobacterium Halothece sp. PCC 7418. Arch Biochem Biophys. 2019 Sep 15;672:108059.

208. Sundaram S, Karakaya H, Scanlan DJ, Mann NH. Multiple oligomeric forms of glucose-6-phosphate dehydrogenase in cyanobacteria and the role of OpcA in the assembly process. Microbiology. 1998;144 (Pt 6:1549–56.

209. Ozkul K, Karakaya H. Characterisation of an opcA Mutant of the Unicellular Cyanobacterium Synechocystis sp. PCC 6803. Curr Microbiol. 2015 Nov;71(5):572–8.

210. Makowka A, Nichelmann L, Schulze D, Spengler K, Wittmann C, Forchhammer K, et al. Glycolytic Shunts Replenish the Calvin-Benson-Bassham Cycle as Anaplerotic Reactions in Cyanobacteria. Mol Plant [Internet]. 2020 Feb 8;

211. Koksharova O, Schubert M, Shestakov S, Cerff R. Genetic and biochemical evidence for distinct key functions of two highly divergent GAPDH genes in catabolic and anabolic carbon flow of the cyanobacterium Synechocystis sp. PCC 6803. Plant Mol Biol. 1998 Jan;36(1):183–94.

212. Eisenhut M, Ruth W, Haimovich M, Bauwe H, Kaplan A, Hagemann M. The photorespiratory glycolate metabolism is essential for cyanobacteria and might have been conveyed endosymbiontically to plants. Proceedings of the National Academy of Sciences of the United States of America. 2008;105(44):17199–204.

213. Eisenhut M, Roell MS, Weber APM. Mechanistic understanding of photorespiration paves the way to a new green revolution. New Phytol. 2019 Sep;223(4):1762–9.

214. Eisenhut M, Kahlon S, Hasse D, Ewald R, Lieman-Hurwitz J, Ogawa T, et al. The plant-like C2 glycolate cycle and the bacterial-like glycerate pathway cooperate in phosphoglycolate metabolism in cyanobacteria. Plant Physiology. 2006;142(1):333–42.

215. Zilliges Y. Glycogen, a dynamic cellular sink and reservoir for carbon. In: Flores E, editor. Cell Biology of Cyanobacteria. Caister Academic Press; 2014.

216. Yoo SH, Lee BH, Moon Y, Spalding MH, Jane JL. Glycogen synthase isoforms in Synechocystis sp. PCC6803: identification of different roles to produce glycogen by targeted mutagenesis. PLoS One. 2014;9(3):e91524–e91524.

217. Fu J, Xu XD. The functional divergence of two glgP homologues in Synechocystis sp PCC 6803. Fems Microbiology Letters. 2006;260(2):201–9.

218. Taroncher-Oldenberg G, Nishina K, Stephanopoulos G. Identification and analysis of the polyhydroxyalkanoate-specific beta-ketothiolase and acetoacetyl coenzyme A reductase genes in the cyanobacterium Synechocystis sp strain PCC6803. Appl Environ Microbiol. 2000;66(10):4440–8.

219. Hein S, Tran H, Steinbuchel A. Synechocystis sp. PCC6803 possesses a two-component polyhydroxyalkanoic acid synthase similar to that of anoxygenic purple sulfur bacteria. Arch Microbiol. 1998;170(3):162–70.

220. Koch M, Doello S, Gutekunst K, Forchhammer K. PHB is Produced from Glycogen Turn-over during Nitrogen Starvation in Synechocystis sp. PCC 6803. Int J Mol Sci [Internet]. 2019 Apr 2;20(8).

221. Zhang S, Bryant DA. The tricarboxylic acid cycle in cyanobacteria. Science. 2011;334(6062):1551–3.

222. Zhang S, Qian X, Chang S, Dismukes GC, Bryant DA. Natural and Synthetic Variants of the Tricarboxylic Acid Cycle in Cyanobacteria: Introduction of the GABA Shunt into Synechococcus sp. PCC 7002. Front Microbiol. 2016;7:1972.

223. Ito S, Koyama N, Osanai T. Citrate synthase from Synechocystis is a distinct class of bacterial citrate synthase. Sci Rep-Uk [Internet]. 2019 Apr 15;9.

224. Katayama N, Takeya M, Osanai T. Biochemical characterisation of fumarase C from a unicellular cyanobacterium demonstrating its substrate affinity, altered by an amino acid substitution. Sci Rep-Uk [Internet]. 2019 Jul 23;9.

225. Takeya M, Ito S, Sukigara H, Osanai T. Purification and Characterisation of Malate Dehydrogenase From Synechocystis sp PCC 6803: Biochemical Barrier of the Oxidative Tricarboxylic Acid Cycle. Front Plant Sci [Internet]. 2018 Jul 13;9.

226. Knoop H, Grundel M, Zilliges Y, Lehmann R, Hoffmann S, Lockau W, et al. Flux Balance Analysis of Cyanobacterial Metabolism: The Metabolic Network of Synechocystis sp PCC 6803. Plos Comput Biol [Internet]. 2013 Jun;9(6).

227. Takeya M, Hirai MY, Osanai T. Allosteric Inhibition of Phosphoenolpyruvate Carboxylases is Determined by a Single Amino Acid Residue in Cyanobacteria. Sci Rep-Uk [Internet]. 2017 Jan 24;7.

228. Yang C, Hua Q, Shimizu K. Metabolic flux analysis in Synechocystis using isotope distribution from C-13-labeled glucose. Metab Eng. 2002 Jul;4(3):202–16.

229. Young JD, Shastri AA, Stephanopoulos G, Morgan JA. Mapping photoautotrophic metabolism with isotopically nonstationary C-13 flux analysis (vol 13, pg 656, 2011). Metab Eng. 2012 Mar;14(2):185–185.

230. Bricker TM, Zhang SL, Laborde SM, Mayer PR, Frankel LK, Moroney JV. The malic enzyme is required for optimal photo autotrophic growth of Synechocystis sp strain PCC 6803 under continuous light but not under a diurnal light regimen. Journal of Bacteriology. 2004;186(23):8144–8.

231. Hasunuma T, Matsuda M, Kato Y, Vavricka CJ, Kondo A. Temperature enhanced succinate production concurrent with increased central metabolism turnover in the cyanobacterium Synechocystis sp PCC 6803. Metab Eng. 2018 Jul;48:109–20.

232. Brey LF, Wlodarczyk AJ, Bang Thofner JF, Burow M, Crocoll C, Nielsen I, et al. Metabolic engineering of Synechocystis sp. PCC 6803 for the production of aromatic amino acids and derived phenylpropanoids. Metab Eng. 2019 Nov 10;57:129–39.

233. Schmidt W, Weckesser J, Mayer H. Lipopolysaccharides in four strains of the unicellular cyanobacterium Synechocystis. Archives of Microbiology. 1980;127(3):217–22.

234. Maeda K, Narikawa R, Ikeuchi M. CugP Is a Novel Ubiquitous Non-GalU-Type Bacterial UDP-Glucose Pyrophosphorylase Found in Cyanobacteria. Journal of Bacteriology. 2014;196(13):2348–54.

235. Mohamed HE, van de Meene AML, Roberson RW, Vermaas WFJ. Myxoxanthophyll is required for normal cell wall structure and thylakoid organization in the cyanobacterium, Synechocystis sp strain PCC 6803. Journal of Bacteriology. 2005;187(20):6883–92.

236. Marin K, Zuther E, Kerstan T, Kunert A, Hagemann M. The ggpS gene from Synechocystis sp. strain PCC 6803 encoding glucosyl-glycerol-phosphate synthase is involved in osmolyte synthesis. Journal of Bacteriology. 1998;180(18):4843–9.

237. Miao XL, Wu QY, Wu GF, Zhao NM. Sucrose accumulation in salt-stressed cells of agp gene deletion-mutant in cyanobacterium Synechocystis sp PCC 6803. Fems Microbiology Letters. 2003;218(1):71–7.

238. Curatti L, Folco E, Desplats P, Abratti G, Limones V, Herrera-Estrella L, et al. Sucrose-phosphate synthase from Synechocystis sp. Strain PCC 6803: Identification of the spsA gene and characterization of the enzyme expressed in Escherichia coli. Journal of Bacteriology. 1998;180(24):6776–9.

239. Salerno GL, Curatti L. Origin of sucrose metabolism in higher plants: when, how and why? Trends Plant Sci. 2003 Feb;8(2):63–9.

240. Kirsch F, Luo Q, Lu X, Hagemann M. Inactivation of invertase enhances sucrose production in the cyanobacterium Synechocystis sp. PCC 6803. Microbiology. 2018 Oct;164(10):1220–8.

241. Hagemann M, Erdmann N. Activation and Pathway of Glucosylglycerol Synthesis in the Cyanobacterium-Synechocystis Sp Pcc-6803. Microbiol-Sgm. 1994 Jun;140:1427–31.

242. Guardiola J, De Felice M, Lamberti A, Iaccarino M. The acetolactate synthase isoenzymes of Escherichia coli K-12. Mol Gen Genet. 1977 Nov 4;156(1):17–25.

243. GarciaDominguez M, Reyes JC, Florencio FJ. Purification and characterization of a new type of glutamine synthetase from cyanobacteria. Eur J Biochem. 1997 Feb 15;244(1):258–64.

244. Navarro F, Martin-Figueroa E, Candau P, Florencio FJ. Ferredoxin-dependent iron-sulfur flavoprotein glutamate synthase (GlsF) from the cyanobacterium Synechocystis sp PCC 6803: Expression and assembly in Escherichia coli. Archives of Biochemistry and Biophysics. 2000;379(2):267–76.

245. Liu LK, Becker DF, Tanner JJ. Structure, function, and mechanism of proline utilization A (PutA). Arch Biochem Biophys. 2017 Oct 15;632:142–57.

246. Zhang H, Liu YJ, Nie XQ, Liu LX, Hua Q, Zhao GP, et al. The cyanobacterial ornithine-ammonia cycle involves an arginine dihydrolase. Nat Chem Biol. 2018 Jun;14(6):575–81.

247. Kurihara S, Oda S, Kato K, Kim HG, Koyanagi T, Kumagai H, et al. A novel putrescine utilization pathway involves gamma-glutamylated intermediates of Escherichia coli K-12. J Biol Chem. 2005 Feb 11;280(6):4602–8.

248. Flores E, Arevalo S, Burnat M. Cyanophycin and arginine metabolism in cyanobacteria. Algal Res [Internet]. 2019 Sep;42.

249. Hudson AO, Singh BK, Leustek T, Gilvarg C. An LL-diaminopimelate aminotransferase defines a novel variant of the lysine biosynthesis pathway in plants. Plant Physiol. 2006 Jan;140(1):292–301.

250. Hudson AO, Gilvarg C, Leustek T. Biochemical and phylogenetic characterization of a novel diaminopimelate biosynthesis pathway in prokaryotes identifies a diverged form of LL-diaminopimelate aminotransferase. Journal of Bacteriology. 2008;190(9):3256–63.

251. Zhao GP, Somerville RL, Chitnis PR. Synechocystis Pcc-6803 Contains a Single-Gene for the Beta-Subunit of Tryptophan Synthase with Strong Homology to the Trpb Genes of Arabidopsis and Maize (Zea-Mays L). Plant Physiol. 1994 Feb;104(2):461–6.

252. Legrand P, Dumas R, Seux M, Rippert P, Ravelli R, Ferrer JL, et al. Biochemical characterization and crystal structure of Synechocystis arogenate dehydrogenase provide insights into catalytic reaction. Structure. 2006;14(4):767–76.

253. Klemke F, Baier A, Knoop H, Jablonsky J, Beyer G, Volkmer T, et al. Identification of the light-independent phosphoserine pathway as an additional source of serine in the cyanobacterium Synechocystis sp. PCC 6803. Microbiology. 2015;161:1050–60.

254. Tirupati B, Vey JL, Drennan CL, Bollinger Jr JM. Kinetic and structural characterization of Slr0077/SufS, the essential cysteine desulfurase from Synechocystis sp. PCC 6803. Biochemistry. 2004;43(38):12210–9.

255. Cameron JC, Pakrasi HB. Glutathione in Synechocystis 6803: a closer look into the physiology of a gshB mutant. Plant Signal Behav. 2011;6(1):89–92.

256. Cameron JC, Pakrasi HB. Essential Role of Glutathione in Acclimation to Environmental and Redox Perturbations in the Cyanobacterium Synechocystis sp. PCC 6803. Plant Physiology. 2010;154(4):1672–85.

257. Kato S, Mihara H, Kurihara T, Yoshimura T, Esaki N. Gene cloning, purification, and characterization of two cyanobacterial NifS homologs driving iron-sulfur cluster formation. Biosci Biotechnol Biochem. 2000 Nov;64(11):2412–9.

258. Jaschkowitz K, Seidler A. Role of a NifS-like protein from the cyanobacterium Synechocystis PCC 6803 in the maturation of FeS proteins. Biochemistry. 2000;39(12):3416–23.

259. Kessler D. Slr0077 of Synechocystis has cysteine desulfurase as well as cystine lyase activity. Biochemical and Biophysical Research Communications. 2004;320(2):571–7.

260. Kessler D, Papenbrock J. Iron-sulfur cluster biosynthesis in photosynthetic organisms. Photosynth Res. 2005 Dec;86(3):391–407.

261. Fontecave M, Ollagnier-de-Choudens S. Iron-sulfur cluster biosynthesis in bacteria: Mechanisms of cluster assembly and transfer. Arch Biochem Biophys. 2008;474(2):226–37.

262. Wollenberg M, Berndt C, Bill E, Schwenn JD, Seidler A. A dimer of the FeS cluster biosynthesis protein IscA from cyanobacteria binds a [2Fe2S] cluster between two protomers and transfers it to [2Fe2S] and [4Fe4S] apo proteins. European Journal of Biochemistry. 2003;270(8):1662–71.

263. Kappock TJ, Ealick SE, Stubbe J. Modular evolution of the purine biosynthetic pathway. Curr Opin Chem Biol. 2000 Oct;4(5):567–72.

264. Zhang Y, Morar M, Ealick SE. Structural biology of the purine biosynthetic pathway. Cell Mol Life Sci. 2008 Nov;65(23):3699–724.

265. Lascu I, Gonin P. The catalytic mechanism of nucleoside diphosphate kinases. J Bioenerg Biomembr. 2000 Jun;32(3):237–46.

266. Larsson KM, Jordan A, Eliasson R, Reichard P, Logan DT, Nordlund P. Structural mechanism of allosteric substrate specificity regulation in a ribonucleotide reductase. Nat Struct Mol Biol. 2004 Nov;11(11):1142–9.

267. Turnbough CL Jr, Switzer RL. Regulation of pyrimidine biosynthetic gene expression in bacteria: repression without repressors. Microbiol Mol Biol Rev. 2008 Jun;72(2):266–300, table of contents.

268. Kilstrup M, Hammer K, Ruhdal Jensen P, Martinussen J. Nucleotide metabolism and its control in lactic acid bacteria. FEMS Microbiol Rev. 2005 Aug;29(3):555–90.

269. Waldrop GL, Holden HM, St Maurice M. The enzymes of biotin dependent CO2 metabolism: What structures reveal about their reaction mechanisms. Protein Sci. 2012 Nov;21(11):1597–619.

270. Lin S, Cronan JE. Closing in on complete pathways of biotin biosynthesis. Molecular bioSystems. 2011;7(6):1811–21.

271. Rodionov DA, Mironov AA, Gelfand MS. Conservation of the biotin regulon and the BirA regulatory signal in Eubacteria and Archaea. Genome Res. 2002 Oct;12(10):1507–16.

272. Sakaki K, Ohishi K, Shimizu T, Kobayashi I, Mori N, Matsuda K, et al. A suicide enzyme catalyzes multiple reactions for biotin biosynthesis in cyanobacteria. Nat Chem Biol [Internet]. 2020 Feb 10;

273. Stancek M, Schnell R, Ryden-Aulin M. Analysis of Escherichia coli nicotinate mononucleotide adenylyltransferase mutants in vivo and in vitro. BMC Biochem. 2005 Sep 9;6:16.

274. Gerdes SY, Kurnasov OV, Shatalin K, Polanuyer B, Sloutsky R, Vonstein V, et al. Comparative genomics of NAD biosynthesis in cyanobacteria. Journal of Bacteriology. 2006;188(8):3012–23.

275. Raffaelli N, Lorenzi T, Amici A, Emanuelli M, Ruggieri S, Magni G. Synechocystis sp. slr0787 protein is a novel bifunctional enzyme endowed with both nicotinamide mononucleotide adenylyltransferase and “Nudix” hydrolase activities. Febs Letters. 1999;444(2–3):222–6.

276. Ishikawa Y, Kawai-Yamada M. Physiological Significance of NAD Kinases in Cyanobacteria. Front Plant Sci [Internet]. 2019 Jun 27;10.

277. Kämäräinen J, Huokko T, Kreula S, Jones PR, Aro EM, Kallio P. Pyridine nucleotide transhydrogenase PntAB is essential for optimal growth and photosynthetic integrity under low-light mixotrophic conditions in Synechocystis sp. PCC 6803. New Phytologist. 2017;214(1):194–204.

278. de Crecy-Lagard V, El Yacoubi B, de la Garza RD, Noiriel A, Hanson AD. Comparative genomics of bacterial and plant folate synthesis and salvage: predictions and validations. Bmc Genomics [Internet]. 2007 Jul 23;8.

279. Hanson AD, Pribat A, Waller JC, de Crecy-Lagard V. “Unknown” proteins and “orphan” enzymes: the missing half of the engineering parts list--and how to find it. Biochem J. 2009 Dec 14;425(1):1–11.

280. Rubio LM, Flores E, Herrero A. Molybdopterin guanine dinucleotide cofactor in Synechococcus sp. nitrate reductase: identification of mobA and isolation of a putative moeB gene. FEBS Lett. 1999;462(3):358–62.

281. Rubio LM, Flores E, Herrero A. The narA locus of Synechococcus sp. strain PCC 7942 consists of a cluster of molybdopterin biosynthesis genes. J Bacteriol. 1998 Mar;180(5):1200–6.

282. Wuebbens MM, Rajagopalan KV. Mechanistic and mutational studies of Escherichia coli molybdopterin synthase clarify the final step of molybdopterin biosynthesis. J Biol Chem. 2003 Apr 18;278(16):14523–32.

283. Du QL, Wang HH, Xie JP. Thiamin (Vitamin B1) Biosynthesis and Regulation: A Rich Source of Antimicrobial Drug Targets? Int J Biol Sci. 2011;7(1):41–52.

284. Rodionov DA, Vitreschak AG, Mironov AA, Gelfand MS. Comparative genomics of thiamin biosynthesis in procaryotes. New genes and regulatory mechanisms. J Biol Chem. 2002 Dec 13;277(50):48949–59.

285. Leonardi R, Jackowski S. Biosynthesis of Pantothenic Acid and Coenzyme A. EcoSal Plus [Internet]. 2007 Apr;2(2).

286. Brand LA, Strauss E. Characterization of a new pantothenate kinase isoform from Helicobacter pylori. J Biol Chem. 2005 May 27;280(21):20185–8.

287. Richts B, Rosenberg J, Commichau FM. A Survey of Pyridoxal 5'-Phosphate-Dependent Proteins in the Gram-Positive Model Bacterium Bacillus subtilis. Front Mol Biosci. 2019;6:32.

288. Laber B, Maurer W, Scharf S, Stepusin K, Schmidt FS. Vitamin B6 biosynthesis: formation of pyridoxine 5'-phosphate from 4-(phosphohydroxy)-L-threonine and 1-deoxy-D-xylulose-5-phosphate by PdxA and PdxJ protein. FEBS Lett. 1999 Apr 16;449(1):45–8.

289. Sheng J, Vannela R, Rittrnann BE. Evaluation of methods to extract and quantify lipids from Synechocystis PCC 6803. Bioresource Technology. 2011;102(2):1697–703.

290. Lea-Smith DJ, Ortiz-Suarez ML, Lenn T, Nurnberg DJ, Baers LL, Davey MP, et al. Hydrocarbons are essential for optimal cell size, division and growth of cyanobacteria. Plant Physiology. 2016;172(3):1928–40.

291. Tasaka Y, Gombos Z, Nishiyama Y, Mohanty P, Ohba T, Ohki K, et al. Targeted mutagenesis of acyl-lipid desaturases in Synechocystis: evidence for the important roles of polyunsaturated membrane lipids in growth, respiration and photosynthesis. EMBO J. 1996 Dec 2;15(23):6416–25.

292. von Berlepsch S, Kunz HH, Brodesser S, Fink P, Marin K, Flügge U ingo, et al. The acyl-acyl carrier protein synthetase from Synechocystis sp. PCC 6803 mediates fatty acid import. Plant physiology. 2012;159(2):606–17.

293. Kaczmarzyk D, Fulda M. Fatty Acid Activation in Cyanobacteria Mediated by Acyl-Acyl Carrier Protein Synthetase Enables Fatty Acid Recycling. Plant Physiology. 2010;152(3):1598–610.

294. Mendez-Perez D, Begemann MB, Pfleger BF. Modular synthase-encoding gene involved in α-olefin biosynthesis in Synechococcus sp. strain PCC 7002. Applied and environmental microbiology. 2011;77(12):4264–7.

295. Schirmer A, Rude MA, Li X, Popova E, del Cardayre SB. Microbial biosynthesis of alkanes. Science. 2010;329(5991):559–62.

296. Rajakovich LJ, Norgaard H, Warui DM, Chang WC, Li N, Booker SJ, et al. Rapid Reduction of the Diferric-Peroxyhemiacetal Intermediate in Aldehyde-Deformylating Oxygenase by a Cyanobacterial Ferredoxin: Evidence for a Free-Radical Mechanism. J Am Chem Soc. 2015 Sep 16;137(36):11695–709.

297. Lea-Smith DJ, Biller SJ, Davey MP, Cotton CAR, Perez Sepulveda BM, Turchyn AV, et al. Contribution of cyanobacterial alkane production to the ocean hydrocarbon cycle. Proceedings of the National Academy of Sciences of the United States of America. 2015;112(44):13591–6.

298. Weier D, Muller C, Gaspers C, Frentzen M. Characterisation of acyltransferases from Synechocystis sp PCC6803. Biochemical and Biophysical Research Communications. 2005;334(4):1127–34.

299. Hagio M, Gombos Z, Varkonyi Z, Masamoto K, Sato N, Tsuzuki M, et al. Direct evidence for requirement of phosphatidylglycerol in photosystem II of photosynthesis. Plant Physiology. 2000;124(2):795–804.

300. Awai K, Kakimoto T, Awai C, Kaneko T, Nakamura Y, Takamiya K, et al. Comparative genomic analysis revealed a gene for monoglucosyldiacylglycerol synthase, an enzyme for photosynthetic membrane lipid synthesis in cyanobacteria. Plant Physiol. 2006;141(3):1120–7.

301. Awai K, Watanabe H, Benning C, Nishida I. Digalactosyldiacylglycerol is required for better photosynthetic growth of Synechocystis sp PCC6803 under phosphate limitation. Plant and Cell Physiology. 2007;48(11):1517–23.

302. Guler S, Seeliger A, Hartel H, Renger G, Benning C. A null mutant of Synechococcus sp. PCC7942 deficient in the sulfolipid sulfoquinovosyl diacylglycerol. J Biol Chem. 1996 Mar 29;271(13):7501–7.

303. Aoki M, Sato N, Meguro A, Tsuzuki M. Differing involvement of sulfoquinovosyl diacylglycerol in photosystem II in two species of unicellular cyanobacteria. Eur J Biochem. 2004 Feb;271(4):685–93.

304. Guler S, Essigmann B, Benning C. A cyanobacterial gene, sqdX, required for biosynthesis of the sulfolipid sulfoquinovosyldiacylglycerol. J Bacteriol. 2000;182(2):543–5.

305. Beld J, Abbriano R, Finzel K, Hildebrand M, Burkart MD. Probing fatty acid metabolism in bacteria, cyanobacteria, green microalgae and diatoms with natural and unnatural fatty acids. Mol Biosyst. 2016 Apr;12(4):1299–312.

306. Cronan JE. Assembly of Lipoic Acid on Its Cognate Enzymes: an Extraordinary and Essential Biosynthetic Pathway. Microbiol Mol Biol R. 2016 Jun;80(2):429–50.

307. Cronan JE, Zhao X, Jiang Y. Function, attachment and synthesis of lipoic acid in Escherichia coli. Adv Microb Physiol. 2005;50:103–46.

308. Liberton M, Saha R, Jacobs JM, Nguyen AY, Gritsenko MA, Smith RD, et al. Global proteomic analysis reveals an exclusive role of thylakoid membranes in bioenergetics of a model cyanobacterium. Molecular & Cellular Proteomics. 2016;15(6):2021–32.

309. Sham LT, Butler EK, Lebar MD, Kahne D, Bernhardt TG, Ruiz N. MurJ is the flippase of lipid-linked precursors for peptidoglycan biogenesis. Science. 2014 Jul 11;345(6193):220–2.

310. Taguchi A, Welsh MA, Marmont LS, Lee W, Sjodt M, Kruse AC, et al. FtsW is a peptidoglycan polymerase that is functional only in complex with its cognate penicillin-binding protein. Nat Microbiol. 2019 Apr;4(4):587–94.

311. Marbouty M, Mazouni K, Saguez C, Cassier-Chauvat C, Chauvat F. Characterization of the Synechocystis strain PCC 6803 penicillin-binding proteins and cytokinetic proteins FtsQ and FtsW and their network of interactions with ZipN. J Bacteriol. 2009;191(16):5123–33.

312. Reith J, Mayer C. Peptidoglycan turnover and recycling in Gram-positive bacteria. Appl Microbiol Biotechnol. 2011 Oct;92(1):1–11.

313. Ruiz N, Kahne D, Silhavy TJ. Transport of lipopolysaccharide across the cell envelope: the long road of discovery. Nat Rev Microbiol. 2009 Sep;7(9):677–83.

314. Kalynych S, Morona R, Cygler M. Progress in understanding the assembly process of bacterial O-antigen. FEMS Microbiol Rev. 2014 Sep;38(5):1048–65.

315. Englund E, Shabestary K, Hudson EP, Lindberg P. Systematic overexpression study to find target enzymes enhancing production of terpenes in Synechocystis PCC 6803, using isoprene as a model compound. Metab Eng. 2018 Sep;49:164–77.

316. Barkley SJ, Desai SB, Poulter CD. Type II isopentenyl diphosphate isomerase from Synechocystis sp strain PCC 6803. Journal of Bacteriology. 2004;186(23):8156–8.

317. Poliquin K, Ershov YV, Cunningham FX, Woreta TT, Gantt RR, Gantt E. Inactivation of sll1556 in Synechocystis strain PCC 6803 impairs isoprenoid biosynthesis from pentose phosphate cycle substrates in vitro. Journal of Bacteriology. 2004;186(14):4685–93.

318. Englund E, Pattanaik B, Ubhayasekera SJ, Stensjo K, Bergquist J, Lindberg P. Production of squalene in Synechocystis sp. PCC 6803. PLoS One. 2014;9(3):e90270–e90270.

319. Welander PV, Hunter RC, Zhang L, Sessions AL, Summons RE, Newman DK. Hopanoids play a role in membrane integrity and pH homeostasis in Rhodopseudomonas palustris TIE-1. J Bacteriol. 2009 Oct;191(19):6145–56.

320. Jurgens UJ, Simonin P, Rohmer M. Localization and distribution of hopanoids in membrane systems of the cyanobacterium Synechocystis PCC 6714. FEMS Microbiol Lett. 1992 May 1;71(3):285–8.

321. Toth TN, Chukhutsina V, Domonkos I, Knoppova J, Komenda J, Kis M, et al. Carotenoids are essential for the assembly of cyanobacterial photosynthetic complexes. Biochim Biophys Acta. 2015 Oct;1847(10):1153–65.

322. Mohamed HE, Vermaas W, Myxoxanthophyll R. Slr1293 in Synechocystis sp. strain PCC 6803 Is the C-3',4' desaturase (CrtD) involved in myxoxanthophyll biosynthesis. J Bacteriol. 2004;186(17):5621–8.

323. Graham JE, Bryant DA. The Biosynthetic Pathway for Synechoxanthin, an Aromatic Carotenoid Synthesized by the Euryhaline, Unicellular Cyanobacterium Synechococcus sp Strain PCC 7002. Journal of Bacteriology. 2008;190(24):7966–74.

324. Maresca JA, Graham JE, Wu M, Eisen J a, Bryant D a. Identification of a fourth family of lycopene cyclases in photosynthetic bacteria. Proceedings of the National Academy of Sciences of the United States of America. 2007;104(28):11784–9.

325. Graham JE, Bryant DA. The biosynthetic pathway for myxol-2' fucoside (myxoxanthophyll) in the cyanobacterium Synechococcus sp. strain PCC 7002. J Bacteriol. 2009;191(10):3292–300.

326. Masamoto K, Wada H, Kaneko T, Takaichi S. Identification of a gene required for cis-to-trans carotene isomerization in carotenogenesis of the cyanobacterium Synechocystis sp. PCC 6803. Plant Cell Physiol. 2001;42(12):1398–402.

327. Proctor MS, Morey-Burrows FS, Canniffe DP, Martin EC, Swainsbury DJK, Johnson MP, et al. Zeta-Carotene Isomerase (Z-ISO) Is Required for Light-Independent Carotenoid Biosynthesis in the Cyanobacterium Synechocystis sp. PCC 6803. Microorganisms. 2022 Sep;10(9):1730.

328. Maeda H, Sakuragi Y, Bryant DA, DellaPenna D. Tocopherols protect Synechocystis sp strain PCC 6803 from lipid peroxidation. Plant Physiology. 2005;138(3):1422–35.

329. Yang Y, Yin CT, Li WZ, Xu XD. alpha-tocopherol is essential for acquired chill-light tolerance in the cyanobacterium Synechocystis sp strain PCC 6803. Journal of Bacteriology. 2008;190(5):1554–60.

330. Sakuragi Y, Maeda H, DellaPenna D, Bryant DA. alpha-tocopherol plays a role in photosynthesis and macronutrient homeostasis of the cyanobacterium Synechocystis sp PCC 6803 that is independent of its antioxidant function. Plant Physiology. 2006;141(2):508–21.

331. Collakova E, DellaPenna D. Isolation and functional analysis of homogentisate phytyltransferase from Synechocystis sp PCC 6803 and arabidopsis. Plant Physiology. 2001;127(3):1113–24.

332. Savidge B, Weiss JD, Wong YHH, Lassner MW, Mitsky TA, Shewmaker CK, et al. Isolation and characterization of homogentisate phytyltransferase genes from Synechocystis sp PCC 6803 and Arabidopsis. Plant Physiology. 2002;129(1):321–32.

333. Schledz M, Seidler A, Beyer P, Neuhaus G. A novel phytyltransferase from Synechocystis sp PCC 6803 involved in tocopherol biosynthesis. Febs Letters. 2001;499(1–2):15–20.

334. Shpilyov AV, Zinchenko VV, Shestakov SV, Grimm B, Lokstein H. Inactivation of the geranylgeranyl reductase (ChlP) gene in the cyanobacterium Synechocystis sp. PCC 6803. Biochim Biophys Acta. 2005;1706(3):195–203.

335. Dahnhardt D, Falk J, Appel J, van der Kooij TA, Schulz-Friedrich R, Krupinska K. The hydroxyphenylpyruvate dioxygenase from Synechocystis sp. PCC 6803 is not required for plastoquinone biosynthesis. FEBS Lett. 2002;523(1–3):177–81.

336. Bonner CA, Jensen RA, Gander JE, Keyhani NO. A core catalytic domain of the TyrA protein family: arogenate dehydrogenase from Synechocystis. Biochemical Journal. 2004;382:279–91.

337. Saw JHW, Schatz M, Brown MV, Kunkel DD, Foster JS, Shick H, et al. Cultivation and Complete Genome Sequencing of Gloeobacter kilaueensis sp. nov., from a Lava Cave in Kīlauea Caldera, Hawai'i. PLoS ONE. 2013;8(10):e76376–e76376.

338. Shintani DK, Cheng ZG, DellaPenna D. The role of 2-methyl-6-phytylbenzoquinone methyltransferase in determining tocopherol composition in Synechocystis sp. PCC6803. FEBS Lett. 2002;511(1–3):1–5.

339. Kozuleva MA, Petrova AA, Mamedov MD, Semenov AY, Ivanov BN. O2 reduction by photosystem I involves phylloquinone under steady-state illumination. FEBS Lett. 2014 Nov 28;588(23):4364–8.

340. Johnson TW, Shen GZ, Zybailov B, Kolling D, Reategui R, Beauparlant S, et al. Recruitment of a foreign quinone into the A(1) site of photosystem I - I. Genetic and physiological characterization of phylloquinone biosynthetic pathway mutants in Synechocystis sp PCC 6803. Journal of Biological Chemistry. 2000;275(12):8523–30.

341. Johnson TW, Naithani S, Stewart C, Zybailov B, Jones AD, Golbeck JH, et al. The menD and menE homologs code for 2-succinyl-6-hydroxyl-2, 4-cyclohexadiene-1-carboxylate synthase and O-succinylbenzoic acid-CoA synthase in the phylloquinone biosynthetic pathway of Synechocystis sp PCC 6803. Biochimica Et Biophysica Acta-Bioenergetics. 2003;1557(1–3):67–76.

342. Emonds-Alt B, Coosemans N, Gerards T, Remacle C, Cardol P. Isolation and characterization of mutants corresponding to the MENA, MENB, MENC and MENE enzymatic steps of 5'-monohydroxyphylloquinone biosynthesis in Chlamydomonas reinhardtii. Plant J. 2017 Jan;89(1):141–54.

343. Fatihi A, Latimer S, Schmollinger S, Block A, Dussault PH, Vermaas WF, et al. A dedicated Type II NADPH Dehydrogenase performs the penultimate step in the biosynthesis of Vitamin K1 in Synechocystis and Arabidopsis. Plant Cell [Internet]. 2015;

344. Pfaff C, Glindemann N, Gruber J, Frentzen M, Sadre R. Chorismate pyruvate-lyase and 4-hydroxy-3-solanesylbenzoate decarboxylase are required for plastoquinone biosynthesis in the cyanobacterium Synechocystis sp. PCC6803. J Biol Chem. 2014;289(5):2675–86.

345. Sadre R, Pfaff C, Buchkremer S. Plastoquinone-9 biosynthesis in cyanobacteria differs from that in plants and involves a novel 4-hydroxybenzoate solanesyltransferase. Biochem J. 2012;442(3):621–9.

346. Anzaldi LL, Skaar EP. Overcoming the heme paradox: heme toxicity and tolerance in bacterial pathogens. Infect Immun. 2010 Dec;78(12):4977–89.

347. Skotnicova P, Sobotka R, Shepherd M, Hajek J, Hrouzek P, Tichy M. The cyanobacterial protoporphyrinogen oxidase HemJ is a new b-type heme protein functionally coupled with coproporphyrinogen III oxidase. J Biol Chem. 2018 Aug 10;293(32):12394–404.

348. Brzezowski P, Ksas B, Havaux M, Grimm B, Chazaux M, Peltier G, et al. The function of PROTOPORPHYRINOGEN IX OXIDASE in chlorophyll biosynthesis requires oxidised plastoquinone in Chlamydomonas reinhardtii. Commun Biol [Internet]. 2019 May 3;2.

349. Kato K, Tanaka R, Sano S, Tanaka A, Hosaka H. Identification of a gene essential for protoporphyrinogen IX oxidase activity in the cyanobacterium Synechocystis sp. PCC6803. Proceedings of the National Academy of Sciences of the United States of America. 2010;107(38):16649–54.

350. Goto T, Aoki R, Minamizaki K, Fujita Y. Functional differentiation of two analogous coproporphyrinogen III oxidases for heme and chlorophyll biosynthesis pathways in the cyanobacterium Synechocystis sp. PCC 6803. Plant Cell Physiol. 2010;51(4):650–63.

351. Yilmaz M, Kang I, Beale SI. Heme oxygenase 2 of the cyanobacterium Synechocystis sp PCC 6803 is induced under a microaerobic atmosphere and is required for microaerobic growth at high light intensity. Photosynthesis Research. 2010;103(1):47–59.

352. Aoki R, Goto T, Fujita Y. A Heme Oxygenase Isoform is Essential for Aerobic Growth in the Cyanobacterium Synechocystis sp PCC 6803: Modes of Differential Operation of Two Isoforms/Enzymes to Adapt to Low Oxygen Environments in Cyanobacteria. Plant and Cell Physiology. 2011;52(10):1744–56.

353. Peter E, Salinas A, Wallner T, Jeske D, Dienst D, Wilde A, et al. Differential requirement of two homologous proteins encoded by sll1214 and sll1874 for the reaction of Mg protoporphyrin monomethylester oxidative cyclase under aerobic and micro-oxic growth conditions. Biochim Biophys Acta. 2009;1787(12):1458–67.

354. Frankenberg N, Mukougawa K, Kohchi T, Lagarias JC. Functional genomic analysis of the HY2 family of ferredoxin-dependent bilin reductases from oxygenic photosynthetic organisms. Plant Cell. 2001;13(4):965–78.

355. Schluchter WM, Glazer AN. Characterization of cyanobacterial biliverdin reductase. Conversion of biliverdin to bilirubin is important for normal phycobiliprotein biosynthesis. J Biol Chem. 1997 May 23;272(21):13562–9.

356. Jensen PE, Gibson LCD, Henningsen KW, Hunter CN. Expression of the chlI, chlD, and chlH genes from the cyanobacterium Synechocystis PCC6803 in Escherichia coli and demonstration that the three cognate proteins are required for magnesium-protoporphyrin chelatase activity. J Biol Chem. 1996 Jul 12;271(28):16662–7.

357. Wilde A, Mikolajczyk S, Alawady A, Lokstein H, Grimm B. The gun4 gene is essential for cyanobacterial porphyrin metabolism. Febs Letters. 2004;571(1–3):119–23.

358. Davison PA, Schubert HL, Reid JD, Iorg CD, Heroux A, Hill CP, et al. Structural and biochemical characterization of Gun4 suggests a mechanism for its role in chlorophyll biosynthesis. Biochemistry. 2005;44(21):7603–12.

359. Sobotka R, Duhring U, Komenda J, Peter E, Gardian Z, Tichy M, et al. Importance of the cyanobacterial Gun4 protein for chlorophyll metabolism and assembly of photosynthetic complexes. J Biol Chem. 2008;283(38):25794–802.

360. Smith CA, Suzuki JY, Bauer CE. Cloning and characterization of the chlorophyll biosynthesis gene chlM from Synechocystis PCC 6803 by complementation of a bacteriochlorophyll biosynthesis mutant of Rhodobacter capsulatus. Plant Mol Biol. 1996 Mar;30(6):1307–14.

361. Minamizaki K, Mizoguchi T, Goto T, Tamiaki H, Fujita Y. Identification of two homologous genes, chlAI and chlAII, that are differentially involved in isocyclic ring formation of chlorophyll a in the cyanobacterium Synechocystis sp. PCC 6803. J Biol Chem. 2008;283(5):2684–92.

362. Chen GE, Canniffe DP, Hunter CN. Three classes of oxygen-dependent cyclase involved in chlorophyll and bacteriochlorophyll biosynthesis. P Natl Acad Sci USA. 2017 Jun 13;114(24):6280–5.

363. Reinbothe C, El Bakkouri M, Buhr F, Muraki N, Nomata J, Kurisu G, et al. Chlorophyll biosynthesis: spotlight on protochlorophyllide reduction. Trends in Plant Science. 2010;15(11):614–24.

364. Islam MR, Aikawa S, Midorikawa T, Kashino Y, Satoh K, Koike H. slr1923 of Synechocystis sp PCC6803 is essential for conversion of 3,8-divinyl(proto)chlorophyll(ide) to 3-monovinyl(proto)chlorophyll(ide). Plant Physiology. 2008;148(2):1068–81.

365. Ito H, Yokono M, Tanaka R, Tanaka A. Identification of a novel vinyl reductase gene essential for the biosynthesis of monovinyl chlorophyll in Synechocystis sp PCC6803. Journal of Biological Chemistry. 2008;283(14):9002–11.

366. Chen GE, Canniffe DP, Barnett SFH, Hollingshead S, Brindley AA, Vasilev C, et al. Complete enzyme set for chlorophyll biosynthesis in Escherichia coli. Sci Adv. 2018 Jan;4(1):eaaq1407.

367. Romine MF, Rodionov DA, Maezato Y, Anderson LN, Nandhikonda P, Rodionova IA, et al. Elucidation of roles for vitamin B12 in regulation of folate, ubiquinone, and methionine metabolism. Proc Natl Acad Sci U S A. 2017 Feb 14;114(7):E1205–14.

368. Helliwell KE, Lawrence AD, Holzer A, Kudahl UJ, Sasso S, Krautler B, et al. Cyanobacteria and Eukaryotic Algae Use Different Chemical Variants of Vitamin B12. Curr Biol. 2016 Apr 25;26(8):999–1008.

369. Fang H, Kang J, Zhang D. Microbial production of vitamin B12: a review and future perspectives. Microb Cell Fact. 2017 Jan 30;16(1):15.

370. Moore SJ, Lawrence AD, Biedendieck R, Deery E, Frank S, Howard MJ, et al. Elucidation of the anaerobic pathway for the corrin component of cobalamin (vitamin B12). Proc Natl Acad Sci U S A. 2013 Sep 10;110(37):14906–11.

371. Flores E, Frias JE, Rubio LM, Herrero A. Photosynthetic nitrate assimilation in cyanobacteria. Photosynthesis Research. 2005;83(2):117–33.

372. Montesinos ML, Muro-Pastor AM, Herrero A, Flores E. Ammonium/Methylammonium permeases of a cyanobacterium - Identification and analysis of three nitrogen-regulated amt genes in Synechocystis sp. PCC 6803. Journal of Biological Chemistry. 1998;273(47):31463–70.

373. Omata T, Andriesse X, Hirano A. Identification and characterization of a gene cluster involved in nitrate transport in the cyanobacterium Synechococcus sp. PCC7942. Mol Gen Genet. 1993 Jan;236(2–3):193–202.

374. Maeda S, Omata T. Substrate-binding lipoprotein of the cyanobacterium Synechococcus sp. strain PCC 7942 involved in the transport of nitrate and nitrite. J Biol Chem. 1997 Jan 31;272(5):3036–41.

375. Luque I, Flores E, Herrero A. Nitrate and nitrite transport in the cyanobacterium Synechococcus sp. PCC 7942 are mediated by the same permease. Biochemica et Biophysica Acta- Bioenergetics. 1994;1184(2–3):296–8.

376. Rubio LM, Herrero A, Flores E. A cyanobacterial narB gene encodes a ferredoxin-dependent nitrate reductase. Plant Mol Biol. 1996 Feb;30(4):845–50.

377. Suzuki I, Sugiyama T, Omata T. Primary Structure and Transcriptional Regulation of the Gene for Nitrite Reductase from the Cyanobacterium Synechococcus PCC 7942. Plant and Cell Physiology. 1993;34(8):1311–20.

378. Valladares A, Montesinos ML, Herrero A, Flores E. An ABC-type, high-affinity urea permease identified in cyanobacteria. Molecular Microbiology. 2002;43(3):703–15.

379. Veaudor T, Cassier-Chauvat C, Chauvat F. Genomics of Urea Transport and Catabolism in Cyanobacteria: Biotechnological Implications. Front Microbiol. 2019;10:2052.

380. Quintero MJ, Montesinos ML, Herrero A, Flores E. Identification of genes encoding amino acid permeases by inactivation of selected ORFs from the Synechocystis genomic sequence. Genome Res. 2001;11(12):2034–40.

381. Suginaka K, Yamamoto K, Ashiida H, Kono Y, Saw Y, Shibata H. Cysteine Uptake for Accumulation of Glutathione by the Cyanobacterium Synechocystis strain PCC 6803. Biosci Biotechnol Biochem. 1998;62(3):424–8.

382. Tottey S, Rich PR, Rondet SAM, Robinson NJ. Two Menkes-type ATPases supply copper for photosynthesis in Synechocystis PCC 6803. Journal of Biological Chemistry. 2001;276(23):19999–20004.

383. Badarau A, Dennison C. Thermodynamics of copper and zinc distribution in the cyanobacterium Synechocystis PCC 6803. Proceedings of the National Academy of Sciences of the United States of America. 2011;108(32):13007–12.

384. Tottey S, Patterson CJ, Banci L, Bertini I, Felli IC, Pavelkova A, et al. Cyanobacterial metallochaperone inhibits deleterious side reactions of copper. Proceedings of the National Academy of Sciences of the United States of America. 2012;109(1):95–100.

385. Giner-Lamia J, Lopez-Maury L, Reyes JC, Florencio FJ, López-Maury L, Reyes JC, et al. The CopRS Two-Component System Is Responsible for Resistance to Copper in the Cyanobacterium Synechocystis sp PCC 6803. Plant Physiology. 2012;159(4):1806–18.

386. Giner-Lamia J, Lopez-Maury L, Florencio FJ. CopM is a novel copper-binding protein involved in copper resistance in Synechocystis sp PCC 6803. Microbiologyopen. 2015;4(1):167–85.

387. Matsuda N, Uozumi N. Ktr-mediated potassium transport, a major pathway for potassium uptake, is coupled to a proton gradient across the membrane in Synechocystis sp. PCC 6803. Biosci Biotechnol Biochem. 2006;70(1):273–5.

388. Nanatani K, Shijuku T, Takano Y, Zulkifli L, Yamazaki T, Tominaga A, et al. Comparative analysis of kdp and ktr mutants reveals distinct roles of the potassium transporters in the model cyanobacterium Synechocystis sp. strain PCC 6803. J Bacteriol. 2015 Feb 15;197(4):676–87.

389. Matsuda N, Kobayashi H, Katoh H, Ogawa T, Futatsugi L, Nakamura T, et al. Na+-dependent K+ uptake Ktr system from the cyanobacterium Synechocystis sp. PCC 6803 and its role in the early phases of cell adaptation to hyperosmotic shock. Journal of Biological Chemistry. 2004;279(52):54952–62.

390. Zanetti M, Teardo E, La Rocca N, Zulkifli L, Checchetto V, Shijuku T, et al. A Novel Potassium Channel in Photosynthetic Cyanobacteria. PLoS One. 2010;5(4).

391. Checchetto V, Segalla A, Allorent G, La Rocca N, Leanza L, Giacometti GM, et al. Thylakoid potassium channel is required for efficient photosynthesis in cyanobacteria. Proceedings of the National Academy of Sciences of the United States of America. 2012;109(27):11043–8.

392. Checchetto V, Formentin E, Carraretto L, Segalla A, Giacometti GM, Szabo I, et al. Functional characterization and determination of the physiological role of a calcium-dependent potassium channel from cyanobacteria. Plant Physiol. 2013;162(2):953–64.

393. Waditee R, Hossain GS, Tanaka Y, Nakamura T, Shikata M, Takano J, et al. Isolation and functional characterization of Ca2+/H+ antiporters from cyanobacteria. The Journal of biological chemistry. 2004;279(6):4330–8.

394. Jiang HB, Cheng HM, Gao KS, Qiu BS. Inactivation of Ca(2+)/H(+) exchanger in Synechocystis sp. strain PCC 6803 promotes cyanobacterial calcification by upregulating CO(2)-concentrating mechanisms. Appl Environ Microbiol. 2013;79(13):4048–55.

395. Nazarenko LV, Andreev IM, Lyukevich AA, Pisareva TV, Los DA. Calcium release from Synechocystis cells induced by depolarization of the plasma membrane: MscL as an outward Ca2+ channel. Microbiology-Sgm. 2003;149:1147–53.

396. Kranzler C, Lis H, Finkel OM, Schmetterer G, Shaked Y, Keren N. Coordinated transporter activity shapes high-affinity iron acquisition in cyanobacteria. Isme Journal. 2014;8(2):409–17.

397. Katoh H, Hagino N, Ogawa T. Iron-binding activity of FutA1 subunit of an ABC-type iron transporter in the cyanobacterium Synechocystis sp strain PCC 6803. Plant and Cell Physiology. 2001;42(8):823–7.

398. Badarau A, Firbank SJ, Waldron KJ, Yanagisawa S, Robinson NJ, Banfield MJ, et al. FutA2 is a ferric binding protein from Synechocystis PCC 6803. Journal of Biological Chemistry. 2008;283(18):12520–7.

399. Katoh H, Grossman AR, Hagino N, Ogawa T. A gene of Synechocystis sp strain PCC 6803 encoding a novel iron transporter. Journal of Bacteriology. 2000;182(22):6523–4.

400. Katoh H, Hagino N, Grossman AR, Ogawa T. Genes essential to iron transport in the cyanobacterium Synechocystis sp. strain PCC 6803. J Bacteriol. 2001;183(9):2779–84.

401. Jiang HB, Lou WJ, Ke WT, Song WY, Price NM, Qiu BS. New insights into iron acquisition by cyanobacteria: an essential role for ExbB-ExbD complex in inorganic iron uptake. ISME J [Internet]. 2014;

402. Keren N, Aurora R, Pakrasi HB. Critical roles of bacterioferritins in iron storage and proliferation of cyanobacteria. Plant Physiology. 2004;135(3):1666–73.

403. Bartsevich VV, Pakrasi HB. Manganese transport in the cyanobacterium Synechocystis sp. PCC 6803. J Biol Chem. 1996;271(42):26057–61.

404. Brandenburg F, Schoffman H, Kurz S, Kramer U, Keren N, Weber AP, et al. The Synechocystis Manganese Exporter Mnx Is Essential for Manganese Homeostasis in Cyanobacteria. Plant Physiol. 2017;173(3):1798–810.

405. Aguilar-Barajas E, Diaz-Perez C, Ramirez-Diaz MI, Riveros-Rosas H, Cervantes C. Bacterial transport of sulfate, molybdate, and related oxyanions. Biometals. 2011;24(4):687–707.

406. Banerjee S, Wei BX, Bhattacharyya-Pakrasi M, Pakrasi HB, Smith TJ. Structural determinants of metal specificity in the zinc transport protein ZnuA from Synechocystis 6803. Journal of Molecular Biology. 2003;333(5):1061–9.

407. Borrelly GP, Rondet SA, Tottey S, Robinson NJ. Chimeras of P-type ATPases and their transcriptional regulators: contributions of a cytosolic amino-terminal domain to metal specificity. Mol Microbiol. 2004 Jul;53(1):217–27.

408. Dainty SJ, Patterson CJ, Waldron KJ, Robinson NJ. Interaction between cyanobacterial copper chaperone Atx1 and zinc homeostasis. Journal of Biological Inorganic Chemistry. 2010;15(1):77–85.

409. Pohland AC, Schneider D. Mg2+ homeostasis and transport in cyanobacteria - at the crossroads of bacterial and chloroplast Mg2+ import. Biol Chem. 2019 Sep 25;400(10):1289–301.

410. Peca L, Kos PB, Vass I. Characterization of the activity of heavy metal-responsive promoters in the cyanobacterium Synechocystis PCC 6803. Acta Biol Hung. 2007;58 Suppl:11–22.

411. Burut-Archanai S, Eaton-Rye JJ, Incharoensakdi A. Na+-stimulated phosphate uptake system in Synechocystis sp PCC 6803 with Pst1 as a main transporter. Bmc Microbiology. 2011;11.

412. Pitt FD, Mazard S, Humphreys L, Scanlan DJ. Functional Characterization of Synechocystis sp Strain PCC 6803 pst1 and pst2 Gene Clusters Reveals a Novel Strategy for Phosphate Uptake in a Freshwater Cyanobacterium. Journal of Bacteriology. 2010;192(13):3512–23.

413. Gomez-Garcia MR, Losada M, Serrano A. Concurrent transcriptional activation of ppa and ppx genes by phosphate deprivation in the cyanobacterium Synechocystis sp strain PCC 6803. Biochemical and Biophysical Research Communications. 2003;302(3):601–9.

414. Zhang HY, Ishige K, Kornberg A. A polyphosphate kinase (PPK2) widely conserved in bacteria. Proceedings of the National Academy of Sciences of the United States of America. 2002;99(26):16678–83.

415. Inaba M, Sakamoto A, Murata N. Functional expression in Escherichia coli of low-affinity and high-affinity Na(+)(Li(+))/H(+) antiporters of Synechocystis. J Bacteriol. 2001;183(4):1376–84.

416. Elanskaya IV, Karandashova IV, Bogachev AV, Hagemann M. Functional analysis of the Na+/H+ antiporter encoding genes of the cyanobacterium Synechocystis PCC 6803. Biochemistry (Mosc). 2002 Apr;67(4):432–40.

417. Tsunekawa K, Shijuku T, Hayashimoto M, Kojima Y, Onai K, Morishita M, et al. Identification and characterization of the Na+/H+ antiporter Nhas3 from the thylakoid membrane of Synechocystis sp. PCC 6803. J Biol Chem. 2009;284(24):16513–21.

418. Hagemann M, Richter S, Mikkat S. The ggtA gene encodes a subunit of the transport system for the osmoprotective compound glucosylglycerol in Synechocystis sp. strain PCC 6803. J Bacteriol. 1997 Feb;179(3):714–20.

419. Mikkat S, Hagemann M. Molecular analysis of the ggtBCD gene cluster of Synechocystis sp strain PCC6803 encoding subunits of an ABC transporter for osmoprotective compounds. Archives of Microbiology. 2000;174(4):273–82.

420. Omata T, Price GD, Badger MR, Okamura M, Gohta S, Ogawa T. Identification of an ATP-binding cassette transporter involved in bicarbonate uptake in the cyanobacterium Synechococcus sp strain PCC 7942. Proceedings of the National Academy of Sciences of the United States of America. 1999;96(23):13571–6.

421. Maeda S, Price GD, Badger MR, Enomoto C, Omata T. Bicarbonate binding activity of the CmpA protein of the cyanobacterium Synechococcus sp strain PCC 7942 involved in active transport of bicarbonate. Journal of Biological Chemistry. 2000;275(27):20551–5.

422. Du J, Forster B, Rourke L, Howitt SM, Price GD. Characterisation of cyanobacterial bicarbonate transporters in E. coli shows that SbtA homologs are functional in this heterologous expression system. PLoS One. 2014;9(12):e115905.

423. Shibata M, Katoh H, Sonoda M, Ohkawa H, Shimoyama M, Fukuzawa H, et al. Genes essential to sodium-dependent bicarbonate transport in cyanobacteria - Function and phylogenetic analysis. Journal of Biological Chemistry. 2002;277(21):18658–64.

424. Price GD, Woodger FJ, Badger MR, Howitt SM, Tucker L. Identification of a SulP-type bicarbonate transporter in marine cyanobacteria. Proceedings of the National Academy of Sciences of the United States of America. 2004;101(52):18228–33.

425. Akai M, Onai K, Morishita M, Mino H, Shijuku T, Maruyama H, et al. Aquaporin AqpZ Is Involved in Cell Volume Regulation and Sensitivity to Osmotic Stress in Synechocystis sp Strain PCC 6803. Journal of Bacteriology. 2012;194(24):6828–36.

426. Akai M, Onai K, Kusano M, Sato M, Redestig H, Toyooka K, et al. Plasma Membrane Aquaporin AqpZ Protein Is Essential for Glucose Metabolism during Photomixotrophic Growth of Synechocystis sp PCC 6803. Journal of Biological Chemistry. 2011;286(28):25224–35.

427. Pope MA, Hodge JA, Nixon PJ. An Improved Natural Transformation Protocol for the Cyanobacterium Synechocystis sp. PCC 6803. Frontiers in Plant Science [Internet]. 2020 [cited 2022 Oct 25];11.

428. Sezonov G, Joseleau-Petit D, D'Ari R. Escherichia coli physiology in Luria-Bertani broth. J Bacteriol. 2007 Dec;189(23):8746–9.

429. Snoep JL, Mrwebi M, Schuurmans JM, Rohwer JM, Teixeira de Mattos MJ. Control of specific growth rate in Saccharomyces cerevisiae. Microbiology (Reading). 2009 May;155(Pt 5):1699–707.

430. Cui J, Sun T, Li S, Xie Y, Song X, Wang F, et al. Improved Salt Tolerance and Metabolomics Analysis of Synechococcus elongatus UTEX 2973 by Overexpressing Mrp Antiporters. Frontiers in Bioengineering and Biotechnology [Internet]. 2020 [cited 2022 May 10];8.

431. Cui J, Sun T, Chen L, Zhang W. Salt-Tolerant Synechococcus elongatus UTEX 2973 Obtained via Engineering of Heterologous Synthesis of Compatible Solute Glucosylglycerol. Front Microbiol. 2021;12:650217.

432. Steuer R. Fast-growing phototrophic microorganisms and the productivity of phototrophic cultures. Biotechnology and Bioengineering [Internet]. [cited 2022 Jul 7];n/a(n/a).

433. Castenholz RW. Culturing methods for Cyanobacteria. Method Enzymol. 1988;167:68–93.

434. Algae UCC of. UTEX Culture Collection of Algae at UT-Austin [Internet]. UTEX Culture Collection of Algae. [cited 2022 May 25]. Available from: https://utex.org/

435. Beer. Bestimmung der Absorption des rothen Lichts in farbigen Flüssigkeiten. Annalen der Physik. 1852;162(5):78–88.

436. Ritchie RJ. Consistent Sets of Spectrophotometric Chlorophyll Equations for Acetone, Methanol and Ethanol Solvents. Photosynth Res. 2006 Jul 1;89(1):27–41.

437. Lea-Smith DJ, Ross N, Zori M, Bendall DS, Dennis JS, Scott S a, et al. Thylakoid terminal oxidases are essential for the cyanobacterium Synechocystis sp. PCC 6803 to survive rapidly changing light intensities. Plant physiology. 2013;162(1):484–95.

438. Synechococcus sp. PCC 11901 genome assembly ASM557713v1 [Internet]. NCBI. [cited 2023 May 14]. Available from: https://www.ncbi.nlm.nih.gov/data-hub/assembly/GCF_005577135.1/

439. Rai S, Lucius S, Kern R, Bauwe H, Kaplan A, Kopka J, et al. The Synechocystis sp. PCC 6803 Genome Encodes Up to Four 2-Phosphoglycolate Phosphatases. Front Plant Sci. 2018;9:1718.

440. Mills LA, McCormick AJ, Lea-Smith DJ. Current knowledge and recent advances in understanding metabolism of the model cyanobacterium Synechocystis sp. PCC 6803. Bioscience Reports. 2020 Apr 3;40(BSR20193325).

441. Lea-Smith D. J, Hanke GT. Manipulating electron transport for synthetic biology applications. In: Hudson P, editor. Cyanobacteria Biotechnology. Wiley-VCH; 2021. p. 33–63.

442. Nomura C, Bryant D. Cytochrome c6 from Synechococcus sp. PCC 7002. In: Peschek G, Loffelhardt W, Schmetterer G, editors. The Phototrophic Prokaryotes. New York, USA: Kluwer Academic/Plenum Publishers; 1997. p. 269–74.

443. Dann M, Leister D. Evidence that cyanobacterial Sll1217 functions analogously to PGRL1 in enhancing PGR5-dependent cyclic electron flow. Nat Commun [Internet]. 2019 Nov 22;10.

444. Schorsch M, Kramer M, Goss T, Eisenhut M, Robinson N, Osman D, et al. A unique ferredoxin acts as a player in the low-iron response of photosynthetic organisms. P Natl Acad Sci USA. 2018 Dec 18;115(51):E12111–20.

445. Battchikova N, Eisenhut M, Aro EMM. Cyanobacterial NDH-1 complexes: Novel insights and remaining puzzles. Biochimica Et Biophysica Acta-Bioenergetics. 2011;1807(8):935–44.

446. Xiong F, LoBrutto R, Vermaas W. The Synechocystis sp. PCC 6803 open reading frame slr0201 that is homologous to sdhC from Archaea codes for a [2Fe-2S] protein. bioRXiv. 2021;

447. Nomura CT, Persson S, Shen G, Inoue-Sakamoto K, Bryant DA. Characterization of two cytochrome oxidase operons in the marine cyanobacterium Synechococcus sp. PCC 7002: inactivation of ctaDI affects the PS I:PS II ratio. Photosynth Res. 2006;87(2):215–28.

448. Kirst H, Formighieri C, Melis A. Maximizing photosynthetic efficiency and culture productivity in cyanobacteria upon minimizing the phycobilisome light-harvesting antenna size. Biochimica Et Biophysica Acta-Bioenergetics. 2014;1837(10):1653–64.

449. Page LE, Liberton M, Pakrasi HB. Reduction of photoautotrophic productivity in the cyanobacterium Synechocystis sp. strain PCC 6803 by phycobilisome antenna truncation. Appl Environ Microbiol. 2012;78(17):6349–51.

450. Kwon JH, Bernat G, Wagner H, Rogner M, Rexroth S. Reduced light-harvesting antenna: Consequences on cyanobacterial metabolism and photosynthetic productivity. Algal Research-Biomass Biofuels and Bioproducts. 2013;2(3):188–95.

451. Collins AM, Liberton M, Jones HDT, Garcia OF, Pakrasi HB, Timlin JA. Photosynthetic pigment localization and thylakoid membrane morphology are altered in Synechocystis 6803 phycobilisome mutants. Plant Physiol. 2012;158(4):1600–9.

452. Liberton M, Collins AM, Page LE, O'Dell WB, O'Neill H, Urban VS, et al. Probing the consequences of antenna modification in cyanobacteria. Photosynthesis Research. 2013;118(1–2):17–24.

453. Liberton M, Chrisler WB, Nicora CD, Moore RJ, Smith RD, Koppenaal DW, et al. Phycobilisome truncation causes widespread proteome changes in Synechocystis sp PCC 6803. Plos One. 2017 Mar 2;12(3).

454. Sugita C, Ogata K, Shikata M, Jikuya H, Takano J, Furumichi M, et al. Complete nucleotide sequence of the freshwater unicellular cyanobacterium Synechococcus elongatus PCC 6301 chromosome: gene content and organization. Photosynth Res. 2007 Jul 1;93(1):55–67.

455. Barbosa MJ, Hoogakker J, Wijffels RH. Optimisation of cultivation parameters in photobioreactors for microalgae cultivation using the A-stat technique. Biomolecular Engineering. 2003 Jul 1;20(4):115–23.

456. Anye Cho B, de Carvalho Servia MÁ, del Río Chanona EA, Smith R, Zhang D. Synergising biomass growth kinetics and transport mechanisms to simulate light/dark cycle effects on photo-production systems. Biotechnology and Bioengineering. 2021;118(5):1932–42.

457. del Rio-Chanona EA, Dechatiwongse P, Zhang D, Maitland GC, Hellgardt K, Arellano-Garcia H, et al. Optimal Operation Strategy for Biohydrogen Production. Ind Eng Chem Res. 2015 Jun 24;54(24):6334–43.

458. Dechatiwongse P, Srisamai S, Maitland G, Hellgardt K. Effects of light and temperature on the photoautotrophic growth and photoinhibition of nitrogen-fixing cyanobacterium Cyanothece sp. ATCC 51142. Algal Research. 2014 Jul 1;5:103–11.

459. Cordara A, Re A, Pagliano C, Alphen PV, Pirone R, Saracco G, et al. Analysis of the light intensity dependence of the growth of Synechocystis and of the light distribution in a photobioreactor energized by 635 nm light. PeerJ. 2018 Jul 27;6:e5256.

460. Zhang D, Dechatiwongse P, Hellgardt K. Modelling light transmission, cyanobacterial growth kinetics and fluid dynamics in a laboratory scale multiphase photo-bioreactor for biological hydrogen production. Algal Research. 2015 Mar 1;8:99–107.

461. Pottier L, Pruvost J, Deremetz J, Cornet JF, Legrand J, Dussap CG. A fully predictive model for one-dimensional light attenuation by Chlamydomonas reinhardtii in a torus photobioreactor. Biotechnol Bioeng. 2005 Sep 5;91(5):569–82.

462. Anye Cho B, Ross BS, du Toit JP, Pott RWM, del Río Chanona EA, Zhang D. Dynamic modelling of Rhodopseudomonas palustris biohydrogen production: Perturbation analysis and photobioreactor upscaling. International Journal of Hydrogen Energy. 2021 Oct 26;46(74):36696–708.

463. Palamae S, Choorit W, Dechatiwongse P, Zhang D, Antonio del Rio-Chanona E, Chisti Y. Production of renewable biohydrogen by Rhodobacter sphaeroides S10: A comparison of photobioreactors. Journal of Cleaner Production. 2018 Apr 20;181:318–28.

464. Zhang D, Dechatiwongse P, Del-Rio-Chanona EA, Hellgardt K, Maitland GC, Vassiliadis VS. Analysis of the cyanobacterial hydrogen photoproduction process via model identification and process simulation. Chemical Engineering Science. 2015 May 25;128:130–46.

465. Wächter A, Biegler LT. On the implementation of an interior-point filter line-search algorithm for large-scale nonlinear programming. Math Program. 2006 Mar 1;106(1):25–57.

466. Nicholson B, Siirola JD, Watson JP, Zavala VM, Biegler LT. pyomo.dae: a modeling and automatic discretization framework for optimization with differential and algebraic equations. Math Prog Comp. 2018 Jun 1;10(2):187–223.

467. Hart William E, Laird Carl D, Watson JP, Woodruff David L, Hackebeil Gabriel A, Nicholson Bethany L, et al. Pyomo-optimization modeling in python. vol. 67. 2017;

468. Mowbray M, Savage T, Wu C, Song Z, Cho BA, Del Rio-Chanona EA, et al. Machine learning for biochemical engineering: A review. Biochemical Engineering Journal. 2021 Aug 1;172:108054.

469. Rogers AW, Vega-Ramon F, Yan J, del Río-Chanona EA, Jing K, Zhang D. A transfer learning approach for predictive modeling of bioprocesses using small data. Biotechnology and Bioengineering. 2022;119(2):411–22.

470. Pinto J, de Azevedo CR, Oliveira R, von Stosch M. A bootstrap-aggregated hybrid semi-parametric modeling framework for bioprocess development. Bioprocess Biosyst Eng. 2019 Nov 1;42(11):1853–65.

471. Gerken-Starepravo L, Zhu X, Cho BA, Vega-Ramon F, Pennington O, Antonio del Río-Chanona E, et al. An MIQP framework for metabolic pathways optimisation and dynamic flux analysis. Digital Chemical Engineering. 2022 Mar 1;2:100011.

472. Sadino-Riquelme MC, Rivas J, Jeison D, Hayes RE, Donoso-Bravo A. Making sense of parameter estimation and model simulation in bioprocesses. Biotechnology and Bioengineering. 2020;117(5):1357–66.

473. Zhang D, Dechatiwongse P, del Rio-Chanona EA, Maitland GC, Hellgardt K, Vassiliadis VS. Dynamic modelling of high biomass density cultivation and biohydrogen production in different scales of flat plate photobioreactors. Biotechnology and Bioengineering. 2015;112(12):2429–38.

474. Cabello J, Morales M, Revah S. Dynamic photosynthetic response of the microalga Scenedesmus obtusiusculus to light intensity perturbations. Chemical Engineering Journal. 2014 Sep 15;252:104–11.

475. Zhang D, Dechatiwongse P, del Rio-Chanona EA, Maitland GC, Hellgardt K, Vassiliadis VS. Modelling of light and temperature influences on cyanobacterial growth and biohydrogen production. Algal Research. 2015 May 1;9:263–74.

476. del Rio-Chanona EA, Ahmed N rashid, Zhang D, Lu Y, Jing K. Kinetic modeling and process analysis for Desmodesmus sp. lutein photo-production. AIChE Journal. 2017;63(7):2546–54.

477. Carvalho AP, Silva SO, Baptista JM, Malcata FX. Light requirements in microalgal photobioreactors: an overview of biophotonic aspects. Appl Microbiol Biotechnol. 2011 Mar 1;89(5):1275–88.

478. Salleh SF, Kamaruddin A, Uzir MH, Mohamed AR, Shamsuddin AH. Modeling the light attenuation phenomenon during photoautotrophic growth of A. variabilis ATCC 29413 in a batch photobioreactor. Journal of Chemical Technology & Biotechnology. 2017;92(2):358–66.

479. Rivera C, Niño L, Gelves G. Modeling of phycocyanin production from Spirulina platensis using different light-emitting diodes. South African Journal of Chemical Engineering. 2021 Jul 1;37:167–78.

480. del Rio-Chanona EA, Liu J, Wagner JL, Zhang D, Meng Y, Xue S, et al. Dynamic modeling of green algae cultivation in a photobioreactor for sustainable biodiesel production. Biotechnology and Bioengineering. 2018;115(2):359–70.

481. Kobayashi I, Nakajima M, Chun K, Kikuchi Y, Fujita H. Silicon array of elongated through-holes for monodisperse emulsion droplets. AIChE Journal. 2002;48(8):1639–44.

482. del Rio-Chanona EA, Wagner JL, Ali H, Fiorelli F, Zhang D, Hellgardt K. Deep learning-based surrogate modeling and optimization for microalgal biofuel production and photobioreactor design. AIChE Journal. 2019;65(3):915–23.

483. Ali H, Solsvik J, Wagner JL, Zhang D, Hellgardt K, Park CW. CFD and kinetic-based modeling to optimize the sparger design of a large-scale photobioreactor for scaling up of biofuel production. Biotechnology and Bioengineering. 2019;116(9):2200–11.

484. Steinmetz M, Le Coq D, Aymerich S, Gonzy-Tréboul G, Gay P. The DNA sequence of the gene for the secreted Bacillus subtilis enzyme levansucrase and its genetic control sites. Mol Gen Genet. 1985;200(2):220–8.

485. Gay P, Le Coq D, Steinmetz M, Berkelman T, Kado CI. Positive selection procedure for entrapment of insertion sequence elements in gram-negative bacteria. Journal of Bacteriology. 1985 Nov;164(2):918–21.

486. Hmelo LR, Borlee BR, Almblad H, Love ME, Randall TE, Tseng BS, et al. Precision-engineering the Pseudomonas aeruginosa genome with two-step allelic exchange. Nat Protoc. 2015 Nov;10(11):1820–41.

487. Gay P, Le Coq D, Steinmetz M, Ferrari E, Hoch JA. Cloning structural gene sacB, which codes for exoenzyme levansucrase of Bacillus subtilis: expression of the gene in Escherichia coli. J Bacteriol. 1983 Mar;153(3):1424–31.

488. Cai YP, Wolk CP. Use of a conditionally lethal gene in Anabaena sp. strain PCC 7120 to select for double recombinants and to entrap insertion sequences. J Bacteriol. 1990 Jun;172(6):3138–45.

489. Lagarde D, Beuf L, Vermaas W. Increased Production of Zeaxanthin and Other Pigments by Application of Genetic Engineering Techniques toSynechocystis sp. Strain PCC 6803. Applied and Environmental Microbiology. 2000 Jan;66(1):64–72.

490. Branco dos Santos F, Du W, Hellingwerf KJ. Synechocystis: Not Just a Plug-Bug for CO2, but a Green E. coli. Frontiers in Bioengineering and Biotechnology [Internet]. 2014 [cited 2022 Sep 27];2.

491. Cheah YE, Albers SC, Peebles CAM. A novel counter-selection method for markerless genetic modification in Synechocystis sp. PCC 6803. Biotechnol Prog. 2013 Feb;29(1):23–30.

492. Aikens J, Turner RJ. Transgenic photosynthetic microorganisms and photobioreactor [Internet]. US8367379B2, 2013 [cited 2022 Sep 21].

493. Xu Y, Green BD. Compositions and methods to remove genetic markers using counter-selection [Internet]. WO2012178101A3, 2013 [cited 2022 Sep 21].

494. Tan X, Liang F, Cai K, Lu X. Application of the FLP/FRT recombination system in cyanobacteria for construction of markerless mutants. Appl Microbiol Biotechnol. 2013 Jul;97(14):6373–82.

495. Zhang Y, Pu H, Wang QS, Cheng S, Zhao WX, Zhang Y, et al. PII is important in regulation of nitrogen metabolism but not required for heterocyst formation in the cyanobacterium Anabaena sp PCC 7120. Journal of Biological Chemistry. 2007;282(46).

496. Danielsen S, Kilstrup M, Barilla K, Jochimsen B, Neuhard J. Characterization of the Escherichia coli codBA operon encoding cytosine permease and cytosine deaminase. Mol Microbiol. 1992 May;6(10):1335–44.

497. Vermes A, Guchelaar HJ, Dankert J. Flucytosine: a review of its pharmacology, clinical indications, pharmacokinetics, toxicity and drug interactions. Journal of Antimicrobial Chemotherapy. 2000 Aug 1;46(2):171–9.

498. Stougaard J. Substrate-dependent negative selection in plants using a bacterial cytosine deaminase gene. The Plant Journal. 1993 May 1;3(5):755–61.

499. Kobayashi T, Hisajima S, Stougaard J, Ichikawa H. A conditional negative selection for Arabidopsis expressing a bacterial cytosine deaminase gene. The Japanese Journal of Genetics. 1995;70(3):409–22.

500. Serino G, Pal Maliga P. A negative selection scheme based on the expression of cytosine deaminase in plastids. The Plant Journal. 1997;12(3):697–701.

501. Dubeau MP, Ghinet MG, Jacques PE, Clermont N, Beaulieu C, Brzezinski R. Cytosine Deaminase as a Negative Selection Marker for Gene Disruption and Replacement in the Genus Streptomyces and Other Actinobacteria. Appl Environ Microb. 2009 Feb 15;75(4):1211–4.

502. Young REB, Purton S. Cytosine deaminase as a negative selectable marker for the microalgal chloroplast: a strategy for the isolation of nuclear mutations that affect chloroplast gene expression. Plant J. 2014 Dec;80(5):915–25.

503. Gale GAR, Schiavon Osorio AA, Puzorjov A, Wang B, McCormick AJ. Genetic Modification of Cyanobacteria by Conjugation Using the CyanoGate Modular Cloning Toolkit. J Vis Exp. 2019 Oct 31;(152).

504. Lambert JM, Bongers RS, Kleerebezem M. Cre-lox-Based System for Multiple Gene Deletions and Selectable-Marker Removal in Lactobacillus plantarum. Applied and Environmental Microbiology. 2007 Feb 15;73(4):1126–35.

505. Vogel AIM, Lale R, Hohmann-Marriott MF. Streamlining recombination-mediated genetic engineering by validating three neutral integration sites in Synechococcus sp. PCC 7002. Journal of Biological Engineering. 2017 Jun 5;11(1):19.

506. Klähn S, Hagemann M. Compatible solute biosynthesis in cyanobacteria. Environmental Microbiology. 2011;13(3):551–62.

507. Ungerer J, Pakrasi HB. Cpf1 Is A Versatile Tool for CRISPR Genome Editing Across Diverse Species of Cyanobacteria. Sci Rep-Uk [Internet]. 2016 Dec 21;6.

508. Xiao Y, Wang S, Rommelfanger S, Balassy A, Barba-Ostria C, Gu P, et al. Developing a Cas9-based tool to engineer native plasmids in Synechocystis sp. PCC 6803. Biotechnol Bioeng. 2018 Sep;115(9):2305–14.

509. Li H, Shen CR, Huang CH, Sung LY, Wu MY, Hu YC. CRISPR-Cas9 for the genome engineering of cyanobacteria and succinate production. Metabolic Engineering. 2016 Nov 1;38:293–302.

510. Niu TC, Lin GM, Xie LR, Wang ZQ, Xing WY, Zhang JY, et al. Expanding the Potential of CRISPR-Cpf1-Based Genome Editing Technology in the Cyanobacterium Anabaena PCC 7120. ACS Synth Biol. 2019 Jan 18;8(1):170–80.

511. Treves H, Küken A, Arrivault S, Ishihara H, Hoppe I, Erban A, et al. Carbon flux through photosynthesis and central carbon metabolism show distinct patterns between algae, C3 and C4 plants. Nat Plants. 2022 Jan;8(1):78–91.

512. Rosgaard L, de Porcellinis AJ, Jacobsen JH, Frigaard NU, Sakuragi Y. Bioengineering of carbon fixation, biofuels, and biochemicals in cyanobacteria and plants. J Biotechnol. 2012;162(1):134–47.

513. Liang F, Lindblad P. Effects of overexpressing photosynthetic carbon flux control enzymes in the cyanobacterium Synechocystis PCC 6803. Metabolic Engineering. 2016 Nov 1;38:56–64.

514. Liang F, Englund E, Lindberg P, Lindblad P. Engineered cyanobacteria with enhanced growth show increased ethanol production and higher biofuel to biomass ratio. Metabolic Engineering. 2018 Mar 1;46:51–9.

515. Liang F, Lindblad P. Synechocystis PCC 6803 overexpressing RuBisCO grow faster with increased photosynthesis. Metabolic Engineering Communications. 2017 Jun 1;4:29–36.

516. De Porcellinis AJ, Nørgaard H, Brey LMF, Erstad SM, Jones PR, Heazlewood JL, et al. Overexpression of bifunctional fructose-1,6-bisphosphatase/sedoheptulose-1,7-bisphosphatase leads to enhanced photosynthesis and global reprogramming of carbon metabolism in Synechococcus sp. PCC 7002. Metabolic Engineering. 2018 May 1;47:170–83.

517. Liu JJ, Orlova N, Oakes BL, Ma E, Spinner HB, Baney KLM, et al. CasX enzymes comprise a distinct family of RNA-guided genome editors. Nature. 2019 Feb;566(7743):218–23.

518. Gordon GC, Korosh TC, Cameron JC, Markley AL, Begemann MB, Pfleger BF. CRISPR interference as a titratable, trans-acting regulatory tool for metabolic engineering in the cyanobacterium Synechococcus sp. strain PCC 7002. Metabolic Engineering. 2016 Nov 1;38:170–9.

519. Posten C. Design principles of photo-bioreactors for cultivation of microalgae. Engineering in Life Sciences. 2009;9(3):165–77.

520. Singh RN, Sharma S. Development of suitable photobioreactor for algae production – A review. Renewable and Sustainable Energy Reviews. 2012 May 1;16(4):2347–53.

521. Huang Q, Jiang F, Wang L, Yang C. Design of Photobioreactors for Mass Cultivation of Photosynthetic Organisms. Engineering. 2017 Jun 1;3(3):318–29.